Efficient Audio Systems

Iversen, Niels Elkjær

Publication date:
2018

Document Version
Publisher's PDF, also known as Version of record

Efficient Audio Systems

Niels Elkjær Iversen
PhD thesis
March 2018

DTU Electrical Engineering
Department of Electrical Engineering

Niels E. Iversen

Efficient Audio Systems

Ph.D. Dissertation, March 2018

Efficient Audio Systems

Author:
Niels E. Iversen

Supervisors:
Michael A. E. Andersen — DTU Elektro, Electronics Group
Arnold Knott — DTU Elektro, Electronics Group

Department of Electrical Engineering
Electronics Group
Technical University of Denmark
Elektrovej building 325
DK-2800 Kgs. Lyngby
Denmark

www.ele.elektro.dtu.dk
Tel: (+45) 45 25 38 00
Fax: (+45) 45 88 01 17
E-mail: hw@elektro.dtu.dk

Release date:	21$^{\text{th}}$ March 2018
Category:	1 (public)
Edition:	First
Comments:	This thesis is submitted in partial fulfillment of the requirements for obtaining the PhD degree at the Technical University of Denmark.

Preface and Acknowledgment

This thesis is a result of three years of research activities at the Technical University of Denmark. During these three years I have had the pleasure of working closely with a lot of people which assistance I will like to acknowledge. They include all of my colleagues within the Electronics Group. Especially I want to thank:

Michael A. E. Andersen for managing the research group so well and for his highly appreciated supervision. Arnold Knott for his excellent supervision during the entire period of my Ph.D. study and for the many happy moments playing table soccer and drinking beers. Henrik Schneider for his interest and assistance in my research activities, especially during my first year of my Ph.D. study. That really helped me getting started! Thomas Birch, Rasmus Ploug and Jens Pejtersen for their support, technical discussion and many hours of fun at the office. Dorte, Hans-Christian and Henriette for all kinds of support, ordering components, filling out travel expenses writing research applications. Thank you very much!

In addition to my colleagues I have been very fortunate to do projects in collaboration with organisations that showed interests in my research. I want to thank:

Miroslav Vasic and Vladan Lazarevic from the CEI group in Madrid for their great hospitality during my external stay and their expertise within Envelope Tracking power supplies. It was a great pleasure working with you for three months. I could not have hoped for a better outcome of my external stay. Carsten and Morten from Point Source Acoustics for their technical assistance in making voice coils and loudspeaker drivers and for many great discussions on loudspeaker efficiency. Ruben and Anton from Soundboks for their collaboration and inputs regarding highly efficient portable audio system projects. Rien and Mikkel from Merus Audio for great discussions on highly efficient audio system and a collaborative publication within the Audio Engineering Society. Dave Houghton from EcosResearch for his inputs and discussion on appropriate test signals and his serious investigation on using my research in new standardization methods for testing audio equipment. Stine and Alberte from The Royal Danish Academy of Fine Arts, School of Architecture, Design and Conservation (KADK) for their dedication to collaborate on artistic installations for Roskilde festival and STRØM festival.

Moreover I have had the joy of supervising approximately 150 DTU students and 90 high school students for a wide range of projects during my Ph.D. study. These projects include five B.Sc. projects and three M.Sc. projects. I have really enjoyed these supervision tasks and I have benefited from the many technical discussions I had with the many talented students. I want to thank everyone that did projects with me especially Nicolai Dahl, Filip Madsen, Tobias Thydal, Sebastian Tengvall, Martijn Duraj and Søren Thorsen for their excellent work within my field of research.

Finally I want to thank my family for their love and support during my Ph.D. study. Especially my beloved wife, Josefine, and duaghter, Sofie, for keeping a smile on my face.

Abstract

A modern audio reproduction system comprises of one input block, the input signal, and three hardware blocks, the power supply, the power amplifier and the loudspeaker. The system is meant to handle an infinite combination of sine waves within the audible range, 20 Hz to 20 kHz, with a dynamic range of up to 120 dB. Being able to do this with low Total Harmonic Distortion plus Noise (THD+N) is the requirement in modern audio reproduction systems. In recent years high efficiency and small size has become key parameters partly due to the fact that audio reproduction systems have evolved into battery driven portable devices. This has made switch-mode technology widely used in audio reproduction systems. However a consequence of shrinking the audio reproduction systems is reliability issues which always is a key parameter.

It is with respect to these key parameters; efficiency, size and reliability, this thesis examines each block of the audio reproduction system identifying limitations and methods to overcome them.

Sine waves are the common test signal when designing audio reproduction systems. Sine waves have a crest factor of 3 dB and based on an analysis of 183 music tracks they are found to represent music poorly. The analysis shows that the average crest factor of music is 15 dB thus causing conventional designs to be improper, favouring sine wave operation. The impact on switch-mode power audio amplifier design from this understanding of the audio input is listed below:

- A new test signal is proposed based on amplitude distribution of real music. It is analytically described and has fundamental periodicity making it a serious replacement signal for conventional sine waves. With a crest factor of 14 dB it is very close to that of actual music which is found to be 15 dB and compared with sine waves that have a 3 dB crest factor the proposed signal is almost a factor seven more precise in modelling the dynamics.
- Experimental results on a conventionally designed 12 V switch-mode power audio amplifier demonstrate a 10 % point efficiency improvement when choosing switching devices based on the proposed signal instead of sine waves.
- A new switching strategy beneficial for power dissipation in switching devices is proposed. Experimental results on a 100 W test amplifier show a 45 °C reduction of operating temperature compared to conventional implementation.
- Measured results on a 150 W prototype amplifier using the proposed strategy show power density of 11.5 W/cm^3. That is almost a factor three higher than recognized state-of-the-art amplifier modules. Moreover it is demonstrated that by using the proposed switching strategy size can be reduced more than a factor two compared to a conventional implementation.

The proposed switching strategy utilizes a high ripple current in the output filter inductance to improve soft switching capabilities when playing audio so that the power dissipation is moved away from the switching devices into the output filter which functions as natural heat sink. The high ripple current affects the amplifier's frequency

response making classical control sub-optimal. An alternative method using full state control is proposed. Experimental results on a 1.9 MHz prototype amplifier show that frequency response ripples are effectively removed while delivering THD+N levels down to 0.01 %.

Conventional power supplies for switch-mode audio power amplifiers supply the amplifier with a fixed voltage. An alternative approach employing envelope tracking known from RF amplifiers is proposed. Measured results on a 100 W prototype system, comprised of a multi-level power supply and a switch-mode audio power amplifier, show that efficiency is improved up to a factor of 6 when playing real audio signals. The temperature rise is strongly reduced, especially for the switching devices of the amplifier where it is halved from 100 °C to 50 °C effectively increasing reliability and life span due to less thermal stress.

The total system efficiency is dominated by the loudspeaker efficiency, in the range 0.2 % to 2 %. To counter that:

- A new voice coil design method is proposed. Analysis shows that the relationship between voice coil fill factor and loudspeaker efficiency is proportional. Using rectangular winding layout may increase the fill factor. Experimental results show a 25 % efficiency improvement when increasing the fill factor from 45 % to 53 %.

Increasing fill factor using a rectangular winding layout will result in a lower nominal resistance of the loudspeaker. This has a positive effect on a system level as it allows the amplifier to deliver more power from the same supply level. Measured results show that by using a 1 Ω load resistance instead of a conventional 4 Ω the efficiency is improved 10 % point at 1 W output power. In systems normally needing a boost converter, like automotive and portable electronics, this improvement can even be greater as the the low load resistance eliminates the need for supply voltage boosting. Measured results demonstrate a 25 % point efficiency improvement at 1 W output power for such systems.

The findings of this thesis show that a high continuous output power is not a key parameter for music applications. The new test signal is currently under investigation by a subcontractor to the EPA U.S Energy Star program for use in test methods for a standard. High peak power is still needed for reproducing the peaks in dynamic audio signals. This points towards that future challenges in audio reproduction system design are high supply voltage levels and better loudspeaker efficiencies. In that sense this thesis outlines methods to overcome these challenges.

Resumé

Et moderne lydgengivelsessystem består af en input blok, input signalet, og tre harware blokke, strømforsyningen, effektforstærkeren og højttaleren. Systemet er beregnet til at hÃĕndtere en uendelig kombination af sinusbølger inden for det hørbare område, 20 Hz til 20 kHz, med et dynamisk spænd på op til 120 dB. At kunne gøre dette med lav en lav Total Harmonic Distortion plus Noise er kravet i moderne lydgengivelsessystemer. I de senere år er effektivitet og størrelse blevet vigtige parametre for forbruger produkter. Dette skyldes til dels, at lydgengivelsessystemer har udviklet sig i retningen af batteridrevne og bærbare enheder. Dette har gjort switch-mode teknologi meget anvendt i lydgengivelsessystemer på grund af den høje effektivitet denne teknologi er kendt for. En konsekvens af, at minimiere størrelsen af lydgengivelsessystemer er dog pålidelighedsproblemer, som altid er en en vigtig parameter i forbruger elektronik.

Det er med hensyn til disse vigtige parametre; effektivitet, størrelse og pålidelighed, at denne afhandling undersøger hver blok af lydgengivelsessystemet, identificerende begrænsninger og foreslår metoder til at overvinde dem.

Sinusbølger er det konventionelle testsignal brugt i forbindelse med design af lydgengivelsessystemer. Sinusbølger har en crest faktor på 3 dB og på baggrund af en analyse af 183 musiknumre må det konkluderes, at de repræsenterer dynamisk musik dårligt. Analysen viser, at den gennemsnitlige crest faktor for musik er 15 dB, hvilket får konventionelle forstærker designs til at yde best ved gengivelse af sinusbølger frem for egentlig musik. Med denne viden er en række opdagelser gjort som har betydning for effektforstærkeren:

- Et nyt test signal baseret på amplitude distribution af ægte musik er blevet udviklet. Det er analytisk beskrevet og har grundlæggende periodicitet, ligesom sinussignaler, hvilket gør det til et seriøst erstatningssignal for konventionelle sinusbølger. Med en crest faktor på 14 dB er den meget tæt på, at have samme dynamiske egenskaber som musik, som en 15 dB crest faktor. Sammenlignet med sinusbølger, der har en 3 dB crest faktor, er det nye signal næsten en faktor syv mere præcis i modellering af dynamikken i musik.

- Eksperimentelle resultater på en konventionel 12 V switch-mode-effektforstærker demonstrerer en effektivitetsforbedring på 10 % point, når man vælger forstærkerens switching-devices baseret på det nye signal i stedet for sinusbølger.

- En ny switching strategi der minimere effekttab i forstærkerens switching-devices er blevet udviklet. Eksperimentelle resultater på en 100 W forstærker prototype demonstrerer en temperatur sænking for forstærkerens switching-devices på 45 °C sammenlignet med en konventionel switching strategi.

- Målinger på en 150 W prototypeforstærker, der bruger den nye switching strategi, viser en effekttæthed på 11.5 W/cm ^{3}. Det er næsten en faktor tre højere end anerkendte state-of-the-art forstærkermoduler. Det fremgår endvidere, at ved at anvende den foreslåede swithing strategi kan størrelsen reduceres mere end en faktor to sammenlignet med en konventionel implementering.

Den nye switching strategi anvender en høj rippelstrøm i udgangsfilteret, til at forbedre forstærkerens soft switching egenskaber. Derved flyttes effekttab væk fra forstærkerens switching-devices. Tilgengæld afsættes et større tab i udgansfilteret som fungerer som en naturlig køleplade. Den høje rippelstrøm påvirker forstærkerens frekvensrespons, hvilket gør klassisk kontrol uhensigtsmæssig. En alternativ kontrol metode, der bruger full state kontrol, foreslås. Eksperimentelle resultater på en 1.9 MHz prototypeforstærker viser, at ringninger i frekvensresponset effektivt fjernes, mens lydgengivelsen er god med THD+N-niveauer ned til 0.01 %.

Konventionelle strømforsyninger til switch-mode forstærkere forsyner forstærkeren med en fast spænding. En alternativ metode, der anvender Envelope Tracking, foreslås. Målte resultater på et 100 W prototypesystem, der består af en en switch-mode forstærker og en strømforsyning med flere tilgængelige forsyningsspændinger at vælge i mellem, viser, at effektivitets forbedring op til en faktor 6, sammenlignet med systemer med fast spændingsforsyninger. Forstærkerens temperatur reduceres tilsvarende kraftigt, særligt for forstærkerens switching-devices, hvor den halveres fra 100 °C til 50 °C. Dette øger pålideligheden og levetiden af systemet på grund af mindre termisk stress.

Den samlede systemeffektivitet domineres af højttalerens effektivitet, hvilken er i området 0.2 % til 2 %. For at imødegå det forslås:

- Et nyt svingspole design. Gennem analyse vises det, at svingspolens fyldfaktor er proportional med højtalerens effektivitet og at fyldfaktoren kan øges ved hjælp at et rektangulært viklingslayout. Eksperimentelle resultater viser en 25 % effektivitet forbedring, når fyldfaktoren øges fra 45 % til 53 %.

Ved at øge fyldfaktoren gennem et rektangulært viklingslayout sænkes højtalerens nominelle modstand. Dette har en positiv effekt på et systemniveau, da det giver forstærkeren mulighed for at levere mere effekt fra samme forsyningsspænding. Målte resultater viser en effektivitets forbdering på 10 % point i forstærkeren ved 1 W udganseffekt, når den nominelle modstand sænkes fra 4 til 1 Ω. I systemer der er afhængige af en boost-konverter, f.eks. batteridrevne systemer, kan denne forbedring være større, da den en lav nominel modstand eliminerer behovet for forøgelse af forsyningsspændingen. Målte resultater viser en effektivitets forbedring på 25 % point ved 1 W udgangseffekt for sådanne systemer.

Denne afhandling viser at en høj vedvarende udgangseffekt ikke er et vigtigt parameter for lydgengivelses systemer til musik applikationer. En høj udgangseffekt er dog stadig væsentligt for at reproducere dynamikken i lyd. Forestående udfordringer for lydgengivelses systmer er høje forsyningsspændinger og en bedre højtalereffektiviteter. Det nye test signal bliver undersøgt af EPA U.S. Energy Star program som en muligh afløser for sinus toner i standardiserede tests.

Contents

List of Figures

1

Introduction

1.1 Background

Audio reproduction systems are a vital part of modern life. Not only for communication purposes such as security announcements in public areas but equally as a cultural stimulation throughout our lives. From background music in a restaurant to large scale rock concerts. All rely on properly designed audio reproduction systems. A modern audio reproduction system should be able to handle an infinite combination of sine waves within the audible range, 20 Hz to 20 kHz, with a dynamic range of up to 120 dB and low Total Harmonic Distortion plus Noise (THD+N). Audio reproduction systems comprise of four blocks; One input- and three hardware-blocks:

- Input signal (input)
- Power supply (electrical hardware)
- Amplifier (electrical hardware)
- Loudspeaker (electro-mechanical hardware)

Switch-mode technology [1] is widely used for power supply and amplifier designs due to very high efficiency in the range of 90% [2, 3] and with very low THD+N down to 0.0005% [4–10].

Due to the high efficiency of switch-mode technology the power density of audio amplifiers have increased. This has resulted in a selection of integrated amplifiers for low- and mid-level output powers [11–15]. At higher output powers ($\geq$100 W) integrated amplifiers become less viable as the power dissipation increases and thus the need for cooling [16]. To develop switch-mode power audio amplifiers with higher power density, techniques used for the latest generation of LED drivers may be considered [17–20]. That involves increasing the switching frequency of the power stage significantly yielding an equally significant size reduction of the bulky components such as filter capacitors and inductors. Combined with new semiconductor technology, such as Gallium Nitride devices (GaN), new design possibilities have emerged [21–25]. GaN in high switching frequency switch-mode power audio amplifiers have demonstrated good results with respect to THD+N however reliability and performance is affected by temperature rise [26–28]. Therefore the management of power dissipation remains the main challenge to overcome in order to increase the power density.

Different types of loudspeaker topologies exist such as moving coil- and balanced-armatures-loudspeakers [29]. The conventional one is the moving coil loudspeaker.

It consists of a driver and a some kind of enclosure [30–34]. Essentially it is an electromechanical motor converting electrical energy into acoustical energy. Compared to the efficiency of switch-mode technology the loudspeaker block offers very poor efficiency in the range 0.2% to 2% and is therefore the limiting factor of the total system efficiency. Methods to improve the efficiency include impedance matching between driver diaphragm and air load. This is done by horn loading the driver as the horn acts like an acoustic transformer [30]. However this method increases the overall size of the speaker, especially for low frequencies as it is proportional to the wave length, making it incompatible with market demands for small sized systems.

Due to the fact that audio reproduction systems have evolved into battery driven portable devices [35] high efficiency and small size are now vital parameters on a system level along with reliability and audio performance, which set up new design challenges to overcome. This Ph.D. thesis aims to provide methods to overcome these challenges within each of the essential blocks of the audio reproduction system and on a system level.

1.2 Thesis scope

With respect to the above mentioned key parameters; efficiency, size, reliability and audio performance, this Ph.D. thesis aims to examine each block of the audio reproduction system, i.e. input signal, power supply, power amplifier and loudspeaker, and identify limitations and methods to overcome them.

The efficiency, η, is defined as the ratio between the output and input power of the Device Under Test (DUT):

$$\eta = \frac{P_{out}}{P_{in}} \cdot 100 \quad [\%] \tag{1.1}$$

Research topics related to efficiency have been test procedures and measurement techniques, loudspeaker design and tracking power supplies.

In this thesis reliability is simplified to safe steady state operating temperatures, defined as temperatures below 100 °C. This is a very simplified representation of the reliability and other factors besides temperature, such as Component Stress Factor (CSF) [36–38], affect reliability and expected life time. Size is referring to the power density, ρ_{power}, defined as the ratio between the output power and the physical volume, V_{DUT}.

$$\rho_{power} = \frac{P_{out}}{V_{DUT}} \quad [\mathrm{W/cm^3}] \tag{1.2}$$

The research topic related to reliability and size has been high power density switch-mode power audio amplifiers.

Audio performance relates the quality of the audio produced by the system. In this thesis it will be quantified by the Total Harmonic Distortion plus Noise (THD+N).

$$\mathrm{THD{+}N} = \frac{\sum_{n=2}^{\infty} A_n + \mathrm{noise}}{A_1} \tag{1.3}$$

Where A_1 is the amplitude of the fundamental and A_n are the harmonics. Research related to audio performance includes self-oscillating modulators and control of switch-mode power audio amplifiers.

The findings have resulted in:

- Patent applications : 1 submitted.
- Peer-review journal publications : 2 published and 1 submitted.
- Peer-review conference publications : 11 published and 1 accepted.

The thesis is build around these publications and they are all included in appendices A-P.

1.3 Thesis structure

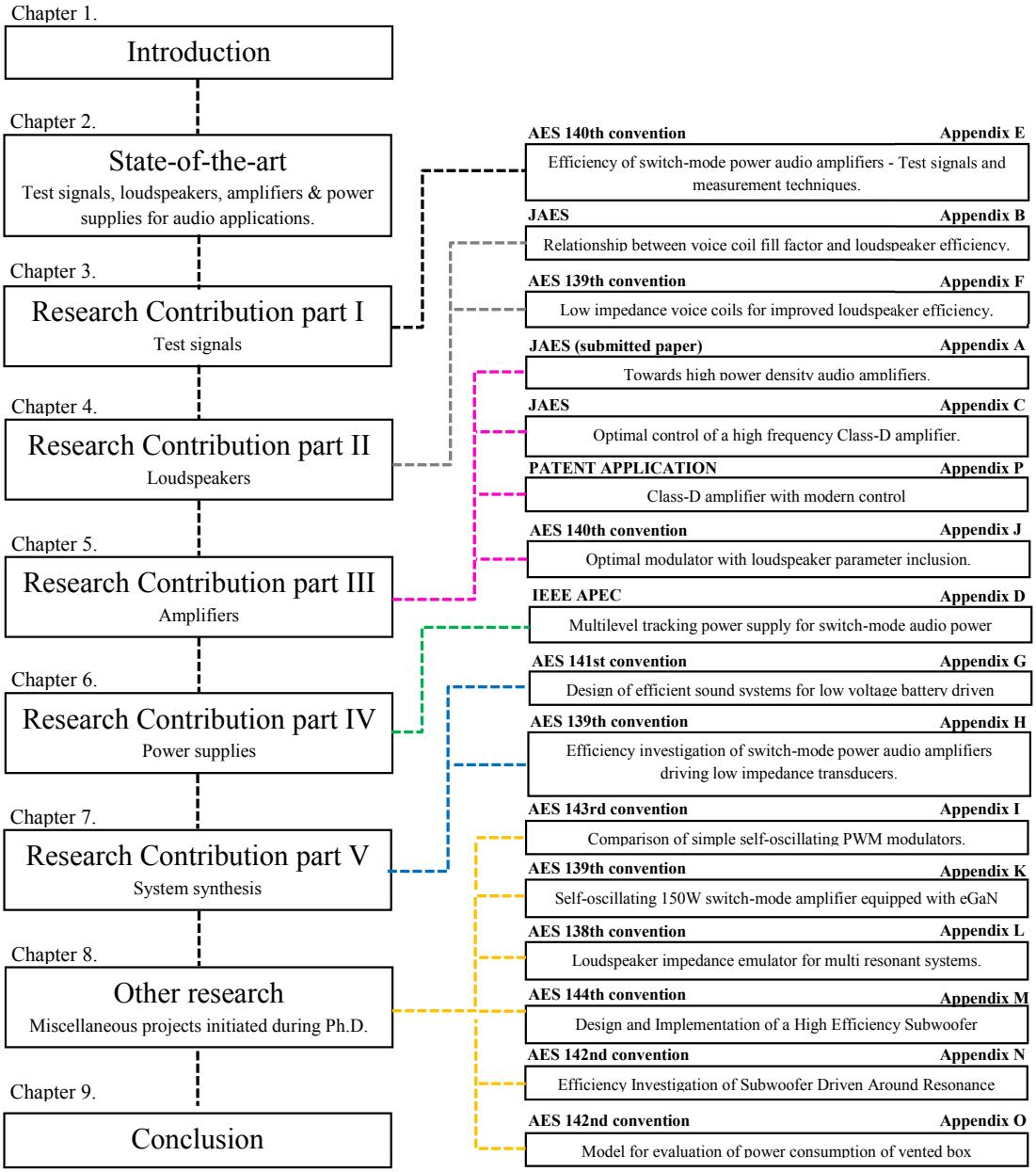

2

State-of-the-art

2.1 Input signals

The input signal to the audio reproduction system is of great importance. Not only because it is what the listener perceives and hopefully enjoys but mainly due to the fact that the input signal has great influence on operating conditions for the different blocks of the audio reproduction system. Moreover specific audio signals are used to evaluate the performance of the individual blocks of the audio system.

This section will analyse well established signals used for testing purposes along with a real audio signal. The signals will be analysed with respect to their Crest Factor (CF), which is the peak-to-rms ratio and provide information about the dynamic behaviour.

$$\mathrm{CF} = 20 \log \left(\frac{V_{pk}}{V_{rms}} \right) \quad [\mathrm{dB}] \tag{2.1}$$

Where V_{rms} is the Root Mean Square (RMS) value of the signal. In addition to that, the frequency content of the signals is also examined.

2.1.1 Sine waves

Sine waves are one of the most commonly used test signals for audio purposes. This is due to the fact that opposed to other signals a sine wave is a pure tone, meaning that it has only one frequency component, i.e. is fundamental frequency. That makes it ideal for evaluating distortion effects and frequency responses of audio amplifiers and loudspeakers. In addition to that it is described mathematically making it easy to evaluate and use for analysis.

$$f(t) = A \sin(\omega t + \theta) \tag{2.2}$$

Where A denotes the amplitude, $\omega = 2\pi f$ is the radial frequency and θ denotes the phase. Moreover the fundamental periodicity allows for easy evaluation of through RMS values which is convenient when evaluating efficiency of audio amplifiers. Though a sine wave does have dynamic properties it has a rather low CF value of 3 dB. Fig. 2.1 shows time- and frequency domain of a 50 Hz sine wave.

2.1.2 Noise signals

Noise signals are characterized as being uniform dynamic signals consisting of a combination of all frequencies. The most simple noise signal is white noise which has an even

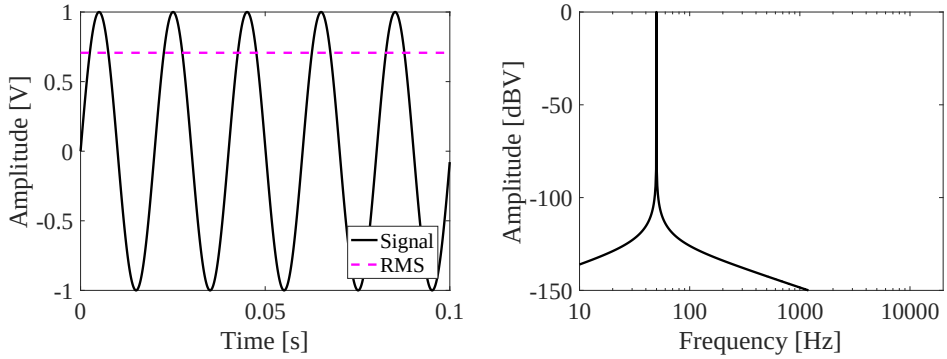

(a) Time domain. **(b)** Frequency domain.

Figure 2.1: 50 Hz sine wave analysed in time- and frequency-domains.

frequency distribution. Similarly to sine waves white noise has a low CF of approximately 5 dB. White noise can be used to evaluate frequency responses in combination with Fourier analysis [39].

Pink noise is different from white noise as it as an uneven frequency distribution. The amplitude spectrum of the pink noise rolls off with 10 dB/decade. This is actually more representative for audio signals than white noise as most energy is placed in the low frequency domain. From a dynamic perspective pink noise has a CF of approximately 14 dB making it much more dynamic than white noise. Due to similarities to music pink noise can be used for thermal stress test on amplifiers and loudspeakers.

Finally there is the IEC-268 standard [40] which is filtered pink noise signal. The filter applied to the pink noise is a high pass placed a low frequencies and a low pass for high frequencies. Using this filtering the amplitude spectrum and CF becomes similar to what one can expect in average music recordings [40]. The IEC-268 signal has a CF of 14 dB. Like the pink noise signal the IEC-268 signal is useful for thermal stress testing. Fig. 2.2 shows time- and frequency domains of the noise signals. Due to the large frequency content and the seemingly random time domain noise signals are not ideal for efficiency and distortion measurements.

2.1.3 Music signals

Opposed to sine waves and noise signals, music signals can actually be an enjoyable listening experience. Music signals are non-uniform and highly dynamic. The dynamics can be vastly different from track to track and genre to genre. Fig. 2.3 shows time- and frequency domains of three music signals from pop, rock and classical genres.

The pop track is *"Daft Punk - Get Lucky"* and it has a CF of 13 dB. On Fig. 2.3 (a) the beat is easily noticeable and Fig. 2.3 (b) shows a frequency spectrum with some resemblance to the spectrum of pink noise and the IEC-268 noise on Fig. 2.2 (d) and (f).

The rock track is *"Lamb of God - Redneck"* and from the time domain analysis in Fig. 2.3 (c) it must be concluded that this track is vastly more compressed than the pop track. In fact it has a CF of 10 dB. The spectrum analysis in Fig. 2.3 (d) is similar to that of the pop track.

Finally there is the classical track *"Chopin - Minute Waltz"*. With a CF of 20 dB this track is much more dynamic than the pop and rock track. Moreover its' frequency spectrum shown in Fig. 2.3 (f) is some what different peaking around 500 Hz. This is due to the instrument of this track being piano solely. In general classical music has more dynamics compared to rock and pop music. This analysis corresponds with previous findings [41–44].

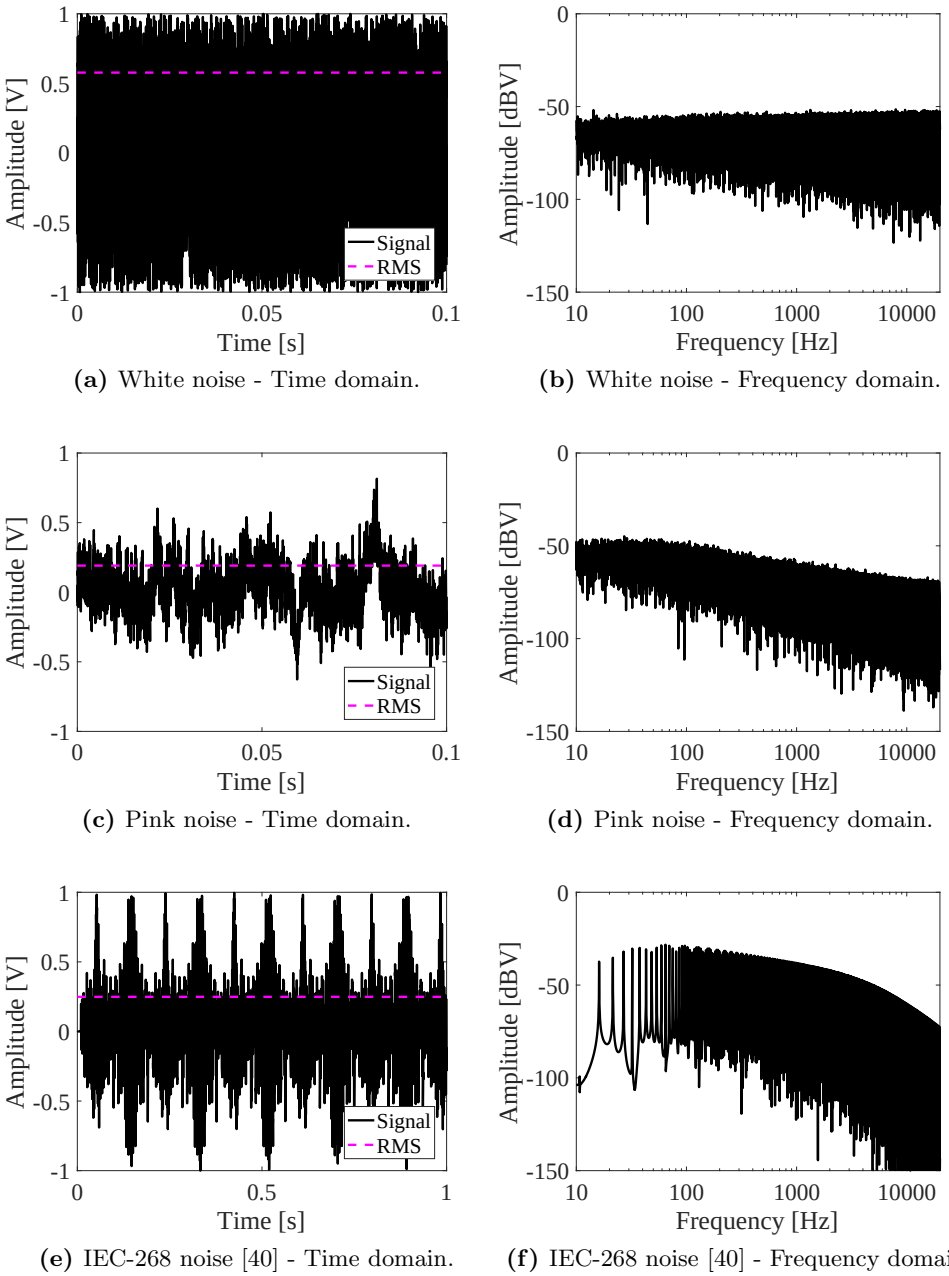

(a) White noise - Time domain. **(b)** White noise - Frequency domain.

(c) Pink noise - Time domain. **(d)** Pink noise - Frequency domain.

(e) IEC-268 noise [40] - Time domain. **(f)** IEC-268 noise [40] - Frequency domain.

Figure 2.2: Noise signals analysed in time- and frequency-domains.

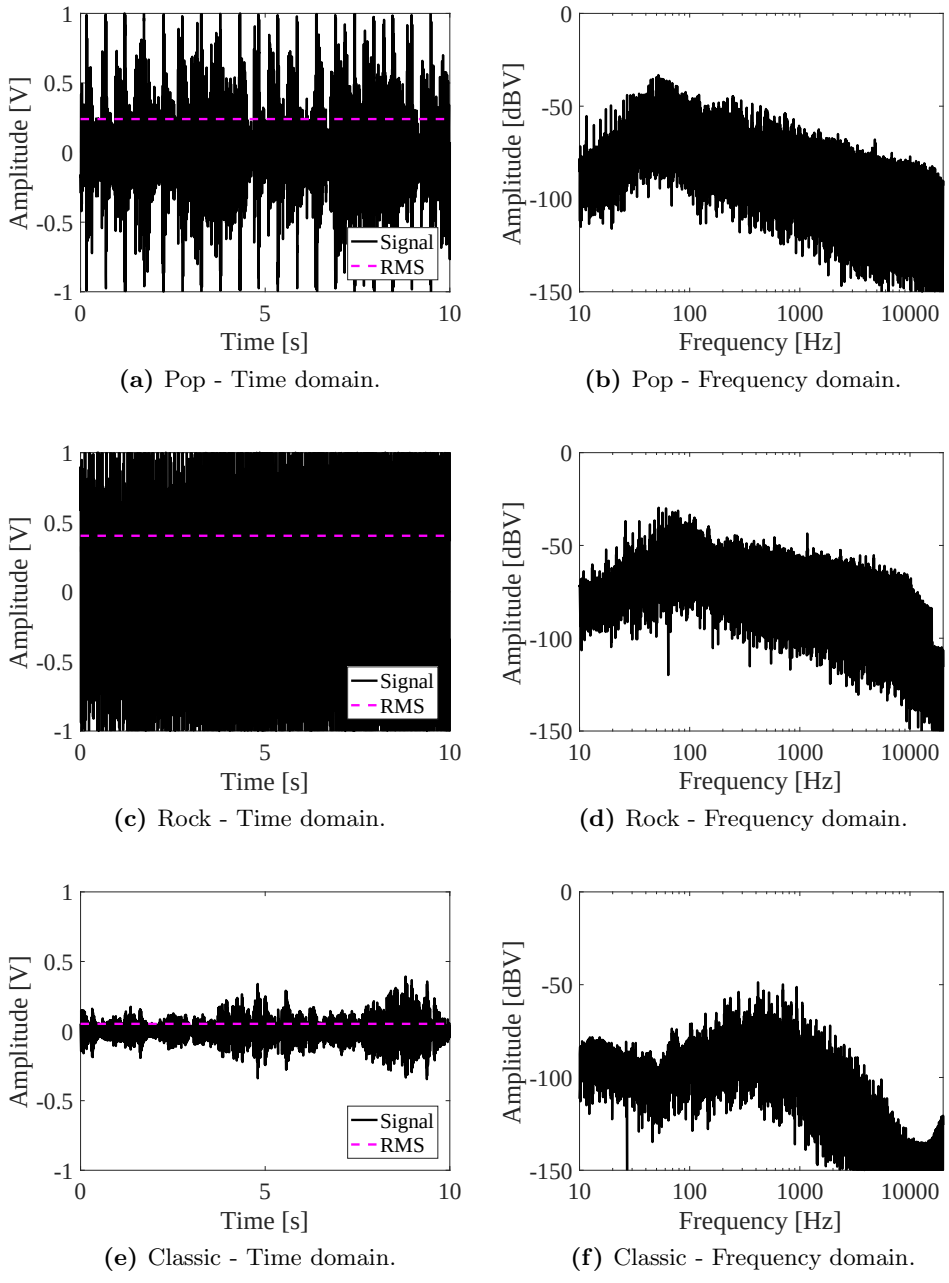

(a) Pop - Time domain.

(b) Pop - Frequency domain.

(c) Rock - Time domain.

(d) Rock - Frequency domain.

(e) Classic - Time domain.

(f) Classic - Frequency domain.

Figure 2.3: Music signals analysed in time- and frequency-domains.

2.1.4 Summary of state-of-the-art audio signals

This section presented an analysis of the most commonly used test signals, their field of use and their relevancy in connection with music signals. Table 2.1 summarizes the dynamic properties of investigated test signals along with original programme material [41].

Table 2.1: Summary of dynamic properties of audio signals.

	Crest Factor (CF) [dB]
Test signals	
Sine wave	3
White noise	5
Pink noise	14
IEC-268 [40]	12
Programme material	
Pop [41]	10.6
Heavy [41]	9.2
Symphonic [41]	17.1
Jazz [41]	13.5
Hip-Hop [41]	8.2
Speech [41]	12.9

2.2 Moving coil loudspeakers

Moving coil loudspeakers are a well described topic [30–34, 45, 46]. A common method to describe loudspeaker operation is through Thiele-Small parameters [32–34]. Using this method this section will present the basic operation and modelling techniques related to this topic. Moreover a summary of existing implementations will be presented in the end of this section along with key performance parameters.

2.2.1 Fundamental operation

Moving coil loudspeakers convert an electrical signal to sound. Fig. 2.4 shows the cross section of a moving coil loudspeaker. The electrical signal is applied across the voice coil (VC). This generates an electro magnetic field which causes the VC to be displaced

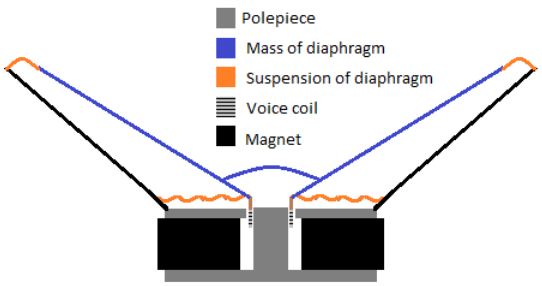

Figure 2.4: Cross section of moving coil loudspeaker.

due to the magnetic field of the permanent magnet. This displacement is transferred mechanically to the diaphragm and finally emitted as sound.

The loudspeaker can be split into three building blocks:

- Electrical
- Mechanical
- Acoustical

The electrical block consists of the VC with a nominal resistance, R_e (the resistance at 0 Hz), and a self-inductance, L_e. The mechanical block consists of the total moving mass of the diaphragm, M_{ms}, the compliance of the suspension, C_{ms}, and some mechanical damping, R_{md}. The mechanical domain determines the loudspeaker driver's resonance frequency, f_S, with a given mechanical quality factor, Q_{ms}.

$$f_S = \frac{1}{2\pi\sqrt{M_{ms}C_{ms}}} \tag{2.3}$$

$$Q_{MS} = \frac{1}{R_{ms}}\sqrt{\frac{M_{ms}}{C_{ms}}} \tag{2.4}$$

The driver will reach its' maximum impedance at the resonance frequency. This is also where the driver is easiest to excite thus its' most efficient operating point [29, 47].

The electrical block is coupled to the mechanical block through the permanent magnet. The coupling relates to the force factor, Bl, which is the product between the static magnetic field strength of the permanent magnet and the length of the wire in the air gap between the pole piece and the top plate. The electrical quality factor of the driver is dependent on both electrical, mechanical and the coupling elements related to the magnet system:

$$Q_{ES} = \frac{R_e}{(Bl)^2}\sqrt{\frac{M_{ms}}{C_{ms}}} \tag{2.5}$$

The two quality factors can be combined into one total quality factor of the loudspeaker driver.

$$Q_{TS} = \frac{Q_{MS}Q_{ES}}{Q_{MS} + Q_{ES}} \tag{2.6}$$

The acoustical block relates to the acoustic impedance behind and in front of the diaphragm, Z_{AB} and Z_{AF} respectively. They relate to the structural design of the loudspeaker, e.g. the enclosure.

2.2.2 Frequency response and impedance

The frequency response relates to the on-axis pressure transfer function of the loudspeaker [30]:

$$p = \frac{\rho_0}{2\pi}\frac{Blv_{spk}S_D}{R_eM_{ms}} \cdot G(s) \cdot T_{u1}(s) \tag{2.7}$$

$G(s)$ models the low frequencies as a second order high pass transfer function while $T_{u1}(s)$ models the high frequencies through a first order low pass transfer function. Moreover v_{spk} is the input voltage from the amplifier and S_D is the diaphragm area.

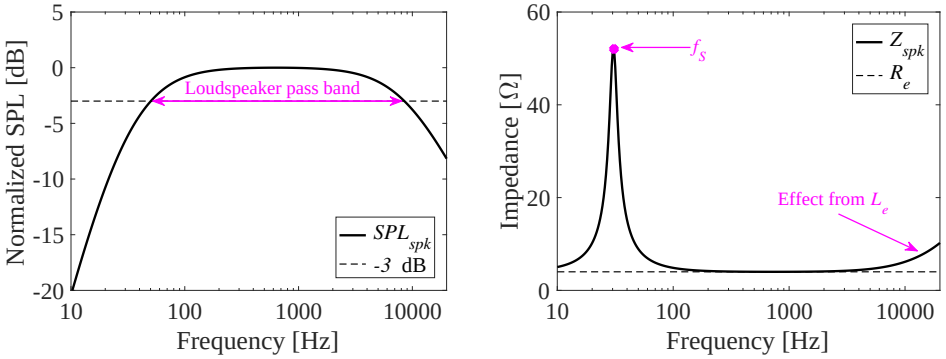

(a) Loudspeaker frequency response **(b)** Loudspeaker impedance

Figure 2.5: Typical response and impedance curves for a low frequency loudspeaker driver.

Combined $G(s)$ and $T_{u1}(s)$ forms a pass band which is the frequency band where the loudspeaker has a flat frequency response. The pass band is limited by the low- and high-cut-off frequencies, also known as the -3 dB cut-off frequencies. The low pass transfer function, $T_{u1}(s)$, can be expressed as:

$$T_{u1}(s) = \frac{1}{1 + \frac{s}{w_{u1}}} \qquad w_{u1}(s) = \frac{M_{ms} R_E}{M_d L_E} \tag{2.8}$$

The high pass transfer function, $G(s)$, can be written as:

$$G(s) = \frac{(s/\omega s)^2}{(s/\omega s)^2 + (1/Q_{TS})(s/\omega s) + 1} \tag{2.9}$$

Where $\omega_s = 2\pi f_S$ relates to the resonance frequency of the driver.

The impedance of the driver can be determined from Ohms law:

$$Z_{spk}(s) = \frac{v_{spk}(s)}{i_{spk}(s)} \tag{2.10}$$

Fig. 2.5 shows the frequency response and impedance for a typical low frequency loudspeaker.

2.2.3 Loudspeaker efficiency

By definition the efficiency is ratio between out- and in-put power. For the loudspeaker this is the ratio between the acoustic power emitted from the diaphragm, P_A, and the electrical power flowing into the voice coil, P_E.

$$\eta_0 = \frac{P_A}{P_E} \tag{2.11}$$

In general the loudspeaker efficiency is rather low, in the range 0.2% to 2%. The pass band efficiency can be expressed as:

$$\eta_0 = \frac{\rho_0 (Bl)^2 S_D^2}{2\pi c R_e M_{ms}^2} \tag{2.12}$$

Where $\rho_0 = 1.18$ kg/m^3 is the density of air and $c = 345$ m/s is the speed of sound in air. A common measure related to the efficiency is the loudspeaker sensitivity, where the Sound Pressure Level (SPL) is measured in dB at 1 meter distance when 1 W is applied to the speaker. The SPL can be expressed as:

$$SPL = 10 \log \left(\frac{P_E \frac{\eta_0}{A}}{P_o} \right) \tag{2.13}$$

Where $P_o = 10^{-12}$ W/m^2 is the reference acoustic sound power and A is the area of the sound surface at a given distance from the driver. A final remark on loudspeaker efficiency is that especially for low frequency drivers high efficiency is difficult to achieve. This is realized when examining eq. (2.12) as it is seen that the efficiency decreases with the mass of the diaphragm. A high mass is needed to generate a low resonance frequency so designers are left with no choice but to increase the diaphragm size significantly to get decent low frequency efficiency. Methods to improve the low frequency efficiency includes impedance matching between driver diaphragm and air load. This could be done by horn loading the driver [30] but comes with the cost of an increased speaker size.

2.2.4 Loudspeaker modelling

A widely accepted method to model loudspeakers is by using small-signal equivalent circuits [30]. Fig. 2.6 shows the conventional small-signal model of a loudspeaker. Here the electrical block is coupled to the mechanical via a voltage controlled voltage source and the mechanical block to acoustical via a voltage controlled current source. i_c is the current in the voice coil, u_D is the diaphragm velocity, f_D is the force, p_D is the acoustical pressure of the diaphragm and U_D is the volume velocity. Z_{AB} and Z_{AF} denotes the acoustic impedance behind and in front of the loudspeaker diaphragm respectively, which relates to the enclosure type. Very common enclosure types include closed box- and vented box-cabinets [32–34]. The loudspeaker model can also be formalized in a standard state space model for Linear Time Invariant (LTI) systems [48]:

$$\dot{x}(t) = Ax(t) + Bu(t) \tag{2.14}$$

$$y(t) = Cx(t) + Du(t) \tag{2.15}$$

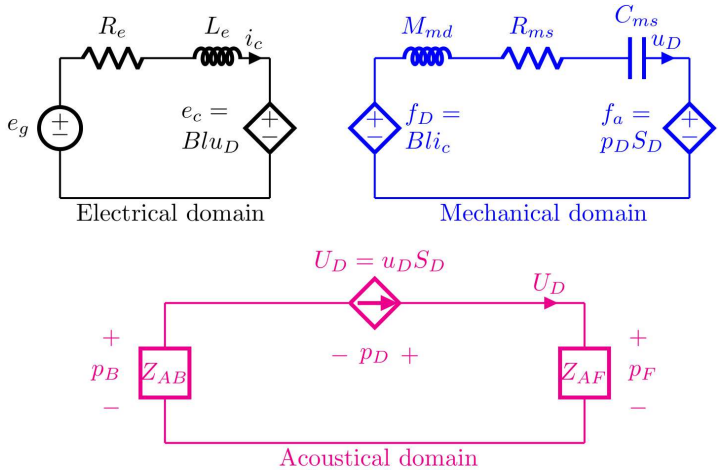

Figure 2.6: Small-signal modelling of loudspeaker.

Where $x(t)$ is the state vector, $\dot{x}(t)$ is its' derivative, A is the system matrix containing the dynamics, B is the input matrix, $u(t)$ is the input signal, C is the output matrix, $y(t)$ is the output vector and D the feed trough matrix which in many cases can be ignored. For a loudspeaker driver mounted in free air the state vector, $x(t)$, the system matrix, A, and the input matrix B can be formalized as:

$$x(t) = \begin{bmatrix} i(t) \\ x_D(t) \\ u_D(t) \end{bmatrix} \qquad A = \begin{bmatrix} -\frac{R_e}{L_e} & 0 & -\frac{Bl}{L_e} \\ 0 & 0 & 1 \\ \frac{Bl}{M_{ms}} & -\frac{1}{C_{ms}M_{ms}} & -\frac{R_{ms}}{M_{ms}} \end{bmatrix} \qquad B = \begin{bmatrix} \frac{1}{L_e} \\ 0 \\ 0 \end{bmatrix} \tag{2.16}$$

The state space modelling can be extended to account for enclosure design [49] and non linearities of the loudspeaker system [48]. These non linearities relate to the force factor, the self-inductance, creep in compliance of suspension and flux modulation [50–53].

2.2.5 Summary of state-of-the-art loudspeakers

Moving coil loudspeakers convert the electrical energy from an audio amplifier into acoustical energy perceived as sound by the listener. They are characterized by a resonance frequency, formed by the moving mass and the compliance of the suspension, and a pass band where the driver has a theoretically flat frequency response. The efficiency in the pass band is nevertheless rather poor, in the range 0.2% to 2%. Table 2.2 summarizes the performance of some existing drivers and speakers available on the market.

Table 2.2: Summary of existing loudspeaker drivers. LF = Low Frequency, FR = Full Range, HL = Horn Loaded, HF = High Frequency.

	η_0 [%]	SPL@1W/1m [dB]	f_S [Hz]	Size	BW [Hz]	Type
[54]	0.4	88	65	5”	63-6300	LF
[55]	1.9	94.9	30	18”	31 200	LF
[56]	0.1	83.2	187	2”	150-20000	FR
[57]	12.6	103	-	284 Liters	50-225	HL
[58]	0.2	85.4	600	3/4”	600-20000	HF

2.3 Switch-mode power audio amplifiers

Switch-mode power audio amplifiers are well described in literature [2, 5, 59–62]. This section will present the basic operation and loss mechanisms for state-of-the-art amplifier implementation. In addition to that a summary of existing results will be presented in the end of this section.

Switch-mode power audio amplifiers consists of three main blocks:

- Modulator
- Power stage
- Output filter

The functionality of the modulator is to generate a Pulse Width Modulated (PWM) representation of the amplifier input. Conventionally this is obtained by comparing the input signal with a high frequency carrier of triangular shape. The frequency of the resulting PWM signal is the switching frequency of the amplifier. The on-time of each pulse in the PWM signal is quantified as the duty cycle, D. Fig. 2.7 demonstrates the PWM generation. Self-oscillating (SO) modulator topologies generates the carrier signal directly from the input signal and will typically reduce the component count. SO modulators are described in [63–65]. The switching power stage of the amplifier is driven by the PWM signal. The output filter suppresses the switching noise from the power stage for Electro Magnetic Interference (EMI) reasons. The output filter may be omitted in some applications [66, 67].

2.3.1 Power stage

The conventional power stage used for switch-mode power audio amplifiers is of a buck topology due to an ideal linear transfer function minimizing distortion effects. It can be realized either in a half- or full-bridge configuration. Half bridge implementation requires dual voltage supplies while the full bridge only requires a single supply but have twice the component count. Full bridge is also referred to as Bridge Tied Load (BTL). Fig. 2.8 (a) shows the full bridge configuration. Q1 to Q4 are the switching devices conventionally implemented with Metal Oxide Semiconductor Field Effect Transistors (MOSFETs). L_f, C_f and the load, R_e, forms the output low pass filter. V_{sw} are the switch-node voltages. The factor two division on L_f ensures that equations presented throughout this section is equally valid for half bridge configurations. The switching devices are switched in pairs and are driven 180° out of phase so that the current flow is as highlighted in Fig. 2.8 (a) where the red line shows the current flow when Q1 and Q3 conduct and the blue line when Q2 and Q4 conduct. A short dead time period, t_{dt}, where all switches are off is needed between turn on and off to avoid unintentionally short circuits. Eq. 2.17 shows the ideal linear relationship between duty cycle and output voltage and current when using a Buck topology.

$$\begin{aligned} V_{out} &= (2D-1)\,V_{DD} \\ I_{out} &= \tfrac{V_{out}}{R_e} \end{aligned} \tag{2.17}$$

Where D is the duty cycle and V_{DD} is the rail-to-rail voltage, i.e. $\pm V_S$ in half bridge- and V_S in full bridge-configuration. The output current will have a ripple component,

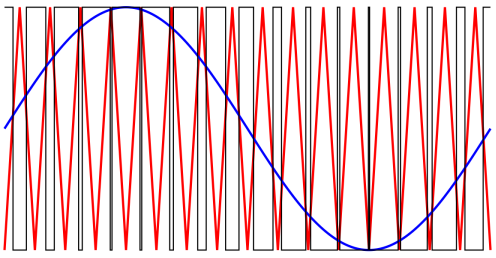

Figure 2.7: Pulse Width Modulated (PWM) representation of the sine wave. Blue = sine input, red = carrier, black = PWM signal.

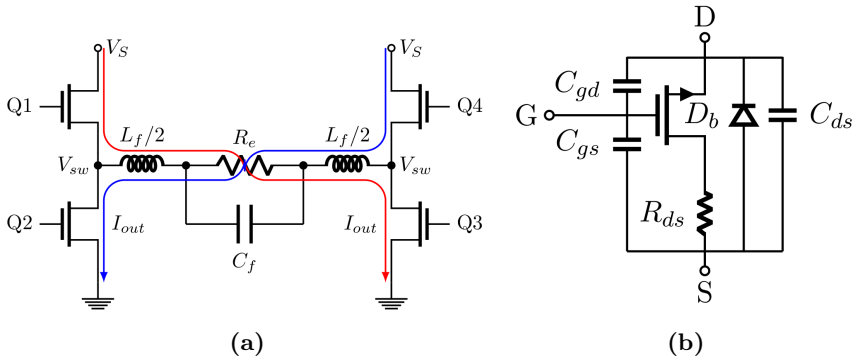

Figure 2.8: **(a)**: Full bridge configuration (BTL) Buck switch-mode power audio amplifier. **(b)**: Model of switching device with parasitic components: G = Gate, D = Drain and S = Source.

Δi_L, caused by the filter inductance:

$$\Delta i_L = \frac{V_{DD} D(1-D)}{2 L_f f_{sw}} \tag{2.18}$$

Switching devices are not ideal. Fig. 2.8 (b) shows the conventional model of a switching device including parasitic components. They are parasitic capacitances, C_{ds}, C_{gs} and C_{gd}, on resistance R_{ds} and a drain source body diode with a forward voltage drop, V_f.

The Buck power stage can undergo four switching conditions:

1. Hard switching occurs when the drain source capacitance, C_{ds}, can not be charged/discharged by the inductor current, I_L, during the dead time period, t_{dt}. The switching node voltage, V_{sw}, will ramp up and down together with the drain current, I_D, in the switching device, causing switching losses.

2. Reduced Voltage Switching (RVS) and Zero Voltage Switching (ZVS) occurs when the drain source capacitance can be partially or completely charged/discharged by the inductor current, I_L, during the dead time period, t_{dt}, minimizing switching losses.

3. When $\Delta i_L > |I_{out}|$ a situation can occur where the parasitic drain source capacitance, C_{ds}, is charged/discharged beyond the rail-to-rail voltage, V_{DD}, causing the body diode, D_b, to conduct.

4. When $|I_{out}| > \Delta i_L$, the body diode, D_b, will continue conducting after turn off.

Fig. 2.9 shows the waveforms of Buck topology for all of the described switching condition.

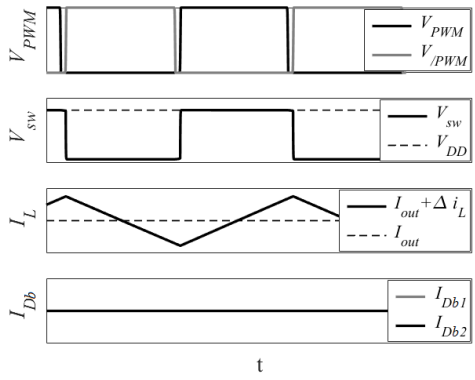

(a) Hard switching.

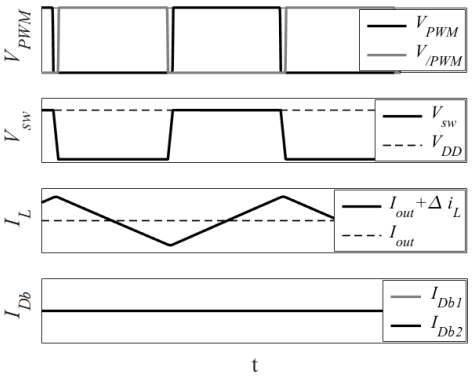

(b) Zero/Reduced Voltage Switching.

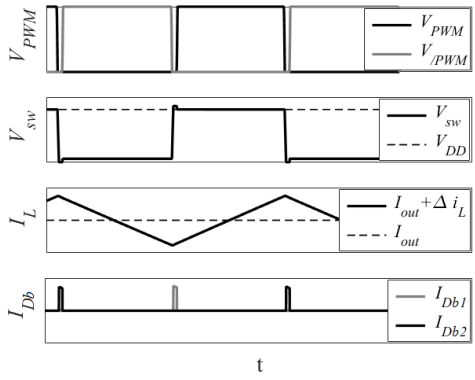

(c) Body diode conduction ($|I_{out}| < \Delta i_L$).

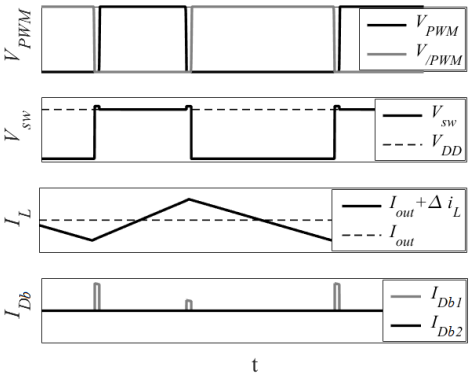

(d) Body diode conduction ($|I_{out}| > \Delta i_L$).

Figure 2.9: Waveforms in Buck power stage for different switching conditions. V_{PWM} is PWM gate signals, V_{SW} is switch-node voltage, I_L is inductor current and I_{Db} is body diode current.

2.3.2 Output filter

The filter inductor, L_f, the filter capacitance, C_f and the load , R_e, forms an output filter with the simplified transfer function:

$$H_f(s) = \frac{1}{\left(\frac{s}{s_0}\right)^2 + \frac{1}{2Q}\left(\frac{s}{s_0}\right) + 1} \tag{2.19}$$

Where s is the Laplace operator, s_0 is the pole of the filter indicating the cut-off frequency, f_c, and Q is quality factor of the filter indicating how much the filter is dampened at its' resonance.

$$s_0 = \frac{1}{\sqrt{L_f C_f}} \qquad f_c = \frac{s_0}{2\pi} \qquad Q = \frac{R_e}{\sqrt{\frac{L_f}{C_f}}} = \frac{R_e}{2\pi 2 L_f f_c} \tag{2.20}$$

The cut-off frequency of the filter is placed well below the switching frequency of the power stage as its' main purpose is to remove the switching residual from the output voltage for efficiency and EMI reasons. The filter should have a flat frequency response within the audio range, i.e. 20 Hz to 20 kHz, and attenuates with 40 dB/decade above the cut-off frequency. Fig. 2.10 shows how a high Q introduces a ripple in the frequency response. Conventional filters are designed for a maximum flat response, i.e. $Q = 0.7$ [59]. The filter has parasitic components which can affect the performance. They are the series resistance, R_{Lf}, and parallel capacitance, C_{Lf}, for the filter inductor and the equivalent series resistance and inductance, ESR and ESL, for the filter capacitance. The parasitic resistances should be kept as low as they introduce losses. Moreover the ESR of the filter capacitance introduces a zero placed at:

$$f_z = \frac{1}{2\pi C_f ESR} \tag{2.21}$$

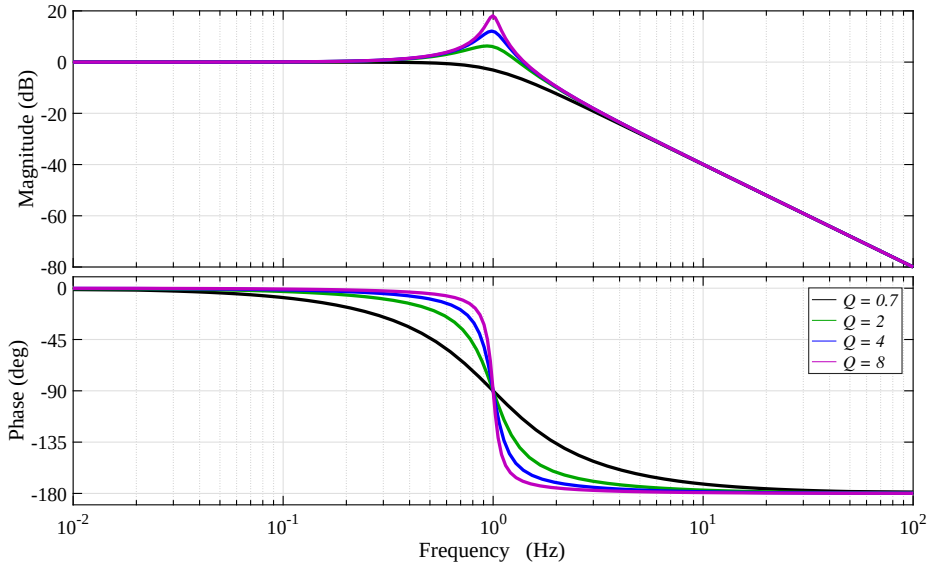

Figure 2.10: Normalized frequency response of output filter for different quality factors.

If the zero is placed too close to the cut-off frequency the roll off of the filter will be decreased from 40 to 20 dB/decade. The parasitic capacitance of the filter inductor sets the self-resonance frequency, SRF, indicating when the inductor stops working inductive and becomes capacitive.

$$\mathrm{SRF}_{Lf} = \frac{1}{2\pi\sqrt{L_f C_{Lf}}} \tag{2.22}$$

Equally the ESL of the capacitance generates a SRF where the filter capacitance becomes inductive.

$$\mathrm{SRF}_{Cf} = \frac{1}{2\pi\sqrt{C_f ESL}} \tag{2.23}$$

2.3.3 Loss mechanisms

This section presents the loss mechanisms related to the amplifier power stage and amplifier.

Gate losses are caused by charge and discharge of gate capacitances, C_{gd} and C_{gs}, of the switching device. The needed charge is defined as the total gate charge, Q_g. The gate losses can be express as:

$$P_{gate} = Q_g V_{gs} f_{sw} \tag{2.24}$$

Where V_{gs} is the gate source voltage of the switching device.

Conduction losses are generated when the drain current, I_D, flows through the switching device during its' on state.

$$P_{cond} = I_D^2 R_{ds} \tag{2.25}$$

Switching losses are generated by the drain source voltage and drain currents of the switching device. These ramp up and down between the on and off states. This power is dissipated in the parasitic drain source capacitance, C_{ds}, as it is charged/discharged by the drain current. This can be express as:

$$P_{sw} = 4\left(\frac{1}{2} C_{ds} V_{ds}^2 f_{sw}\right) \tag{2.26}$$

The factor four relates to the fact that the loss appears two times for each switching period, during rise and fall, and that the effective drain source capacitance is doubled due to two switches are tied to same node.

The parasitic capacitances can be charged/discharged by the instantaneous inductor current, $i_L(t)$, during the dead time period reducing the drain source voltage, V_{ds}, facilitating RVS and ZVS.

$$V_{ds} = V_{DD} - V_{Cds} \tag{2.27}$$

Where V_{Cds} is the voltage over the drain source capacitance. V_{Cds} can be expressed from the charge current and charge time which are the inductor current and the dead time period:

$$V_{Cds} = \frac{t_{dt} i_L}{2C_{ds}} \tag{2.28}$$

Where $i_L = I_{out} + \Delta i$ is instantaneous inductor current during the switching event. If the drain source capacitance is theoretically charged beyond the sum of the rail-to-rail voltage and the forward voltage drop of the diode, then the body diode will start conducting, thus clamping the drain source capacitance voltage to $V_{DD} + V_f$. The same relation applies for discharging where the capacitance will be clamped to $-V_f$. Therefore voltage over the drain source capacitance can be expressed as:

$$V_{Cds} = \begin{cases} -V_f & \forall \frac{t_{dt} i_L}{2C_{ds}} < -V_f \\ V_{DD} + V_f & \forall \frac{t_{dt} i_L}{2C_{ds}} > V_{DD} + V_f \\ \frac{t_{dt} i_L}{2C_{ds}}, & \text{otherwise} \end{cases} \tag{2.29}$$

Reverse conduction losses occur when the body diode in the switching device starts or continues to conduct the instantaneous inductor current during the dead time period. Due to the forward voltage drop of the body diode power will be dissipated

$$P_{reverse} = i_L V_f t_{cond} f_{sw} \tag{2.30}$$

t_{cond} is the conducting period of the body diode. The duration of conduction relates to the charge/discharge time of the drain source capacitance and is expressed as:

$$t_{cond} = \begin{cases} t_{dt} - \left| \frac{(V_{DD}+V_f)2C_{ds}}{i_L} \right| & \forall \left| \frac{t_{dt} i_L}{2C_{ds}} \right| > V_{DD} + V_f \\ 0 & \text{otherwise} \end{cases} \tag{2.31}$$

Filter losses are mainly caused by the filter inductance and can be separated into winding- and core-losses.

$$P_{Lf} = P_{winding} + P_{core} \tag{2.32}$$

Where winding losses are the combination of DC and AC losses in the inductor wire.

$$P_{wire} = I_L^2 \left(R_{DC} + R_{AC} \right) \tag{2.33}$$

Core losses relate to flux density, B, the magnetic field strength, H and the volume of the core, $A_c l_m$ [1] and can be expressed as:

$$W = (A_c l_m) \int_{onecycle} H dB \tag{2.34}$$

Which basically expresses that the loss per cycle equals the volume of the core multiplied with the area of the B-H loop. Precise modelling of core losses is a research topic on its own and data sheet for magnetic materials usually provide simplified methods to estimate losses [68].

The total losses is expressed as the sum of the different loss components:

$$P_{tot} = P_{gate} + P_{cond} + P_{sw} + P_{reverse} + P_{Lf} \tag{2.35}$$

By evaluating the total loss for all desired operating points a loss model, P_{loss}, can be generated [69]:

$$P_{loss,d} = \begin{pmatrix} P_{tot,1} \\ P_{tot,2} \\ \vdots \\ P_{tot,d} \end{pmatrix} \tag{2.36}$$

Where d is the operating point specifying a specific duty cycle. Equally the duty cycle distribution, ϕ, of the amplifier power stage can be formalized as:

$$\phi = \begin{pmatrix} \phi_1 & \phi_2 & \cdots & \phi_d \end{pmatrix} \tag{2.37}$$

The duty cycle distribution is directly related to the amplitude distribution of the amplifier input signal [60]. By formalizing the loss model and duty cycle distribution in this way the total loss for any given duty cycle distribution can be evaluated as:

$$P_{tot,\phi} = \phi_d \cdot P_{loss,d} \tag{2.38}$$

2.3.4 Control

Control is very important in switch-mode power audio amplifiers as the performance requirements are high. This section outlines varies control methods.

2.3.4.1 Stability considerations

Classical control is designed from stability considerations evaluated through bode plots. Controllers are typically of a negative feed back type even though feed forward systems also exist [70]. A system is said to be stable when the open loop phase shift, at unity gain, is less than -180 °. This relates to the phase margin, θ_m:

$$\theta_m = 180 - \theta_{0\text{dB}} \tag{2.39}$$

Where $\theta_{0\text{dB}}$ is the phase shift at unity gain. As long as $\theta_m > 0$ the system is stable. However a high margin of $\approx 45°$ is preferable to ensure high stability. Some of the most conventional controllers are PI and PI-Lead controllers and they are both well described in literature [1, 71] so design procedures will not be repeated here. PI controller aims to improve static errors while PI-Lead introduces a positive phase shift to improve phase margins and thereby stability. Considering the system shown in Fig. 2.11 the open

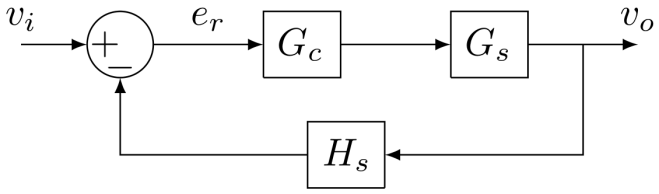

Figure 2.11: Simple control system.

loop transfer function, G_o, can be expressed as:

$$G_o = G_c G_s H_s \tag{2.40}$$

Where G_c is the controller transfer function, G_s is a subsystem transfer function, e.g. the switch-mode power stage, and H_s is a feed back gain. For a switch-mode power stage transfer function, $G(s)$, is dominated by the low pass filter transfer function from eq. (2.19). For an amplifier system, a PI controller takes the error signal, e_r, and improves the low frequency errors which is good, since in comparison with the switching frequency, the audio band is a low frequency band. Fig. 2.12 (a) show the bode plot

of a PI controller designed for a switch-mode power audio amplifier. The controller has a negative phase shift of 90° when acting like integrator. If applied directly to the amplifier power stage the open loop transfer function becomes:

$$G_o = G_{pi} G_s H_s \tag{2.41}$$

Where G_{pi} is the PI controller transfer function. Fig. 2.12 (b) shows the resulting open loop response. Though a decent loop gain is achieved for low frequencies the phase margin is negative yielding that the phase shift of the PI controller causes the system to be unstable. To counter that one can implement a Lead compensation which adds a positive phase shift to the system. Fig. 2.12 (c) shows that the Lead compensation provides a positive phase shift while acting like a differentiator. When applied to the PI controller a PI-Lead controller is realized and the open loop transfer function becomes:

$$G_o = G_l G_{pi} G_s H_s \tag{2.42}$$

Where G_l is the Lead compensation transfer function. Fig. 2.12 (d) shows that the system now has a positive phase margin and therefore is stable. There exists many other controller configurations with this design approach where the system stability is considered. For switch-mode power audio amplifiers these types of controllers can provide good audio performance with THD+N levels at 0.01 % [26, 72, 73].

2.3.4.2 Carrier considerations

To achieve very good audio performance one can consider the perturbations in the carrier signal and try to linearise it. This cannot be achieved from a stability consideration perspective and alternative methods must be used.

The quality of the carrier signal is very important for the amplifier THD+N performance, as the sampling of the input signal, generating the PWM signal, relies upon it. In Fig. 2.7 the carrier signal is depicted a perfect triangle which would yield a perfect sampling. However the carrier signal will have some perturbations with non-linear characteristics. These perturbations origin from the output of the amplifier which is fed back to the input and into the error signal, e_r, according to Fig. 2.11, thus affecting the carrier signal.

Different approaches have been proposed to counter the carrier non-linearities. One method is to dimensioning the feed back loop as a pure integrator from the switch-node voltage (see Fig. 2.8) to the modulator input. In this way it is ensured that the perturbations will have triangular shape since the switch-node voltage is a square wave and therefore its' integral a triangle. With the linear shape of the perturbations the sampling of the audio signal will not be affected and audio performance will improve [5, 7, 8]. Other approaches include notch filters to kill the perturbations. However a dedicated attention to the carrier waveform and its' linearity yields very good audio performance with THD+N well below 0.01 % and even below 0.001 % for some cases. [4, 74, 75].

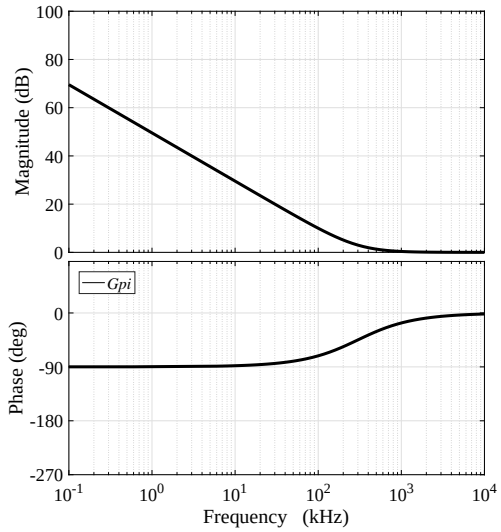

(a) PI controller.

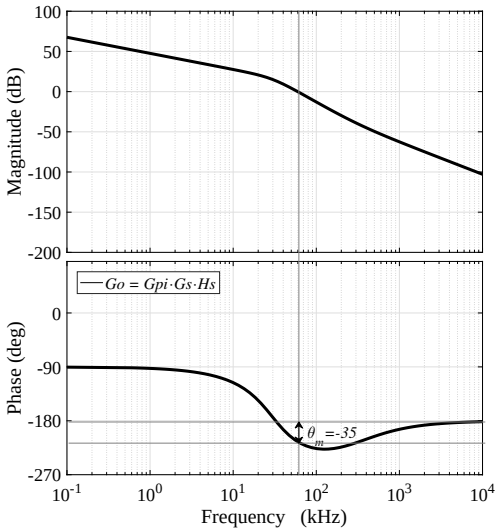

(b) Open loop with PI controller.

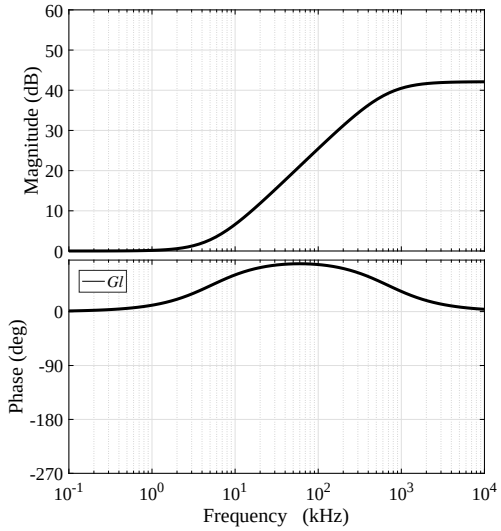

(c) Lead compensation.

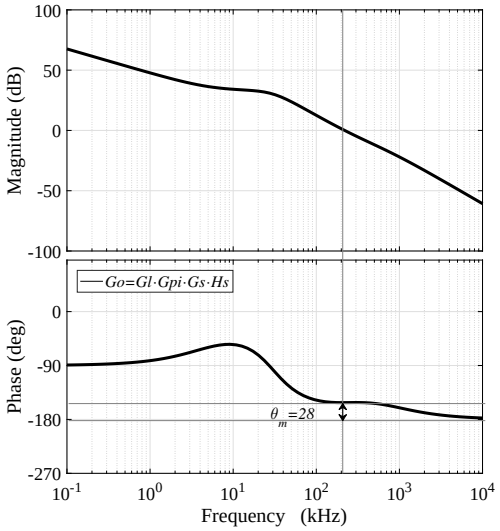

(d) Open loop with PI-Lead controller.

Figure 2.12: Bode plots of controllers and resulting open loops.

2.3.5 Summary of state-of-the-art switch-mode power audio amplifiers

This section have presented the basic blocks of switch-mode power audio amplifiers. Table 2.3 summarizes existing amplifier key parameters for amplifiers in the low- and mid-power level.

Table 2.3: Summary of existing amplifiers

	P_{out} [W]	η [%]	ρ_{power} [W/cm^3]	THD+N [%]	Notes
[15]	100	90	-	0.02	Integrated circuit
[14]	140	90	-	0.03	Integrated circuit
[27]	50	-	-	0.05	GaNFET
[4]	100	-	-	0.0006	MOSFET
[16]	180	-	3.9	0.02	MOSFET
[76]	400	-	7.4	0.03	MOSFET

2.4 Switch-mode power supplies

Switch-Mode Power Supplies (SMPS) are used for a wide range of applications due to their high efficiency. These include renewable energy systems, LED drivers, Radio Frequency (RF) amplifiers and many more [77–80]. In fact switch-mode power audio amplifiers can be viewed as a special case of an AC/DC SMPS or inverter with very strict specifications for bandwidth (BW), Dynamic Range (DR), Total Harmonic Distortion (THD) etc.

In this section SMPSs for switch-mode power audio amplifiers are presented and the current state of the art summarized.

2.4.1 SMPS for audio applications

The Power supply Unit (PSU) is an important part of audio reproducing systems as they supply the system with power. Depending on the application the PSU can be as simple as a battery supplying the amplifier. However systems solely driven by a battery are limited to low power applications as the battery voltage in consumer products seldom is above 12 V. To achieve a higher supply voltage a boosting converter must be used. In addition to that a pure battery supply is simply insufficient for many applications. For instance in off-line audio reproducing systems where the grid voltage must be rectified and converted to a suitable supply voltage for the amplifier. Such systems could be home Hi-Fi audio systems, cinema sound and large scale professional audio systems.

To ensure that the system efficiency is as high as possible a SMPS is used to minimize losses:

$$\eta_{sys} = \eta_{smps} \cdot \eta_{amp} \cdot \eta_{spk} \tag{2.43}$$

The types of losses occurring in a SMPS are more or less the same as for the switch-mode power audio amplifier, primarily switching-, conduction-, inductor- and transformer-losses, the latter only relevant transformer based converters.

2.4.2 Topologies

One of the most basic topologies there exists is the buck topology, described in section 2.3 and shown in BTL configuration in Fig. 2.8. It is capable of stepping an input voltage down. However there exist many different SMPS topologies [1]. Fig. 2.13 shows three very commonly used topologies. Namely the boost-, the flyback- and the forward-topology.

The boost topology has a DC transfer function given by:

$$\frac{V_o}{V_i} = \frac{1}{1-D} \tag{2.44}$$

Evaluating the formula it is observed that this transfer function has step-up capabilities hence the name "boost". The boost topology is very useful in battery driven applications where the battery voltage is too low to get the desired output power from the speaker [81].

The flyback topology relies on a coupled inductor functioning both as a transformer and an inductor. This design provides both step up and step down capabilities, galvanic isolation and a low component count making it one of the most, if not the most, used SPMS topology for a wide range of applications. For audio applications it is used for off line systems in all kind of power ranges [82–84]. The DC transfer function is given by:

$$\frac{V_o}{V_i} = n\frac{D}{1-D} \tag{2.45}$$

Where n is the transformer turns ratio of secondary turns divided by primary turns.

The forward topology, like the flyback, provides both step up and step down capabilities besides galvanic isolation. However it has a higher component count. This is due to the fact that the Forward topology utilizes a dedicated transformer to transfer energy directly to its' secondary side which basically is a buck converter. This design

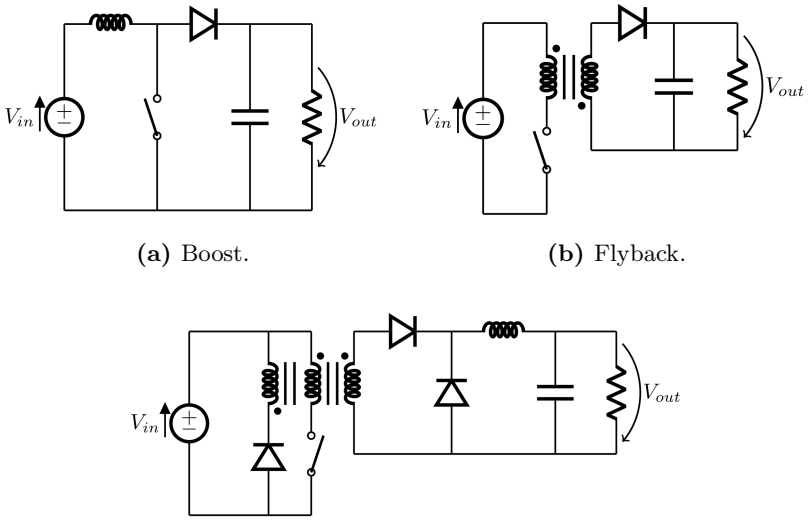

(a) Boost.

(b) Flyback.

(c) Forward.

Figure 2.13: Commonly used SMPS topologies for audio applications.

makes it more energy efficient compared to the flyback. The DC transfer function is given by:

$$\frac{V_o}{V_i} = nD \tag{2.46}$$

Like the flyback it is used for off line systems [85].

2.4.3 Summary of state-of-the-art SMPS for audio applications

This section has briefly presented the basic function of SMPS and described three very commonly used topologies, namely the boost-, flyback- and forward-topology. They can be implemented with a wide range of features to improve performance and efficiency. These features include synchronous rectification and active clamping [1]. The boost topology is suited for battery driven applications while the forward and flyback-topology have off-line capabilities. All of them have a duty cycle dependent DC transfer function.

3

Research contribution part I Test signals

This section builds upon the theory presented in section 2.1 and the results related to the article entitled ”Efficiency of Switch-Mode Power Audio Amplifiers - Test Signals and Measurement Techniques” [60] attached in Appendix E.

3.1 A new test signal

As stated in the introduction of this thesis efficiency is a key parameter in audio reproduction systems and therefore switch-mode technology is widely used. Efficiencies in the vicinity of 90% have been reported for switch-mode power audio amplifiers [2], [26]. The conventional method for evaluating the efficiency utilizes a sine signal which is swept in terms of amplitude, resulting in an efficiency versus output power plot. Fig. 3.1 shows a simulation of a typical amplifier efficiency using conventional sine wave amplitude sweep. However sine waves do not posses the dynamic properties of music signals as shown in section 2.1. Due to high Crest Factor (CF) the RMS output power is much lower when playing music compared to when playing sine waves. This is due to the fact that the CF relates to the output power [60]:

$$\mathrm{CF} = 10 \log \left(\frac{P_{pk}}{P_{rms}} \right) \tag{3.1}$$

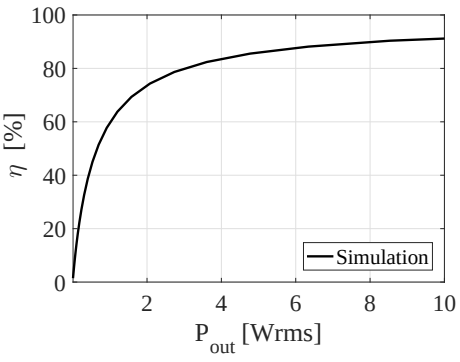

Figure 3.1: Typical amplifier efficiency using conventional sine wave amplitude sweep.

Where P_{pk} is the peak output power of the amplifier. For this reason the amplifier efficiencies obtained in previous work [2, 26] are not representative for the intended amplifier operation, i.e. playing music. In that sense the conventional efficiency measurement unfairly favours sine wave operation leading to inappropriate choice of amplifier components, e.g power stage switching devices.

To counter that, this section presents an elaborate analysis of audio dynamics based on a large music library. Based on this analysis an alternative test signal is proposed. The proposed signal has similar periodic properties as sine waves and can be evaluated analytically. However it also contains the dynamic properties equivalent to that of music. The frequency content of the proposed signal is analysed and compared to the known signals presented in section 2.1. Finally a series of measurements on a 12 V prototype amplifier demonstrates how the proposed signal can replace sine waves for efficiency measurements and how that affects the choice of switching devices.

3.1.1 Audio dynamics

As discussed in section 2.1 and [41–43] audio signals, e.g. music, have high dynamics. In addition to this, the dynamics of music have large variations. Besides the crest factor, the amplitude distribution can be used to illustrate this. Fig. 3.2 shows the amplitude distribution of three different tracks from classic, pop and rock genres. To find the average distribution of audio signals, a music library containing 183 audio tracks from a vast selection of genres have been analysed. Fig. 3.3 (a) shows the amplitude distribution of the audio tracks along with that of a sine wave. This distribution can be translated directly into a duty cycle distribution when a linear relationship is assumed. From the distribution it is clear, that there exists a fundamental difference between sine waves and real audio tracks. While the mean distribution of audio has a maximum around zero amplitude the sine wave distribution have a minimum. The mean crest factor of the analysed audio tracks was found to be 15 dB. Having the duty cycle distribution allows for estimation of losses according to eq. (2.38) presented in section 2.3.

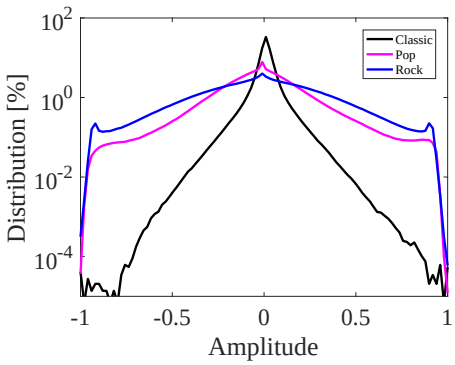

Figure 3.2: Amplitude distribution of three music tracks from different genres.

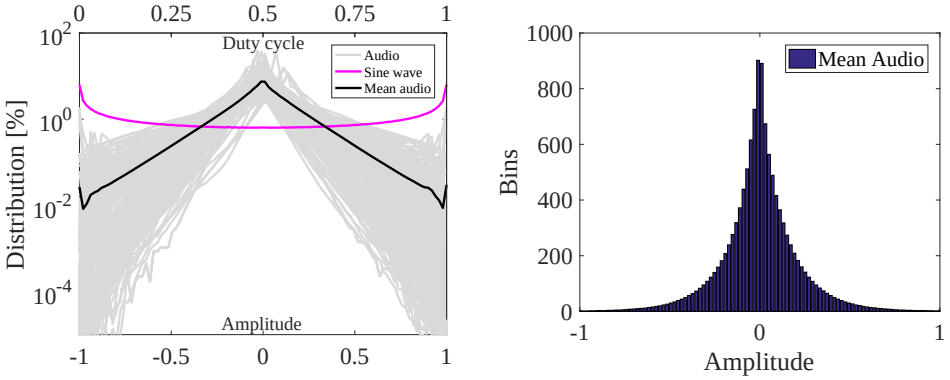

(a) Amplitude- and duty cycle-distribution. **(b)** Bin representation.

Figure 3.3: Distribution analysis of audio tracks and sine waves.

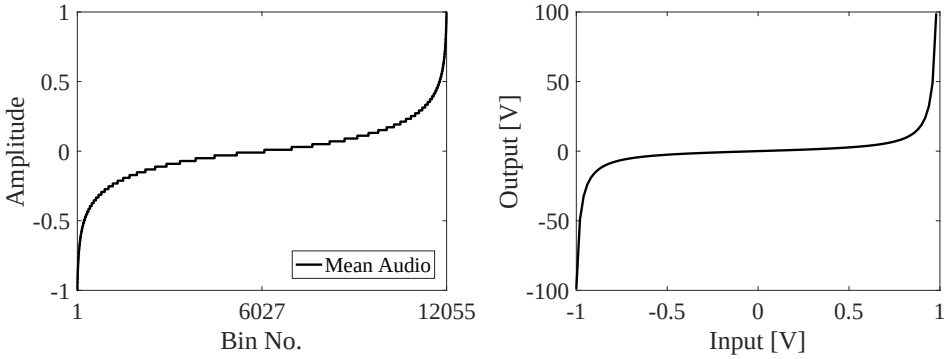

(a) Mean audio waveform evaluated directly from distribution and amplitude. **(b)** Transfer function of BTL Cuk converter.

Figure 3.4: Similarity of mean audio waveform and non-linear power converter transfer function.

3.1.2 Proposal of new test signal

Fig. 3.3 (b) shows the distribution analysis represented in bins versus amplitude. This is a convenient representation form as it allows for creating a signal directly from the distribution analysis. Fig. 3.4 (a) shows this signal where the bin distribution is combined into an array of bins correlated with their respective amplitudes. The shape is highly non-linear and similar to what can be found for non-linear power converters such as the BTL Cuk converter [86, 87] with the input to output transfer function of:

$$\frac{V_o}{V_{in}} = \frac{D - (1 - D)}{D\,(1 - D)} \tag{3.2}$$

Where D is the duty cycle. Fig. 3.4 (b) shows the BTL Cuk transfer function. By manipulating eq. (3.2) to the power of $^{1}/_{4}$ and setting $D = 0.5 + K \cdot \sin(\omega t)$, where $K = 0.49995$ and $\omega = 2\pi f$ a function, $\psi(t)$, with near perfect fit is obtained. The manipulated equation expresses the formula for the proposed test signal:

$$\psi(t) = \left(\frac{(0.5 + K \cdot \sin(\omega t)) - (1 - (0.5 + K \cdot \sin(\omega t)))}{(0.5 + K \cdot \sin(\omega t)) \cdot (1 - (0.5 + K \cdot \sin(\omega t)))} \right)^{1/4} \tag{3.3}$$

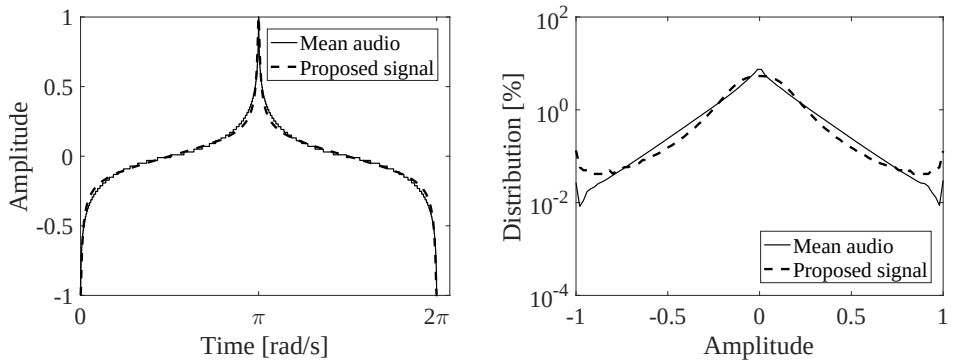

(a) Full period of mean audio waveform and proposed test signal.

(b) Amplitude distribution of mean audio and propsed test signal.

Figure 3.5: Comparison of between mean audio analysis and proposed test signal.

Fig. 3.5 shows both amplitude and distribution comparison between the mean audio analysis and the proposed signal. The proposed test signal has a crest factor of 14 dB. The error compared the analysis can be evaluated using:

$$\%_{error} = \left| \frac{10^{\left(\frac{\mathrm{CF}_{sig}}{20}\right)} - 10^{\left(\frac{\mathrm{CF}_{aud}}{20}\right)}}{10^{\left(\frac{\mathrm{CF}_{aud}}{20}\right)}} \right| \tag{3.4}$$

Where CF_{sig} and CF_{aud} are the signal- and mean audio-crest factors respectively. Evaluating eq. (3.4) for the proposed signal yields a 11 % error while the same evaluation for sine waves yields a error of 75 %. In that sense the proposed signal models the dynamic behaviour of audio almost a factor seven more precisely than sine waves. Fig. 3.6 shows the time- and frequency-domain analysis of the proposed test signal in the case of a 50 Hz fundamental frequency. Opposed to the noise signals presented in section 2.1 the proposed signal has a clear shape in the time domain. In the frequency domain the proposed signal has a high number of harmonics. Like the IEC268- and pink-noise signals it rolls of for higher frequencies thus emulating real audio to some extent. However the roll off is slightly steeper with 16 dB/decade.

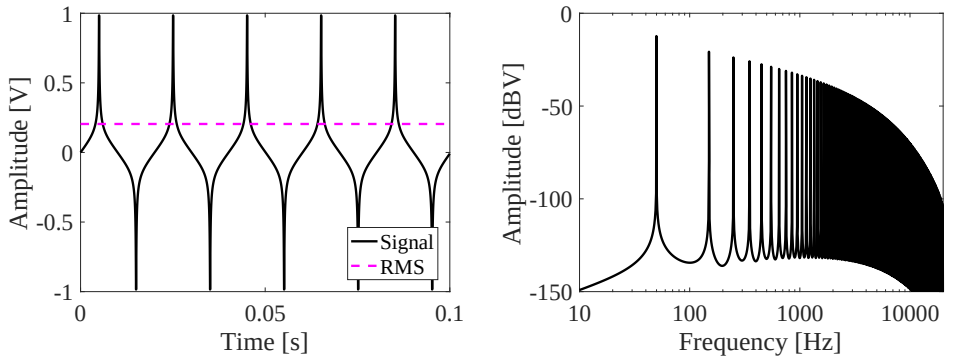

(a) Time domain.

(b) Frequency domain.

Figure 3.6: Proposed test signal with fundamental at 50 Hz analysed in time- and frequency-domains.

	Design1	Design2	Units	Prototype amplifier
Supply voltage - V_{SS}	12	12	V	
Switching frequency - f_{sw}	350	350	kHz	
Load - R_e	8	8	Ω	
MOSFETs - Q_g	24	6.1	nC	
MOSFETs - C_{oss}	247	80	pF	
MOSFETs - R_{ds}	24	540	mΩ	
Power stage	BTL	BTL		

Table 3.1: Implemented prototype amplifiers and specifications.

3.1.3 Efficiency measurement

To demonstrate the impact of using the proposed signal the efficiency of two 12 V prototype switch-mode power audio amplifiers was evaluated. The amplifiers are of a BTL buck topology and are identical except from their switching devices. Design1 is equipped with low drain source resistance, R_{ds}, MOSFETs and Design2 with low parasitic capacitance MOSFETs, e.g C_{ds}, C_{gd} and C_{gs} (see Fig. 2.8 (b) for reference). A MOSFET can not have both low drain source resistance and parasitic capacitances due to the fundamentals of transistor design [88]. Table 3.1 shows the specifications for the implemented prototypes. The efficiency is measured using an amplitude sweep stopping at clipping, i.e. when the peak output voltage hits the supply voltage rail. The input and output voltages and currents are measured with high precision multi meters [89]. Fig. 3.7 (a) and (b) shows the measured efficiency on linear- and logarithmic-scale using a sine wave as test signal. Design1 reaches 86% and looking at the linear scale it appears to have the overall better efficiency. Design2 peaks with an efficiency of 76%. Fig. 3.7 (c) and (d) shows the measured efficiency using the proposed test signal. The first thing to notice is that the output power is lowered significantly due to the dynamic properties of the test signal. Secondly Design2 is now observed to be the design with the overall best efficiency which is especially evident when looking at the logarithmic scale. At $P_{out} = 0.2$ Wrms the difference is 10 % point. Both designs reach a peak efficiency of approximately 70 %.

3.2 Summary of research contribution within test signals

This section have presented the development of a new test signal which in its' current iteration can replace sine waves for efficiency measurements. The test signal is based on a crest factor and amplitude distribution analysis of 183 audio tracks from a vast selection of genres. The average crest factor of the analysed audio was 15 dB. The proposed test signal has a fundamental periodicity like sine waves but possesses dynamic properties like audio signals with a crest factor of 14 dB. Opposed to noise signals the proposed test signal is expressed mathematically as a periodic function with a distinct shape in the time domain. This makes it easy to generate and use for analysis purposes. Moreover this feature enables relatively easy detection of distortion effect from amplifiers as the top of the signal will be clipped.

Measurements on prototype amplifiers show that the conventional efficiency evaluation is misleading favouring components choices beneficial for sine wave operation instead of

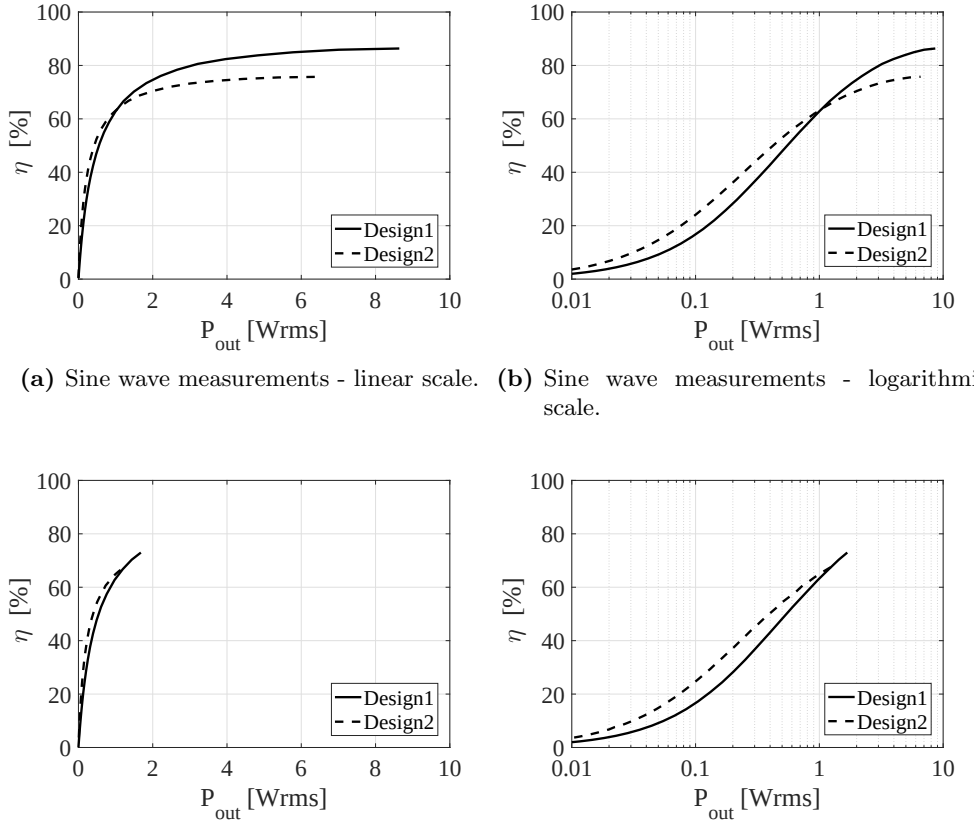

(a) Sine wave measurements - linear scale.

(b) Sine wave measurements - logarithmic scale.

(c) Proposed signal measurement - linear scale.

(d) Proposed signal measurement - logarithmic scale.

Figure 3.7: Measured efficiency of prototypes amplifiers using sine waves and proposed test signal.

music. Using the proposed test signal, it was demonstrated that a 10 % point efficiency improvement could be obtained for audio operation by changing the switching devices. Besides efficiency measurements the proposed signal can be used to conduct thermal stress tests on amplifiers. Due to a slightly steeper frequency roll off of 16 dB/decade compared to IEC268- and pink noise, it is less suited for loudspeaker thermal stress tests though it still emulates the frequency content to some extent and at least much better than a pure sine wave. Table 3.2 shows a summary of test signals presented in this thesis including their evaluated error, obtained through eq. (3.4), when compared to mean crest factor of audio of 15 dB.

Table 3.2: Summary of test signals and their properties.

	CF [dB]	$\%_{error}$ [%]	Frequency roll off	Periodic function
Sine wave	3	75	No	Yes
White noise	5	68	0 dB/dec.	No
Pink noise	14	11	-10 dB/dec.	No
IEC-268 [40]	12	29	-10 dB/dec.	No
Prop. test signal [60]	14	11	-16 dB/dec.	Yes

4

Research contribution part II Loudspeakers

This section builds upon the theory presented in section 2.2 and the results related to the articles entitled "Low impedance voice coils for improved loudspeaker efficiency" and "Relationship between voice coil fill factor and loudspeaker efficiency" [90, 91] attached in Appendix B and F.

4.1 Voice coil fill factor

The loudspeaker efficiency is very low in the range of 0.2% to 2%. To improve the loudspeaker efficiency one can increase the fill factor of the voice coil (VC) [92]. The fill factor, κ, can be expressed as the ratio between the area of the conductor and the total winding area:

$$\kappa = \frac{A_c}{A_w} \tag{4.1}$$

Where A_c is the area of the conductor and A_w is the total winding area. This section presents an elaborate analysis of how the fill factor relates to the efficiency and how it affects the frequency response. Moreover practical considerations on winding layouts are performed. Finally experimental results on VC prototypes verify the presented analysis and shows a 25 % efficiency improvement, corresponding to 1 dB, when increasing the fill factor from 45% to 53%.

4.1.1 Relationship of fill factor and efficiency

Assuming that the loudspeaker efficiency equation (eq. 2.12) presented in section 2.2 is accurate, it is observed that efficiency, η_0, is proportional to the Bl^2/R_e ratio for a given loudspeaker driver.

$$\eta_0 \propto \frac{Bl^2}{R_e} \tag{4.2}$$

To increase the efficiency the obvious solution appears to be either lowering the load resistance, R_e, or increasing the force factor, Bl. However it can be shown, that these solutions cancel each other. This is realized when considering how the DC resistance and force factor are related to the winding area of the loudspeaker driver. Fig. 4.1 shows a conceptual model of a loudspeaker driver and its VC. V_d is the winding depth, V_w is the winding width, A_d is the air gap depth and V_r is the radius of the VC.

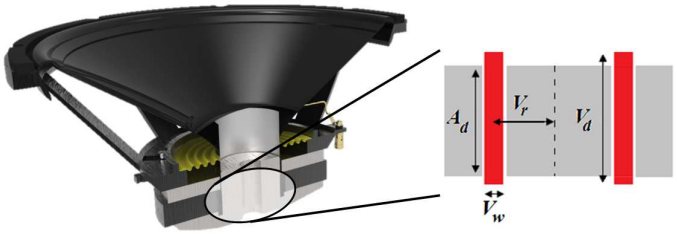

Figure 4.1: Loudspeaker driver and voice coil (VC) winding area.

Taking these geometries into consideration the DC resistance and the force factor can be expressed as:

$$R_e = \frac{l_w}{\sigma A_{wire}} = \frac{NV_o}{\sigma \frac{V_w V_d}{N}} = \frac{N^2 V_o}{\sigma V_w V_d} \tag{4.3}$$

$$Bl = Bl_w \frac{A_d}{V_d} = BNV_o \frac{A_d}{V_d} \tag{4.4}$$

l_w is the total length of the conducting wire, A_{wire} is its' cross sectional area, $V_o = 2\pi V_r$ is the VC circumsphere, N is the number of turns and σ is the conductivity of the conductor. Inserting eq. (4.3) and (4.4) into eq. (4.2) it is found that the ratio between the force factor squared and the DC resistance is a constant value determined by the magnet system geometry, the strength its' static magnetic field and the conductor conductivity:

$$\eta_0 \propto \frac{(Bl)^2}{R_e} = \frac{B^2 V_o V_w A_d^2 \sigma}{V_d} = \textbf{constant} \tag{4.5}$$

However this relation is only valid if one assumes that the entire winding area can be filled by the conductor. Taken the fill factor into account the load resistance can be expressed as:

$$R_e = \frac{N^2 V_o}{\sigma V_w V_d \kappa} \tag{4.6}$$

and eq. (4.5) can be rewritten as:

$$\eta_0 \propto \frac{(Bl)^2}{R_e} = \frac{B^2 V_o V_w A_d^2 \sigma \kappa}{V_d} \neq \textbf{constant} \tag{4.7}$$

As for the load resistance the total moving mass, M_{ms}, can be expressed with a fill factor dependency:

$$M_{ms} = M_{d+cf} + M_{vc} \tag{4.8}$$

Where $M_{d+cf} = M_d + M_{cf}$ is the diaphragm plus coil former mass and $M_{vc} = V_d V_w V_o \rho_{wire} \kappa$ is the VC wire mass where ρ_{wire} is the density of the wire material. Substituting eq. (4.7) and (4.8) into eq. (2.12) the loudspeaker efficiency can be expressed as a function of the fill factor.

$$\eta_0(\kappa) = \frac{\rho_0 S_D^2 B^2 V_o V_w A_d^2 \sigma \kappa}{2\pi c V_d \left(M_d + M_{cf} + V_d V_w V_o \rho_{wire} \kappa\right)^2} \tag{4.9}$$

The optimum fill factor can be found be solving for the derivative of eq. 4.9:

$$\begin{aligned} \eta_0'(\kappa) &= 0 \downarrow \\ \kappa_{optimal} &= \frac{M_d + M_{cf}}{V_d V_w V_o \rho_{wire}} \end{aligned} \tag{4.10}$$

Due to the fact that the maximum fill factor is $\kappa = 1$, i.e. 100%, eq. (4.10) is only true for cases where $M_d + M_{cf} \geq V_d V_w V_o \rho_{wire}$. Therefore eq. (4.10) is redefined as the driver's mass ratio, M_{ratio}, due to the fact that it is the ratio between the masses. Namely the mass of the diaphragm plus the coil former and the theoretical maximum mass of the VC.

$$M_{ratio} = \frac{M_d + M_{cf}}{V_d V_w V_o \rho_{wire}} \tag{4.11}$$

Fig. 4.2 (a) shows that for higher mass ratios the efficiency improvement for an increased fill factor increases. For high mass ratios, e.g. $M_{ratio} \geq 20$, the loudspeaker efficiency has almost a linear relationship with the fill factor thus making it proportional to the fill factor:

$$\eta_0 \propto \kappa \tag{4.12}$$

4.1.2 Impact on frequency response

Using the on axis pressure transfer function from eq. (2.7) the frequency response can be evaluated. Considering only low frequencies Fig. 4.2 (b) shows that the -3 dB cut-off frequency, f_l, is shifted upwards in frequency. This is due to the fact that total quality factor of the loudspeaker driver is related to the fill factor in an inverse proportional matter causing the low frequency cut-off frequency to increase [91]:

$$Q_{TS} \propto \frac{1}{\kappa} \tag{4.13}$$

4.1.3 Voice coil winding layouts

Fig. 4.3 shows three different winding layouts. It is obvious that the fill factor increases from Fig. 4.3 (a) to (b) to (c) as the tiny air gaps between windings are eliminated.

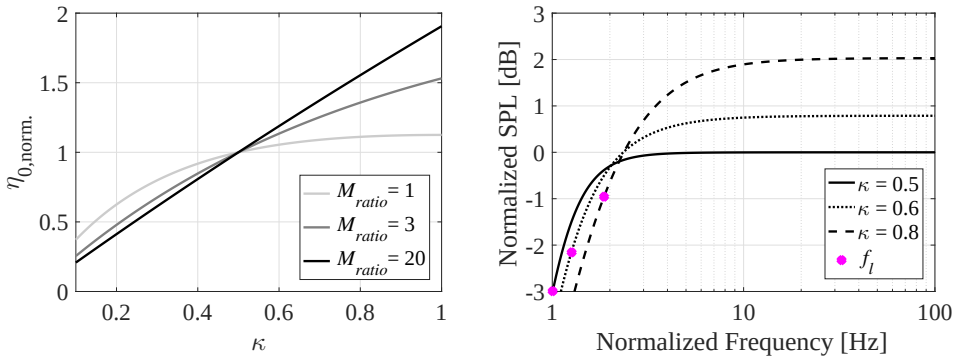

(a) Impact on efficiency for different mass ratios.

(b) Normalized frequency responses with -3 dB cut-off frequencies, f_l. $M_{ratio} = 20$.

Figure 4.2: Mass ratio's relationship with efficiency and fill factor's influence on frequency response.

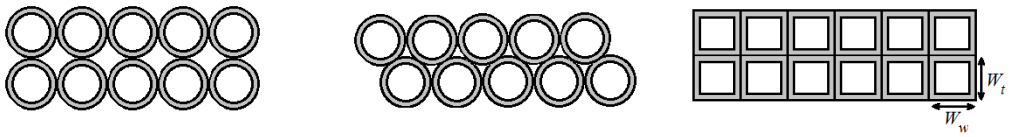

(a) Round layout 1. **(b)** Round layout 2. **(c)** Rectangular layout.

Figure 4.3: Voice coil (VC) winding layouts.

The fill factors of each type of layout can be evaluated as [90, 91]:

$$\kappa_{round,1} = \frac{A_c}{A_w} = \frac{\pi\left(r_w - \frac{t_{iso}}{2}\right)^2}{\left(2r_w\right)^2} \tag{4.14}$$

$$\tag{4.15}$$

$$\kappa_{round,2} = \frac{A_c}{A_w} = \frac{\pi\left(r_w - \frac{t_{iso}}{2}\right)^2}{\left(2+\sqrt{3}\right)r_w^2} \tag{4.16}$$

$$\tag{4.17}$$

$$\kappa_{rec} = \frac{A_c}{A_w} = \frac{\left(W_w - t_{iso}\right)\left(W_t - t_{iso}\right)}{W_w W_t} \tag{4.18}$$

Where t_{iso} is the total insulation thickness on both sides of the wire and r_w is the radius of the round wires while W_w and W_t is the winding width and thickness respectively. For the rectangular layout the resulting wire resistance can be evaluated as:

$$R_e = \frac{lw}{\sigma A} = \frac{NV_o}{\sigma W_{t,cu}(W_w - t_{iso})} = \frac{NV_o}{\sigma W_{t,cu}\left(\frac{V_d}{0.5N} - t_{iso}\right)} \tag{4.19}$$

Fig. 4.4 shows the comparison of the fill factors for the different winding layouts as a function of the ratio between the insulation thickness and wire diameter, t_{iso}/d_w. For the rectangular layouts $d_w = W_t$. Fig. 4.4 shows that the rectangular layout generally can achieve higher fill factors especially for low thickness to width ratio, W_t/W_d.

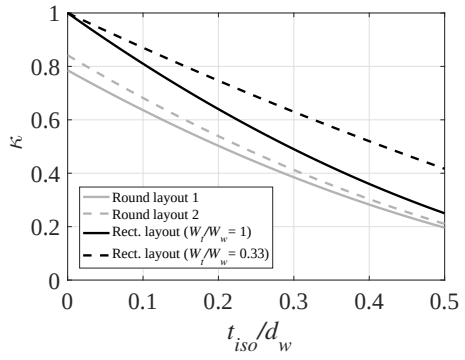

Figure 4.4: Fill factor comparison of different winding layouts.

4.1.4 Experimental results

To verify the presented theory, i.e. the relation between VC fill factor and loudspeaker efficiency, a series of measurements was performed on VC prototypes implemented in the same magnet system. The implemented VCs use a rectangular winding layout and have same geometry. The main difference is the thickness to width ratio, W_t/W_d. For the same VC geometry a lower thickness to width ratio causes a lower resulting wire resistance according to eq. (4.19). Moreover a standard VC was implemented as reference utilizing conventional round layout 2 for windings. All VCs use a copper material as conductor.

The prototypes were measured on their nominal resistances, R_e, and force factors, Bl. From that the Bl^2/R_e ratio can be determined which for high mass ratios are expected to have proportional relationship with the fill factor. The nominal resistance was measured using a high precision multi meter [89]. The force factor was measured by pulling the VC out of the magnet system with a constant velocity while measuring the induced voltage on the VC terminals. The relation can be derived from Lorentz's force law and the Coulombian Force Attraction described in [93] and [53].

$$\begin{aligned} F &= i \cdot Bl \\ V &= u \cdot Bl \end{aligned} \tag{4.20}$$

Where F is a force, i is an electrical current, V is the induced voltage on the voice coil terminals and u is the velocity of the voice coil movement inside the air gap.

Moreover the VC masses was measured using a high precision weight [94]. Knowing the mass the fill factor can be determined from:

$$\kappa = \frac{M_{Cu}}{V_d V_o V_w \rho_{Cu}} \tag{4.21}$$

$M_{Cu} = M_{vc} - M_{cf} - M_{lw}$ is the mass of the copper where M_{vc}, M_{cf} and M_{lw} are the mass of the total VC, the coil former and the connection litz wires respectively. $\rho_{Cu} = 8960$ kg/m^3 is the copper density.

Table 4.1 shows the specifications and measured results of the implemented VCs. The efficiency improvement,$\Delta\eta$, with respect to VC3 (the VC with the lowest fill factor) is evaluated for a high mass ratio of $M_{ratio} = 20$. This is done both based on the measurements and from theoretical evaluations obtained through Fig. 4.2 (a). There exist a good correlation between the expected results and the measurements. An approximate efficiency of 1 dB, corresponding to 25 %, is detected going from a fill factor of 45% to 53%. However the VCs using rectangular layout have generally a lower fill factor than the more conventional VC4. This is due to the fact that the voice coil manufacturer applied an additional insulation coating on the VCs using rectangular layout. The resulting fill factor suffers from that.

4.2 Summary research contribution within loudspeakers

This section have demonstrated theoretically and experimentally that the loudspeaker efficiency can be expressed as a function of the fill factor and the geometry of the

	VC1	VC2	VC3	VC4	Units	Prototype VCs
Layout	Rect.	Rect.	Rect.	Rnd.2		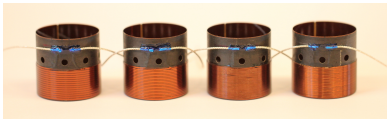
Bl	1.45	2.03	2.88	5.14	Tm	
R_e	0.32	0.66	1.53	3.82	Ω	
κ	53	51	45	53	%	
Bl^2/R_e	6.65	6.25	5.42	6.91	Ω/Tm	
$\Delta\eta_{meas.}$	0.89	0.62	ref.	1.05	dB	
$\Delta\eta_{sim.}$	0.71	0.54	ref.	0.71	dB	

Table 4.1: Summary of specifications and results of implemented prototype VCs.

magnet system. For loudspeaker drivers with high mass ratio the relation between the VC fill factor and loudspeaker efficiency is directly proportional. In addition to this it was found that a high fill factor will shift the low frequency upwards resulting in a higher -3 dB cut-off frequencies. Analysis of different VC winding layouts showed that a rectangular winding layout can facilitate higher fill factors. This results in a lower nominal resistance compared to conventional designs (4-8 Ω). Four VC designs were implemented. Due to insulation issues the fill factor of the VCs using rectangular layout did not exceed that of the conventional round layout. Nevertheless experimental results verified the presented hypothesis, i.e. that efficiency is proportional to VC fill factor for high mass ratios. An efficiency improvement of approximately 1 dB was detected, which corresponds to an improvement of 25 %. This improvement is actually massive and it could be even higher. This is due to the fact that the fill factor of the reference voice coil using conventional round wire was measured to be 53% which leaves plenty of head room for future optimizing.

5

Research contribution part III Amplifiers

This section builds upon the theory presented in section 2.1 and 2.3 and the results are related to the articles entitled "Towards higher power density audio amplifiers" and "Optimal Control of a High-Frequency Class-D Amplifier" [61, 95] attached in Appendix A and C.

5.1 High power density switch-mode power audio amplifiers

As stated in the introduction of this thesis management of power dissipation in switch-mode power audio amplifiers is the main challenge to overcome in order to achieve high power density audio amplifiers delivering $P_{out} \geq 100$ Wrms.

This section presents a new switching strategy for switch-mode power audio amplifiers beneficial for power dissipation in the switching devices. The strategy is based on the expected duty cycle distribution of real audio signals and utilizes a high output filter ripple current combined with full state control [95] to improve soft switching capabilities while keeping good audio performance.

An experimental comparison between a conventional- and a proposed-implementation of 100 Wrms amplifiers is performed. Results show the losses are distributed more evenly between output filter and switching devices when using the proposed switching strategy. In addition to this a temperature reduction of up to 45 °C on the switching devices is observed when comparing the proposed implementation to the conventional.

Finally a size optimized 150 Wrms amplifier is implemented using the proposed switching strategy. Measured results demonstrate a power density of 11.5 W/cm^3 with THD+N levels down to 0.03%. Temperature measurements show that the amplifier is operating at safe temperatures below 100 °C even with a sine wave output power of 100 Wrms.

5.1.1 Proposed switching strategy

The proposed switching aims to improve soft switching capabilities of amplifier power stage when playing real audio signals, i.e. Zero Voltage Switching (ZVS) and Reduced

Voltage Switching (RVS). To do so the expected duty cycle distribution of audio signals must be known. Section 3.1 presented an analysis of the amplitude- and duty cycle-distribution. Fig. 5.1 (a) shows the expected duty cycle distribution of the power stage for audio signals and sine waves respectively with the 90% intervals marked for comparison. It is observed that sine waves utilizes almost full modulation 90% of the time while audio signals in average only uses one third of that. Therefore the switching strategy will aim to improve soft switching capabilities within that range, i.e. $D = 0.34$ to $D = 0.66$.

To facilitate RVS and ZVS on all switching devices for a given duty cycle span the ripple current, Δi_L, in the output filter inductor must be larger than the continuous output current, I_{out}, for all duty cycles within the span. This can be expressed as a requirement using eq. (2.18) and (2.17):

$$\frac{V_{DD} D\,(1-D)}{2 L_f f_{sw}} > \frac{(2D-1)\,V_S}{R_e} \tag{5.1}$$

Examining eq. (5.1) it is realized that the ripple current decreases as the duty cycle moves away from idle, $D = 0.5$, for Fixed Frequency (FF) modulation. Therefore a Self-Oscillating (SO) modulation scheme is preferred. In addition to that the size of the ripple current is dependent on the output filter quality factor, Q, as the filter inductance, L_f follows eq. (2.20). Fig. 5.1 (b) shows the ratio between the ripple and output current for different filter quality factors. As long as the ratio is larger than one eq. (5.1) is satisfied and ZVS/RVS can theoretically be achieved on all switching devices. Fig. 5.1 (b) shows that aiming for a filter quality factor of $Q = 4$ with a SO modulation scheme can facilitate ZVS and RVS within the desired duty cycle span, i.e. $D = 0.34$ to $D = 0.66$. A high ripple current causes AC losses of output filter inductor to increase. However it is expected that the heat capacity of the filter inductor normally will be larger than that of the switching devices due to their physical size. In that sense losses are transferred from the switching devices to the output filter inductor which will act as a natural heat sink. The amount of soft switching experienced by a power stage

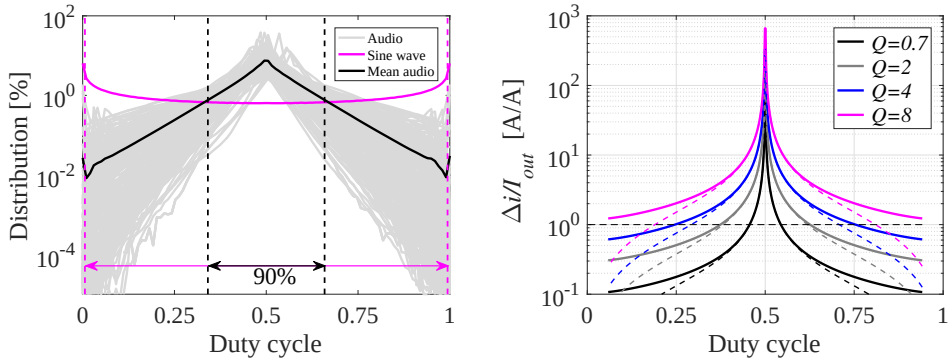

(a) Duty cycle distribution form Fig. 3.3 (b) with 90% intervals marked.

(b) Ratio between ripple- and continuous output-current for various filter Q. SO modulation (solid) and FF modulation (dashed).

Figure 5.1: Proposed switching strategy uses high output filter Q to facilitate ZVS and RVS for the vast majority of the expected duty cycle distribution when playing real audio signals.

Table 5.1: Specifications of amplifier prototypes for experimental comparison.

	Prior art	Proposed	Units	Amplifier prototype
Cut-off frq (f_c)	40	40	kHz	
Filter ind. (L_f)	23	4	μH	
Filter cap. (C_f)	0.35	2	μF	
Quality Factor (Q)	0.7	4		
Idle switch Frq (f_{sw})	500	500	kHz	
Supply voltage (V_S)	50	50	V	
Dead time (t_{dt})	10	10	ns	
Gain (G)	32.5	32.5	dB	
Load (R_e)	8	8	Ω	
Power stage	BTL	BTL		
Modulation	SO	SO		
Control	Full state	Full state		

switch can be expressed as the soft switching factor, V_P [96, 97]. For switching devices in a switch-mode power audio amplifier the soft switching factor can be written as:

$$V_P = \frac{V_{Cds}}{V_S} = \frac{t_{dt} i_L}{2 C_{ds} V_s} \tag{5.2}$$

To control amplifiers using the proposed switching strategy full state control can be used. Full state control is preferred over classical output control, such as PI and PID regulators, as it provides control of system pole placement [95]. This is a desired feature for a switch-mode power audio amplifier with a high filter quality factor as the resonant peak in the transfer function can be dealt with while keeping good audio performance. Full state control will be elaborated in section 5.2.

5.1.2 Experimental comparison

To evaluate the performance difference between the proposed switching strategy and a conventional implementation, two prototype amplifiers were implemented. The amplifiers are identical in terms of modulation scheme, power stage configuration and control type. They differ in terms of the output filter design. The proposed amplifier utilizes the proposed switching strategy with a filter quality factor of $Q = 4$. The prior art amplifier utilizes a conventional maximum flat implementation of the output filter, $Q = 0.7$. Both amplifiers uses MOSFETs [98], SO modulation and full state control. The states used for feedbacks are the inductor current, I_L, the output current, I_{out}, and the output voltage, V_{out}. Table 5.1 shows the specifications of the prototype amplifiers.

5.1.2.1 Audio performance comparison

Fig. 5.2 shows that the two amplifiers have similar audio performance. Fig. 5.2 (a) shows excellent Total Harmonic Distortion plus Noise (THD+N) levels down to 0.03% measured A-weighted with a 100 Hz sine wave on an UPP Audio Analyzer from Rohde Schwartz. The proposed amplifier performs slightly better. However this is related to small adjustments in the loop gain of the two amplifier prototypes. Therefore it can not be concluded that the proposed switching strategy improves THD+N levels. Fig. 5.2 shows the open- and closed-loop frequency response which for closed loop configurations are practically identical. More interesting is the open loop response of

the proposed amplifier where a gain for higher frequencies is observed. This gain is caused by the high quality factor output filter which introduces a resonant peak in the frequency response as discussed in section 2.3.

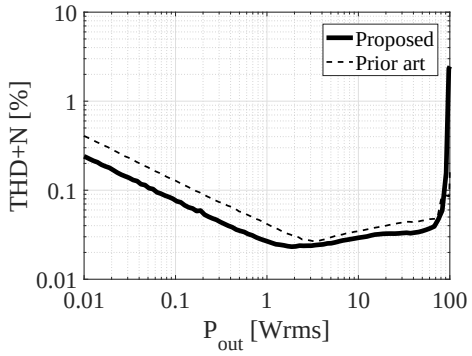

(a) THD+N @100 Hz.

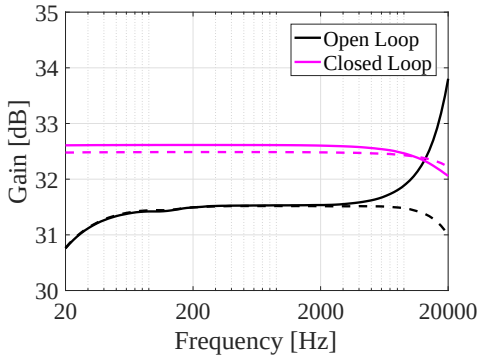

(b) Open- and closed-loop frequency response.

Figure 5.2: Measured audio performance of implemented amplifier prototypes. Proposed (solid) and prior art (dashed).

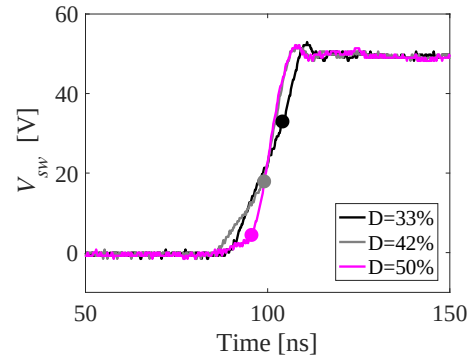

(a) Rising edge wave form. Prior art.

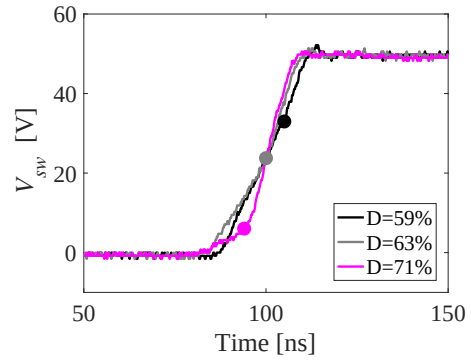

(b) Rising edge wave form. Proposed.

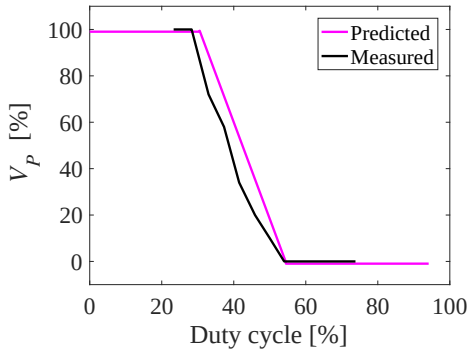

(c) Soft switching factor. Prior art.

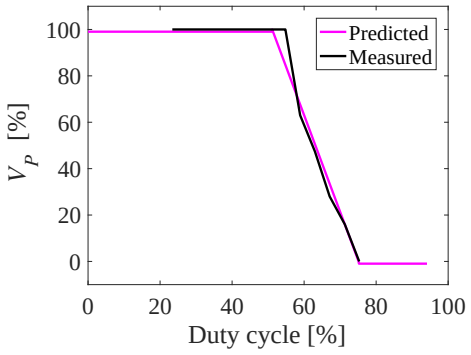

(d) Soft switching factor. Proposed.

Figure 5.3: Measured soft switching capabilities of implemented amplifier prototypes. Dots marked V_{Cds}.

5.1.2.2 Soft switching comparison

To compare the soft switching capabilities of the implemented amplifiers it is desired to evaluate the soft switching factor. This can be done by measuring the rising edge switching waveform using an oscilloscope for different duty cycles while tracking the voltage over the parasitic drain source capacitance, V_{Cds}. Fig. 5.3 (a) and (b) show the rising edge of the switching waveforms for both amplifiers with V_{Cds} marked for different duty cycles, D. Knowing the voltage over the parasitic drain source capacitance voltage over the MOSFET and the soft switching factor, defined in [96, 97], can be found using eq. (2.27) and eq. (5.2). Fig. 5.3 (c) and (d) show that the soft switching capabilities are improved in the proposed amplifier as ZVS and RVS are achieved for a larger duty cycle span. Measurements corresponds very well with predictions derived from eq. (2.27), eq. (2.29) and eq. (5.2). The amplifiers are effectively hard switching at a soft switching factor of $V_P = 0$ % and for the prior art amplifier this limit is found to be at 55 % duty cycle while for the proposed amplifier it is at 75 %. The measurements are performed for the high side MOSFETs but by assuming symmetry in the power stage design they are equally valid for the low side MOSFETs.

5.1.2.3 Temperature comparison

The improved soft switching capabilities of the MOSFETs translate into reduced MOSFET operating temperature. Fig. 5.4 (a) and (b) shows the measured operating temperature of the amplifiers tested at full power with the test signal proposed in section 3.1 modelling the expected amplitude distribution of real audio signals [60]. The temperature of the MOSFETs is strongly reduced in the proposed amplifier ($\Delta T_{1-4} \approx 45°\text{C}$) while the output filter temperature is increased ($\Delta T_{5-6} \approx 13°\text{C}$). This corresponds with the expectations. Fig. 5.4 (c) and (d) confirms this even for a high output power using a sine wave test signal. The MOSFET temperature is reduced in the proposed amplifier design ($\Delta T_{1-4} \approx 15°\text{C}$). The reduction is less than observed for the proposed test signal of section 3.1. This is expected as the switching strategy of the proposed amplifier is mainly designed for improving the switching losses for real audio signals. However a clear improvement is still observed. In general the power dissipation is spread more evenly between the switching MOSFETs and filter in the proposed amplifier design. All thermal images of the amplifiers were taken using the T650 SC thermal camera from FLIR.

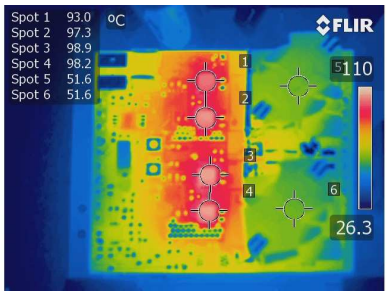

(a) Test signal of section 3.1 - Prior art amplifier.

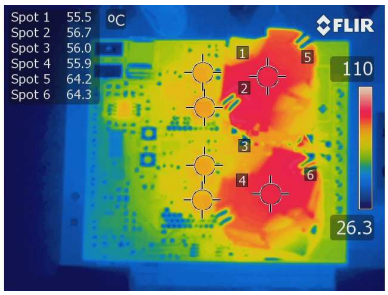

(b) Test signal of section 3.1 - Proposed amplifier.

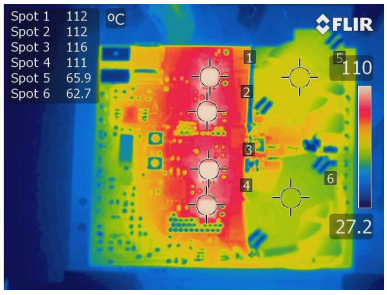

(c) Sine signal - Prior art amplifier.

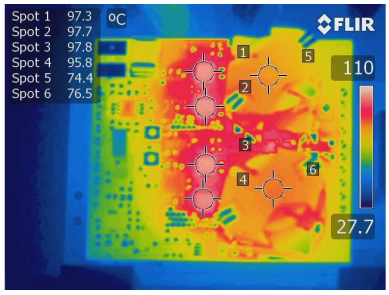

(d) Sine signal - Proposed amplifier.

Figure 5.4: Temperatures of amplifiers after 20 minutes of operation. (a) and (b) uses proposed test signal of section 3.1 at 300 Hz (P_{out} = 7.5 W). (c) and (d) uses 1000 Hz sine (P_{out} = 85 W). Spot 1 to 4 are switching MOSFETs and spot 5 and 6 are output filter inductors.

5.1.3 High Power density switch-mode power audio amplifier

To demonstrate the potential for high power density amplifiers using the proposed switching strategy the proposed amplifier of table 5.1 was developed into a high power density amplifier. Except from the size which is smaller for the high power density amplifier, the specifications are more or less the same, e.g. supply voltage of $V_S = 50$ V, high quality factor of $Q = 4$, a 500 kHz switching frequency, etcetera. However due to minor adjustments in the full state control feedback circuit the maximum output power is increased to $P_{out} = 150$ Wrms. In addition to that the high power density amplifier utilizes a four layer Printed Circuit Board (PCB) with an updated layout for leading heat away from the switching devices. This layout utilizes copper planes in multiple layers to add as much thermal mass to the switching devices as possible. Finally the high power density amplifier utilizes GaNFETs instead of conventional MOSFETs to minimize parasitic capacitances and thereby gate and switching losses [21]. With a boxed volume of 13 cm^3 the power density becomes 11.5 W/cm^3.

5.1.3.1 Experimental results

To evaluate the performance of the high power density amplifier a series of measurement was performed.

Fig. 5.5 (a) shows the measured A-weighted THD+N@100 Hz. The measurement is performed using an UPP Audio Analyzer from Rohde Schwartz. The distortion

is observed to be below 0.1% for output powers ranging from 0.1 to 100 Wrms with a minimum of 0.03% while clipping with 3% at 150 Wrms. Fig. 5.5 (b) shows the measured efficiency of the high power density amplifier. Due to the high supply voltage level the efficiency is only 25% at 1 Wrms but rises quickly to 74% at 10 Wrms and peaks with 90% at maximum output power. The efficiency was measured by measuring input and output voltages and currents using high precision multimeters [89]. The operating temperature of the high efficiency amplifier was evaluated with thermal images taken with a T650 SC thermal camera from FLIR and temperature logging of the output

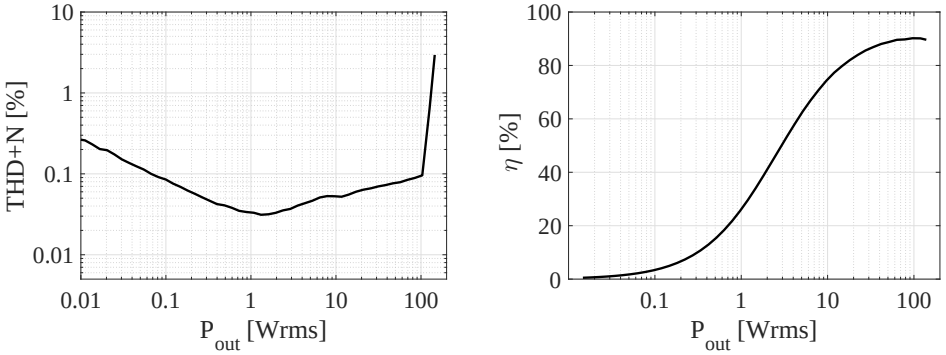

(a) THD+N @100 Hz. **(b)** Efficiency measured with sine wave.

Figure 5.5: Measured THD+N and efficiency of the high efficiency audio amplifier.

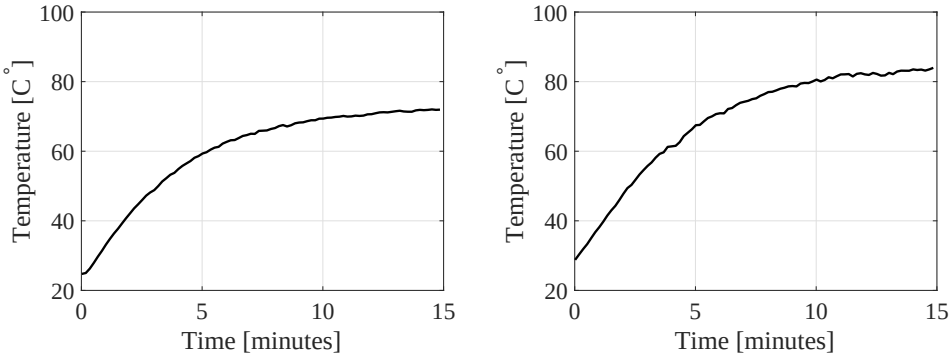

(a) Idle operation inductor temperature. **(b)** P_{out} = 100 Wrms inductor temperature.

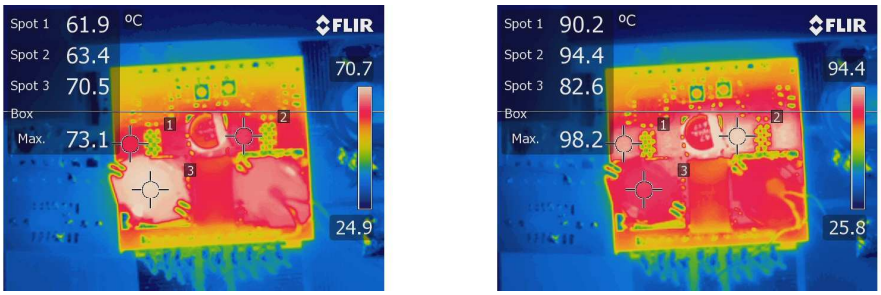

(c) Idle operation after 15 minutes. **(d)** P_{out} = 100 Wrms (sine wave) after 15 minutes.

Figure 5.6: Temperature of high power density audio amplifier. Spot 1 and 2 are switching GaNFETs and spot 3 is output filter inductor.

filter inductor using thermistors in conjunction with a high precision multimeter [89]. Fig. 5.6 (a) and (b) shows the measured output filter inductor reaches a steady state temperature after 15 minutes. Since the inductors are assumed to have the largest heat capacity the whole amplifier is assumed to be in steady state after 15 minutes. Fig. 5.6 (c) and (d) shows the thermal images of the amplifier after 15 minutes of operation, i.e. steady state conditions. Both in idle and at 100 Wrms output power the temperature never exceeds 100 °C. The temperature of the output inductors are quite high in idle and better core material should be a topic of future work. The cores used in this amplifier was RM5 cores with N87 material [68]. The performance is summarized in table 5.2.

Table 5.2: Performance of high power density audio amplifier.

	Performance	**Units**	**Amplifier prototype**
Gain	32.5	dB	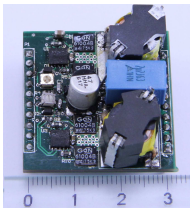
P_{out} @ 8Ω	150	Wrms	
η_{max}	90	%	
Boxed volume	13	cm^3	
Power density (ρ_{power})	11.5	W/cm^3	
Temperature @ 100 Wrms	$\leq$ 100	°C	
THD+N	0.03	%	

5.2 Optimal control for switch-mode power audio amplifiers

The proposed switching strategy described in section 5.1 utilizes a high filter inductance ripple current to improve soft switching capabilities. This means that the quality factor, Q, of the output filter is rather high and therefore introduces a resonant peak in the open loop frequency response opposed to conventional designs aiming for maximal flat response. Conventional control methods such as voltage controlled PI- and PI-Lead -regulators are not well suited for controlling a high Q amplifier power stage. This is due to the fact the the resonant peak in the open loop frequency response will determine the amount of feedback gain the control loop can deliver without becoming unstable, i.e. without having critical phase margins close to or above -180 °. For this reason conventional PI- or PI-Lead -regulators will performed better in conventional designs than in a high Q design. Therefore it is relevant to investigate an alternative control method.

This section presents the design and results of an optimal controller for a high Q switch-mode power audio amplifier [95]. The controller utilizes full state control meaning that it uses multiple feed back paths enabling damping of the output filter effectively removing the resonant peak from the frequency response. The controller is implemented on a 1.9 MHz switch-mode power audio amplifier equipped with GaNFETs and results show down to 0.01% distortion.

5.2.1 State space model

Opposed to conventional control methods the proposed full state controller requires a state space model of the system. The state modelled can be described using the standard state space model for Linear Time Invariant (LTI) systems shown in eq. 2.15 and below for convenience:

$$\dot{x}(t) = Ax(t) + Bu(t) \tag{5.3}$$
$$y(t) = Cx(t) + Du(t) \tag{5.4}$$

The system is in this case the switch-mode power audio amplifier which can be modelled as the simplified circuit model shown in Fig. 5.7. Where V_{in} is the amplifier input voltage and G is the amplifier gain. L_f, R_{Lf} and I_L denotes the filter inductance, its' series resistance and the current flowing through it respectively while C_f is the filter capacitance. R_e and L_e relates to the voice coil nominal resistance and self inductance. V_{out} and I_{out} is the amplifier output voltage and current. Formalized into the state space form the system matrix, A, and the input matrix, B, becomes:

$$A = \begin{bmatrix} -\frac{R_{Lf}}{L_f} & 0 & -\frac{1}{L_f} \\ 0 & -\frac{R_e}{L_e} & \frac{1}{L_e} \\ \frac{1}{C_f} & -\frac{1}{C_f} & 0 \end{bmatrix} \quad B = \begin{bmatrix} \frac{G}{L_f} \\ 0 \\ 0 \end{bmatrix} \tag{5.5}$$

The state vector, $x(t)$ contains three states, namely the filter inductor current, the output current and the output voltage:

$$x(t) = \begin{bmatrix} I_L \\ I_{out} \\ V_{out} \end{bmatrix} \tag{5.6}$$

Due to non-linearities in the switch-mode power stage and modulator an integration term is added to the system so that input to output tracking capabilities are improved, effectively reducing distortion in the amplifier output. The integration acts as an I controller for an error signal, $e(t)$, and can be included in the state space model by

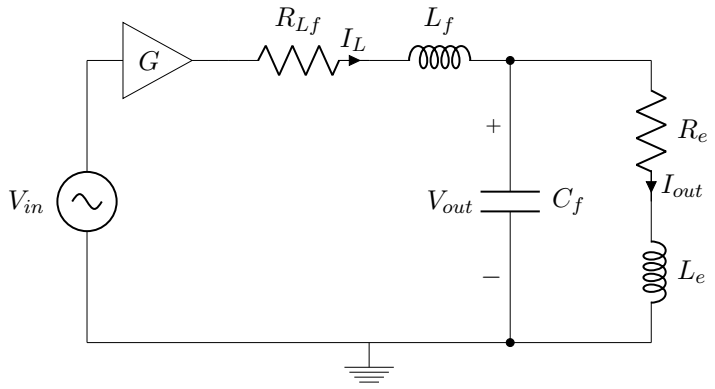

Figure 5.7: Signle ended circuit model of amplifier systems.

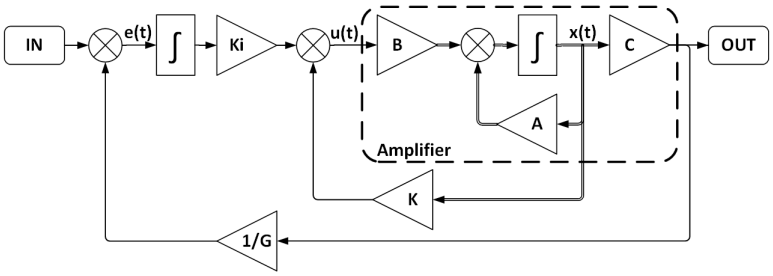

Figure 5.8: Amplifier with control. K consists the elements of K_∞ associated with the three state vectors while Ki is the element of K_∞ associated with the integration term.

applying an integral transform:

$$A_i = \begin{bmatrix} A & 0 \\ -C & 0 \end{bmatrix}, \quad B_i = \begin{bmatrix} B \\ 0 \end{bmatrix}, \quad x(t) = \begin{bmatrix} I_L \\ I_{out} \\ V_{out} \\ q \end{bmatrix} \tag{5.7}$$

This results in an extra state, q, in the state vector, containing the negative values of the output voltage which is used as a negative feedback to generate the error signal, $e(t)$.

5.2.2 Linear Quadratic Regulator

To design the full state controller, the Linear Quadratic Regulator (LQR) method is used. The LQR method turns the controller design into an optimization routine based on the cost function. It ensures stability and is therefore a type of controller designed from a stability consideration. The method finds the optimal gain matrix, K, containing the gain from each state in the system. The cost function used is the following quadratic performance index [99, 100]:

$$J(u) = \lim_{t\to\infty} \int_0^t x^T(t) R_1 x(t) + u(t)^T R_2 u(t)\, \mathrm{dt} \tag{5.8}$$

Where $x(t)$ is the system state vector and $u(t)$ is the system control signal. R_1 and R_2 are weighting, or so called penalty matrices, used to emphasize the performance of specific states and control signals. The limiting constant solution, P_∞, to the performance index, $J(u)$, can found by solving the Algebaric Ricatti Equation [100].

$$0 = A^T P_\infty + P_\infty A + R_1 - P_\infty B R_2^{-1} B^T P_\infty \tag{5.9}$$

The steady state gains, K_∞, for the full state controller can then be evaluated as:

$$K_\infty = R_2^{-1} B^T P_\infty \tag{5.10}$$

Fig. 5.8 shows the complete amplifier system design with feedback paths.

5.2.3 Experimental results

To evaluate the performance of a full state controlled amplifier a prototype amplifier was implemented. The prototype uses GaNFETs and is switched at a fairly high

Table 5.3: Specifications of amplifier prototype system.

	Performance	Units	Amplifier prototype
Quality Factor (Q)	4.5		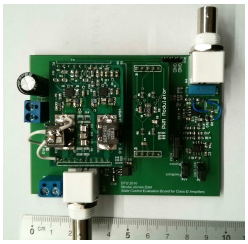
Cut-off Frq. (f_c)	155	kHz	
Idle switch Frq. (f_{sw})	1.9	MHz	
P_{out} @ 8Ω	9	Wrms	
Supply voltage (V_S)	50	V	
Load resistance (R_e)	8	Ω	
Load self-inductance (L_e)	2	nH	
Gain	19.2	dB	

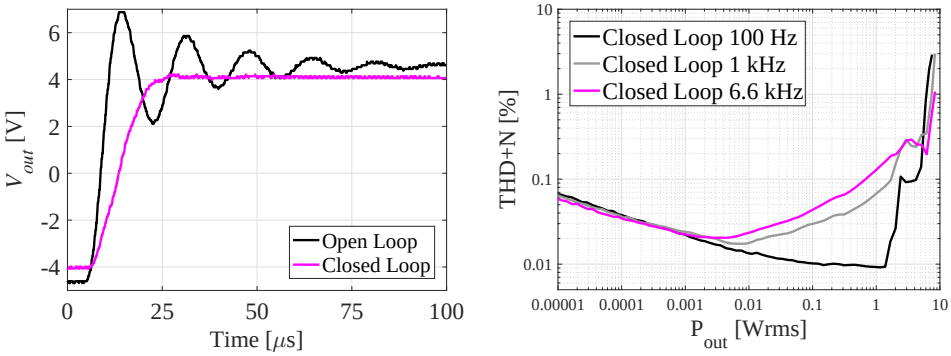

(a) Step response of implemented amplifier. **(b)** THD+N of implemented amplifier.

Figure 5.9: Measured step response and THD+N of implemented amplifier prototypes using full state control.

switching frequency of 1.9 MHz. Moreover it has a high output filter quality factor of $Q = 4.5$ causing a resonance peak in the frequency response. The feedback gains used in the prototype were designed using the Matlab `lqr()` function which returns the needed feedback gains. These gains were then translated into component values and implemented in the amplifier circuit. Table 5.3 shows the specification of the designed and implemented amplifier prototype.

Fig. 5.9 (a) shows the measured open- and closed-loop step response. The oscillation seen on the open loop measurements is caused by the resonant peak introduced by the high filter Q. In the closed loop configuration the oscillations are effectively dampened so that a steady state condition is achieve after approximately 16 μs, i.e. more than factor five faster than the open loop response. Fig. 5.9 (b) shows the closed loop A-weighted THD+N. The measured results show excellent audio performance down to 0.01% with consistent levels below 0.1% over a large power range.

5.3 Summary

This chapter has presented a new switching strategy enabling very high power density switch-mode power audio amplifiers for output powers above 100 Wrms. The proposed switching strategy utilizes a high output filter inductance ripple current to improve soft switching capabilities of the switching devices. An experimental comparison on 100 Wrms amplifier prototypes showed that the proposed switching strategy reduces

Table 5.4: Summary of contribution within high power density audio amplifiers.

	P_{out} [W]	η [%]	ρ_{power} [W/cm^3]	THD+N [%]	Notes
[15]	100	90	-	0.02	Integrated circuit
[14]	140	90	-	0.03	Integrated circuit
[27]	50	-	-	0.05	GaNFET
[4]	100	-	-	0.0006	MOSFET
[16]	180	-	3.9	0.02	MOSFET
[76]	400	-	7.4	0.03	MOSFET
This work	150	90	11.5	0.03	GaNFET

the operating temperature of the switching devices with up to 45 °C when compared to a conventional implementation without sacrificing audio performance as THD+N levels down to 0.03 % were measured. Based on that a high power density audio amplifier prototype was designed with a measured power density of 11.5 W/cm^3 and THD+N levels still down to 0.03 %. Operating temperatures were monitored and found safe below 100 °C up to 100 Wrms steady state output power. Table 5.4 summarizes the achievements of this work compared to state-of-the art. To control amplifiers using this type of switching strategy a full state control method is design utilizing the Linear Quadratic Regulator (LQR) method. The controller design is explain and demonstrated on a 1.9 MHz amplifier prototypes. Results show that oscillations caused by the high Q output filter can effectively be removed while THD+N levels reaches down to 0.01%. This control method extended to include loudspeaker parameters as shown in [101]. The combination of high ripple current and full state control has been formalized into a patent application, Appendix P, which has been submitted to the European patent office.

6

Research contribution part IV Power supplies

This section builds upon the theory presented in section 2.3 and the results related to the article entitled "Multilevel tracking power supply for switch-mode audio power amplifiers" [102] attached in Appendix D.

6.1 Multilevel tracking power supply

In switch-mode power audio amplifiers it is desired to avoid clipping as this produces audible distortion on the output signal to the amplifier. Fig. 6.1[103] shows the consequence of having an insufficient rail voltage, V_S. As established in section 2.3, eq. (2.26), the switching losses, P_{sw}, relates to the switching devices' drain-source voltage, V_{ds}, squared:

$$P_{sw} = 4\left(\frac{1}{2}C_{ds}V_{ds}^2 f_{sw}\right) \tag{6.1}$$

In the case of a conventional hard switched power stage the drain-source voltage equals the supply rail voltage, $V_S = V_{ds}$. Combining this with the fact that the continuous output power is rather low when playing music due to the dynamics of music signals described in section 2.1 and 3.1 it becomes clear that the switch-mode power audio amplifier efficiency will be low and dominated by switching losses. An excessive loss within the amplifier can cause undesired thermal stress on amplifier components limiting life time reliability. In addition to that it increases the size of required heat sinks and acts as the limiting factor for play back time in battery driven audio reproducing systems such as bluetooth speakers.

For Radio Frequency (RF) power amplifiers a similar problem exists. Highly dynamic

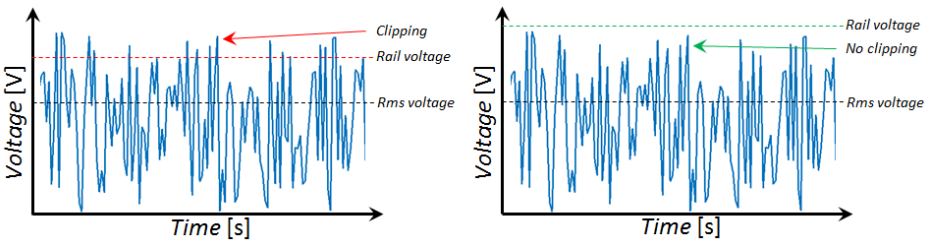

Figure 6.1: Music signal gets distorted when rail voltages are insufficient.

radio signals degrade the amplifier efficiency [80, 104, 105]. To solve this problem within RF power amplifiers Envelope Tracking (ET) and Envelope Elimination and Restoration (EER) have been proposed [69, 106–108].

This section proposes a similar approach for switch-mode power audio amplifiers where a multilevel power supply with ET capabilities will be designed for a conventional implementation of a 100 W prototype switch-mode power audio amplifier. Results show that the low power efficiency is improved with up to a factor of six and the operating temperature for the switching devices can be halved. The proposed approach is not to be confused with previous work where a continuous tracking is suggested for switch-mode amplifiers [109, 110]. Opposed to that the approach presented in this chapter uses discrete level tracking. This is not to be confused with conventionally class-H and class-G topologies as those are characterized by having a linear amplifier power stage, opposed to the switch-mode power stage of switch-mode power audio amplifier [111].

6.1.1 Design

The task for the ET power supply is to supply the audio amplifier with just enough voltage at any given time to avoid clipping of the amplifier output signal. This means that during quiet passages of an audio track the supply voltage will be low and at more wild passages it will be high. In order to do so the proposed power ET supply utilizes an analogue multiplexer which selects the amplifier supply voltage, V_S , from four evenly spaced predefined DC voltage levels. Fig. 6.2 (a) shows a simplified schematic of the analogue multiplexer. The control signals, $S1-3$ are generated from evaluation of the amplifier input signal amplitude. Fig. 6.2 (b) show a High Percision Peak Detector (HPPD) which is used for this amplitude evaluation. Based on the input signal amplitude the correct level to avoid undesired clipping of the amplifier output signal is selected. Practically this is achieved by sending the output of the HPPD, $V_{in,pk}$, to three comparators with a hysteresis and individual thresholds, v_{th1-3}. The control signals, $S1-3$, are enabled when the audio input triggers these thresholds:

$$V_{in,pk} > v_{th1-3} \tag{6.2}$$

The tracking speed is set by the time constant of the HPPD, τ_{HPPD}, formed by $C1$ and $R2$. Fig. 6.3 (a) shows the predicted behaviour ET power supply voltage, V_S and amplifier output voltage. The tracking speed is a trade-off parameter as faster tracking speed in theory reduces the losses in the audio amplifier but causes excessive

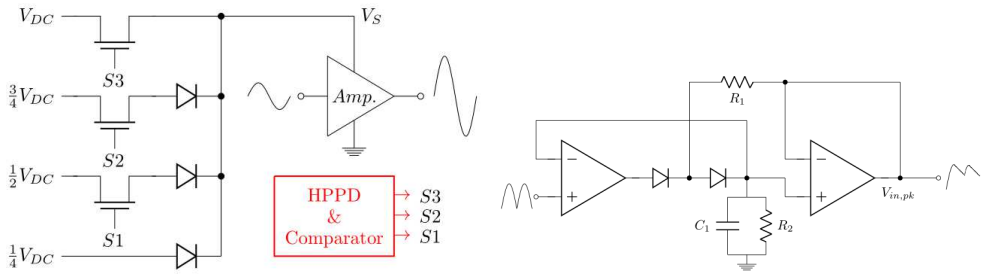

(a) Analogue multiplexer. **(b)** HPPD circuit.

Figure 6.2: Concept of proposed ET power supply consisting of a four level analogue multiplexer and a High Precission Peak Detector (HPPD tracking circuit).

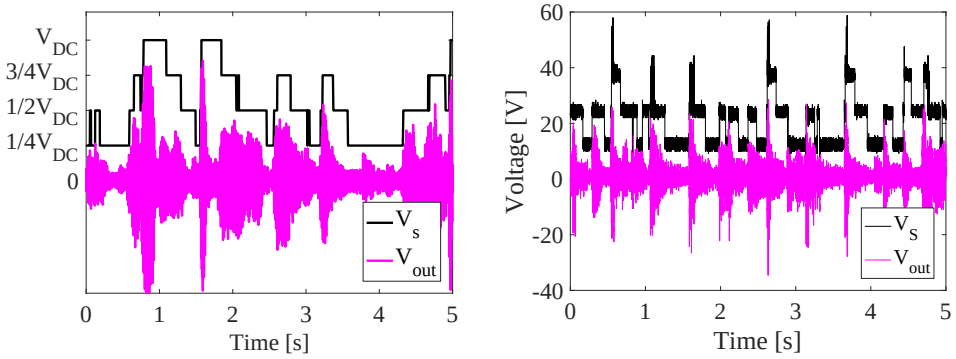

(a) Estimated behaviour - "*Ella & Louis - Can't we be friends*". **(b)** Measured behaviour - "*Daft Punk - Get Lucky*".

Figure 6.3: Envelope Tracking (ET) power supply voltage, V_S, and amplifier output in case dynamic audio signal. V_{DC} is the maximum DC voltage of the predefined voltage levels for the multiplexer.

switching in the multiplexer thus generating losses. The impact on amplifier efficiency when using the proposed ET power supply can be theorised by using the loss model, $P_{tot,\phi}$, presented in section 2.3, eq. (2.38).

6.1.2 Experimental results

To verify the theorized efficiency benefit of using an ET power supply, a prototype system was implemented consisting of an analogue multiplexer with four fixed an evenly spaced voltage levels, a HPPD comparator control circuit and a 100 Wrms switch-mode power audio amplifier. Table 6.1 shows the specifications of the implemented prototype system. According to the specifications the output of the multiplexer takes its' lowest value $V_S = 12.5$ V when $V_{in,pk} < v_{th1}$ and its' highest value $V_S = 50$ V when $V_{in,pk} > v_{th3}$. Moreover the tracking speed of the implementation is rather slow, $\tau_{HPPD} = 12$ seconds, thus avoiding excessive multiplexer switching. Fig. 6.3 (b) shows the measured behaviour of the ET power supply- and amplifer-output voltages in case of a real dynamic audio signal. In this case it is "*Daft Punk - Get Lucky*". It is observed that the proposed power supply do track the audio signal as expected.

Table 6.1: Specification of implemented multilevel supply and amplifier system.

Specifications	Value	Units	System prototype
V_{DC}	50.0	V	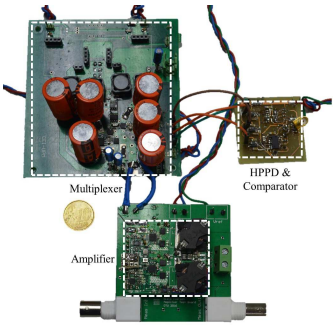
$1/2V_{DC}$	25.0	V	
$3/4V_{DC}$	37.5	V	
$1/4V_{DC}$	12.5	V	
v_{th1}	0.2	V	
v_{th2}	0.4	V	
v_{th3}	0.6	V	
P_{out} @ 8Ω	100	Wrms	
τ_{HPPD}	12	s	

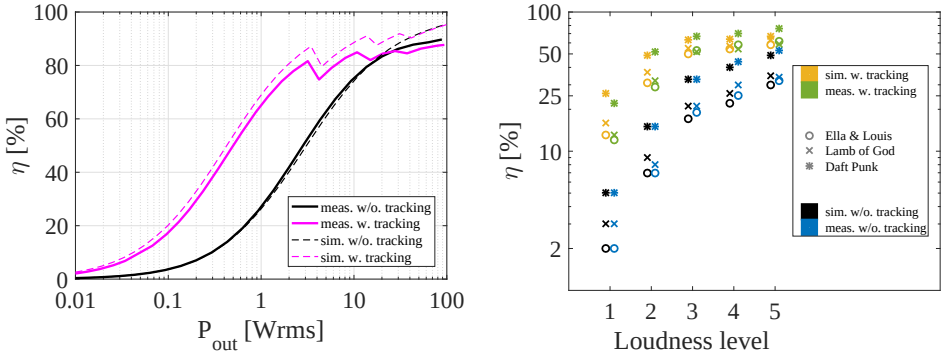

(a) Sine wave. **(b)** Audio - First 20 seconds

Figure 6.4: Simulated and measured efficiencies for sine wave and audio tracks. The corresponding output powers for the audio tracks' loudness levels are shown in Table 6.3.

Table 6.2: Crest factors of selected audio tracks.

	Name	Artist	Genre	CF
1	Can't We Be Friends	Ella & Louis	Jazz	20.4 dB
2	Redneck	Lamb of God	Metal	8.9 dB
3	Get Lucky	Daft Punk	Pop	13.0 dB

The efficiency of the system is measured using a sine wave amplitude sweep. Input and output voltages and currents was measured using high precision multi meters [89]. Fig. 6.4 (a) shows that the low power efficiency is significantly improved from < 20 % to > 50 % at $P_{out} = 0.5$ Wrms. That is almost a factor three improvement. Moreover there is a good correlation between expectations and measurements. However sine wave do not represent real audio very well and therefore the efficiency is also measured with real dynamic music signals at different loudness levels [112, 113]. Table 6.2 shows the three test signals chosen for the measurements and their crest factor (CF). Moreover Table 6.3 shows the corresponding output power for five different loudness levels, where loudness level 5 is at full power. A DPO3014 oscilloscope from Tektronix equipped with high precision current and voltage probes was used to capture the highly dynamic input and output voltages/currents from which the input and output power could be evaluated can translated into efficiency. For test purposes only the first twenty seconds of the music tracks were considered. Fig. 6.4 (b) shows the measured efficiency when measured with actual music signals. Good correlation between expectations and actual measurements are still observed. Errors between measurements and expectations are in many cases less than 10 %. Moreover the efficiency is vastly improved for all loudness levels. The greatest improvement is found for loudness level 1 where the efficiency is improved from 2 % to 12 % for the jazz track. That is a factor six. This shows that the tracking speed does not need to be very high in order to produce significant improvements.

Table 6.3: Corresponding output power for different loudness levels.

Loudness level vs. output power					
Loudness level	1	2	3	4	5
First 20 seconds					
Ella & Louis	0.06 W	0.20 W	0.56 W	0.80 W	1.20 W
Lamb of God	0.08 W	0.25 W	0.71 W	1.00 W	1.50 W
Daft Punk	0.14 W	0.47 W	1.34 W	1.90 W	2.80 W
Full track					
Ella & Louis	0.10 W	0.33 W	0.93 W	1.3 W	1.96 W
Lamb of God	0.14 W	0.46 W	1.32 W	1.86 W	2.77 W
Daft Punk	0.18 W	0.59 W	1.69 W	2.38 W	3.56 W

The efficiency improvement means that less power is being dissipated inside the switch-mode power audio amplifier. This will cause the operating temperature to be reduced. To quantify this reduction of operating temperature Fig. 6.5 shows thermal images of the amplifier operating with and without the ET power supply. The measurements show that the operating temperature is reduced up to a factor 2 for the switching devices where the temperature goes from approximately 100 °C without ET power supply to 50 °C with. For the filter inductors the temperature is reduced approximately 20 °C from $\approx$ 50 °C to $\approx$30 °C. Table 6.4 summarizes the measured operating temperatures.

6.2 Summary

This section has presented an Envelope Tracking (ET) power supply technique applied to a switch-mode power audio amplifier. Due to the highly dynamic behaviour of audio it was theorized that the switch-mode power audio amplifier would gain similar benefits with respect to efficiency as Radio Frequency (RF) amplifiers do for highly dynamic radio signals when using ET power supplies. A 100 W prototype system was implemented consisting of a four level analogue multiplexer with ET capabilities provided by a control circuit based on High Precision Peak Detection (HPPD) of the amplifier input signal. Measured results demonstrate a massive efficiency improvements for a range of loudness levels. The maximum improvements were found at low loudness levels where improvements of up to a factor of six were detected. Equally the operating temperature of the amplifier was vastly reduced. For the switching devices the temperature was halved from 100 °C without ET power supply to 50 °C with.

Table 6.4: Summary of temperature measurements shown in fig. 6.5

Mean temperatures				
	w/o. tracking		w. tracking	
Input	MOSFETs	Ind.	MOSFETs	Ind.
Idle	94.5 C°	46.9 C°	37.2 C°	29.1 C°
Ella & Louis	97.5 C°	51.6 C°	46.2 C°	33.3 C°
Lamb of God	98.3 C°	52.8 C°	55.0 C°	35.9 C°
Daft Punk	98.2 C°	52.5 C°	53.8 C°	35.7 C°

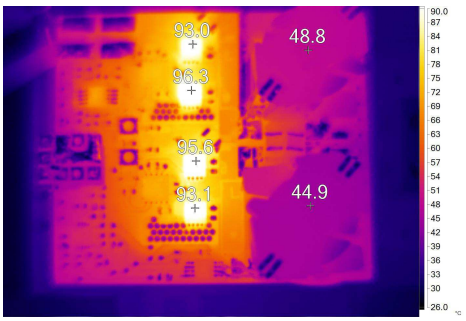

(a) Idle - Without tracking.

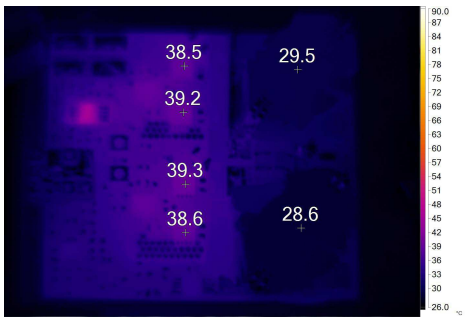

(b) Idle - With tracking.

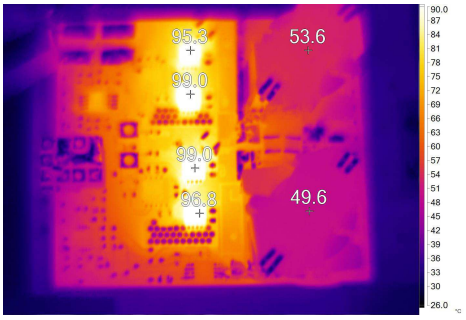

(c) *Ella & Louis* - Without tracking.

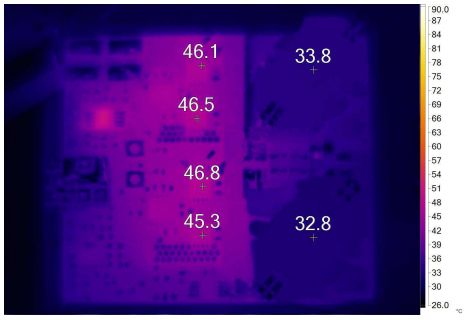

(d) *Ella & Louis* - With tracking.

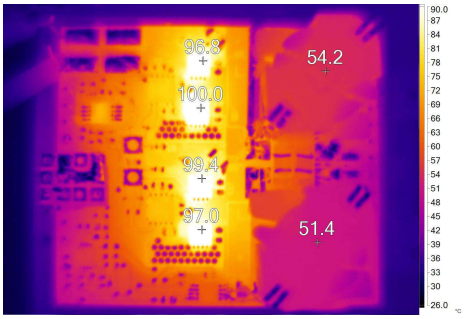

(e) *Lamb of God* - Without tracking.

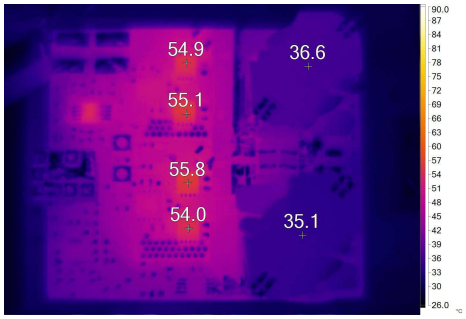

(f) *Lamb of God* - With tracking.

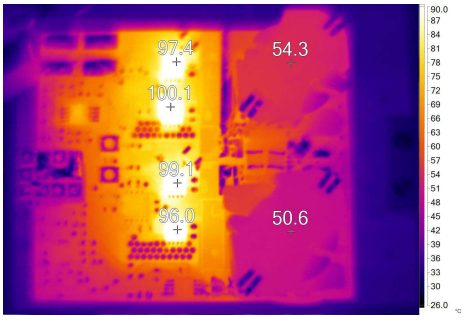

(g) *Daft Punk* - Without tracking.

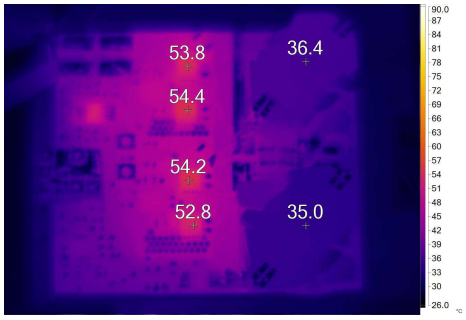

(h) *Daft Punk* - With tracking.

Figure 6.5: Measured temperatures of amplifier with- and with-out tracking at loudness level 5. Performed with Fluke thermal camera.

7

Research contribution part V System synthesis

This section combines some of the findings presented in section 3.1, 4.1 and 5.1. The results presented in this section are related to the articles entitled "Efficiency Investigation of Switch-Mode Power Audio Amplifiers Driving Low Impedance Transducers" and "Design of Efficient Sound Systems for Low Voltage Battery Driven Applications" [103, 114] attached in Appendix G and H.

7.1 Highly efficient audio systems using low impedance transducers

As a system designer one needs to take different aspects of the audio chain into consideration including the listener and his/her demands. This section presents a design flow enabling designers to choose supply voltages and nominal loudspeaker resistances to accommodate highly efficient audio reproducing systems.

Fig. 7.1 (a) shows a typical sound system with a listener placed at distance, r, from the sound source. As a system designer one wants to supply the listeners with their

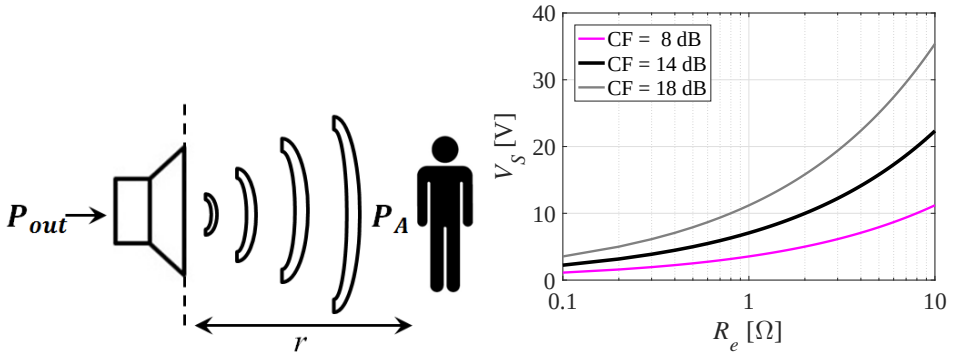

(a) Sound system with listener at a distance of r away from transducer [103].

(b) V_S vs. R_e at different crest factors (CFs) for a 93 dB@1meter sound system with a 0.61 % efficient driver.

Figure 7.1: The listeners desired SPL translated into a voltage rail vs. nominal resistance curve.

preferred Sound Pressure Level (SPL) when playing music. The Sound Pressure Level at the listeners position can be evaluated using eq. (2.13):

$$SPL = 10 \log \left(\frac{P_E \frac{\eta_0}{A}}{P_o} \right) \tag{7.1}$$

Where, P_E is electrical input power from the amplifier, P_A is acoustical output power from the loudspeaker driver, η_0 is the loudspeaker efficiency, $P_o = 10^{-12}$ W/m^2 is the reference acoustic sound power and $A = 2\pi r^2$ is the area of the sound surface at the distance, r, from the driver. To generate a high sound pressure level of 93 dB@1m from a standard loudspeaker with $\eta_0 = 0.61$ % the needed RMS power can be found to be 2 Wrms by solving for P_E in eq. (7.1). The needed peak power to supply a given RMS power relates to the crest factor (CF) of the music signal being played back over the system.

$$P_{pk} = P_{RMS} \cdot \left(\exp \frac{CF \cdot \ln(10)}{10} \right) \tag{7.2}$$

The peak power relates directly to the amplifier supply rail voltage, V_S, and the nominal resistance of the loudspeaker, R_e.

$$P_{pk} = \frac{|V_{DD}|^2}{R_L} \tag{7.3}$$

$$V_{DD} = \sqrt{R_L P_{pk}} \tag{7.4}$$

As shown in section 2.1 and 3.1 and in [41–43] the CF for real music signals is in the range 8 to 20 dB.

Having the information about loudspeaker efficiency and desired sound pressure level enables designers to plot the supply rail voltage, V_S, requirement of the amplifier vs. nominal resistance of the loudspeaker, R_e. Fig. 7.1 (b) shows the V_S vs. R_e curve for a desired output SPL of 93 dB@1meter with a 0.61 % efficient loudspeaker driver. With this curve the designer can quickly evaluate that for a 12 V battery driven system, a nominal resistance of $R_e = 1\ \Omega$ is preferable to avoid the need for a boosting power supply. A nominal resistance of $R_e = 1\ \Omega$ can in itself be beneficial for the loudspeaker efficiency as the fill factor can be increased using rectangular windings as shown in section 4.1 and [90, 91].

To summarize the system design flow is:

1. Determine listeners SPL need.
2. Translate SPL into needed electrical power using eq. (7.1) and (7.2).
3. Translate electrical power into a V_S vs. R_e curve using eq. (7.4) to examine design. options.
4. Chose the appropriate V_S and R_e.

7.1.1 Experimental results on commercial amplifiers

Using the above example with a desired SPL of 93 dB@1meter and a 0.61 % efficient loudspeaker driver two prototypes systems was designed for a 12 V battery driven

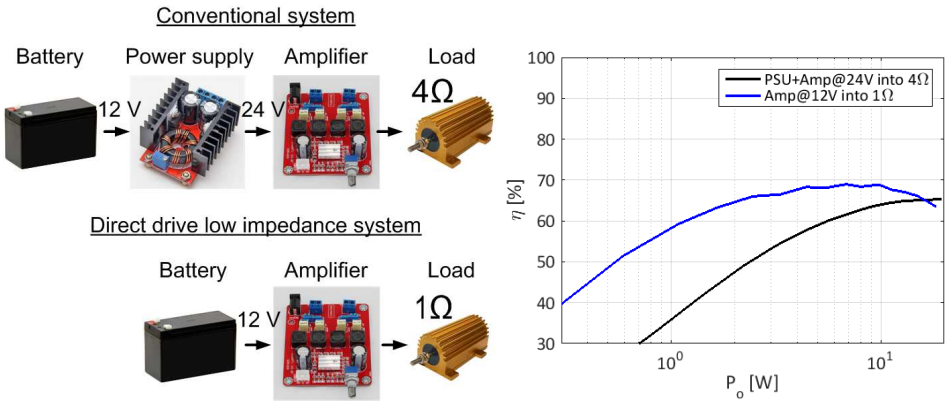

(a) Realized prototypes systems. **(b)** Measured efficiency.

Figure 7.2: Implemented prototype systems and corresponding efficiency measurements.

application. One using conventional $R_e = 4\ \Omega$ loudspeaker driver in conjunction with a boosting Power Supply Unit (PSU) and one using an unconventional $R_e = 1\ \Omega$ loudspeaker driver for a direct battery drive. For simplicity the driver was emulated as a pure ohmic resistance. Fig. 7.2 (a) shows the two systems. The amplifier is a commonly used module in consumer electronics [15] and the boosting PSU is of switch-mode technology and has up to approximately 90 % efficiency [103]. Fig. 7.2 (b) shows the measured efficiency of the two systems. Even though the used amplifier is not optimized for a low impedance loudspeaker driver the low impedance system has much better low power efficiency, e.g. more than 20 % point at 1 W output power, reaching nearly a factor two improvement.

7.1.2 Making the driver

This section serves to demonstrate that audio reproduction systems utilizing low impedance drivers are realistic. Therefore a low impedance 4" prototype driver was implemented and mounted in a vented box enclosure. The voice coil (VC) of the driver was imple-

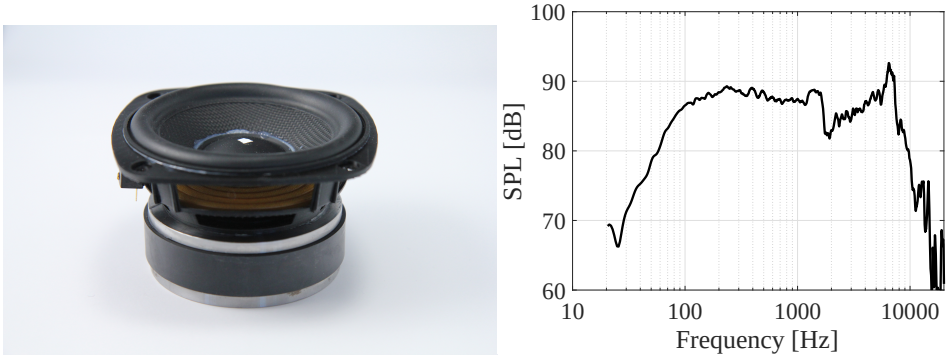

(a) Realized driver prototype. **(b)** On axis SPL (1.13V@40cm) measured in anechoic conditions in 2π environment, e.g. half sphere.

Figure 7.3: Low impedance prototype driver.

mented with a rectangular winding layout corresponding to that presented on Fig. 4.3 (c). However the fill factor of the voice coil was not especially high due to additional insulation coverings on the wire. In addition to that the driver basket was 3D printed and diaphragm, suspension, voice coil and magnet system glued together. Fig. 7.3 shows the implemented prototype and its' on-axis frequency response. The frequency response reveals a very conventional behaviour from a 4" driver with a pass band evaluated to be approximately from 80 Hz to 7 kHz. This is good considering that the VC winding layout and nominal resistance are unconventional design choices. Table 7.1 show the small signal parameters of driver.

Q_{TS}	V_{AS}	f_S	R_E	$SPL_{1W@1m}$	η_0
0.55	3.9L	61Hz	1.7Ω	83.6dB	0.145%

Table 7.1: Measured small signal parameters of implemented driver.

7.2 Summary

This chapter has shown how some of the ideas and findings of this thesis can come in to play in system level design tasks. The crest factor (CF) limits the continuous output power and therefore low impedance drivers can be used to benefit the amplifier and system efficiency for battery driven applications as the need for boosting power supplies units (PSUs) can be omitted. Low impedance drivers can actually be implemented with the proposed rectangular winding layout presented in section 4.1 and from measurements the frequency response can be evaluated as an acceptable result. A design flow method has been presented enabling system designers to identify specifications for a given application.

8

Other research

During the Ph.D. study many interesting projects related to the research topic were investigated. The most thoroughly investigated, both theoretically and experimentally, have been presented in the research contribution chapters (chapter 3 to 7). However a range of additional interesting projects were initiated during this Ph.D., many of them conducted in cooperation with talented B.Sc. and M.Sc. students. This section will briefly present the most promising of these project and their results.

8.1 Self-oscillating modulators

This section presents theory and results related to the article entitled "Comparison of Simple Self-Oscillating PWM Modulators" [63] attached in Appendix I. The project was initiated as a special course [115].

Opposed to conventional fixed frequency (FF) modulators, SO topologies generates the carrier signal directly from the input and will typically reduced the component count.

The study evaluates and compares distortion effects for two different types of SO modulators, namely the Astable Integrating Modulator (AIM) presented in [5] and the proposed Hysteresis Offset Modulator (HOM) of [63]. Appendix I provides a thorough analysis investigated SO topologies. Fig. 8.1 (a) shows the implemented modulator board for test purposes and Fig. 8.1 (b) shows through measurements and simulations that the proposed HOM has a more linear characteristic and therefore has up to 2% lower Total Harmonic Distortion (THD).

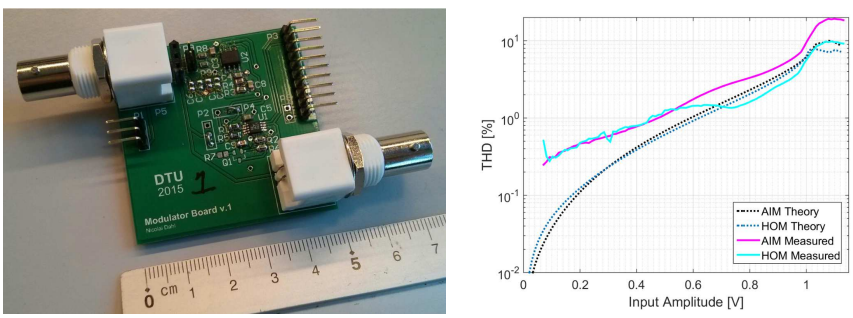

(a) Implemented SO modulator board.

(b) Measured and simulated THD of HOM and AIM.

Figure 8.1: THD comparison and implementation of SO modulators.

8.2 Resonant mode subwoofers

This section presents theory and results related to the articles entitled ”Design and Implementation of a High Efficiency Subwoofer” and ”Efficiency Investigation of Subwoofer Driven Around Resonance Frequency” [116, 117] attached in Appendix M and N. The research was initiated as special courses [118, 119].

As established numerous times in this thesis the loudspeaker efficiency is rather poor typically in the range 0.2% to 2%. However this is only when considering the pass band efficiency. Another method to evaluate the efficiency is the Constant Input Power (CIP) frequency response which reveals the loudspeaker efficiency in the frequency domain [47]. The efficiency at the loudspeaker's resonance frequency is much better than in the pass band. The study provided in Appendix M and N try to exploit this in the design of subwoofers in order improve the loudspeaker efficiency.

Two designs are investigated:

- A 4th order bandpass enclosure (Fig. 8.2 (a)).
- A two way system consisting of vented box speakers (Fig. 8.2 (b)).

Both designs aim at having a high gain for frequencies laying outside a resonance. Fig. 8.2 (c) shows how the simulated frequency response takes a high gain between the two impedance peaks generated from the driver's resonance and the enclosure resonance. This high gain is attenuated with Digital Signal Processing (DSP) to get a flat frequency response with high efficiency.

Results show that an average sensitivity of 96dB@1m/1W, corresponding to an efficiency of 2.5 % can be achieved for a low frequency band from 48 Hz to 90 Hz.

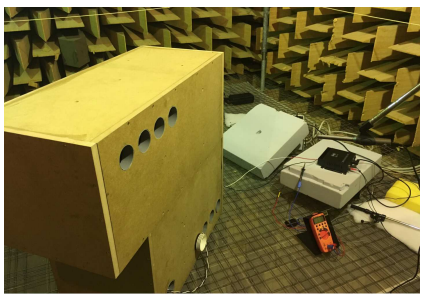

(a) 4th order bandpass implementation.

(b) 2-way implementation.

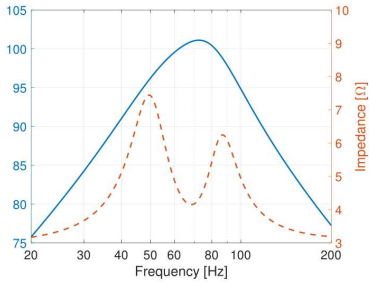

(c) Simulated impedance and frequency response.

Figure 8.2: Resonant mode subwoofers.

8.3 High frequency GaN amplifier

This section presents theory and results related to the article entitled "Self-oscillating 150W switch-mode amplifier equipped with eGaN-FETs" [26] attached in Appendix K. The research was initiated as a M.Sc. thesis [72].

This study investigated the possibilities for making a switch-mode power audio amplifier equipped with GaNFETs operating at a high switching frequency enabling faster control. Opposed to the amplifiers presented in chapter 5 this amplifier utilizes conventional switching strategy and control. Fig. 8.3 (a) shows the implemented amplifier prototype designed to run at 2 MHz switching frequencies. Besides advantages in control speed a high switching frequency reduces the size of the output filter components making the whole amplifier smaller compared to conventional implementations operating at lower switching frequencies.

Fig. 8.3 (b) shows that the implemented prototype has good audio performance with THD down to 0.004 %. However Fig. 8.3 (c) shows that the implemented prototype had thermal issues with temperatures reaching up to 82.6 °C in idle and was effectively hard switching at higher output powers making force cooling a necessity. Methods to overcome thermal issues have been described in chapter 5.

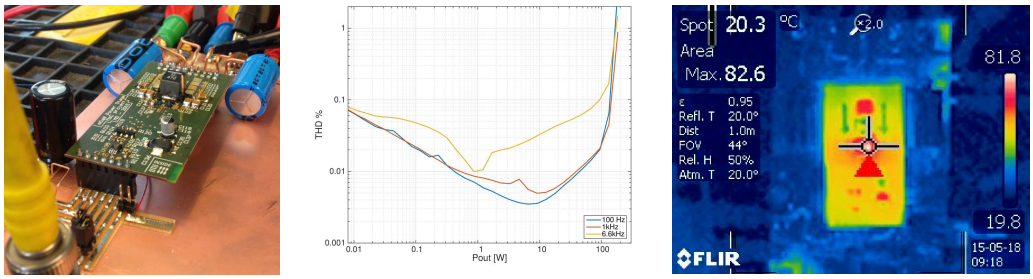

(a) Amplifier prototype. **(b)** Measured THD+N. **(c)** Measured temperature in idle.

Figure 8.3: High frequency GaN amplifier.

8.4 Power consumption model

This section presents theory and results related to the article entitled "Model for evaluation of power consumption of vented box loudspeakers" [49] attached in Appendix O. The project was conducted in collaboration with Soundboks and Merus Audio. The research was initiated as special courses [120, 121].

The motivation for doing this project was to derive a simple power consumption model so that the actual power consumption when playing music easily could be derived. This is relevant when designers want to estimate playback time from batteries. The conventional way of modelling power consumption is to model the speaker as a pure ohmic resistance. However such a simple loudspeaker impedance is far from the reality [45, 46, 122]. Using this method gives misleading results. Therefore this project derived a simple state space model on the simplified form:

$$\dot{x}(t) = Ax(t) + Bu(t) \tag{8.1}$$

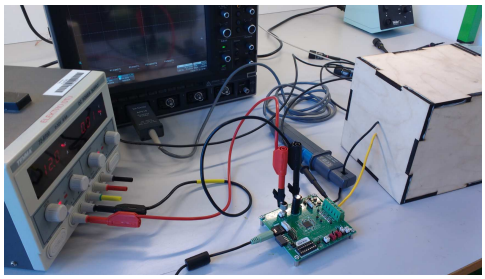

(a) Measurement setup for verifying model.

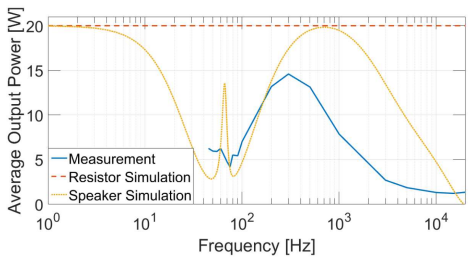

(b) Measured results.

Figure 8.4: Measurements set up and results for verifying proposed power consumption model.

Appendix O can be consulted for full print of state vector, $x(t)$, system matrix, A, and input matrix, B. Having the model in state space form allows for modelling the power consumption in the time domain which is convenient when the desire is to estimate the power consumption for a music signal over time.

To test the model a test bench was created consisting of a real prototype vented box loudspeaker which also was modelled using the model. The average power consumption over time was then measured for various signals. Fig. 8.4 (a) shows the measurement set up and Fig. 8.4 (b) shows the measured and simulated results compared to the conventional pure ohmic model. The results showed that the derived state space model predicted the power consumption much better than the conventional method. However the accuracy is sensitive to imperfections in the actual speaker implementations since the model assumes an ideal implementation.

8.5 Loudspeaker impedance emulator

This section presents theory and results related to the article entitled "Loudspeaker impedance emulator for multi resonant systems" [46] attached in Appendix L. The project was initiated as a M.Sc. thesis [123]

As mentioned in section 8.4 pure ohmic resistors are a poor representation of a loudspeaker impedance. This causes measurements using pure ohmic resistors to modelled

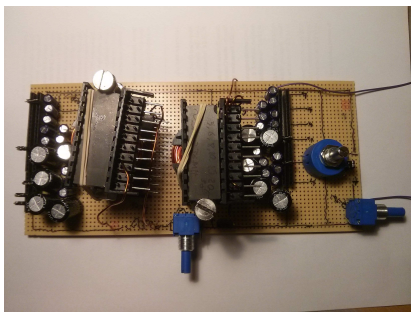

(a) Implemented emulator prototype.

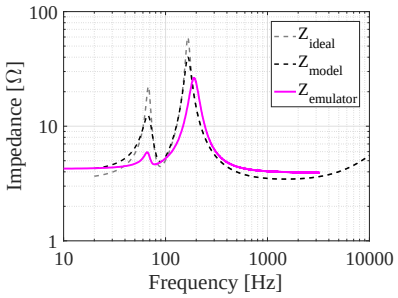

(b) Measured and simulated impedances.

Figure 8.5: Multi resonant impedance emulator.

the loudspeaker to be inaccurate or misleading. To address this issue a loudspeaker impedance emulator was designed able to emulate the impedance of different loudspeaker drivers and designs. That include the capability to emulate the impedance of driver mounted in closed- and vented-box enclosures besides the free air configuration. Fig. 8.5 (a) shows the implemented prototype utilizing tunable inductors, capacitance and resistances to emulate the electrical, mechanical and acoustical properties of a given loudspeaker design. Fig. 8.5 (b) shows how the impedance emulator matches the simulated impedance of a vented box cabinet.

8.6 Festival installations

During the Ph.D. study a couple of projects for actual music festivals was performed. They were performed in collaboration with Roskilde festival, STRØM festival and The Royal Danish Academy of Fine Arts, School of Architecture, Design and Conservation (KADK). Both projects was part of DTU courses [124, 125].

STRØM festival is a Danish festival for electronical music and workshops held in Copenhagen. For the 2015 event a project called the interactive dance floor was developed for the festival in collaboration with KADK. The functionality of the dance floor was basically to adjust the play back volume from a highly efficient loudspeaker according to the activity on the dance floor. The more participants the higher the volume. The project ended up being an installation for a children's event during the festival. KADK developed the visual design of the dance floor while DTU delivered the technical solution to accommodate the desired functionality. Fig. 8.6 (a) shows the final installation during the festival. The Ph.D. contributed with supervision throughout the project and the implementation and design of the speaker.

Roskilde Festival is the biggest music festival in Scandinavia and has existed since the 1970s. During the last decade it have been visited by approximately 100.000 festival goers each year including volunteer workers. For the 2016 event DTU Electro collaborated with KADK on a project putting focus on renewable energy. The project was called "Lingering lights" and its' functionality was to harvest energy from the sun during day time using a PV panel and use this energy for an aesthetic light display during nights. Once again KADK developed the visual design while DTU delivered the technical solution. The technical solution included custom designed battery solar charger based on a DC-DC buck converter, LED installation for the light display with LED programming using DSP for light fading. Fig. 8.6 (b) and (c) show the installation at the festival site during day- and night-time. The Ph.D. contributed with supervision throughout the project and the implementation and design of the DC-DC buck converter solar charger.

(a) Interactive dance floor for STRØM festival.

(b) PV installation for Roskilde festvial during day.

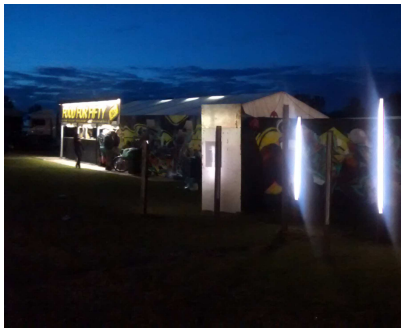

(c) PV installation for Roskilde festvial during night.

Figure 8.6: Multi resonant impedance emulator.

9

Conclusion

9.1 Summary of experimental work

This thesis has investigated multiple topics within audio reproducing systems and a wide selection of experiments and prototypes have been developed to uncover new knowledge within this field. All conducted experiments and activities have been related to the four main pillars of this Ph.D.

- Input signals
- Power supplies
- Amplifiers
- Loudspeakers

Fig. 9.1, 9.2 and 9.3 show the prototypes, modules and installations related to this Ph.D. study. To learn more about specific prototypes or test set ups please consult the appendices.

(a) Test signal amplifier. Appendix E [60].

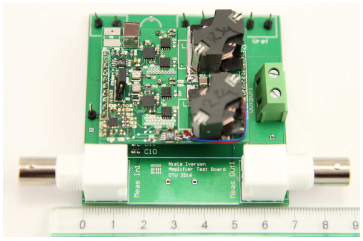

(b) High power density amplifier rev. 1, Appendix A [61].

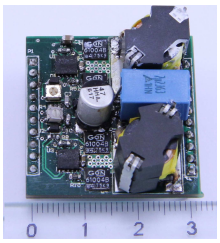

(c) High power density amplifier rev. 2. Section 5.1.

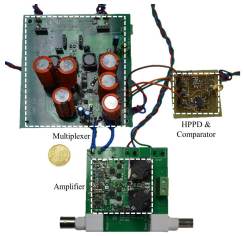

(d) Envelope Tracking power supply system. Appendix D [102].

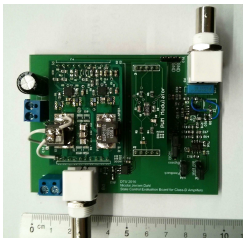

(e) High frequency, full state control amplifier. Appendix C [95].

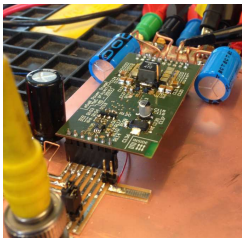

(f) High frequency amplifier. Appendix K [26].

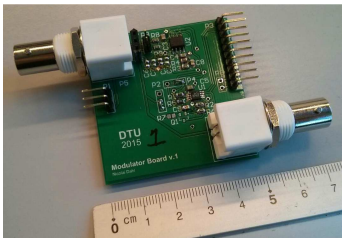

(g) SO modulator board. Appendix I [63].

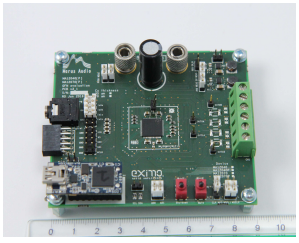

(h) Merus Audio amplifier used in Appendix G [114].

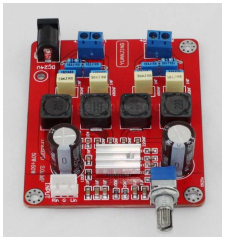

(i) Texas Instrument amplifier used in Appendix H [103].

(j) Unknown Boost converter used in Appendix H [103].

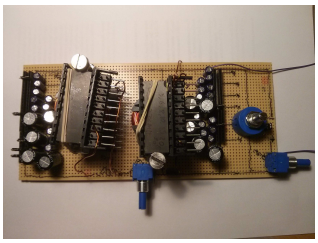

(k) Emulator prototypes. Appendix L [46].

Figure 9.1: Electrical prototypes and modules used for experimental research during the Ph.D. study.

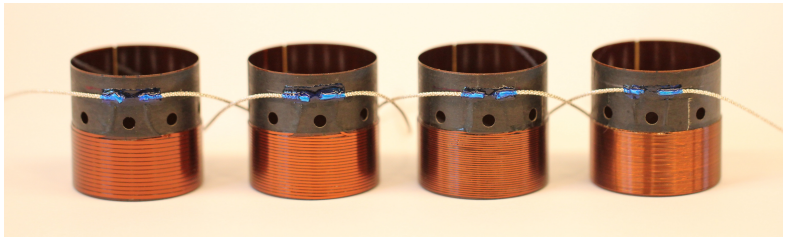

(a) VC prototypes. Appendix B and F [90, 91].

(b) Prototype driver. Appendix G [114].

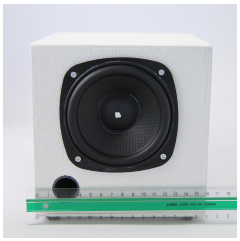

(c) Prototype speaker. Appendix G [114].

(d) Prototype speaker. Appendix N [116].

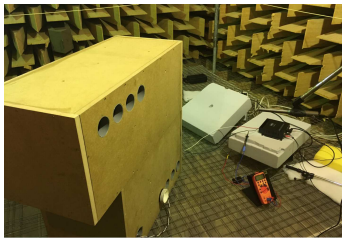

(e) Prototype speaker. Appendix M [117].

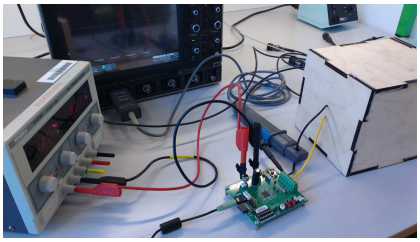

(f) Test bench with speaker prototype. Appendix O [49].

Figure 9.2: Loudspeaker prototypes and tests used for experimental research during the Ph.D. study.

(a) STRØM festival prototype installation.

(b) Roskilde festival prototype installation.

Figure 9.3: Festivals installations developed during the Ph.D. study.

9.2 Summary of results

All these experiments have produced a lot of results. This section summarises the main results and conclusion that can be made upon the end of this Ph.D. study.

Audio reproduction systems comprise of four main blocks, namely input, power supply, power amplifier and loudspeaker. Besides good audio performance key performance parameters are: efficiency, size and reliability. With respect to these key parameter this thesis have examined each block of the audio reproduction system and identified challenges and proposed methods to overcome them.

It was found that sine waves are a poor test signal for evaluating the efficiency of switch-mode power audio amplifiers and that results using this method are misleading for actual usage as they favour sine wave operation. In order to make efficiency measurements more representative for real usage a new test signal was proposed. With a crest factor of 14 dB it was found to represent the dynamics of real audio, having a 15 dB rest factor, very well. In comparison sine waves have a crest factor of 3 dB. Experimental results on a conventionally designed 12 V switch-mode power audio amplifier demonstrated a 10 % efficiency improvement when choosing switching devices based on the proposed signal instead of sine waves.

In addition to that, a new switching strategy beneficial for power dissipation in switching devices was developed. The strategy utilizes a high ripple current in the output filter inductance to improve soft switch capabilities when playing audio so that the power dissipation is moved away from the switching devices and dissipated in the output filter instead which functions as natural heat sink due to the larger surface. The high ripple current affects the amplifier's frequency response making classical control sub-optimal and therefore unconventional full state control methods were applied for the switch-mode power audio amplifiers.

An experimental comparison on 100 W amplifier prototypes showed a 45 °C reduction of operating temperature compared to a conventional implementation. Moreover a high power density prototype amplifier using the proposed strategy was developed. Results showed excellent audio performance down to 0.03 %, output powers up to 150 W and a power density of 11.5 W/cm^3. That is factor 2-3 higher than recognized state-of-the-art amplifier modules. The full state control method was tested on a 1.9 MHz prototype amplifier and experimental results showed that frequency response ripples are effectively removed while THD+N levels down to 0.01 %.

To minimize losses in the switch-mode power audio amplifier an alternative power supply approach was proposed. This approach employed envelope tracking to track the amplifier input signal and adjust the supply voltage accordingly. Measured results on a 100 W prototype system, comprised of a multi-level power supply and a switch-mode audio power amplifier, showed that efficiency improvements up to a factor of 6 when playing real audio signals was detected. In addition to that the temperature rise in the amplifier was strongly reduced, especially for the switching devices where it was halved from 100°C to 50°C effectively increasing reliability and life span due to less thermal stress.

It was found that the total system efficiency is dominated by the loudspeaker efficiency, which is in the range 0.2 % to 2 %. It was found that the efficiency of the loudspeaker related to the voice coil fill factor. Experimental results showed a 10 % point efficiency

improvement when increasing the fill factor from 45 % to 53 %. In addition to that it was found that by increasing fill factor using a rectangular winding layout result in a lower nominal resistance of the loudspeaker. This had a positive effect on a system level as it allows the amplifier to deliver more power from the same supply level. Measured results showed that by using a 1 Ω load resistance instead of a conventional 4 Ω the efficiency is improved 10 % at 1 W output power. This improvement can even be greater in system normally relying on a boost converter, such as automotive systems, as the low load resistance eliminates the need for supply voltage boosting. Measured results demonstrated more than 20 % point efficiency improvement at 1 W output power for such systems.

The main research contributions is summarized below:

- A new test signal. The signal represents the dynamics of music almost a factor seven more precisely than conventional sine waves. Using it for efficiency tests of amplifiers affects the choice of components when compared to a conventional sine wave test and 10 % point efficiency improvement is demonstrated.
- A new voice coil design method. Analysis shows that the relationship between voice coil fill factor and loudspeaker efficiency is proportional. Experimental results show a 25 % efficiency improvement when increasing the fill factor from 45 % to 53 %.
- A new amplifier switching strategy utilizing a high quality factor output filter is proposed. This strategy is beneficial for power dissipation in power stage switching devices when playing actual music. Using this strategy allows for high power density amplifiers up to 11.5 W/cm^3.
- An alternative method using full state control is proposed as a controller for amplifer power stages with high output filter quality factor. Experimental results on a 1.9 MHz prototype amplifier show that frequency response ripples are effectively removed while delivering THD+N levels down to 0.01 %.
- A Envelope Tracking power supply is proposed as a method to minimize amplifier loss and temperature while playing music. Measured results on a 100 W prototype system show up to a factor 6 efficiency improvement and a halving of the temperature, from 100 °C to 50 °C, when playing real audio tracks.

The findings of this thesis show that a high continuous output power is not a key parameter for music applications. The new test signal is currently under investigation by EPA U.S Energy Star program for use in test methods for standardization. High peak power is still needed for reproducing the peaks in dynamic audio signals. This points towards that future challenges in audio reproduction system design are high supply voltage levels and better loudspeaker efficiencies. In that sense this thesis have outlined methods to overcome future challenges.

Bibliography

[1] R. W. Erickson and D. Maksimovic, *Fundamentals of Power Electronics*. Kluwer Academic Publishers Group, 2001.

[2] K. Nielsen, "Audio power amplifier techniques with energy efficient power conversion," Ph.D. dissertation, Technical University of Denmark, Department of Electrical Engineering, 1998.

[3] A. Ikriannikov and N. A. Wilson, "New concept for class D audio amplifiers for lower cost and better performance," *IEEE Transactions on Consumer Electronics*, vol. 57, no. 3, pp. 1218–1226, August 2011.

[4] B. Putzeys, "Simple self-oscillating class D amplifier with full output filter control," in *Audio Engineering Society Convention 118*, May 2005. [Online]. Available: http://www.aes.org/e-lib/browse.cfm?elib=13169

[5] S. Poulsen, "Towards active transducers," Ph.D. dissertation, Technical University of Denmark, Department of Electrical Engineering, 2004.

[6] M. C. W. Høyerby, "High-performance control in radio frequency power amplification systems," Ph.D. dissertation, Technical University of Denmark, Department of Electrical Engineering, 2008.

[7] S. Poulsen and M. A. E. Andersen, "Simple PWM modulator topology with excellent dynamic behavior," in *Applied Power Electronics Conference and Exposition, 2004. APEC '04. Nineteenth Annual IEEE*, vol. 1, 2004, pp. 486–492 Vol.1.

[8] M. C. W. Høyerby and M. A. E. Andersen, "Carrier distortion in hysteretic self-oscillating class-D audio power amplifiers: Analysis and optimization," *IEEE Transactions on Power Electronics*, vol. 24, no. 3, pp. 714–729, March 2009.

[9] M. A. E. Andersen and M. C. W. Høyerby, "Derivation and analysis of a low-cost, high-performance analogue bpcm control scheme for class-D audio power amplifiers," in *Audio Engineering Society Conference: 27th International Conference: Efficient Audio Power Amplification*, Sep 2005. [Online]. Available: http://www.aes.org/e-lib/browse.cfm?elib=13260

[10] S. H. Lee, J. Y. Shin, H. Y. Lee, H. J. Park, K. L. Lund, K. Nielsen, and J. W. Kim, "A 2W, 92% efficiency and 0.01% THD+N class-D audio power amplifier for mobile applications, based on the novel SCOM architecture," in *Proceedings of the IEEE 2004 Custom Integrated Circuits Conference (IEEE Cat. No.04CH37571)*, Oct 2004, pp. 291–294.

[11] S. C. Choi, J. W. Lee, W. K. Jin, J. H. So, and S. Kim, "A design of a 10-w single-chip class D audio amplifier with very high efficiency using cmos technology," *IEEE Transactions on Consumer Electronics*, vol. 45, no. 3, pp. 465–473, Aug 1999.

[12] M. A. Rojas-Gonzalez and E. Sanchez-Sinencio, "Design of a class D audio amplifier ic using sliding mode control and negative feedback," *IEEE Transactions on Consumer Electronics*, vol. 53, no. 2, pp. 609–617, May 2007.

[13] M. Høyerby, J. K. Jakobsen, J. Midtgaard, and T. H. Hansen, "A 2 x 70 W monolithic five-level class-D audio power amplifier in 180 nm BCD," *IEEE Journal of Solid-State Circuits*, vol. 51, no. 12, pp. 2819–2829, Dec 2016.

[14] *MA12040 - Filterless and High-Efficiency +4V to +18V Audio Amplifier with Analog Input*, Merus Audio, 2017.

[15] *TPA3116D2 15-W, 30-W, 50-W Filter-Free Class-D Stereo Amplifier Family With AM Avoidance*, Texas Instruments, 2017.

[16] *UCD180LP - High Efficiency Power Amplifier Module (Low Profile OEM Version)*, Hypex. [Online]. Available: https://www.hypex.nl/product/ucd180lp-oem/55#tab_specifications

[17] M. P. Madsen, "Very high frequency switch-mode power supplies," Ph.D. dissertation, Technical University of Denmark, Department of Electrical Engineering, 2015.

[18] M. Madsen, A. Knott, and M. A. E. Andersen, "Low power Very High Frequency switch-mode power supply with 50 V input and 5 V output," *IEEE Transactions on Power Electronics*, vol. 29, no. 12, pp. 6569–6580, Dec 2014.

[19] J. A. Pedersen, M. P. Madsen, J. D. MÃÿnster, T. Andersen, A. Knott, and M. A. E. Andersen, "US mains stacked Very High Frequency self-oscillating resonant power converter with unified rectifier," in *2016 IEEE Applied Power Electronics Conference and Exposition (APEC)*, March 2016, pp. 1842–1846.

[20] A. D. Sagneri, D. I. Anderson, and D. J. Perreault, "Optimization of integrated transistors for Very High Frequency DC-DC converters," *IEEE Transactions on Power Electronics*, vol. 28, no. 7, pp. 3614–3626, July 2013.

[21] A. Lidow, J. Strydom, M. de Rooij and D. Reusch, *GaN Transistors for Efficient Power Conversion*. John Wiley and Sons, 2014.

[22] D. Reusch, "Impact of parasitics on performance," EPC white paper, 2013.

[23] J. Strydom and D. Reusch, "Dead-time optimization for maximum efficiency," EPC white paper, 2013.

[24] A. Lidow and J. Strydom, "eGan FET drivers and layout considerations," EPC white paper, 2012.

[25] D. Reusch, "Optimizing PCB layout," EPC white paper, 2014.

[26] M. Duraij, N. E. Iversen, L. P. Petersen, and P. Boström, "Self-oscillating 150 W switch-mode amplifier equipped with egan-fets," in *Audio Engineering Society Convention 139*, Oct 2015. [Online]. Available: http://www.aes.org/e-lib/browse.cfm?elib=17936

[27] R. O. Ploug, A. Knott, and S. B. Poulsen, "Gan power stage for switch mode audio amplification," in *Audio Engineering Society Convention 138*, May 2015. [Online]. Available: http://www.aes.org/e-lib/browse.cfm?elib=17697

[28] J. Chung, R. McKenzie, and W. T. Ng, "A comparison between gan and silicon based class D audio power amplifiers with pulse density modulation," in *2016 13th IEEE International Conference on Solid-State and Integrated Circuit Technology (ICSICT)*, Oct 2016, pp. 90–93.

[29] J. Jensen, "Nonlinear distortion mechanisms and efficiency of balanced-armature loudspeakers," Ph.D. dissertation, Technical University of Denmark, Department of Electrical Engineering, 2014.

[30] J. W. Marshall Leach, *Introduction to Electroacoustics and Audio Amplifier Design*. Kendall/Hunt Publishing Company, 2003.

[31] H. F. Olson, *Acoustical Engineering*. Van Nostrand, 1957.

[32] R. H. Small, "Closed-box loudspeaker systems-part 1: Analysis," *J. Audio Eng. Soc*, vol. 20, no. 10, pp. 798–808, 1972. [Online]. Available: http://www.aes.org/e-lib/browse.cfm?elib=2022

[33] R. H. Small, "Closed-box loudspeaker systems-part 2: Synthesis," *J. Audio Eng. Soc*, vol. 21, no. 1, pp. 11–18, 1973. [Online]. Available: http://www.aes.org/e-lib/browse.cfm?elib=2011

[34] N. Thiele, "Loudspeakers in vented boxes: Part 1," *J. Audio Eng. Soc*, vol. 19, no. 5, pp. 382–392, 1971. [Online]. Available: http://www.aes.org/e-lib/browse.cfm?elib=2173

[35] R. Tiwari. (2014) Bluetooth speakers market worth $7 billion by 2019. [Online]. Available: https://www.prnewswire.com/news-releases/bluetooth-speakers-market-worth-7-billion-by-2019-283587821.html

[36] A. M. S. S. Andrade, E. Mattos, L. Schuch, H. L. Hey, and M. L. S. Martins, "Synthesis and comparative analysis of very high step-up dc-dc converters adopting coupled inductor and voltage multiplier cells," *IEEE Transactions on Power Electronics*, vol. PP, no. 99, pp. 1–1, 2017.

[37] M. C. Mira, A. Knott, and M. A. E. Andersen, "A three-port topology comparison for a low power stand-alone photovoltaic system," in *2014 International Power Electronics Conference (IPEC-Hiroshima 2014 - ECCE ASIA)*, May 2014, pp. 506–513.

[38] R. Pittini, M. C. Mira, Z. Zhang, A. Knott, and M. A. E. Andersen, "Analysis and comparison based on component stress factor of dual active bridge and isolated full bridge boost converters for bidirectional fuel cells systems," in *2014 International Power Electronics and Application Conference and Exposition*, Nov 2014, pp. 1026–1031.

[39] J. H. Davis, "Methods of applied mathematics with a software overview," *Methods of Applied Mathematics With a Software Overview*, pp. 5–684, 2016.

[40] I. Electrotechnical Commission, "Iec 268-1 sound system equipment, part 1: General," 1985.

[41] P. J. Chapman, "Programme material analysis," in *Audio Engineering Society Convention 100*, May 1996. [Online]. Available: http://www.aes.org/e-lib/browse.cfm?elib=7501

[42] M. Mijic, D. Masovic, D. Sumarac Pavlovic, and M. Petrovic, "Statistical properties of music signals," in *Audio Engineering Society Convention 126*, May 2009. [Online]. Available: http://www.aes.org/e-lib/browse.cfm?elib=14898

[43] R. A. R. van der Zee and A. J. M. van Tuijl, "Test signals for measuring the efficiency of audio amplifiers," in *Audio Engineering Society Convention 104*, May 1998. [Online]. Available: http://www.aes.org/e-lib/browse.cfm?elib=8532

[44] R. Bakker and M. Duffy, "Maximising the efficiency of a class-D audio amplifier output stage," in *2017 28th Irish Signals and Systems Conference (ISSC)*, June 2017, pp. 1–5.

[45] N. E. Iversen and A. Knott, "Small signal loudspeaker impedance emulator," *J. Audio Eng. Soc*, vol. 62, no. 10, pp. 676–682, 2014. [Online]. Available: http://www.aes.org/e-lib/browse.cfm?elib=17545

[46] N. E. Iversen and A. Knott, "Loudspeaker impedance emulator for multi resonant systems," in *Audio Engineering Society Convention 138*, May 2015. [Online]. Available: http://www.aes.org/e-lib/browse.cfm?elib=17713

[47] J. Jensen, "A new method for evaluating loudspeaker efficiency in the frequency domain," in *Audio Engineering Society Convention 131*, Oct 2011. [Online]. Available: http://www.aes.org/e-lib/browse.cfm?elib=16590

[48] P. Brunet, "Nonlinear system modeling and identification of loudspeakers," Ph.D. dissertation, Northeastern University, Boston, Massachusetts, 2014.

[49] F. S. Madsen, S. Thorsen, N. E. Iversen, and A. Knott, "Model for evaluation of power consumption of vented box loudspeakers," in *Audio Engineering Society Convention 142*, May 2017. [Online]. Available: http://www.aes.org/e-lib/browse.cfm?elib=18601

[50] W. Klippel, "Loudspeaker nonlinearities âĂŞ causes, parameters, symptoms," in *Audio Engineering Society Convention 119*, Oct 2005. [Online]. Available: http://www.aes.org/e-lib/browse.cfm?elib=13346

[51] A. W. King and F. T. Agerkvist, "Position dependence of fractional derivative models for loudspeaker voice coils with lossy inductance," in *Audio Engineering Society Convention 142*, May 2017. [Online]. Available: http://www.aes.org/e-lib/browse.cfm?elib=18600

[52] L. Risbo, F. T. Agerkvist, C. Tinggaard, M. Halvorsen, and B. Putzeys, "Force factor modulation in electro dynamic loudspeakers," in *Audio Engineering Society Convention 141*, Sep 2016. [Online]. Available: http://www.aes.org/e-lib/browse.cfm?elib=18411

[53] M. Halvorsen, C. Tinggaard, and F. T. Agerkvist, "Flux modulation in the electrodynamic loudspeaker," in *Audio Engineering Society Convention 138*, May 2015. [Online]. Available: http://www.aes.org/e-lib/browse.cfm?elib=17741

[54] *5FE100 - 5" Low frequency driver*, faitalPro. [Online]. Available: http://www.faitalpro.com/en/products/LF_Loudspeakers/product_details/index.php?id=401010100

[55] *Definimax 4018LF - 18" Low frequency driver*, Eminence. [Online]. Available: http://www.eminence.com/pdf/Definimax_4018LF.pdf

[56] *TC6FC00-04 - 2" Full range driver*, Peerless by Tymphany. [Online]. Available: https://www.tymphany.com/wp-content/themes/pathfinders/specsheet.php?id=665

[57] *F118 MK2 - 18" Horn loaded driver*, Funktion-One.

[58] *Illiminator - 3/4" dome tweeter*, Scan speak. [Online]. Available: http://www.scan-speak.dk/datasheet/pdf/d2004-602000.pdf

[59] T. Instruments, "Design considerations for class-D audio power amplifiers," Tech. Rep., 1999.

[60] N. E. Iversen, A. Knott, and M. A. E. Andersen, "Efficiency of switch-mode power audio amplifiers - Test signals and measurement techniques," in *Audio Engineering Society Convention 140*, May 2016. [Online]. Available: http://www.aes.org/e-lib/browse.cfm?elib=18198

[61] N. E. Iversen, N. J. Dahl, A. Knott, and M. A. E. Andersen, "Towards high power density audio amplifiers," *Submitted for Journal of Audio Engineering Society*, march, 2018.

[62] Y. H. Liu, "Novel modulation strategies for class-D amplifier," *IEEE Transactions on Consumer Electronics*, vol. 53, no. 3, pp. 987–994, Aug 2007.

[63] N. Dahl, N. E. Iversen, A. Knott, and M. A. E. Andersen, "Comparison of simple self-oscillating PWM modulators," in *Audio Engineering Society Convention 140*, May 2016. [Online]. Available: http://www.aes.org/e-lib/browse.cfm?elib=18260

[64] A. Knott, G. R. Pfaffinger, and M. A. E. Andersen, "A self-oscillating control scheme for a boost converter providing a controlled output current," *IEEE Transactions on Power Electronics*, vol. 26, no. 9, pp. 2707–2723, Sept 2011.

[65] S. Poulsen and M. A. E. Andersen, "Hysteresis controller with constant switching frequency," *IEEE Transactions on Consumer Electronics*, vol. 51, no. 2, pp. 688–693, May 2005.

[66] A. R. Oliva, S. S. Ang, and T. V. Vo, "A multi-loop voltage feedback filterless class-D switching audio amplifier using unipolar pulse-width-modulation," *IEEE Transactions on Consumer Electronics*, vol. 50, no. 1, pp. 312–319, Feb 2004.

[67] H. S. Kim, S. W. Jung, H. M. Jung, J. K. Shin, and P. Choi, "Low cost implementation of filterless class D audio amplifier with constant switching frequency," *IEEE Transactions on Consumer Electronics*, vol. 52, no. 4, pp. 1442–1446, Nov 2006.

[68] *Ferrites and Accessories*, Siemens Matsushita Components.

[69] M. Vasic, O. Garcia, J. A. Oliver, P. Alou, D. Diaz, and J. A. Cobos, "Multilevel power supply for high-efficiency rf amplifiers," *IEEE Transactions on Power Electronics*, vol. 25, no. 4, pp. 1078–1089, April 2010.

[70] A. I. Colli-Menchi, J. Torres, and E. Sanchez-Sinencio, "A feed-forward power-supply noise cancellation technique for single-ended class-D audio amplifiers," *IEEE Journal of Solid-State Circuits*, vol. 49, no. 3, pp. 718–728, March 2014.

[71] O. Jannerup and P. H. Maksimovic, *Regulerings Teknik*. Polyteknisk forlag, 2009.

[72] M. S. Duraj, "High freqeucny class D amplifier with eGaN-FETs," Master's thesis, Technical University of Denmark, Department of Electrical Engineering, 2015.

[73] R. O. Ploug, "Gan audio amplifier with advanced control and reduced output filter," Master's thesis, Technical University of Denmark, Department of Electrical Engineering, 2015.

[74] C. Neesgaard and L. Risbo, "PWM amplifier control loops with minimum aliasing distortion," in *Audio Engineering Society Convention 120*, May 2006. [Online]. Available: http://www.aes.org/e-lib/browse.cfm?elib=13497

[75] B. Halcro, "Low distortion class-D amplifier using carrier reference signal symmetry modulation," 2004, WO 2004/073161.

[76] *UCD400LP - High Efficiency Power Amplifier Module (Low Profile OEM Version)*, Hypex.

[77] M. C. Mira, Z. Zhang, A. Knott, and M. A. E. Andersen, "Power flow control of a dual-input interleaved buck/boost converter with galvanic isolation for renewable energy systems," in *2015 IEEE Applied Power Electronics Conference and Exposition (APEC)*, March 2015, pp. 3007–3012.

[78] A. Knott, T. M. Andersen, P. Kamby, J. A. Pedersen, M. P. Madsen, M. Kovacevic, and M. A. E. Andersen, "Evolution of very high frequency power supplies," *IEEE Journal of Emerging and Selected Topics in Power Electronics*, vol. 2, no. 3, pp. 386–394, Sept 2014.

[79] M. Madsen, A. Knott, and M. A. E. Andersen, "Low power very high frequency switch-mode power supply with 50 v input and 5 v output," *IEEE Transactions on Power Electronics*, vol. 29, no. 12, pp. 6569–6580, Dec 2014.

[80] M. Vasic, O. Garcia, J. A. Oliver, P. Alou, D. Diaz, R. Prieto, and J. A. Cobos, "Envelope amplifier based on switching capacitors for high-efficiency rf amplifiers," *IEEE Transactions on Power Electronics*, vol. 27, no. 3, pp. 1359–1368, March 2012.

[81] *Test Report PMP9491*, Texas Instruments, 2015.

[82] *PMP20195 Test Results*, Texas Instruments, 2016.

[83] P. Ljusev and M. A. E. Andersen, "Four-quadrant flyback converter for direct audio power amplification," in *2005 European Conference on Power Electronics and Applications*, Sept 2005, pp. 10 pp.–P.

[84] *ICEpower100AS1/2 - One and Two Channel 100 W ICEpower Amplifiers with Integrated Universal Mains Power Supply*, ICEpower, 2016. [Online]. Available: https://icepower.dk/products/amplifier-power-modules/as-series/

[85] *ICEpower300AS1 - 300W ICEpower Amplifier with Integrated Power Supply*, ICEpower, 2016. [Online]. Available: https://icepower.dk/products/amplifier-power-modules/as-series/

[86] N. Iversen, T. Birch, and A. Knott, "Utilization of non-linear converters for audio amplification," in *Audio Engineering Society Conference: 48th International Conference: Automotive Audio*, Sep 2012. [Online]. Available: http://www.aes.org/e-lib/browse.cfm?elib=16426

[87] S. Cuk and W. Erickson, "A conceptually new high-frequency switched-mode power amplifier technique eliminates current ripple," in *Proceedings of Powercon5*, May 1978, pp. G3.1–G3.22.

[88] D. J. T.C. Carusone and K. Martin, *Analog Integrated Circuit Design.* John Wiley and Sons, 2012.

[89] *Agilent 34401A Multimeter, User's guide*, Agilent Technologies.

[90] N. E. Iversen, A. Knott, and M. A. E. Andersen, "Low impedance voice coils for improved loudspeaker efficiency," in *Audio Engineering Society Convention 139,* ***Best Student Technical Papers Award***, Oct 2015. [Online]. Available: http://www.aes.org/e-lib/browse.cfm?elib=17946

[91] N. E. Iversen, A. Knott and M. A. E. Andersen, "Relationship between voice coil fill factor and loudspeaker efficiency," *J. Audio Eng. Soc*, vol. 64, no. 4, pp. 241–252, 2016. [Online]. Available: http://www.aes.org/e-lib/browse.cfm?elib=18132

[92] S. Poulsen and M. A. E. Andersen, "Practical considerations for integrating switch mode audio amplifiers and loudspeakers for a higher power efficiency," in *Audio Engineering Society Convention 116*, May 2004. [Online]. Available: http://www.aes.org/e-lib/browse.cfm?elib=12682

[93] D. K. Cheng, *Field and Wave Electromagnetics.* Addison-Wesley publishing company, 1989.

[94] *Operating instructions, PG-S balances (0.001g, 0.01g)*, Mettler Toledo.

[95] N. Dahl, N. Iversen, A. Knott, and M. A. E. Andersen, "Optimal control of a high frequency class-D amplifier," *J. Audio Eng. Soc*, vol. 66, no. 1/2, pp. 34–43, 2018. [Online]. Available: http://www.aes.org/e-lib/browse.cfm?elib=19374

[96] K. S. Meyer, M. A. E. Andersen, and F. Jensen, "Parameterized analysis of zero voltage switching in resonant converters for optimal electrode layout of piezoelectric transformers," in *2008 IEEE Power Electronics Specialists Conference*, June 2008, pp. 2543–2548.

[97] T. Andersen, "Piezoelectric transformer based power supply for dielectric electro active polymers," Ph.D. dissertation, Technical University of Denmark, Department of Electrical Engineering, 2012.

[98] *OptiMOS*^{TM} *Power-Transistor, BSZ150N10LS3*, Infineon, 2013.

[99] S. A. Lindiya, K. Vijayarekha, and S. Palani, "Deterministic LQR controller for dc-dc buck converter," in *Power and Energy Systems: Towards Sustainable Energy (PESTSE), 2016 Biennial International Conference on.* IEEE, 2016, pp. 1–6, https://doi.org/10.1109/PESTSE.2016.7516450.

[100] E. Hendricks, O. Jannerup, and P. H. Sørensen, *Linear systems control: deterministic and stochastic methods*. Springer Science & Business Media, 2008, https://doi.org/10.1007/978-3-540-78486-9.

[101] N. Dahl, N. E. Iversen, and A. Knott, "Optimal modulator with loudspeaker parameter inclusion," in *Audio Engineering Society Convention 143*, Oct 2017. [Online]. Available: http://www.aes.org/e-lib/browse.cfm?elib=19221

[102] N. E. Iversen, V. Lazarevic, M. Vasic, A. Knott, M. A. E. Andersen, and J. A. Cobos, "Multilevel tracking power supply for switch-mode audio power amplifiers," in *2018 International Power Electronics and Application Conference and Exposition (APEC)*, 2018.

[103] N. E. Iversen, H. Schneider, A. Knott, and M. A. E. Andersen, "Efficiency investigation of switch-mode power audio amplifiers driving low impedance transducers," in *Audio Engineering Society Convention 139*, Oct 2015. [Online]. Available: http://www.aes.org/e-lib/browse.cfm?elib=17935

[104] Q. Jin, M. Vasic, O. Garcia, P. Alou, J. A. Oliver, and J. A. Cobos, "Optimized design of gan switching capacitor based envelope tracking power supply for satellite applications," in *2016 IEEE Applied Power Electronics Conference and Exposition (APEC)*, March 2016, pp. 2409–2414.

[105] V. Lazarevic, M. Vasic, O. Garcia, Q. Jin, P. Alou, J. A. Oliver, and J. A. Cobos, "A comparative analysis of two approaches in eer based envelope tracking power supplies," in *2017 IEEE Applied Power Electronics Conference and Exposition (APEC)*, March 2017, pp. 3252–3258.

[106] Z. Wang, "Envelope tracking power amplifiers for wireless communications," Artech House, 2014, Boston.

[107] V. Yousefzadeh, E. Alarcon, and D. Maksimovic, "Three-level buck converter for envelope tracking applications," *IEEE Transactions on Power Electronics*, vol. 21, no. 2, pp. 549–552, March 2006.

[108] L. R. Kahn, "Single-sideband transmission by envelope elimination and restoration," *Proceedings of the IRE*, vol. 40, no. 7, pp. 803–806, July 1952.

[109] A. Yamauchi, H. Schneider, A. Knott, I. H. H. Jørgensen, and M. A. E. Andersen, "Investigation of energy consumption and sound quality for class-D audio amplifiers using tracking power supplies," in *Audio Engineering Society Convention 138*, May 2015. [Online]. Available: http://www.aes.org/e-lib/browse.cfm?elib=17711

[110] R. Bakker and M. Duffy, "Improving the efficiency of class-D audio amplifier systems using envelope tracking DC-DC power supplies," in *2018 International Power Electronics and Application Conference and Exposition (APEC)*, 2018.

[111] J. Angus, "Ultra efficient linear amplifiers," in *Audio Engineering Society Convention 142*, May 2017. [Online]. Available: http://www.aes.org/e-lib/browse.cfm?elib=18613

[112] EBU , "R 128: Loudness normalisation and permitted maximum level of audio signals," 2014.

[113] EBU , "Tech 3343: Loudness normalisation and permitted maximum level of audio signals," 2016.

[114] N. E. Iversen, R. Oortgiesen, A. Knott, M. A. E. Andersen, and M. Høyerby, "Design of efficient sound systems for low voltage battery driven applications," in *Audio Engineering Society Convention 141*, Sep 2016. [Online]. Available: http://www.aes.org/e-lib/browse.cfm?elib=18454

[115] N. J. Dahl, "Comparison of modulators for audio switch-mode power amplifiers," Internal DTU report, 2015.

[116] T. Thydal, N. E. Iversen, and A. Knott, "Efficiency investigation of subwoofer driven around resonance frequency," in *Audio Engineering Society Convention 142*, May 2017. [Online]. Available: http://www.aes.org/e-lib/browse.cfm?elib=18576

[117] S. Tengvall, N. E. Iversen, and A. Knott, "Design and implementation of a high efficiency subwoofer," in *Accepted for 144th Audio Engineering Soceity convention, Milan*, May 2018.

[118] T. Thydal, "Efficiency investigation of subwoofer driven around resonance frequency," Internal DTU report, 2016.

[119] S. Tengvall, "Desing and implementation of a high efficiency subwoofer," Internal DTU report, 2017.

[120] F. S. Madsen, "Model for evaluation of efficiency of switch-mode power audio amplifiers," Internal DTU report, 2016.

[121] S. Thorsen, "Model for evaluation of efficiency of switch-mode power audio amplifiers," Internal DTU report, 2016.

[122] N. E. Iversen and A. Knott, "Small-signal loudspeaker impedance emulator," in *Audio Engineering Society Convention 136,* ***Best Student Technical Papers Award***, Apr 2014. [Online]. Available: http://www.aes.org/e-lib/browse.cfm?elib=17200

[123] N. E. Iversen, "Review of potential loudspeaker impedance emulator implementations," Master's thesis, Technical University of Denmark, Department of Electrical Engineering, 2014.

[124] F. S. Madsen, N. J. Dahl, and M. R. Kramer, "Interaktivt dansegulv til strøm festival 2015," Internal DTU report, 2015.

[125] K. B. Andreas Stokholm, Jakob Bindslev and M. Braagaard, "Grønt lys pa roskilde festival," Internal DTU report, 2016.

A

Towards high power density audio amplifiers

Submitted for Journal of Audio Engineering Society, March, 2018

Towards higher power density amplifiers*

Niels E. Iversen, *AES Student Member*, **Nicolai J. Dahl,** *AES Student Member*, **Arnold Knott,** *AES Member*, **Michael A.E. Andersen,** *AES Member*,
(neiv@elektro.dtu.dk) (s134066@student.dtu.dk) (akn@elektro.dtu.dk) (mea@elektro.dtu.dk)

Technical University of Denmark, Kgs. Lyngby, Denmark

This paper proposes a new switching strategy for switch-mode power audio amplifiers beneficial for the power dissipation in the switching devices of the power stage. The strategy is based on a thorough analysis of the loss mechanism and operating conditions of the power stage and how they relate to the audio input. The strategy utilizes a high ripple current combined with full state control to improve soft switching capabilities. Measured results on 100 W test amplifiers show that the proposed strategy reduces the power dissipation within the switches causing up to 45°C reduction of the operating temperature while keeping low THD+N levels, down to 0.03 %. Power density of implemented amplifiers are 6 W/cm^3.

0 Introduction

Switch-mode technology has during the last decade become the conventional choice for audio amplification. This is due to the superior efficiency this technology offers compared with classical amplifier topologies as class-A and -AB. The efficiency of a switch-mode audio power amplifier (class-D) can theoretically reach an efficiency of 100%. In practice efficiencies well above 90 % have been achieved [1]. Furthermore the audio performance of these amplifiers have improved over time so that very low Total Harmonic Distortion plus Noise (THD+N) levels can be achieved [2, 3, 4, 5]. The high efficiency of switch-mode technology enables high power density amplifiers. This has resulted in a selection of integrated amplifiers for low- and mid-level output powers [6, 7, 8]. However for higher output powers ($\geq$100 W) integrated amplifiers as well as small packaged discrete switching devices become less viable as the power dissipation increases and thus the need for cooling. In previous work the power density has been improved by using Gallium Nitride (GaN) devices combined with high switching frequency thus minimizing the size of bulky components in the output filter [9]. However, by increasing the switching frequency more switching losses are introduced causing undesired high operating temperatures. In addition to this temperature changes can affect the audio performance [10]. Therefore the management of power dissipation remains the main challenge to overcome in order to increase the power density of audio amplifiers.

This paper will deal with this challenge by proposing an improved switching strategy utilizing a high output filter ripple current in conjunction with full state control [11] to improve soft switching capabilities while keeping good audio performance. The result is that the power dissipation is distributed more evenly across the different elements of the amplifier leading to a decrease of operating temperature in limiting parts of the power stage, i.e. the switching devices. The method is demonstrated on 100 W test amplifiers with low THD+N levels, down to 0.03 %. A temperature reduction of up to 45 °C on the switching devices is observed.

1 Switch-Mode Audio Power Amplifiers

This section presents the basic operation of switch-mode audio power amplifiers and their inherent loss mechanism. Moreover, the typical operating conditions of the amplifier, when playing music, will be analysed and based on this analysis an improved switching strategy will be proposed.

Switch-mode audio power amplifiers can be split into three essential blocks. They are:

- Modulator
- Power stage
- Output filter

The basic operation of the modulator is to generate a Pulse Width Modulated (PWM) signal representing the amplifier input. This is typically done by comparing the low frequency input signal (20 Hz to 20 kHz) with a high frequency carrier, typically of triangular shape, which generates a pulse train at a given frequency, the switching fre-

*Arnold Knott, e-mail: akn@elektro.dtu.dk

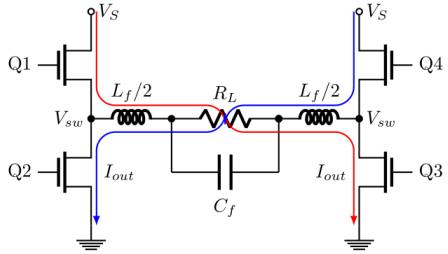

Figure 1: Full bridge configuration (BTL) of switch-mode audio power amplifier buck power stage.

quency. The length or on-time of the pulses is also known as the duty cycle, D, of the PWM signal. Modulators can also be of a self-oscillating topology (SO) where the carrier signal is generated directly from the input [12, 13, 14]. These type of modulators will generate a varying switching frequency which decreases as the level of modulation increases. The PWM signal is used to drive the switching power stage. The power stage is where the amplification takes place. The PWM representation of the input signal is amplified according to the amplifier gain. The output filter is used to suppress switching noise for Electro Magnetic Interference (EMI) reasons.

1.1 Power stage

The power stage consists of switching devices which are switched on and off using the PWM signal. The most common switching device for switch-mode power applications is the Metal Oxide Semiconductor Field Effect Transistor (MOSFET). The power stage of switch-mode audio power amplifiers are typically using a buck topology. This topology can be realized either in a half- or full-bridge configuration. The half bridge requires a dual voltage supply while the full bridge only requires a single supply. This paper focuses on a full-bridge configuration also referred to as a Bridge Tied Load (BTL). Fig. 1 shows the full bridge configuration. Q1 to Q4 are the switching devices, L_f, C_f and the load impedance (here modelled as the resistor R_L) forms the output low pass filter attenuating the switching frequency on the output while V_{sw} denotes the switch-node voltages. The factor two division on the output filter inductance ensures that equations presented in this paper is equally valid for a half bridge configuration. The switches in the half bridges are driven 180° out of phase. The current flow is highlighted in Fig. 1 where the red line shows the current flow when Q1 and Q3 conduct and the blue line when Q2 and Q4 conduct. Note that opposed to conventional DC-DC converters the audio amplifier power stage needs to be synchronous rectified as the current should be able to flow in both directions through the load. To prevent an undesired short circuit through the half bridge a period where both switches are off should be implemented. This period is known as the dead time, t_{dt} [15].

The buck topology is very attractive for audio applications due to an ideally linear transfer function which minimizes the distortion:

$$V_{out} = (2D-1)V_{DD}$$
$$I_{out} = \frac{V_{out}}{R_L} \quad (1)$$

Where V_{out} is the output voltage, D is the duty cycle, R_L is the load resistance and V_{DD} is the rail to rail voltage, i.e. $-V_S$ to V_S in half bridge- and ground to V_S in full bridge-configuration. The inductor in the output filter introduces a ripple. The magnitude of this ripple relates to the filter inductance, the switching frequency and the output voltage generated from one half bridge at a given duty cycle.

$$\Delta i_L = \frac{V_{DD}D(1-D)}{2L_f f_{sw}} \quad (2)$$

The four switches are not ideal and therefore the switch model shown in Fig. 2 is introduced. It includes the parasitic components which are the parasitic capacitances, C_{ds}, C_{gs} and C_{gd}, the on resistance R_{ds} and the drain to source body diode which will have a given forward voltage drop, V_f. There exists four different switching conditions which are relevant in order to estimate the losses in the power stage.

1. Hard switching occurs when the parasitic drain source capacitance, C_{ds}, of the switching device can not be charged/discharged by the inductor current I_L during the dead time period t_{dt}. This can either be due to a very small dead time period, a large parasitic capacitance or an insufficient inductor current. The switching node voltage, V_{sw}, will ramp up and down together with the drain current, I_D, in the switching device, causing switching losses.
2. Reduced Voltage Switching (RVS) and Zero Voltage Switching (ZVS), on the other hand occurs when the parasitic drain source capacitance of the switching device can be partially or completely charged/discharged by the inductor current during the dead time period minimizing switching losses.
3. When the ripple in the inductor current is larger than the output current, $\Delta i_L > |I_{out}|$, a situation can occur where the parasitic drain source capacitance is charged or discharged beyond the rail to rail voltage, V_{DD}. In this sit-

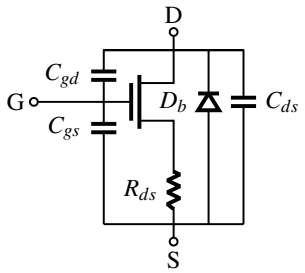

Figure 2: Switching device, e.g. MOSFET, including the parasitic on resistance, R_{ds}, the drain source capacitance, C_{ds}, the gate capacitances, C_{gs} and C_{gd} and the drain to source body diode, D_b. G = Gate, D = Drain and S = Source.

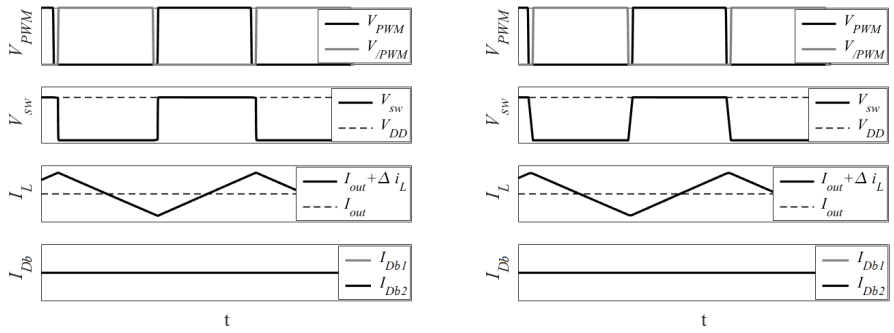

(a) Hard switching.

(b) Zero/Reduced Voltage Switching.

(c) Body diode conduction ($|I_{out}| < \Delta i_L$).

(d) Body diode conduction ($|I_{out}| > \Delta i_L$).

Figure 3: Waveforms in Buck power stage for different switching conditions. V_{PWM} is PWM gate signals, V_{SW} is switch-node voltage, I_L is inductor current and I_{Db} is body diode current.

uation the body diode of the switching device start conducting which causes some losses in the switching device due to the forward voltage drop of the body diode.

4. Finally, when the output current is larger than the ripple, $|I_{out}| > \Delta i_L$, the body diode of the switching device will continue conducting after turn off causing additional losses.

Fig. 3 shows the waveforms for the four described switching condition. Since the power stage is intended for audio use the duty cycle of the PWM signal driving the switching devices will vary according to the audio input. This means that power stage most likely will undergo all four switching conditions. This will be elaborated in section 1.4.

1.2 Output filter

As mentioned the output filter is formed by the filter inductor, L_f, the filter capacitance, C_f and the load impedance which can be simplified as a purely resistive load, R_L. The filter is a second order low pass filter with the simplified transfer function:

$$H_f(s) = \frac{1}{\left(\frac{s}{s_0}\right)^2 + \frac{1}{2Q}\left(\frac{s}{s_0}\right) + 1} \tag{3}$$

Where s is the Laplace operator, s_0 is the pole of the filter indicating the cut-off frequency, f_c, and Q is quality factor of the filter indicating how much the filter is dampened at its' resonance.

$$s_0 = \frac{1}{\sqrt{L_f C_f}} \tag{4}$$

$$f_c = \frac{s_0}{2\pi} \tag{5}$$

$$Q = \frac{R_e}{\sqrt{\frac{L_f}{C_f}}} = \frac{R_e}{2\pi 2 L_f f_c} \tag{6}$$

This resonance frequency is also commonly referred to as the cut-off frequency. It should be placed well below the switching frequency as the main purpose of the filter is to remove the switching transient from the output for efficiency and EMI reasons. The filter should have a flat frequency response in the audio bandwidth, i.e. 20 Hz to 20 kHz, while attenuating with 40 dB/decade above the cut-off frequency. The filter will have a quality factor, Q, which determines how much the filter is dampened at its resonance.

A high Q introduces a resonant peak in the filters frequency response as shown in Fig. 4. This peak is unwanted especially within the audio band thus conventional filter designs will aim for a maximum flat response, i.e. $Q = 0.7$ [16]. There exist parasitic components within the filter that

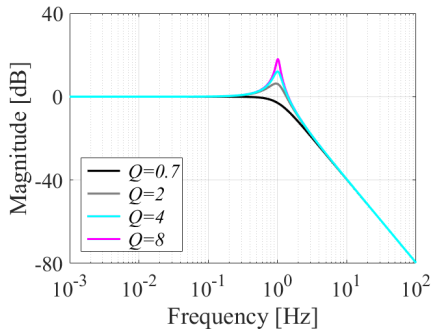

Figure 4: Frequency response of output filter for different quality factors.

will affect the filter characteristics. These parasitics include the series resistance, R_{Lf} and parallel capacitance, C_{Lf}, for the filter inductor and the equivalent series resistance and inductance, ESR and ESL, of the filter capacitance. Special care should be taken when choosing the filter capacitance due to the fact that its' ESR will introduce a zero placed at:

$$f_z = \frac{1}{2\pi C_f ESR} \tag{7}$$

If this zero is placed too close to the cut-off frequency it will affect the filter performance. First of all the roll off of the filter will be decreased from 40 to 20 dB/decade. Secondly the resonating current formed by the filter inductor and capacitance will be attenuated as the ESR will cause some power to be dissipated within the capacitance. For these two reasons the ESR of the capacitance should be kept to a minimum. This yields for a practical implementation using ceramic SMD capacitors. In the same manner the series resistance of the inductor will attenuate the resonating current as some power is dissipated. The series resistance is frequency dependent so it is important to ensure that the AC resistance is fairly low at the switching frequency to minimize losses. The parasitic capacitor of the inductor sets the self-resonance frequency, SRF, of the filter inductor which indicates when the inductor stops working inductive but instead becomes capacitive.

$$\mathrm{SRF}_{Lf} = \frac{1}{2\pi\sqrt{L_f C_{Lf}}} \tag{8}$$

Equally the equivalent series inductance of the capacitance generates a self-resonating frequency after which the capacitance becomes inductive.

$$\mathrm{SRF}_{Cf} = \frac{1}{2\pi\sqrt{C_f ESL}} \tag{9}$$

1.3 Loss mechanism

This section will describe loss mechanism related to the switching power stage and the output filter. The main loss mechanisms will be described and equations for estimating the losses presented.

1.3.1 Gate loss

Gate losses are generated by charging and discharging the gate capacitances, C_{gd} and C_{gs}, of the switching device. The needed charge is normally specified in transistor data sheet as the total gate charge, Q_g. The gate losses can be determined knowing the gate source voltage of the switching device, V_{gs}, and the switching frequency.

$$P_{gate} = Q_g V_{gs} f_{sw} \tag{10}$$

1.3.2 Conduction loss

Conduction losses are generated when the switching device is on. During this state the drain current, I_D, is flowing causing some power to be dissipated in the on resistance.

$$P_{cond} = I_D^2 R_{ds} \tag{11}$$

1.3.3 Switching loss

Switching losses occur during the switching events between the on and off states. The drain current is flowing during the on state while no current flows in the off state. This current ramps up and down and together with the drain source voltage this will cause power to be dissipated. This power is actually dissipated in the parasitic drain source capacitance of the switching device, C_{ds}, as it is charged/discharged by the drain current.

$$P_{sw} = 4\left(\frac{1}{2} C_{ds} V_{ds}^2 f_{sw}\right) \tag{12}$$

The factor four is introduced as the loss happens two times during one switching period, during rise and fall, and as the effective capacitance is doubled as two switches are tied to the switch-node. However, the switching loss can be minimized if the parasitic capacitances is charged/discharged by the instantaneous inductor current, $i_L(t)$, during the dead time period effectively reducing the drain source voltage, V_{ds}, facilitating RVS and ZVS.

$$V_{ds} = V_{DD} - V_{Cds} \tag{13}$$

Where V_{Cds} is the voltage over the parasitic capacitance. To facilitate ZVS for Q1 and Q3 in the full bridge shown in Fig. 1, V_{Cds} should be charged to the rail voltage prior to turn on and discharged to ground prior to turn off. V_{Cds} can be estimated knowing the charging current and the charge time which are the inductor current and the dead time period respectively. The instantaneous inductor current during the dead time period can be assumed to be the sum of the output current and the amplitude of the ripple.

$$i_L = I_{out} + \Delta i \tag{14}$$

The voltage over the parasitic capacitance thus become:

$$V_{Cds} = \frac{t_{dt} i_L}{2C_{ds}} \tag{15}$$

However, if the capacitance voltage theoretically can be charged beyond the sum of the rail to rail voltage and the forward voltage drop in the diode, the body diode will start conducting thus clamping the voltage to $V_{DD} + V_f$. The same relation applies for discharging where the capacitance will be clamp to $-V_f$. Thus the voltage over the

parasitic capacitance can be described as:

$$V_{Cds} = \begin{cases} -V_f & \forall \frac{t_{dt} i_L}{2C_{ds}} < -V_f \\ V_{DD} + V_f & \forall \frac{t_{dt} i_L}{2C_{ds}} > V_{DD} + V_f \\ \frac{t_{dt} i_L}{2C_{ds}}, & \text{otherwise} \end{cases} \quad (16)$$

1.3.4 Reverse conduction loss

This loss occur in the situation where the body diode in the switching device starts or continues conducting the instantaneous inductor current during the dead time period. Due to the forward voltage drop in the body diode some power will be dissipated.

$$P_{reverse} = i_L V_f t_{cond} f_{sw} \quad (17)$$

t_{cond} denotes the conducting period of the body diode. This period depends on the charge/discharge time of the drain source capacitance. The conduction period can be described as:

$$t_{cond} = \begin{cases} t_{dt} - \left| \frac{(V_{DD}+V_f)2C_{ds}}{i_L} \right| & \forall \left| \frac{t_{dt} i_L}{2C_{ds}} \right| > V_{DD} + V_f \\ 0 & \text{otherwise} \end{cases} \quad (18)$$

1.3.5 Filter loss

The loss in the output filter is mainly due to the filter inductance. These losses can be separated into winding losses and core losses.

$$P_{Lf} = P_{winding} + P_{core} \quad (19)$$

The winding losses can furthermore be separated into DC and AC losses.

$$P_{wire} = I_L^2 (R_{DC} + R_{AC}) \quad (20)$$

The core losses relates to the core material and the flux, B, in it. The flux should be kept at a level so that the core does not saturate. In the case of an air core inductor the core is lossless. Core losses can be estimated quite well [17]. However, this paper assumes core losses to be a fraction of the wire losses for simplification.

1.3.6 Total loss

The total loss can now be expressed as the sum of the different loss components:

$$P_{tot} = P_{gate} + P_{cond} + P_{sw} + P_{reverse} + P_{Lf} \quad (21)$$

For maximum output power the conduction losses, P_{cond} and the filter losses, P_{Lf}, will normally be the dominant losses. In that sense these losses limit the maximum efficiency. However, in idle operation, or close to idle operation, where the output power is low, the losses related to the parasitic capacitances become significant, i.e. P_{gate} and P_{sw}. The reverse conduction losses are normally negligible, due to the fact that the forward voltage drop of the body diode and its' conduction time in many cases is rather small. Keeping this in mind switching scenario shown in Fig. 3(c) will in many cases only cause very low switching losses since the voltage over the device is equal to the forward voltage of the body diode. However, if the output current is large a significant loss can be generated. For amplifiers with high output power the switching losses can become challenging since the supply voltage increases. Significant switching losses will heat up the device and ultimately destroy it if the heat is not dissipated elsewhere. Cooling fans can be used to secure safe operation however they increase the overall size and cost of the amplifier and produce undesired audible noise. In section 1.5 alternative method of dealing with this challenge will be presented.

1.4 Audio dynamics

The input signal to the audio amplifier is naturally a dynamic audio signal. For test purposes sine waves are a commonly used signal. However, sine waves do not represent real audio signals [18, 19, 20, 21]. In previous work a large music library have been analysed in terms of amplitude distribution [21]. Fig. 5 shows the amplitude distribution of a sine wave and the audio tracks from the music library. With the 90 % distributions marked for comparison it is clear that there exists a fundamental difference between real audio signals and sine waves. As shown in Fig. 5 the amplitude distribution can be directly translated into a duty cycle distribution when a linear input to output transfer function is assumed. It is observed that when playing maximum output power a sine wave signal will utilize almost full modulation 90 % of the time while real music in average only utilize one third of that. This should be kept in mind when designing the power stage. Though the amplifier should be able to handle full power sine waves for short periods of time it make sense to optimize switching conditions of the power stage for real use with audio.

1.5 Improved switching strategy

Switching losses can be of significant magnitude even at low power causing the temperature of the switching device to rise eventually destroying it. Therefore it is relevant to secure that ZVS, RVS and body diode conduction are the most typical switching conditions, shown in Fig. 3(b) and 3(c), as the switching losses in theses cases will be fairly low. From Fig. 5 the 90 % duty cycle distribution

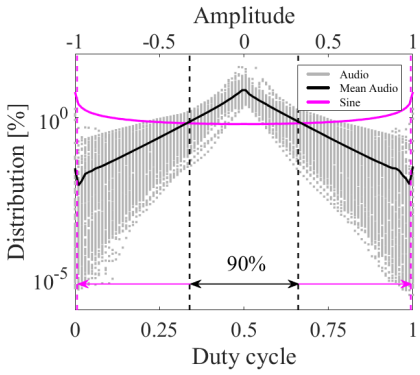

Figure 5: Amplitude and duty cycle distribution for audio tracks and sine wave.

span for real music can be evaluated to be from $D = 0.34$ to $D = 0.66$. Optimizing the switching condition for this duty cycle span will decrease the switching losses, and thus also the temperature of the switching device securing a more robust design.

To facilitate ZVS and RVS for a given duty cycle span the reactive ripple current in the output filter inductor must be dimensioned so that the ripple current is larger than continuous output current for all duty cycles within that span. That is $\Delta i > I_{out}$. This requirement can be written using (1) and (2).

$$\frac{V_{DD}D(1-D)}{2L_f f_{sw}} > \frac{(2D-1)V_S}{R_L} \tag{22}$$

Examining the above equation it is realized that as the duty cycle moves away from idle, $D = 0.5$, the ripple current will decrease for a power stage with a fixed switching frequency. This makes it challenging to facilitate ZVS and RVS over a large duty cycle span. Therefore a self-oscillating modulation scheme should be preferred since the switching frequency will decrease with the level of modulation [12]. In fact it can be shown that the ripple current will be more or less constant for all duty cycles using self-oscillating modulators. Shaping the ripple current's amplitude can be done by adjusting the quality factor of the output filter according to (2) and (6). Fig. 6 illustrates how the ZVS/RVS region increases with higher quality factors and a self-oscillating modulation scheme as it shows the ratio between the ripple- and the continuous output-current vs. duty cycle for various quality factors for both conventional fixed frequency- and self-oscillating-modulation. As long as the ratio is larger than one (22) is satisfied and RVS and ZVS can in principle be facilitated on all switching devices. A high ripple current increases the AC losses in the filter inductor increasing their temperature. However, it is expected that the heat capacity of the inductors normally will be much larger than that of the switching devices due to their physical size. For that reason it makes sense to dissipate some extra energy in the inductors to lower the power dissipation in the switches. The

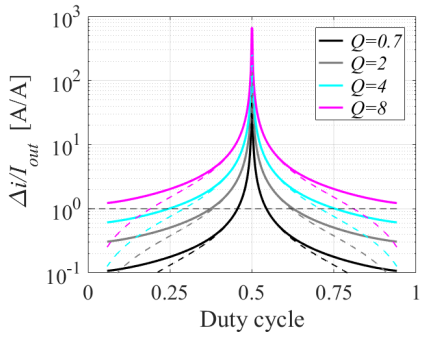

Figure 6: Ratio between ripple- and continuous output-current vs. duty cycle current for various quality factors. Self-oscillating modulation (solid) and fixed frequency modulation (dashed).

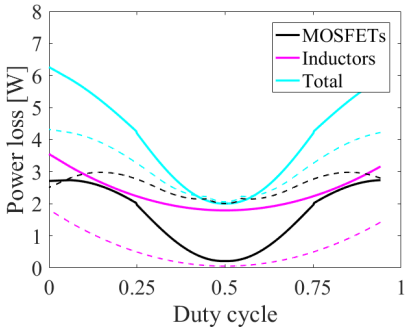

Figure 7: Estimated amplifier losses. Proposed amplifier (solid) and prior art amplifier (dashed).

amount of soft switching present in the individual power stage switch can be expressed as a soft switching factor, V_P [22, 23]. For the switches in the amplifier power stage the soft switching factor can be written as:

$$V_P = \frac{V_{Cds}}{V_S} = \frac{t_{dt} i_L}{2C_{ds}V_s} \tag{23}$$

To control amplifiers using this switching strategy full state control can be used. Full state control is preferred over classical output control, such as PI and PID regulators, as it provides control of system pole placement [11]. This is a desired feature for a switch-mode power audio amplifier with a high filter quality factor as the resonant peak in the transfer function can be effectively removed while keeping good audio performance.

2 Design and Implementation

Two amplifiers were designed and implemented on two layer 4 x 5 cm^2 Printed Circuit Boards (PCBs). The amplifiers are identical in their structure and use same topology for modulator, power stage, output filter and control and can deliver a continuous output power of 100 W. The boxed volume power density is 6 W/cm^3. The specifications of the amplifiers are shown in Table 1. Both amplifiers use a self-oscillating modulator and full state control. The states

Table 1: Specifications of implemented amplifiers

	Prior art	**Proposed**	
Cutoff frq (f_c)	40	40	kHz
Filter ind. (L_f)	23	4	μH
Filter cap. (C_f)	0.35	2	μF
Quality Factor (Q)	0.7	4	
Idle switch Frq (f_{sw})	500	500	kHz
Supply voltage (V_S)	50	50	V
Dead time (t_{dt})	10	10	ns
Gain (G)	32.5	32.5	dB
Load (R_L)	8	8	Ω
Power stage	BTL Buck	BTL Buck	
Modulation	SO	SO	
Control	Full state	Full state	

used for feedback in this implementation is the inductor current, I_L, the output current, I_{out}, and the output voltage, V_{out}. Both amplifiers use a 100V MOSFET from infineon in a small 3.2 X 3.2 mm^2 PG-TSDSON-8 package [24]. In addition to that the filter inductors of both amplifiers are wound with litz wire on RM7 cores using N87 material to keep the AC resistance as low as possible. The amplifiers differ on filter design where one use prior art methods, i.e. a low quality factor of $Q = 0.7$, while the other use the proposed switching strategy with a high quality factor of $Q = 4$. This difference makes a huge impact on the power losses in the amplifier. Fig. 7 shows the predicted losses in the proposed amplifier (solid line) and the prior art amplifier (dashed line). Even though the total losses are slightly higher in the proposed amplifier it is observed that power dissipation within the switching MOSFETs is reduced with a factor of two for duty cycles ranging from 0.34 to 0.66, corresponding to the 90 % distribution of average music, as explained in section 1.5. The reduction of power losses within the MOSFETs is expected to lower the operating temperature, especially for music signals. Fig. 8 shows one of the implemented amplifiers connected to a dedicated measurement board.

3 Measurements

A series of measurements has been performed on the implemented amplifiers to investigate their performance on key parameters. They include measurements of amplifier distortion, soft switching capabilities and operating temperatures.

3.1 Total Harmonic Distortion

Fig. 9 shows the measured Total Harmonic Distortion plus Noise (THD+N) vs. output power for a 100 Hz sine wave measured A-weighted with the UPP Audio Analyzer from Rohde & Schwarz. 100 Hz is used as it is a commonly used test frequency. Both amplifiers show excellent performance with THD+N down to 0.03% which is comparable to available consumer products [7, 8]. This demonstrates that full state control is applicable for audio applications.

3.2 Soft switching capabilities

The soft switching capabilities are measured by driving the power stage at fixed duty cycles and measuring the switching waveforms. Fig. 10(a) and 10(b) show the rising edge of the switching waveforms for both amplifiers. The voltage over the parasitic capacitance at the switching event is highlighted. This provides information concerning the soft switching capabilities on the high side MOSFET. Knowing the voltage over the parasitic capacitance the drain source voltage of the MOSFET and the soft switching factor can be found using (13) and (23). Fig. 10(c) and 10(d) shows improved soft switching capabilities in the proposed amplifier as ZVS and RVS are achieved for a larger duty cycle span. The measurements corresponds very well with predictions derived from (13), (16) and (23). The amplifiers are effectively hard switching at a soft switching factor of $V_P = 0\%$ and for the prior art amplifier this limit is found to be at 55% duty cycle while for the proposed amplifier it is at 75%. The measurements are performed for the high side MOSFETs but by assuming symmetry in the power stage design they are equally valid for the low side MOSFETs.

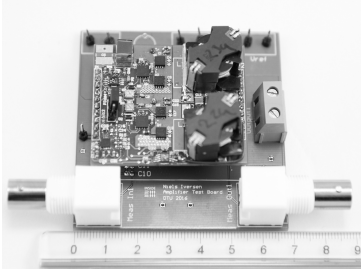

Figure 8: Realized switch-mode power audio amplifier.

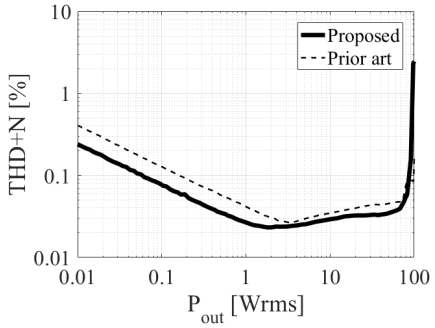

Figure 9: THD+N @100 Hz. Proposed amplifier (solid) and prior art amplifier (dashed).

3.3 Operating temperature

The operating temperature is measured when using a dynamic test signal, representing audio [21], and sine waves. Measurements were performed with the T650 SC thermal camera from FLIR. To ensure steady state conditions measurements was performed after 20 minutes of continuous operation. Fig. 11(a) and 11(b) show thermal pictures of the two amplifiers at full power using the dynamic test signal. The temperature of the switching MOSFETs are strongly reduced in the proposed amplifier ($\Delta T_{1-4} \approx 45°$C) while the output filter temperature is increased ($\Delta T_{5-6} \approx 13°$C) due to higher inductor losses. Fig. 11(c) and 11(d) show thermal pictures of the two amplifiers at a relative high power level, $P_{out} = 85$ W, using a sine wave signal. Is is seen that the temperatures of the switching MOSFETs are reduced in the proposed amplifier design ($\Delta T_{1-4} \approx 15°$C). This temperature reduction is less than observed for the dynamic test signal. This is expected as the switching strategy of the proposed amplifier is mainly designed for improving the switching losses for real audio signals as illustrated in Fig. 7. However a clear improvement is still observed.

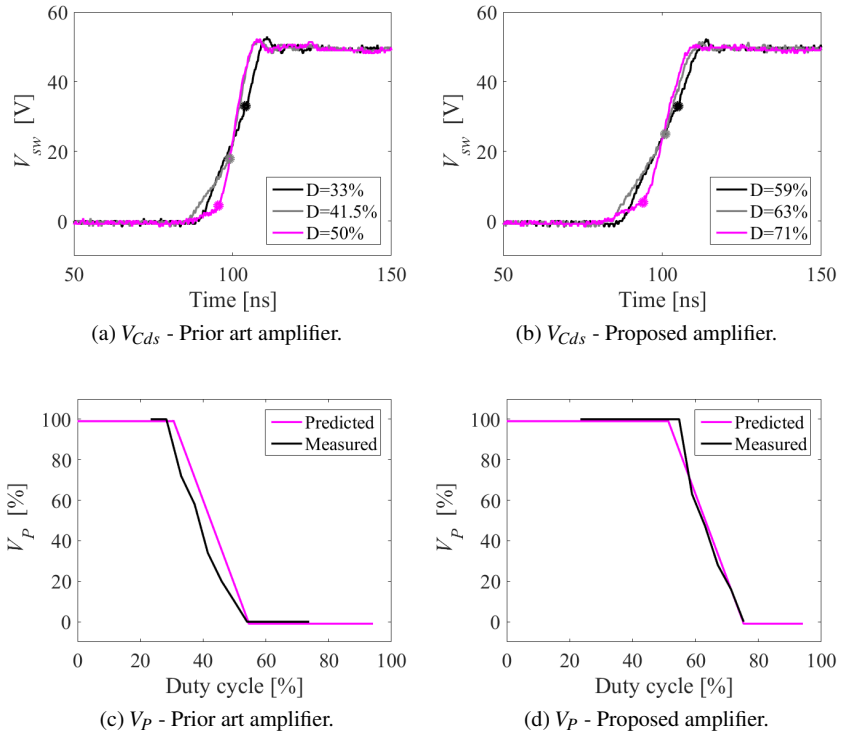

(a) V_{Cds} - Prior art amplifier.

(b) V_{Cds} - Proposed amplifier.

(c) V_P - Prior art amplifier.

(d) V_P - Proposed amplifier.

Figure 10: Measured soft switching capabilities.

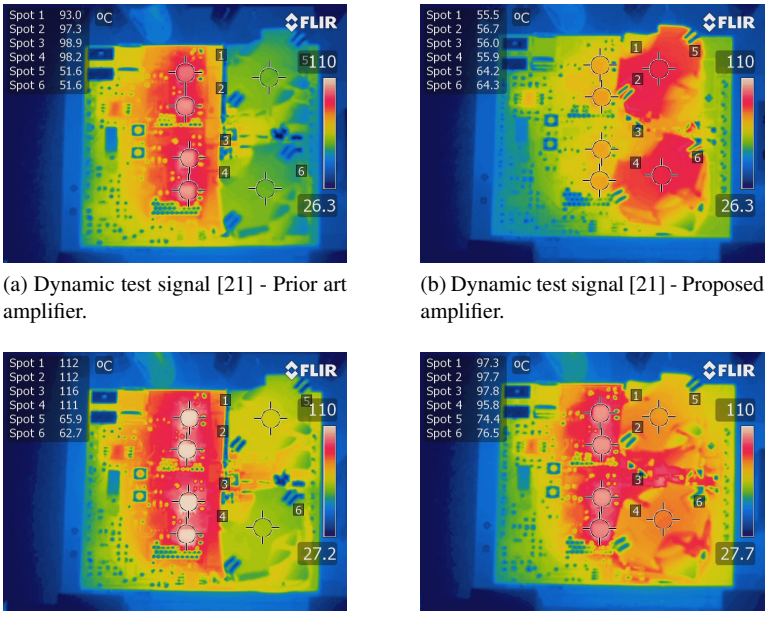

(a) Dynamic test signal [21] - Prior art amplifier.

(b) Dynamic test signal [21] - Proposed amplifier.

(c) Sine signal - Prior art amplifier.

(d) Sine signal - Proposed amplifier.

Figure 11: Temperatures of amplifiers after 20 minutes of operation. a) and b) uses dynamic test signal [21] at 300 Hz (P_{out} = 7.5 W). c) and d) uses 1000 Hz sine (P_{out} = 85 W). Spot 1 to 4 are switching MOSFETs and spot 5 and 6 are output filter inductors.

4 Conclusion

This paper has described the main challenge to overcome in order to achieve high power density audio amplifiers. This is management of the power dissipation within the switching power stage. A thorough analysis of the inherent loss mechanisms in switch-mode audio power amplifiers and their relation to the amplifier input signal has been presented. A new switching strategy, based on a high inductor ripple current, to improve soft switching capabilities of the switching devices has been proposed. The high inductor ripple current is realized when designing the output filter with a high quality factor. Though this design method improves the soft switching capabilities the frequency response of the amplifier is affected as a significant resonance is introduced. However, this is compensated with the use of full state control.

Two amplifiers were implemented to verify that the presented switching strategy in fact reduces the power dissipation in the MOSFETs. One amplifier utilizing conventional switching strategy and the other one the proposed. Both amplifier were capable of delivering 100 W into 8 Ω with a 32.5 dB gain and power densities of 6 W/cm^3. Measured results showed that the soft switching capability was improved when using the proposed switching strategy. This was especially evident when amplifying signals with dynamic properties similar to real audio as thermal pictures revealed a temperature reduction of 45 °C. Even for sine wave operation at 85 W a temperature reduction of 15 °C was measured. The proposed method causes higher inductor losses. However, as the heat capacity of the inductors are much larger than that of the small MOSFET packages this does not give rise to thermal issues. The proposed method ensures that the power dissipation is spread more evenly between the MOSFETs and the filter inductors when compared to the prior art methods. Moreover, the implemented amplifiers showed excellent THD+N levels, down to 0.03 %.

The authors believe that by applying the proposed switching technique combined with full state control power densities of 10 to 20 W/cm^3 are a realistic future scenario.

5 Bibliography

[1] K. Nielsen, "Audio power amplifier techniques with energy efficient power conversion", Ph.D. thesis, Volume 1, Technical University of Denmark 1998.

[2] B. Putzeys, "Simple self-oscillating class D amplifier with full output filter control", in *118th Audio Engineering Society Convention*, Barcelona, May 28-31, 2005.

[3] C. Neesgaard and L. Risbo, "PWM amplifier control loops with minimum aliasing distortion", in *Audio Engineering Society Convention 120*, May 2006.

[4] S. Poulsen and M. A. E. Andersen , "Simple PWM modulator topology with excellent dynamic behaviour", in *IEEE Applied Power Electronics Conference*, 2004. DOI: 10.1109/APEC.2004.1295852.

[5] M. C. W. Høyerby and M. A. E. Andersen, "Carrier distortion in hysteretic self-oscillating class-d audio power amplifiers: Analysis and optimization", in *IEEE Transactions on Power Electronics*, Vol. 24, No. 3, pp. 714-729, March 2009. DOI: 10.1109/TPEL.2008.2007956.

[6] M. Høyerby, J. Kragh, J. Midtgaard and T. H. Hansen, "A 2 70 W monolithic five-level class-D audio power amplifier in 180 nm BCD", in *IEEE Transactions of Solid-State Circuits*, Vol. 51, No. 12, pp. 2819-2829, December 2016. DOI: 10.1109/JSSC.2016.2600251.

[7] Data sheet, "MA12040 - Filterless and high-efficiency +4V to +18V audio amplifier with analog input", Merus Audio, 2017.

[8] Data sheet, "TPA3116D2 15-W, 30-W, 50-W filter-free class-D stereo amplifier family with AM avoidance", Texas Instruments, 2017.

[9] M. Duraj, N. E. Iversen, L. P. Petersen and P. Boström, "Self-oscillating 150 W switch-mode amplifier equipped with eGaN-FETs", in *139th Audio Engineering Society Convention*, New York, October 29-November 1, 2015.

[10] J. Chung, R. McKenzie, W. Tung Ng, "A comparison between GaN and silicon based class D audio power amplifiers with pulse density modulation", in *13th IEEE International Conference on Solid-State and Integrated Circuit Technology*, 2016. DOI:10.1109/ICSICT.2016.7998847.

[11] N. J. Dahl, N. Iversen, A. Knott and M. A. E. Andersen, "Optimal control of a high frequency class-D amplifier", *J. Audio Eng. Soc*, vol. 66, no. 1/2, pp. 34textbf–43, 2018.

[12] N. J. Dahl, N. E. Iversen, Arnold Knott, and Michael A.E. Andersen, "Comparison of simple self-oscillating PWM modulators", in *140th Audio Engineering Society Convention*, Paris, June 4-7, 2016.

[13] A. Knott, G. Pfaffinger and M. A. E. Andersen, "A self-oscillating control scheme for a boost converter providing a controlled output current", in *IEEE Transactions on Power Electronics*, Vol. 26, No. 9, pp. 2707-2723, September 2011. DOI: 10.1109/TPEL.2011.2126600.

[14] S. Poulsen and M. A. E. Andersen, "Hysteresis controller with constant switching frequency", in *IEEE Transactions on Consumer Electronics*, Vol. 51, No. 2, pp. 688-683, May 2005. DOI: 10.1109/TCE.2005.1468020.

[15] F. Koeslag and T. Mouton, "Accurate characterization of pulse timing errors in class-D audio amplifier output stages", in *37th Audio Engineering Society International Conference*, Hillerœd, August 28-30, 2009.

[16] Application Report, "Design Considerations for Class-D Audio Power Amplifiers", Texas Instruments, 1999.

[17] Erickson and Maksimovic, *"Fundamentals of Power Electronics"*, Second Edition, Kluwer Academic Publishers.

[18] P. J. Chapman, "Programme material analysis", in *100th Audio Engineering Society Convention*, Copenhagen, May 11-14, 1996.

[19] R. A. R. van der Zee and A. J. M. van Tuijl, "Test Signals for Measuring the Efficiency of Audio Amplifiers", in *102th Audio Engineering Society Convention*, Amsterdam, May 16-19, 1998.

[20] H. Schneider, L. C. Jensen, L. P. Petersen, A. Knott and M. A. E. Andersen, "Requirements specification for amplifiers and power supplies in active loudspeakers", in *137th Audio Engineering Society Convention*, Los Angeles, October 9-12, 2014.

[21] N. E. Iversen, A. Knott and M. A. E. Andersen, "Efficiency of Switch-Mode Power Audio Amplifiers - Test Signals and Measurement Techniques", in *140th Audio Engineering Society Convention*, Paris, 4-7 June, 2016.

[22] K. S. Meyer and M. A. E. Andersen, "Parameterized analysis of Zero Voltage Switching in resonant converters for optimal electrode layout of piezoelectric transformers", in *IEEE Power Electronics Speciealists Conference*, 2008. DOI: 10.1109/PESC.2008.4592323.

[23] T. Andersen, "Piezoelectric transformer based power supply for dielectric electro active polymers", Ph.D. Thesis, Technical University of Denmark, 2012.

[24] Data sheet, OptiMOS^{TM} Power-Transistor, BSZ150N10LS3, Infineon, Rev. 2.2, 2013.

THE AUTHORS

Niels Elkjær Iversen

Nicolai J. Dhal

Arnold Knott

Michael A. E. Andersen

Niels Elkjær Iversen is a Ph.D student at the electronics group at the Technical University of Denmark, Kongens Lyngby, Denmark. He received his M.Sc degree in December 2014. His research interest include electrical aspects of audio such as switch-mode power audio amplifiers, measurement techniques and transducer modelling.

●

Nicolai J. Dahl is an Electrical Engineering student at Technical University of Denmark where he started in 2013. His main focuses in his studies are: control theory, audio electronics and signal processing and he has since early 2014 continuously worked with class D amplifiers and their power supplies. Currently Nicolai working on his M.Sc. degree specializing in control theory for automation.

●

Arnold Knott received the Diplom-Ingenieur (FH) degree from the University of Applied Sciences in Deggendorf, Germany, in 2004. From 2004 until 2009 he has been working with Harman/Becker Automotive Systems GmbH in Germany and USA, designing switch-mode audio power amplifiers and power supplies for automotive applications. In 2010 he earned the Ph.D. degree from the Technical University of Denmark, Kongens Lyngby, Denmark working on a research project under the title "Improvement of out of band Behaviour in Switch-Mode Amplifiers and Power Supplies by their Modulation Topology". From 2010 to 2013 he was Assistant Professor and since 2013 Associate Professor at the Technical University of Denmark. His interests include switch-mode audio power amplifiers, power supplies, integrated circuit design, transducers, radio frequency electronics and electromagnetic compatibility.

●

Michael A.E. Andersen received the M.Sc.E.E. and Ph.D. degrees in power electronics from the Technical University of Denmark, Kongens Lyngby, Denmark, in 1987 and 1990, respectively. He is currently a Professor of power electronics at the Technical University of Denmark. Since 2009, he has been Deputy Head of Department at the Department of Electrical Engineering. He is the author or coauthor of more than 200 publications. His research interests include switch-mode power supplies, piezoelectric transformers, power factor correction, and switch-mode audio power amplifiers

B

Relationship between voice coil fill factor and loudspeaker efficiency

In Journal of Audio Engineering Society, vol. 64, no. 4, pp. 241-252, May 2016.

Journal of the Audio Engineering Society
Vol. 64, No. 4, April 2016 (© 2016)
DOI: http://dx.doi.org/10.17743/jaes.2016.0006

Relationship between Voice Coil Fill Factor and Loudspeaker Efficiency

NIELS ELKÆR IVERSEN, *AES Student Member*, **ARNOLD KNOTT,** *AES Member*, **AND**
(neiv@elektro.dtu.dk) (akn@elektro.dtu.dk)

MICHAEL A.E. ANDERSEN, *AES Member*
(ma@elektro.dtu.dk)

Technical University of Denamrk, Kgs. Lyngby, Denmark

In modern audio systems utilizing switch-mode amplifiers, the total efficiency is dominated by the rather poor efficiency of the loudspeaker. For decades voice coils have been designed so that nominal resistances of 3 to 8 Ω are obtained, despite modern audio amplifiers using switch-mode technology, can be designed to much lower loads. A thorough analysis of the loudspeaker efficiency is presented and its relation to the voice coil fill factor is described. In addition to this the influence of the driver's mass ratio is investigated and it is found that high mass ratios are beneficial for the efficiency of drivers using high fill factor voice coils. Different voice coil winding strategies are described and their fill factors analyzed. It is found that by lowering the nominal resistance of a voice coil, using rectangular wire, one can increase the fill factor. However a practical realization of four voice coil designs could not prove this due to wire insulation issues. Despite that a good correlation between theory and experimental results is found, it is shown that the efficiency is dependent on the fill factor as predicted. Moreover the fill factor of a conventional 4 Ω voice coil was measured to be 53%, which leaves plenty of room for future fill factor optimization.

0 INTRODUCTION

A system designed for high quality audio reproduction involves many different blocks. These often include power supply, Digital Signal Processing (DSP), pre-amplifier, amplifier, cross-over network, loudspeaker enclosure, and transducer. However all these blocks can be boiled down to three essential blocks that are:

- Power supply
- Amplifier
- Transducer

Modern power supplies and amplifiers are widely utilizing switch-mode power technology, which is described in [1]. This is due to the high efficiency this technology offers, which theoretically can reach 100%. In practice the theoretical efficiency cannot be reached but it is possible to reach efficiencies above 90% [2] and [3]. Moreover switch-mode power audio amplifiers delivers excellent audio performance with Total Harmonic Distortion (THD) beneath 0.005% [4]. The transducer of the sound system is the loudspeaker driver that normally is mounted in a carefully designed enclosure. Loudspeaker drivers and their enclosures are well described in literature [5], [6], [7]. The impedance of the driver consists of an acoustical-, a mechanical-, and an electrical-part and is carefully described in [8] and [9]. The nominal resistance of the driver is characterized by the voice coil resistance. This resistance is also known as the DC resistance, corresponding to the resistance at 0 Hz. For decades it has been widely accepted to aim for voice coil DC resistances between 3 and 8 Ω. However modern switch-mode power audio amplifiers can easily be designed to deliver power to lower load resistances. A reduction of the load resistance leads to a downgrade of the amplifier's voltage rail requirement for a given output power as discussed in [10], and as shown in [11] a low rail voltage can benefit the efficiency of the switch-mode power audio amplifier due to lower switching losses. In addition to this the switch-mode power supply can be spared in battery driven systems, such as portable and automotive sound systems, when the DC resistance becomes so low, that the battery voltage is sufficient for generating a desired sound pressure level. On the transducer side a lower voice coil DC resistance can be obtained using rectangular or foil windings resulting in higher fill factors that can benefit the efficiency of the transducer, as discussed in [12].

Conventional low frequency loudspeaker drivers, such as woofers and sub-woofers, are known to have very poor efficiency, typically in the range 0.2–2% depending, among

others, on the magnet system, diaphragm size, and weight and driver type. Throughout this paper the focus will be on the efficiency on these kinds of drivers. The overall efficiency for an audio system, from electrical input to acoustical output, is simply the product of the efficiencies of the subsystems. For a system consisting of a power supply, an audio amplifier, and a loudspeaker the total efficiency becomes:

$$\eta_{tot} = \eta_{supply} \cdot \eta_{amp} \cdot \eta_{spk} \tag{1}$$

Since the efficiency of the amplifier and the power supply is much higher than that of the loudspeaker, it is clear that the overall efficiency for such systems normally will be dominated by the poor efficiency of the loudspeaker. One method to compensate for the poor efficiency of the driver is to improve the impedance match between the driver diaphragm and the air load. This can be done by using various types of acoustical horns [7]. However for low frequency drivers, acoustical horns tend to increase the overall size of the speaker significantly and therefore they will not be discussed further in this paper.

This paper will focus on how low impedance voice coils with high fill factors can benefit the efficiency of the loudspeaker driver and thereby the whole sound system. In addition to this the fill factor's impact on the driver's frequency characteristic will be investigated. Moreover the paper will present different voice coil designs and winding strategies and describe how they can be used to obtain high fill factor voice coils. Finally experimental results will be presented to support the presented theory.

1 LOUDSPEAKER EFFICIENCY

The efficiency of a loudspeaker driver is simply the ratio between the acoustic power emitted from the diaphragm, P_A, and the electrical power flowing into the voice coil, P_E.

$$\eta_0 = \frac{P_A}{P_E} \tag{2}$$

A more common measure is the loudspeaker driver's sensitivity, where the Sound Pressure Level (SPL) is measured in dB at a given distance with a given input power. The SPL can be expressed as:

$$SPL = 10\log\left(\frac{P_E \frac{\eta_0}{A}}{P_o}\right) \tag{3}$$

Where $P_o = 10^{-12}$ W/m^2 is the reference acoustic sound power and A is the area of the sound surface at a given distance from the driver. Normal sensitivity measurements are measured at 1W@1m with the driver mounted in an infinite baffle, thus playing into a half sphere environment. A half sphere environment corresponds to $A = 2\pi r^2$, where r is the radius of the half sphere. With $r = 1$ meter we get a 8 dB reduction in sensitivity. The Sound Pressure Level at 1W@1m can then be expressed as:

$$SPL_{1W@1\mathrm{m}} = 10\log\left(\frac{\eta_0}{P_o}\right) - 8\mathrm{dB} \tag{4}$$

The sensitivity is normally in the range 85–95 dB. In literature [7] the efficiency is expressed as a function of the force factor, Bl, the diaphragm area, S_D, the DC resistance of the voice coil, R_E, and the total mass of the diaphragm when attached to the voice coil, M_{ms}:

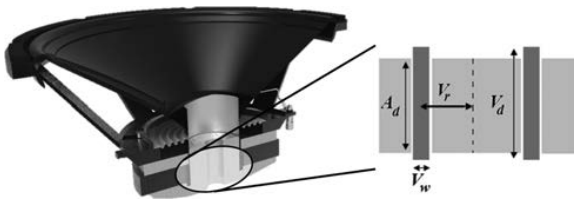

Fig. 1. Loudspeaker driver and voice coil winding area.

$$\eta_0 = \frac{\rho_0 (Bl)^2 S_D^2}{2\pi c R_E M_{ms}^2} \tag{5}$$

Where $\rho_0 = 1.18$ kg/m^3 is the density of air and $c = 345$ m/s is the speed of sound in air. The force factor is the product between the the static magnetic field strength of the permanent magnet and the length of the wire in the air gap. Note that Eq. (5) is a simplified approximation of the loudspeaker efficiency that does not describe how the frequency response behaves. However the frequency response of loudspeaker drivers will be examined later in Sec. 2. For now it is assumed that Eq. (5) is accurate. Thus the efficiency expression can be simplified to be proportional to the Bl^2/R_E ratio for a given driver:

$$\eta_0 \propto \frac{Bl^2}{R_E} \tag{6}$$

From this it seems obvious that one can increase the efficiency by lowering the DC resistance or by increasing the force factor. However these two solutions cancel each other. This can be shown when considering how the DC resistance and force factor are related to the winding area of the loudspeaker driver. A conceptual model of a loudspeaker driver and its voice coil is shown in Fig. 1. V_d is the winding depth, V_w is the winding width, A_d is the air gap depth, and V_r is the radius of the voice coil. Normally the winding depth will be bigger than the air gap depth to compensate for non linearities caused by the displacement [13] resulting in an overhung voice coil design.

Assuming that the entire winding area can be filled with wire the force factor and DC resistance can be written as follows:

$$\begin{aligned} R_E &= \frac{l_w}{\sigma A_{wire}} = \frac{N V_o}{\sigma \frac{V_w V_d}{N}} = \frac{N^2 V_o}{\sigma V_w V_d} \\ Bl &= Bl_w \frac{A_d}{V_d} = BN V_o \frac{A_d}{V_d} \end{aligned} \tag{7}$$

Where l_w is the total length of the wire, A_{wire} is the cross sectional area of the wire, $V_o = 2\pi V_r$ is the circumsphere of the voice coil, N is the number of turns, and σ is the conductivity of the conductor. For copper the conductivity is $\sigma_{Cu} = 5.96 \cdot 10^7$ S/m. Considering Eq. (5) we find the ratio between the force factor squared and the DC resistance to be constant value determined by the geometry of the magnet system, the strength of the static magnetic field, and the conductivity of the conductor. This means that the

efficiency will be independent of efforts to decrease or increase the DC resistance or the force factor respectively.

$$\begin{aligned}\frac{(Bl)^2}{R_E} &= \frac{B^2N^2V_o^2\left(\frac{A_d}{V_d}\right)^2}{\frac{N^2V_o}{\sigma V_w V_d}} \downarrow \\ \frac{(Bl)^2}{R_E} &= \frac{B^2V_oV_wA_d^2\sigma}{V_d} = \textbf{constant}\end{aligned} \tag{8}$$

However the above expression is only valid if one assumed that the entire available winding area is filled with conducting material, which in practice is not possible. Therefore one has to consider the fill factor, κ, of the voice coil, i.e., the ratio between the area of the conductor and the total winding area:

$$\kappa = \frac{A_c}{A_w} \tag{9}$$

Where κ is the fill factor, A_c is the area of the conductor and A_w is the total winding area. Taking the fill factor into account we get:

$$\begin{aligned}R_E &= \frac{N^2V_o}{\sigma V_w V_d \kappa} \\ \frac{(Bl)^2}{R_E} &= \frac{B^2V_oV_wA_d^2\sigma\kappa}{V_d} \neq \textbf{constant}\end{aligned} \tag{10}$$

Moreover the total moving mass of the driver, M_{ms}, can also be expressed as a function of the fill factor:

$$\begin{aligned}M_{ms} &= M_{d+cf} + M_{vc} \\ M_{d+cf} &= M_d + M_{cf} \\ M_{vc} &= V_dV_wV_o\rho_{wire}\kappa\end{aligned} \tag{11}$$

Where M_d is the mass of the diaphragm, M_{cf} is the mass of the coil former, M_{vc} is the mass of the voice coil wire, and ρ_{wire} is the density of the wire material. Now it is possible to express the efficiency of the loudspeaker driver as a function of the fill factor by substituting Eq. (10) and Eq.(11) into Eq. (5):

$$\eta_0(\kappa) = \frac{\rho_0 S_D^2 B^2 V_o V_w A_d^2 \sigma\kappa}{2\pi c V_d \left(M_d + M_{cf} + V_dV_wV_o\rho_{wire}\kappa\right)^2} \tag{12}$$

From Eq. (12) it is seen that the efficiency, expressed as a function of the fill factor, is a ratio between a linear function and a second order polynomial of the simplified form of:

$$\eta_0(\kappa) = \frac{\kappa}{(a + b\cdot\kappa)^2} \tag{13}$$

where a and b are constants. Considering positive values of κ we find the efficiency to have a shape as shown in Fig. 2. In this particular example it is seen that the maximum of efficiency is found at a theoretical fill factor of 50%. In general the fill factor corresponding to the maximum efficiency can be found by solving for the derivative of the

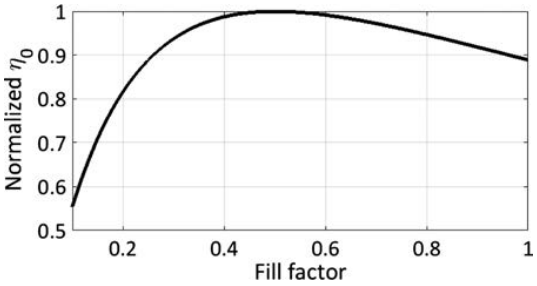

Fig. 2. The efficiency as a function of the fill factor.

efficiency function. In the simplified expression from Eq. (13) we find:

$$\begin{aligned}\eta_0'(\kappa) &= \frac{1}{(a + b\cdot\kappa)^2} - \frac{2b\cdot\kappa}{(a + b\cdot\kappa)^3} \\ \eta_0'(\kappa) &= \frac{1}{(a + b\cdot\kappa)^2} - \frac{2b\cdot\kappa}{(a + b\cdot\kappa)^3} = 0 \downarrow \\ \kappa_{optimal} &= \frac{a}{b}\end{aligned} \tag{14}$$

Applying this solution to Eq. (12) yields:

$$\begin{aligned}\eta_0'(\kappa) &= 0 \downarrow \\ \kappa_{optimal} &= \frac{M_d + M_{cf}}{V_dV_wV_o\rho_{wire}}\end{aligned} \tag{15}$$

However this is only true for cases where:

$$M_d + M_{cf} \leq V_dV_wV_o\rho_{wire} \tag{16}$$

This is due to the fact that the theoretical maximum fill factor is $\kappa = 1$, i.e., 100%. Therefore we will redefine Eq. (15) as the driver's mass ratio:

$$M_{ratio} = \frac{M_d + M_{cf}}{V_dV_wV_o\rho_{wire}} \tag{17}$$

This mass ratio should not be confused with the coil-mass-to-cone-mass ratio discussed in [14] and [15]. The mass ratio presented in this paper is the ratio between the mass of the diaphragm plus the coil former and the theoretical maximum mass of the voice coil, i.e., the scenario where the entire winding area is filled with a solid ring of conducting material. It is quite common that typical low frequency drivers will have a mass ratio above one. For these cases the optimal fill factor is $\kappa = 1$, meaning that these drivers' efficiencies would benefit from a fill factor optimization. However the impact on the efficiency achieved by this fill factor optimization is dependent on how far above 1 the mass ratio is. This is shown on Fig. 3 where the efficiency is normalized around a fill factor of 50%, which is not an uncommon fill factor for voice coil designs. From the figure it is seen that the impact on the efficiency becomes greater for higher mass ratios. Moreover the figure shows that the efficiency function achieves an approximately straight slope for high mass ratios. Therefore we can simplify the efficiency expression to be proportional with fill factor:

$$\eta_0 \propto \kappa \tag{18}$$

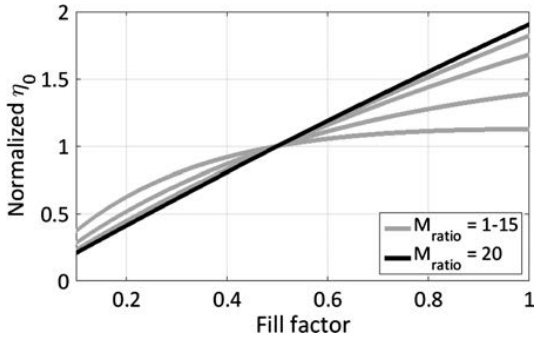

Fig. 3. Impact on efficiency for different mass ratios.

2 IMPACT ON FREQUENCY RESPONSE

As mentioned in Sec. 1 the expression for the loudspeaker driver's efficiency, presented in Eq. (5), is simplified and does not describe how this efficiency relates to the frequency response of the driver. This section investigates this relation by examining how the small-signal parameters are related to the frequency response and its' dependency on the fill factor.

The small-signal parameters are well described in literature, [5], [6], [7], and are also referred to as Thiele-Small parameters. These parameters include the force factor, diaphragm area and acoustic mass, DC resistance, and quality factors. These parameters are useful to determine the frequency response of the driver. This is evident from the on-axis pressure transfer function of the loudspeaker driver that is given by [7]:

$$p = \frac{\rho_0}{2\pi}\frac{Ble_g S_d}{R_E M_{ms}} \cdot G(s) \cdot T_{u1}(s) \tag{19}$$

Where $G(s)$ is a high pass transfer function modelling the low frequency content, $T_{u1}(s)$ is a low pass transfer function modelling the high frequency content, and e_g is the input voltage from the amplifier. Considering Eq. (10), which shows that the Bl^2/R_E ratio is proportional to the fill factor, it can be realized that the pressure transfer function from Eq. (19) can be simplified to be proportional with the square root of the fill factor multiplied with the high- and low-pass transfer functions $G(s)$ and $T_{u1}(s)$:

$$p \propto \sqrt{\kappa} \cdot G(s) \cdot T_{u1}(s) \tag{20}$$

Similarly an expression for the efficiency can be derived keeping in mind that the efficiency is related to the acoustic power P_A as shown in Eq. (2). The acoustic power relates to the pressure function squared:

$$P_A \propto p^2 \tag{21}$$

Hence the efficiency can be expressed as:

$$\begin{aligned} &\eta_0 \propto p^2 \downarrow \\ &\eta_0 \propto \kappa \cdot G(s)^2 \cdot T_{u1}(s)^2 \end{aligned} \tag{22}$$

However this is not entirely correct. This is due to the fact that the radiation pattern will narrow for higher frequencies due to diffraction effects as described in [7] (p. 108). This effect is dependent on the diaphragm size. The bigger the diaphragm, the earlier this effect will be visible in the efficiency frequency response.

The low pass transfer function, $T_{u1}(s)$ determines the high frequency roll off related to the self inductance of the voice coil, L_E, the total moving mass, the total mass of the diaphragm, and the the DC resistance:

$$\begin{aligned} T_{u1}(s) &= \frac{1}{1+\frac{s}{w_{u1}}} \\ w_{u1}(s) &= \frac{M_{ms}R_E}{M_d L_E} \end{aligned} \tag{23}$$

As long as the mass of the diaphragm is the dominating mass the fill factor will have a negligible impact on the M_{Ms}/M_d ratio. However since the self inductance is related to the number of turns on the voice coil squared the R_E/L_E ratio is forced to decrease when the fill factor increases, since less turns are required. This leads to a lower high frequency roll off. However one can compensate by inserting a copper cap inside the magnet system that reduces the self inductance thus increasing the roll off frequency [16].

Since the focus is on low frequency drivers the above mentioned effects will be neglected in this paper. Instead the focus will be on the the high pass transfer function, $G(s)$, which determines the frequency response for low frequencies. This transfer function is related to the total quality factor, Q_{TS}, and the resonance frequency, f_S, of the driver:

$$G(s) = \frac{(s/\omega s)^2}{(s/\omega s)^2 + (1/Q_{TS})(s/\omega s) + 1} \tag{24}$$

Where $\omega_s = 2\pi f_s$ relates to the resonance frequency, which is characterized by the mechanical compliance of the diaphragm suspension, C_{ms}, and the total moving mass M_{ms}:

$$f_S = \frac{1}{2\pi\sqrt{M_{ms}C_{ms}}} \tag{25}$$

For an optimal flat response the total quality factor should be approximately 0.7. Lower values cause a reduction of the low frequency content and higher values causes a ripple in the frequency response. The total quality factor is related to the driver's electrical- and mechanical-quality factors, Q_{ES} and Q_{MS}:

$$Q_{TS} = \frac{Q_{MS}Q_{ES}}{Q_{MS}+Q_{ES}} \tag{26}$$

To describe its' dependency on the fill factor both the electrical- and mechanical-quality factors must be investigated in more detail.

2.1 Electrical Quality Factor

From literature, [7], the electrical quality factor can be expressed as:

$$Q_{ES} = \frac{R_E}{(Bl)^2}\sqrt{\frac{M_{ms}}{C_{ms}}} \tag{27}$$

Where C_{ms} is the mechanical compliance of the diaphragm suspension. In Eq. (10) it was shown that the relationship between the force factor, Bl and the DC resistance, R_E, could

be expressed as a function of the fill factor. Similarly it was shown in Eq. (11) that the total moving mass, M_{ms}, also could be expressed as a function of the fill factor. Applying these two equations to Eq. (27) yields:

$$\begin{aligned} Q_{ES}(\kappa) &= \frac{\frac{N^2 V_o}{\sigma V_w V_d \kappa}}{\left(BNV_o \frac{A_d}{V_d}\right)^2} \sqrt{\frac{M_{d+cf}+V_d V_w V_o \rho_{wire}\kappa}{C_{ms}}} \downarrow \\ Q_{ES}(\kappa) &= \frac{Vd}{\sigma V_o V_w B^2 A d^2 \kappa} \sqrt{\frac{M_{d+cf}+V_d V_w V_o \rho_{wire}\kappa}{C_{ms}}} \end{aligned} \tag{28}$$

Assuming that the mass of the diaphragm is the dominating mass in the driver ($M_d + M_{cf} \gg V_d V_w V_o \rho_{wire}$), meaning that a large mass ratio is assumed, it is possible to simplify the expression so that it can be realized that the electrical quality factor is approximately inversely proportional to the fill factor:

$$Q_{ES}(\kappa) \approx \frac{Vd}{\sigma V_o V_w B^2 A d^2 \kappa} \sqrt{\frac{M_{d+cf}}{C_{ms}}} \tag{29}$$

Thus

$$Q_{ES} \propto \frac{1}{\kappa} \tag{30}$$

2.2 Mechanical Quality Factor

The mechanical quality factor is given by:

$$Q_{MS} = \frac{1}{R_{ms}} \sqrt{\frac{M_{ms}}{C_{ms}}} \tag{31}$$

Where R_{ms} is the mechanical resistance of the diaphragm suspension, normally provided in loudspeaker driver data sheets. Similar to the electrical quality factor, the mechanical quality factor can be expressed as a function of the fill factor by substituting Eq. (11) into Eq. (31):

$$Q_{MS}(\kappa) = \frac{1}{R_{ms}} \sqrt{\frac{M_{d+cf} + V_d V_w V_o \rho_{wire}\kappa}{C_{ms}}} \tag{32}$$

Again it is assumed that the mass of the diaphragm is the dominating mass, to simplify the expression and realize that the mechanical quality factor is independent of the fill factor:

$$\begin{aligned} Q_{MS}(\kappa) &\approx \tfrac{1}{R_{ms}} \sqrt{\tfrac{M_{d+cf}}{C_{ms}}} \downarrow \\ Q_{MS}(\kappa) &\approx \textbf{constant} \end{aligned} \tag{33}$$

2.3 Total Quality Factor

Now an expression for the total quality factor as a function of the fill factor can be obtained by substituting Eqs. (28) and (32) into Eq. (26):

$$\begin{aligned} &Q_{TS}(\kappa) \\ &= \frac{\left(M_{d+cf} + V_d V_w V_o \rho_{wire}\kappa\right) V_d}{C_{ms} \sqrt{\frac{M_{d+cf}+V_d V_w V_o \rho_{wire}\kappa}{C_{ms}}} \left(\sigma V_o V_w B^2 A d^2 \kappa + R_{ms} V_d\right)} \end{aligned} \tag{34}$$

Using the assumption that the mass of the diaphragm is the dominating mass allows for simplification and realization that the total quality factor of the driver is inversely proportional to the fill factor:

$$Q_{TS}(\kappa) \approx \frac{M_{d+cf} V_d}{C_{ms} \sqrt{\frac{M_{d+cf}}{C_{ms}}} \left(\sigma V_o V_w B^2 A d^2 \kappa + R_{ms} V_d\right)} \tag{35}$$

Thus

$$Q_{TS} \propto \frac{1}{\kappa} \tag{36}$$

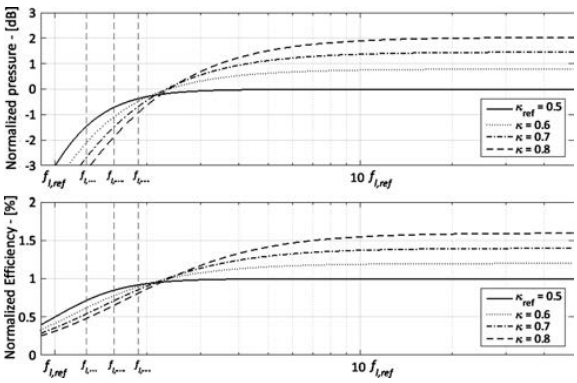

Fig. 4. Normalized frequency responses for increasing fill factors. The vertical dashed lines shows how the –3 dB the cut-off frequency, f_l, increases with the fill factor. Moreover it is seen that the normalized pressure and efficiency is improved in pass band as the fill factor increases. The reference response (solid line) has an optimal flat response.

2.4 Frequency Responses

Based on the above analysis it is possible to derive expressions that explains the pressure- and efficiency-transfer functions relationship to the fill factor for low frequencies. By inserting Eq. (24) into Eqs. (20) and (22) the following expressions are obtained:

$$p \propto \sqrt{\kappa} \cdot \frac{(s/\omega s)^2}{(s/\omega s)^2 + (1/Q_{TS})(s/\omega s) + 1} \tag{37}$$

$$\eta_0 \propto \kappa \left(\frac{(s/\omega s)^2}{(s/\omega s)^2 + (1/Q_{TS})(s/\omega s) + 1} \right)^2 \tag{38}$$

where $Q_{TS} \propto 1/\kappa$. This means that for higher fill factors it is expected that the total quality factor will decrease for a given driver. This has the consequence that the frequency response will be shifted upwards, meaning that the driver's –3 dB cut-off frequency, f_l, increases. Fig. 4 shows the normalized pressure and efficiency frequency responses, plotted for four different fill factors. The frequency responses are normalized with respect to an optimal flat reference response with a fill factor of 50%, i.e., $\kappa_{ref} = 0.5$. The figure shows that the efficiency is improved in the pass band as the fill factor increases. Note that these frequency responses and the expression from Eqs. (37) and (38) assumes that the mass ratio of the driver is large. This is not always the case and for low mass ratio scenarios the efficiency improvement in the pass band will be reduced according to Fig. 3.

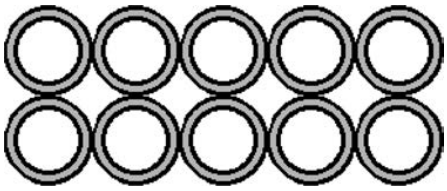

Fig. 5. Round winding layout 1.

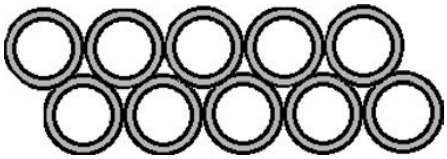

Fig. 6. Round winding layout 2.

3 FILL FACTOR OF VOICE COIL LAYOUTS

After the analysis performed in Secs. 1 and 2 an understanding of how a high fill factor can improve the efficiency of the loudspeaker driver has been established. This section presents an analysis of how to practically improve the fill factor of voice coils. This includes an analysis of conventional voice coil layouts using round wire and unconventional layouts using rectangular wire.

3.1 Round Winding Layout 1

Conventional voice coil designs utilize round wire in two layers. The concept of the winding layout is shown in Fig. 5. It is evident that the round shape causes some air gaps to exist between the wire. For this winding layout the maximum fill factor becomes:

$$\kappa_{round,1} = \frac{A_c}{A_w} = \frac{\pi r_w^2}{(2r_w)^2} = \frac{\pi}{4} \approx 0.79 \tag{39}$$

where r_w is the radius of the wire. Taking the insulation of the wire into account the fill factor will be even lower.

$$\kappa_{round,1} = \frac{A_c}{A_w} = \frac{\pi\left(r_w - \frac{t_{iso}}{2}\right)^2}{(2r_w)^2} \tag{40}$$

where t_{iso} is the total insulation thickness on both sides of the wire. In conventional voice coil designs using this winding layout DC resistances between 3 and 8 Ω are quite normal.

3.2 Round Winding Layout 2

During production of voice coils with round wire in two layers, the windings are often squeezed together as shown in Fig. 6. It is seen that the round shape still causes some tiny air gaps to exist. However the size of the air gaps are reduced compared to the layout from Fig. 5. This leads to an increment of the maximum fill factor:

$$\kappa_{round,2} = \frac{A_c}{A_w} = \frac{\pi r_w^2}{\left(2+\sqrt{3}\right) r_w^2} = \frac{\pi}{\left(2+\sqrt{3}\right)} \approx 0.84 \tag{41}$$

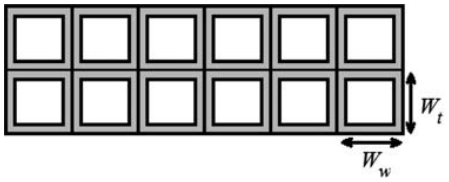

Fig. 7. Winding layout utilizing rectangular wire.

With insulation the fill factor of this winding layout becomes:

$$\kappa_{round,2} = \frac{A_c}{A_w} = \frac{\pi\left(r_w - \frac{t_{iso}}{2}\right)^2}{\left(2+\sqrt{3}\right) r_w^2} \tag{42}$$

3.3 Rectangular Winding Layout

Considering an unconventional voice coil winding layout utilizing rectangular wire, as shown in Fig. 7, it is possible to achieve a higher fill factor.

$$\kappa_{rec} = \frac{A_c}{A_w} = \frac{(W_w - t_{iso})(W_t - t_{iso})}{W_w W_t} \tag{43}$$

where W_w is the winding width and W_t is the winding thickness. In this winding layout there exists no air gap between the wires and therefore the theoretical maximum fill factor is $\kappa_{rec} = 1$, i.e., 100%. In order to fill out the entire winding area, the width of the rectangular wire will change as a function of the DC resistance of the voice coil. For lower DC resistances less turns are required, resulting in a greater wire width and thereby higher fill factor. For this reason the fill factor can be increased by lowering DC resistance and thereby the number of turns. Knowing the voice coil width, V_w, the air gap depth, A_d, the voice coil circumsphere V_o, and the winding depth, V_d, one can determine the exact number of turns for a given DC resistance and insulation thickness. This is done by realizing that for a given voice coil geometry the DC resistance is only dependent on the number of turns and the insulation thickness.

$$R_E = \frac{lw}{\sigma A} = \frac{NV_o}{\sigma W_{t,cu}(W_w - t_{iso})} = \frac{NV_o}{\sigma W_{t,cu}\left(\frac{V_d}{0.5N} - t_{iso}\right)} \tag{44}$$

where $W_{t,Cu} = W_t - t_{iso}$ is the actual thickness of the copper in the wire. By solving for the number of turns N in Eq. (44) we get:

$$N = \frac{-R_E W_{t,Cu} t_{iso}\sigma + \sqrt{R_E^2 W_{t,Cu}^2 t_{iso}^2 \sigma^2 + 8 R_E V_o V_d W_{t,Cu}\sigma}}{2V_o} \tag{45}$$

From this the actual width of the copper in the wire can be determined as:

$$W_{w,Cu} = W_w - t_{iso} = \frac{Vd}{0.5N} - t_{iso} \tag{46}$$

This is valid for a voice coil with two layers. When the number of turns becomes equal to one, $N = 1$, only one layer exists and a theoretical filling factor of 100% is obtained. In this case the voice coil becomes a one layer solid ring of conducting material. However the DC resistance will be very small, close to zero, which will make it difficult to drive, even with modern switch-mode audio power amplifiers.

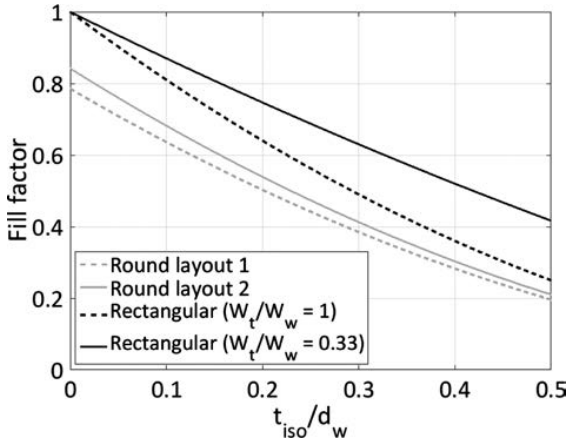

Fig. 8. Fill factor comparison of different winding layouts.

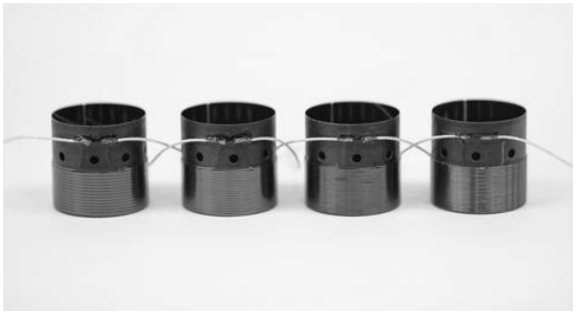

Fig. 9. Implemented voice coils. From left to right: Design 1, 2, 3 and 4.

3.4 Comparison of Winding Layouts

Fig. 8 shows a comparison between the different voice coil winding layouts. Note that the x-axis has the relative scale t_{iso}/d_w, where d_w is the diameter of the wire or, for the rectangular wire, the thickness, W_t. It is seen that the voice coil layout using rectangular wire can achieve a higher fill factor than that of the layouts using round wire. For the rectangular wire the decrement rate of the fill factor as the insulation thickness increases, is dependent on the shape of the wire. For high ratios of W_t/W_w there will be a fast decrement rate of the fill factor and for low ratios there will be a slower decrement rate.

4 MEASUREMENTS AND EXPERIMENTAL RESULTS

Four different voice coil designs were implemented. Three low impedance voice coils using the rectangular winding layout described in Sec. 3.3 and one standard voice coil using a round winding layout. In total 20 voice coils of each design were produced. Fig. 9 shows four samples of the implemented voice coil designs. Even though the designs using rectangular wire should be able to achieve higher fill factors than the design using round wire, this cannot be guaranteed in this project. This is due to the fact that the voice coil manufacturer used in this project applies an additional insulation coating on the designs using rectangular wire. This is to ensure proper insulation between the wires. The resulting fill factor suffers from this extra coating. It should be mentioned that several techniques exist that avoids this extra coating. One of them is to design a one layer voice coil that eliminates the need for additional insulation. However this solution would introduce a new challenge on how to get the access to both voice coil terminals. Another solution is to use another coating technique that allows for thin insulation on rectangular wires in multiple layers. However this solution might affect the power handling of the driver, since the insulation might be weaker.

A series of measurements was performed on five samples of each of the implemented voice coil designs. These measurements include the DC resistance, the force factor, and the mass. The DC resistance and the force factor are interesting since the ratio between them are expected to be non constant as a function of the fill factor, as predicted by Eq. (10). Moreover the Bl^2/R_E ratio can be assumed to be proportional with the efficiency as establish in Eq. (6) and if a high mass ratio is assumed we can assume this ratio to be proportional with the fill factor as shown in Eq. (18). In this way it is possible to estimate the efficiency improvement gained by optimizing the fill factor. The mass is interesting as it reveals the fill factor differences between the different designs.

Fig. 11 shows a close up of the DUT and the magnet system.

4.1 Force Factor—*Bl*

As mentioned in Sec. 1 the force factor is the product between the static magnetic field strength, B, and the effective length of the wire which cuts it, l, i.e., the actual length of the wire inside the air gap. The force factor is an important parameter as it is the motor that converts electrical impulses to mechanical movements. This conversion happens by the interaction between the electromagnetic field, generated by the current running in the voice coil and the static magnetic field of the permanent magnet. The relation can be derived from Lorentz's force law and the Coulombian Force Attraction described in [17] and [18].

$$\begin{aligned} F &= i \cdot Bl \\ V &= u \cdot Bl \end{aligned} \tag{47}$$

where F is a force, i is an electrical current, V is the induced voltage on the voice coil terminals and u is the velocity of the voice coil movement inside the air gap. From this it is evident that the force factor can be estimated by moving the voice coil at a fixed velocity while measuring the induced voltage on the voice coil terminals:

$$Bl = \frac{V}{u} \tag{48}$$

The measurement is carried out by the use of a controlled step motor. The step motor controls the movement of a pole on which the Device Under Test (DUT) is mounted (i.e., the voice coil). Before the measurement starts the voice coil is placed in the magnet system at its bottom position. Then the step motor pulls the voice coil up at a constant velocity while a multimeter measures the voltage on the voice coil

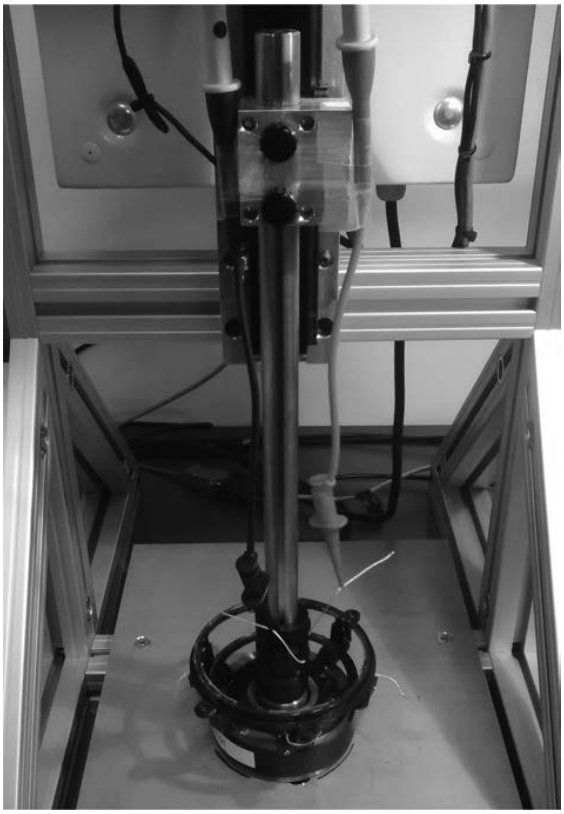

Fig. 10. Measurment setup.

Table 1. Measured force factor on the four different voice coil designs.

	Force factor - *Bl* [T · m]	
Design	*Min*	*Max*
Design 1	1.448	1.456
Design 2	2.031	2.024
Design 3	2.872	2.882
Design 4	5.120	5.150

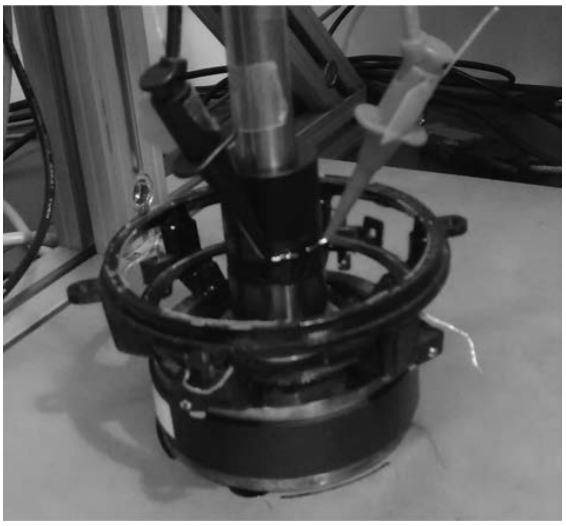

Fig. 11. Close up on voice coil and magnet system.

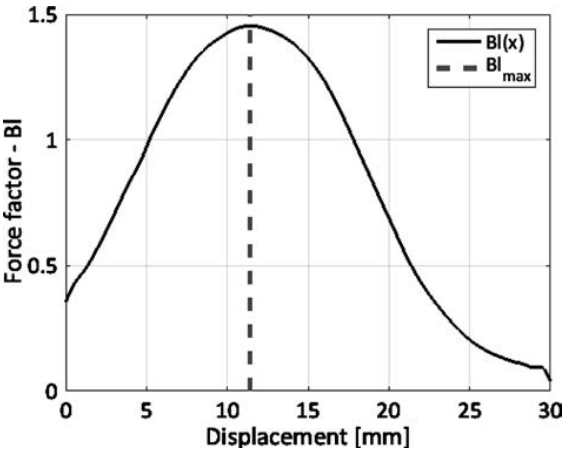

Fig. 12. *Bl* vs. displacement curve. The curve is generated as the average of five successive measurements on the same voice coil. This specific curve is for voice coil Design 1.

terminals. The force factor can then be estimated using Eq. (48). The step motor velocity was set to $u = 12$ mm/s. The measurement setup is shown in Fig. 10. Fig. 12 shows the measured force factor as a function of the step motor's position for one of the realized voice coil designs. The initial displacement of 0 mm corresponds to the voice coil's bottom position in the magnet system. The curve generated is an average curve based on five successive measurements on the same voice coil. Five samples of each voice coil design was measured using this method and the measured force factor is very consistent as shown in Table 1. Moreover Table 1 shows that the force factor increases with the DC resistance. This is expected as the effective wire length goes up with the DC resistance causing the *Bl* product to increase. Finally it is worth noticing that the force factor is highly non-linear. This will affect the distortion pattern and the efficiency of driver to some level as discussed in [13]. However the impact of the force factor's non linearities is worst at large excursion levels that will correspond to a high low frequency sound pressure level which, for a normal listening scenario, is uncommon. Anyway it is definitely something to be aware of when designing the driver's magnet system and several techniques exist to make the force factor more linear. That includes overhung voice coils and a dual voice coil system as discussed in [19].

5 DC RESISTANCE—R_E

The DC resistance of the four implemented voice coil designs was measured with a standard digital multimeter similar to the Agilent 34401A models [20]. The resistance was measured with an accuracy within 10 mΩ. For all measurements the multimeter probes were placed right at the voice coil terminals as shown in Fig. 11, bypassing the litz

Table 2. Measured DC resistance on the four different voice coil designs.

	DC Resistance - R_E [Ω]	
Design	*Min*	*Max*
Design 1	0.31	0.33
Design 2	0.65	0.66
Design 3	1.52	1.53
Design 4	3.79	3.84

Table 3. Measured mass and fill factor on the four different voice coil designs.

	M_{vc} [mg]		M_{Cu} [mg]		κ [%]
Design	*Min*	*Max*	*Min*	*Max*	*Typical*
Design 1	4.854	4.880	4.008	4.034	53
Design 2	4.686	4.704	3.840	3.858	51
Design 3	4.270	4.348	3.424	3.502	45
Design 4	4.839	4.891	3.993	4.045	53

wire. This is done to avoid the additional resistance of the litz wire that will distort the measurements especially for the low impedance voice coil designs. This also means that in a real loudspeaker using a low impedance voice coil design, the amplifier should be placed in close proximity to the voice coil terminals, to avoid conduction losses in the litz wire, thus almost integrating the amplifier into the driver. The measured DC resistances are also very consistent as shown in Table 2.

5.1 Mass—M_{vc}

The mass of the four designs was measured using a high precision weight, similar to Mettler Toledo's PG-S series [21], capable of measuring with a resolution of 1 mg. Moreover the mass of the coil former and the litz wire was measured. Assuming that the mass of the insulation material is insignificant it is possible to estimate the fill factor as the ratio between the measured mass of the copper and the theoretical maximum mass of the copper:

$$\begin{aligned} M_{Cu} &= M_{vc} - M_{cf} - M_{lw} \\ \kappa &= \frac{M_{Cu}}{V_d V_o V_w \rho_{Cu}} \end{aligned} \tag{49}$$

where $\rho_{Cu} = 8960$ kg/m^3 is the density of copper and M_{lw} it the mass of the litz wire. The mass of the coil former and the litz wire was measured to be $M_{cf} = 0.546$ g and $M_{lw} = 0.300$ g. For practical reasons it was not possible to measure these parameters for each of the designed voice coils, so it will be assumed that these measurements are valid for all of the implemented voice coils. The total mass of five samples of each design was measured. Using Eq. (49) the mass of the copper and the fill factor was calculated. The results are displayed in Table 3. Considering Design 1, 2, and 3, it is seen that as the mass goes up the DC resistance decreases causing the W_t/W_w ratio of the rectangular wire to decrease, obtaining a higher fill factor as predicted by Fig. 8. The mass of the round winding layout (Design 4) is very similar to that of Design 1 meaning the two designs will have approximately the same fill factor. Therefore it is expected that the Bl^2/R_E ratio for these two designs will be rather similar. However the mass, and thus also the fill factor, of the voice coil using round winding layout should have been less than the designs using rectangular winding layouts. However the additional layer of insulation on the designs using rectangular winding layout eliminates this advantage.

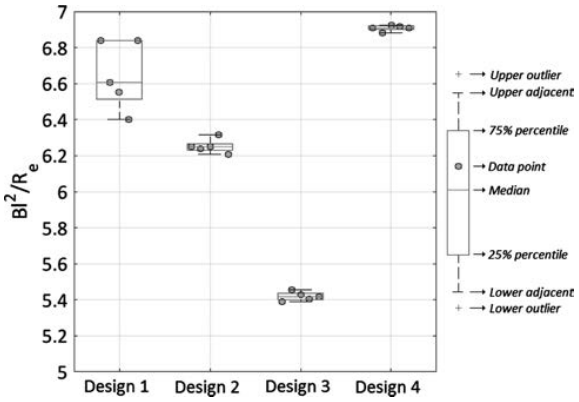

Fig. 13. Bl^2/R_E for the four different voice coils designs.

5.2 Bl^2/R_E—Ratio

From the measured force factor and DC resistance the Bl^2/R_E ratio can be calculated. As mentioned this ratio can be assumed to be proportional with the efficiency for large mass ratios as shown in Eq. (6). Fig. 13 shows the obtained results plotted as a box plot with visible data points. Considering Design 1, 2, and 3 it is seen that the Bl^2/R_E ratio behaves as predicted, i.e., higher Bl^2/R_E ratios for lower voice coil impedance. Moreover it is seen that the standard deviation increases for low impedance designs. This is especially evident for the box plot concerning Design 1. This is due to the fact that low impedance design will be much more sensitive to small measurement errors related to the DC resistance. As mentioned the DC resistance was measured with a resolution of approximately 10 mΩ. This resolution becomes less sufficient for low impedance designs where an apparently small error will represent a significant percentage of the measured DC resistance, thus causing an equal significant error on the Bl^2/R_E ratio.

6 IMPACT ON THE EFFICIENCY

The improvement of the loudspeaker efficiency, in dB, generated by an increased Bl^2/R_E ratio can be calculated as:

$$\Delta\eta = 10\log\left(\frac{x_{ratio}}{y_{ratio}}\right) \tag{50}$$

where x_{ratio} and y_{ratio} represent the Bl^2/R_E ratio of two different designs and $\Delta\eta$ is the efficiency difference in dB between the two. This is only valid when assuming a large mass ratio. Equally the efficiency improvement can be theoretically estimated by using the fill factor estimations from

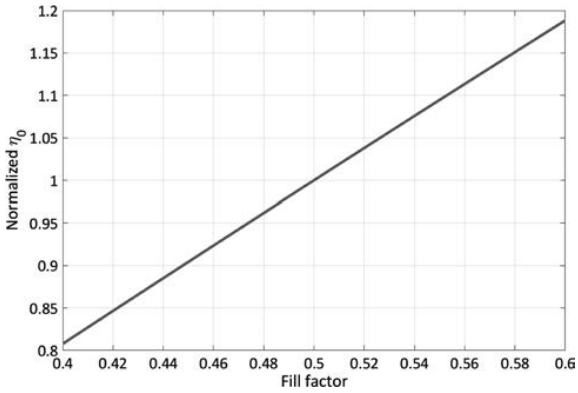

Fig. 14. Impact on efficiency for a large mass ratio ($M_{ratio} = 20$).

Table 4. Efficiency improvement of the different designs seen relative to Design 3.

Design	Bl^2/R_E *Mean*	κ [%]	η_{norm}	Δη [dB] *Meas*	Δη [dB] *Theory*
Design 1	6.65	53	1.06	0.89	0.71
Design 2	6.25	51	1.02	0.62	0.54
Design 3	5.42	45	0.90	–	–
Design 4	6.91	53	1.06	1.05	0.71

Table 3 and the corresponding normalized efficiency that can be read off Fig. 3.

$$\Delta\eta = 10\log\left(\frac{x_\eta}{y_\eta}\right) \tag{51}$$

where x_η and y_η represent the normalized efficiency of the two different designs. Fig. 14 shows a close up of Fig. 3 for a large mass ratio ($M_{ratio} = 20$). The normalized efficiency for the different fill factors can be read fairly easily off this graph. Using Eqs. (50), (51), and Fig. 14 the actual efficiency improvement can be compared to the theoretical predicted. This comparison is shown in Table 4. The improvement is seen relative to Design 3, which has the lowest fill factor. Moreover the Bl^2/R_E ratio used to perform these calculations is the mean ratio for each voice coil design. From Table 4 it is seen, considering Design 1 and 3, that a fill factor optimization from 45% to 53% generates an efficiency improvement of approximately 1 dB, which in percentages corresponds to an improvement of 25%. Moreover it is evident that there is a quite good correlation between the theoretical estimation and the measured efficiency improvement. However there are some deviations. For all voice coil designs the measured efficiency improvement is higher than the estimation. This could be caused by the rather rough estimation of the fill factor described in Sec. 5.1. In addition to this, it is expected that there will exist deviations between measurements and theory. Nevertheless it is clearly seen that the measurements follow the hypothesis that a higher fill factor can generate more efficient loudspeakers. Since the measurement has not been conducted on fully assembled drivers it has not been possible to measure the frequency responses. However it is expected that the frequency response will behave and change with the fill factor according the analysis presented in Sec. 2.

7 CONCLUSION

This paper has presented a thorough analysis of the loudspeaker efficiency and its relation to the fill factor of the voice coil. This analysis showed that the efficiency can be expressed as a function of the fill factor and the geometry of the magnet system. In addition to this the influence of the driver's mass ratio was discussed and it was found that drivers with high mass ratios will benefit more from fill factor optimization than drivers with low mass ratio. Moreover the fill factor's impact on the frequency response of the driver has been investigated for low frequencies. It was found that a high fill factor will shift the low frequency upwards resulting in a higher –3 dB cut-off frequencies. On the practical side, different voice coil winding layouts have been described and analyzed with respect to their fill factors. It was found that by using rectangular wire to realize voice coils with low DC resistance the fill factor could be increased compared to that of conventional voice coils using round wire. However it should be mentioned that by using low impedance voice coil the cables connecting the loudspeaker with the amplifier should be as short as possible in order to reduce conduction losses. This indicates that these kind of voice coils are best suited for active loudspeaker systems. Four different voice coil designs were implemented. Due to insulation issues the fill factor of the voice coils using rectangular wire did, in practice, not exceed that of the conventional wire. However several solutions were suggested and discussed. The four implemented voice coil designs were measured on relevant parameters, i.e., the force factor, the DC resistance, and the mass. Based on the measurements the Bl^2/R_E ratio was calculated and from this the efficiency improvement was estimated assuming a large mass ratio. The measurement based Bl^2/R_E ratio confirmed the predicted hypothesis that a higher fill factor can increase the loudspeaker efficiency. The efficiency difference between the designs having the lowest and highest fill factors was theoretically estimated and compared to the measured results. Again a good correlation between theory and measurements was found and an efficiency improvement of approximately 1 dB was detected, which corresponds to an improvement of 25%. This improvement is actually massive and it could be even higher. This is due to the fact that the fill factor of the reference voice coil using conventional round wire was measured to be 53%, which leaves plenty of head room for future optimizing.

8 FUTURE WORK

Future work includes measurement on a fully assembled loudspeaker driver to verify that the efficiency is dependent on the fill factor as indicated in this paper and therefore can be measured in a the Sound Pressure Level test (SPL). In addition to this the predictions from Sec. 2, regarding the frequency response, should be experimentally verified.

Secondly, future work includes a new design of a fill factor optimized voice coil. It could use rectangular wire and have low impedance as done in this paper, but then the additional insulation layer should be avoided. In addition to this it is expected that the voice coil cost will increase when using rectangular wire compared to round wire. However this additional cost is not expected to be the dominating cost in a complete loudspeaker build. Finally, audio power amplifiers capable of handling low impedance drivers are to be developed; but with the use of switch-mode technology this should be possible. The authors encourage the development of a new loudspeaker design, with high fill factors, high mass ratios, and low DC resistance. This could allow for a new series of highly efficient drivers.

9 ACKNOWLEDGMENTS

The authors would like to thank Carsten Thingaard and Morten Halvorsen from PointSource Acoustics for their good advice and their know-how on measurement techniques on particular voice coils. Moreover the authors would like to thank Henrik Schneider from the Electronics Group, in the Department of Electrical Engineering, at the Technical University of Denmark, for many good discussions on the subject of efficiency improvement of loudspeakers.

1. REFERENCES

[1] Erickson and Maksimovic, *Fundamentals of Power Electronics*, Second Edition (Kluwer Academic Publishers, 2001).

[2] K. Nielsen, "*Audio Power Amplifier Techniques With Energy Efficient Power Conversion,*" Ph.D. thesis, Volume 1, Technical University of Denmark (1998).

[3] A. Yamauchi, A. Knott, I. H. H. Jorgensen and M. A. E. Andersen, "Frequency Dependent Loss Analysis and Minimization of System Losses in Switch-Mode Audio Power Amplifiers," presented at the *137th Convention of the Audio Engineering Society* (2014 Oct.), convention paper 9193.

[4] S. Poulsen, "Simple PWM Modulator Topology with Excellent Dynamic Behavior," *Applied Power Electronics Conference and Exposition* (2004).

[5] R. H. Small, "Closed-Box Loudspeaker Systems," *J. Audio Eng. Soc.*, vol. 20, pp. 383–395 (1972 June).

[6] A. N. Thiele, "Loudspeakers in Vented Boxes, Parts I and II," *J. Audio Eng. Soc.*, vol. 19, pp. 382–392 (1971 May); vol. 19, pp. 471–483 (1971 June).

[7] W. MarshallJr. Leach, *Introduction to Electroacoustics and Audio Amplifier Design* (Kendall/Hunt Publishing Company, 2003).

[8] H. F. Olson, *Acoustical Engineering* (Professional Audio Journals, Inc., 1957).

[9] N. E. Iversen and A. Knott, "Small Signal Loudspeaker Impedance Emulator," *J. Audio Eng. Soc.,* vol. 62, pp. 676–682 (2014 Oct.).

[10] N. E. Iversen, H. Schneider, A. Knott and M. A. E. Andersen, "Efficiency Investigation of Switch-Mode Power Audio Amplifiers Driving Low Impedance Transducers," presented at the *139th Convention of the Audio Engineering Society* (2015 Oct.), convention paper 9377.

[11] A. Yamauchi, H. Schneider, A. Knott, I. H. H. Jorgensen and M. A. E. Andersen, "Investigation of Energy Consumption and Sound Quality for Class-D Audio Amplifiers Using Tracking Power Supplies," presented at the *138th Convention of the Audio Engineering Society* (2015 May), convention paper 9287.

[12] S. Poulsen and M. A. E. Andersen, "Practical Considerations for Integrating Switch Mode Audio Amplifiers and Loudspeakers for a Higher Power Efficiency," presented at the *116th Convention of the Audio Engineering Society* (2004 May), convention paper 6155.

[13] Klippel Wolfgang, "Loudspeaker Non linearities. Causes, Parameters, Symptoms," Klippel GmbH, Dresden, Germany.

[14] G. W. Sioles, "Tweeter Design Considerations," *J. Audio Eng. Soc.*, vol. 4, pp. 105–109 (1956 July).

[15] F. Massa, "Signal Translating Apparatus," U.S. Patent 2214591 A, September 10, 1940.

[16] K. Thorborg and C. Futtrup, "Electrodynamic Transducer Model Incorporating Semi-Inductance and Means for Shorting AC Magnetization," *J. Audio Eng. Soc.*, vol. 59, pp. 612–627 (2011 Sep.).

[17] D. K. Cheng, *Field and Wave Electromagnetics*, Second edition (Addison-Wesley Publishing Company).

[18] M. Halvorsen, C. Tinggaard and F. Agerkvist, "Flux Modulation in the Electrodynamic Loudspeaker," presented at the *138th Convention of the Audio Engineering Society* (2015 May), convention paper 9317.

[19] F. Kochëndorfer and A. Voishvillo, "Comparative Static and Dynamic FEA Analysis of Single and Dual Voice Coil Midrange Transducers," presented at the *139th Convention of the Audio Engineering Society* (2015 Oct.), convention paper 9414.

[20] Technologies Agilent, "Agilent 34401A Multimeter," User's Guide.

[21] Mettler Toledo, "Operating Instructions, METTLER TOLEDO, PG-S balances (0.001g, 0.01g)."

[22] N. E. Iversen, A. Knott and M. A. E. Andersen, "Low Impedance Voice Coils for Improved Loudspeaker Efficiency," presented at the *139th Convention of the Audio Engineering Society* (2015 Oct.), convention paper 9389.

THE AUTHORS

Niels Elkjær Iversen

Arnold Knott

Michael A. E. Andersen

Niels Elkjær Iversen is a Ph.D. student at the electronics group at the Technical University of Denmark (DTU), Kongens Lyngby, Denmark. He received his B.Sc. degree in electrical engineering from DTU in 2012 and completed his M.Sc. education in December 2014. During his studies he has sumitted several papers for AES conventions, conferences. and the *AES Journal* all concerning electrical aspects of audio such as amplifier design, measurement techniques, and transducer modelling. The Audio Engineering Society has appointed his research the "Student Technical Papers Award" on two occasions, at the 136th convention in Berlin [9] and at the 139th convention in New York [22] respectively. Throughout his career his main interest has been reproduction of sound with focus on switch-mode power audio amplifiers and design and modelling of electric acoustic transducers.

•

Arnold Knott received the Diplom-Ingenieur (FH) degree from the University of Applied Sciences in Deggendorf, Germany, in 2004. From 2004 until 2009 he has been working with Harman/Becker Automotive Systems GmbH in Germany and USA, designing switch-mode audio power amplifiers and power supplies for automotive applications. In 2010 he earned the Ph.D. degree from the Technical University of Denmark, Kongens Lyngby, Denmark, working on a research project under the title "Improvement of Out of Band Behaviour in Switch-Mode Amplifiers and Power Supplies by their Modulation Topology." From 2010 to 2013 he was Assistant Professor and since 2013 Associate Professor at the Technical University of Denmark. His interests include switch-mode audio power amplifiers, power supplies, integrated circuit design, transducers, radio frequency electronics, and electromagnetic compatibility.

•

Michael A.E. Andersen received the M.Sc.E.E. and Ph.D. degrees in power electronics from the Technical University of Denmark, Kongens Lyngby, Denmark, in 1987 and 1990, respectively. He is currently a Professor of power electronics at the Technical University of Denmark. Since 2009, he has been Deputy Head of Department at the Department of Electrical Engineering. He is the author or coauthor of more than 200 publications. His research interests include switch-mode power supplies, piezoelectric transformers, power factor correction, and switch-mode audio power amplifiers.

C

Optimal control of a high frequency Class-D amplifier

In Journal of Audio Engineering Society, vol. 66, no. 1/2, pp. 33-42, Jan./Feb. 2018.

Dahl N., Iversen N., Knott A., and Andersen M. A. E.,
"Optimal Control of a High-Frequency Class-D Amplifier,"
J. Audio Eng. Soc., vol. 66, no. 1/2, pp. 33–42, (2018 January/February.).
DOI: https://doi.org/10.17743/jaes.2017.0046

Optimal Control of a High-Frequency Class-D Amplifier

NICOLAI DAHL, *AES Student Member*, **NIELS IVERSEN,** *AES Student Member*,
(nicolai@jerram.dk) (neiv@elektro.dtu.dk)

ARNOLD KNOTT, AND MICHAEL A. E. ANDERSEN, *AES Member*
(akn@elektro.dtu.dk) (ma@elektro.dtu.dk)

Technical University of Denmark, Kgs. Lyngby, Denmark

Control loops have been used with switch-mode audio amplifiers to improve the sound quality of the amplifier. Because these amplifiers use a high-frequency modulation, precautions in the controller design must be taken. Further, the quality factor of the output filter can have a great impact on the controller's capabilities to suppress noise and track the audio signal. In this paper design methods for modern control are presented. The control method proves to easily overcome the challenge of designing a good performing controller when the output filter has a high quality factor. The results show that the controller is able to produce a clear improvement in the Total Harmonic Distortion with up to a 30 times improvement compared to open-loop with a clear reduction in the noise. This places the audio quality on pair with current solutions.

0 INTRODUCTION

During the last decade, switch-mode audio amplifiers have become a common choice for audio applications. This is due to the superior efficiency these amplifiers offer compared to other traditional linear amplifiers. With efficiencies in the vicinity of 90% [1, 2], the achievements of high power density systems is possible. In terms of linearity, switch-mode amplifiers have shown great performance with Total Harmonic Distortion as low as 0.001%, [3–5]. The switch-mode power amplifier works by modulating the input audio into a high-frequency level discrete signal that drives a power stage. The modulation process of the signal is one of the primary sources of distortion due to the non-linearities in the process [3, 6, 7]. Another source of distortion is the power stage [8, 9]. The power stage is connected directly to the supply voltage, which results in disturbances in the supply voltage being reflected in the audio. To prevent these disturbances and non-linearities from introducing excessive distortion and noise to the amplified audio signal, the principals of feedback and control theory have been utilized to correct and suppress the unwanted behaviors of the switch-mode power amplifier.

To this day the majority of switch-mode power amplifiers have been using the principals of classical control due to its straight forward theory and the ease of implementing it in Single Input Single Output (SISO) systems [10, 11]. However, limitations in the theory often result in the control solution being only sub-optimal. Depending on the system, the limitations of the method can be so severe that no satisfactory solution can be obtained. This can, in audio applications, result in less reduction of distortion and noise than what is possible. One way to address this is through the means of modern control theory. Modern control, unlike output control, considers all the states of the system hence allowing for very precise control of the dynamics.

In this paper the principles of state space modelling, and how it can be used in conjunction with class-D amplifiers, is shown. Modern control theory methods will be applied to design and simulate a full state feedback integrating controller for use with a high-frequency bridge tied class-D amplifier. The benefits and drawbacks of using modern control for class-D amplifiers will be discussed. Finally, measured results obtained from an implemented test board will be presented to support the simulations.

1 STATE SPACE AVERAGE MODELING

The state space average model is a special case of state space modeling that is used to describe piecewise continuous systems such as Switch Mode Power Supply (SMPS). Here the method has been widely used since it provides an internal model of the system thus making it suitable for describing the small signal transfer properties of the system [12–14]. The state space average model works by modeling all the states a system can assume during a switching period, separately. The models are then averaged with a

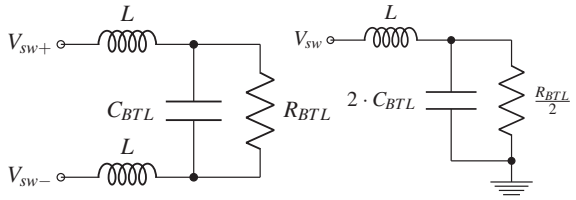

(a) Differential Filter (b) Single Ended Filter

Fig. 1. Transformation from differential to single ended filter

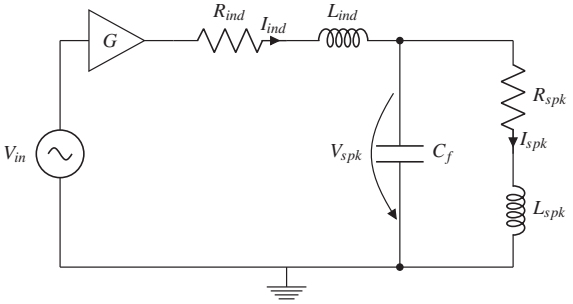

Fig. 2 . The circuit modeled in the state space model

weighted average based on the duty cycle that corresponds to the chosen linearization point. The duty cycle represents the percentage of time in a switching period where the level discrete signal of the modulator will be high.

1.1 Filter Transformation

For a class-D amplifier with a bridge tied load (Fig. 1a) the system can take two states assuming the dead time can be neglected. This will give the following outputs from the power stage to the output filter:

$$V_{sw+} = \begin{cases} V_{cc} & \forall\, dT_{sw} \\ 0 & \forall\, \bar{d}T_{sw} \end{cases}$$
$$V_{sw-} = \begin{cases} 0 & \forall\, dT_{sw} \\ V_{cc} & \forall\, \bar{d}T_{sw} \end{cases} \tag{1}$$

Where V_{sw+} and V_{sw-} are the differential output pair, d is the duty cycle, V_{cc} is the supply voltage for the power stage and T_{sw} is the time of the switching period. The differential nature of the bridge tied amplifier will increase the model complexity due to the existence of more internal states compared to a single ended configuration. To keep the model complexity to a minimum, the symmetry of the differential design is utilized to transform the system into a single ended equivalent system by using the methods presented in [15]. Fig. 1a shows the differential filter and 1b its single ended equivalent with the necessary scaling of component values to achieve the same filter properties as the differential filter. Here C_{BTL} and R_{BTL} are the capacitance and load for the bridge tied system that changes value when transformed.

The filter transformation further simplifies the outputs from the power stage to the output filter to be a single output that is symmetric around the reference voltage. Eq. (2) shows the transformed output.

$$V_{sw} = \begin{cases} V_{cc} & \forall\, dT_{sw} \\ -V_{cc} & \forall\, \bar{d}T_{sw} \end{cases} \tag{2}$$

Since audio is an AC signal, the linearization point is set to be the reference voltage where the duty cycle is $d = 0.5$. This leads to the state space average model being identical to a standard state space model that will be used to describe the system. Eq. (3) shows the standard form of a state space model for a Linear Time Invariant (LTI) system.

$$\dot{x}(t) = Ax(t) + Bu(t)$$
$$y(t) = Cx(t) + Du(t) \tag{3}$$

1.2 State Space Model

In general it is desired to model all the internal states since it will provide the most accurate description of the system. However, when designing an analog full state controller only the internal states that are directly measurable are of interest. This is because the full state controller must have a feedback path for every state which makes it crucial that the state is accessible [16]. In theory an observer could be implemented to model the states that are not directly measurable, but in practice it would be too unpractical to implement an analog observer. If digital control is used instead a more comprehensive description of the amplifier and loudspeaker can be made through state estimation. However, loudspeakers are very non-linear in the operational region thus adaptive methods [17] or more linear magnet-only loudspeakers [18] should be considered for the best results. This, however, is out of the scope of this paper.

The directly measurable states in the class-D amplifier are: the speaker voltage V_{spk}, the speaker current I_{spk}, and the inductor current I_{ind}. All three states are included in the state vector $x(t)$ (Eq. (4)).

$$x(t) = \begin{bmatrix} I_{ind} \\ I_{spk} \\ V_{spk} \end{bmatrix} \tag{4}$$

The output filter of the amplifier is a 2nd order low pass filter, thus only two states are needed to describe it (V_{spk} and I_{ind}). The inclusion of a third state (I_{spk}) makes it possible to model the speaker as a resistor and an inductor in series. Here the inductor represents the self-inductance of the voice coil of the loudspeaker thus increasing the model order of the speaker from a 0th order to a 1st order model. Fig. 2 shows the modeled circuit.

Here G is the gain through the modulator and the power stage. Eq. (5) provides an approximative gain through the amplifier based on the voltage amplification and the desired maximum modulation index M_{max}.

$$G = \frac{V_{spk}}{V_{in}} \cdot M_{max} \tag{5}$$

Table 1. Class-D Amplifier Specifications

Cutoff Frq (f_c)	155	kHz
Quality Factor (Q)	4.5	
Idle Switch Frq (f_{sw})	1.9	MHz
Max Modulation Index (M_{max})	76	%
Input Voltage pk-pk (V_{in})	2	V
Gain (G)	19.2	dB
Max Output Power (P_{rms})	9	W
Load Resistance (R_{spk})	8	Ω
Load Inductance (L_{spk})	2	nH

The input to the state space model $u(t)$ is in this case the audio input $V_{in}(t)$. From this the system matrix A (Eq. (6)) and the input matrix B becomes:

$$A = \begin{bmatrix} -\frac{R_{ind}}{L_{ind}} & 0 & -\frac{1}{L_{ind}} \\ 0 & -\frac{R_{spk}}{L_{spk}} & \frac{1}{L_{spk}} \\ \frac{1}{C_f} & -\frac{1}{C_f} & 0 \end{bmatrix} \quad B = \begin{bmatrix} \frac{G}{L_{ind}} \\ 0 \\ 0 \end{bmatrix} \tag{6}$$

The output of the system is selected to be the voltage across the speaker for convenience. The output could also be the current through the speaker. This would give a better control of the speaker dynamics but also increase the requirements for the accuracy of the self-inductance of the voice coil thus making the amplifier less acceptable for different speakers. Based on the selected output the output matrix C and feed through matrix D becomes:

$$C = \begin{bmatrix} 0 & 0 & 1 \end{bmatrix} \qquad D = 0 \tag{7}$$

With the linear state space model constructed, component values can be assigned. The supplied class-D amplifier will have component values that ensures that the specifications in Table 1 are met. The amplifier will be tested into a resistive load hence the inductance of the load is assumed to be close to zero and is estimated to be 2 nH. Doing the filter transformation will result in the system and input matrix (Eq. (8)).

$$A = \begin{bmatrix} -\frac{37\text{m}\Omega}{1\mu\text{H}} & 0 & -\frac{1}{1\mu\text{H}} \\ 0 & -\frac{4\Omega}{1\text{nH}} & \frac{1}{1\text{nH}} \\ \frac{1}{1.32\mu\text{F}} & -\frac{1}{1.32\mu\text{F}} & 0 \end{bmatrix} \quad B = \begin{bmatrix} \frac{9.12}{1\mu\text{H}} \\ 0 \\ 0 \end{bmatrix} \tag{8}$$

2 OPEN-LOOP SYSTEM RESPONSE

The found values allow for an analysis of the open-loop system response. Fig. 3 shows the bode plot of the open-loop system. Here it is seen that the frequency response follows the response of an underdamped 2nd order low pass filter. The underdamping results in a large resonance peak, 13 dB higher than DC, at the natural frequency (138.6 kHz). This is typically unwanted in a class-D amplifier since the damped oscillation it creates, impedes the ability to improve the fidelity when using classical control since an increase in the gain at the resonance frequency will also increase the resonance. However, in modern control, this problem is easily solved, and thus the resonance peak can be used to improve the distribution of heat in the power stage by moving losses from the switching devices to the filter [19].

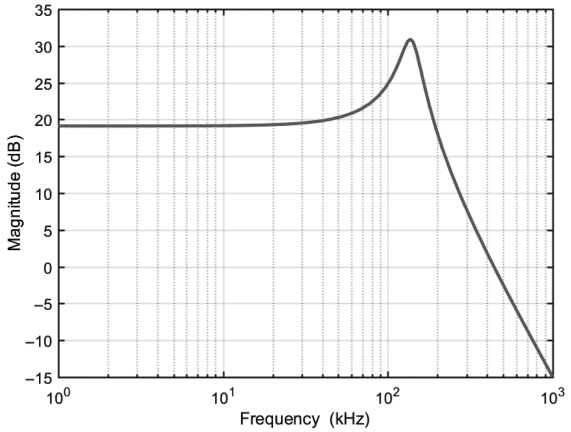

Fig. 3. Calculated open-loop bode plot

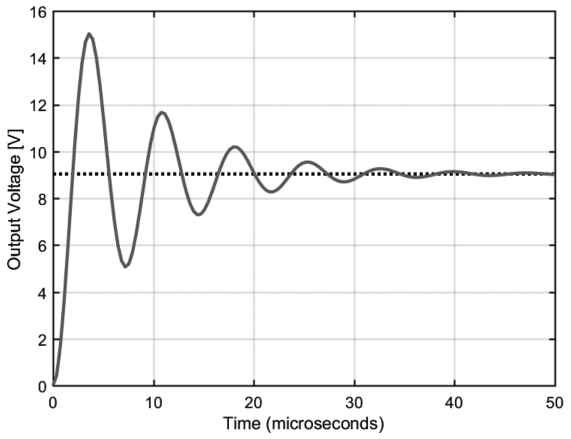

Fig. 4. Calculated open-loop step response

To get a better understanding of the amount of oscillation produced from the resonance peak, a step response is conducted. Fig. 4 shows the step response of the open-loop system. Here it is clear that the oscillation generates extensive overshoots (70.4%) and settles to within 2% of the final value in 40.3 μs. Both of these properties must be reduced to improve the response of the system.

3 CONTROLLER DESIGN

3.1 Controllability

One requirement must be fulfilled when designing a full state controller. This is the need for the important states of the system to be controllable. A state is controllable when the state can be affected by the input of the system. If a state is not controllable it must at least be stabilizable such that the state will not diverge over time. To investigate the controllability, the controllability matrix, which consists of multiple combinations of the system matrix and input matrix, is used [16]. From the controllability matrix the amount of controllable states can be determined based on

the rank of the matrix. If the rank is full all states are controllable. Matrix 9 shows the controllability matrix for the class-D amplifier system and Eq. (10) the resulting rank.

$$M_c = \begin{bmatrix} B & AB & A^2B \end{bmatrix} = \begin{bmatrix} -\frac{G}{L_{ind}} & -\frac{G \cdot R_{nd}}{L_{ind}^2} & -\frac{G \cdot (L_{ind} - C \cdot R_{ind}^2)}{C \cdot L_{ind}^3} \\ 0 & 0 & \frac{G}{C \cdot L_{spk} \cdot L_{ind}} \\ 0 & \frac{G}{C \cdot L_{ind}} & -\frac{G \cdot R_{ind}}{C \cdot L_{ind}^2} \end{bmatrix} \tag{9}$$

$$\text{Rank}(M_c) = 3 \tag{10}$$

Since all the states are proven controllable, the methods for designing a full state integral controller can be applied.

3.2 Integral Transformation

Due to the non-linearities in the class-D amplifier coming from the modulator and output filter an integration term is desirable. The integration term is added to improve the tracking capabilities such that the class-D amplifier to a certain extend maintains:

$$V_{spk} \propto V_{in} \quad \forall\, V_{in} \subseteq V_{span} \tag{11}$$

Where V_{span} is the chosen range of input voltage the amplifier can take without clipping. This property is especially useful when the controller is used in the actual implementation since it counteracts the non-linear behaviors. The integration term will result in an I controller for the error signal $e(t)$, and thus be in series with the class-D amplifier. Because of this, it is essential that the time constant for the integrator will result in a bandwidth greater than the bandwidth of the signal into the system to ensure proper tracking. For the class-D amplifier, this means that the bandwidth of the integrator should be so high that audio content can pass through it without being attenuated. Audio is present within 20 Hz to 20 kHz. Thus the integrator will easily be able to meet this requirement due to the cutoff frequency of the output filter being at 155 kHz, providing plenty of bandwidth to work with.

To include the integrator term into the state space model, an integral transformation is applied:

$$A_i = \begin{bmatrix} A & 0 \\ -C & 0 \end{bmatrix}, \quad B_i = \begin{bmatrix} B \\ 0 \end{bmatrix}, \quad C_i = [C \quad 0] \tag{12}$$

This results in an extra state for the integrator (q) in the state space model, hence the new state vector becomes:

$$x(t) = \begin{bmatrix} I_{ind} \\ I_{spk} \\ V_{spk} \\ q \end{bmatrix} \tag{13}$$

The integration state q simply consists of the negative output of the system that in this case is $-V_{spk}$. This is used as the negative feedback to generate the error signal for the I controller. With the integrator transform done, the Linear Quadratic Regulator design approach can be applied to the system [20, 16].

3.3 Linear Quadratic Regulator

The Linear Quadratic Regulator (LQR) is an optimization method used in modern control to find the optimal full state controller with time varying gains. However, time varying gains are often not practical nor necessary, hence a simplified steady state LQR method has been developed that will be used for the system. This method optimizes a cost function with the mostly used cost function being the following quadratic performance index [20, 16]:

$$J(u) = \lim_{t \to \infty} \int_0^t x^T(t) R_1 x(t) + u(t)^T R_2 u(t)\, \mathrm{dt} \tag{14}$$

Here $x(t)$ is the state of the system and $u(t)$ the control signal to the system. R_1 and R_2 are penalty matrices that are used to emphasize the performance of specific states and control signals. It is desired to minimize the index $J(u)$ in Eq. (14).

$$\min J(u) \qquad \text{s.t.} \quad \dot{x}(t) = A_i x(t) + B_i u(t) \tag{15}$$

This can only be solved numerically for non-linear systems that easily becomes very time consuming. By using a linearized state space model this is avoided and static optimization can be used to find optimal steady state gains for the full state feedback controller. It can be shown that the limiting constant solution P_∞ to the performance index can be found by solving the Algebraic Riccati Equation (Eq. (16)) [16].

$$0 = A^T P_\infty + P_\infty A + R_1 - P_\infty B R_2^{-1} B^T P_\infty \tag{16}$$

From this the optimal constant gains for the full state controller become:

$$K_\infty = R_2^{-1} B^T P_\infty \tag{17}$$

For the class-D amplifier it is desired to compensate for any non-linearities as fast as possible and to reduce the damped oscillation on the output. To realize this, the penalty matrix R_1 is designed to heavily penalize the integration state. This will move the pole of the integrator to the left in the s-plane and make it settle somewhere close to the poles of the 2nd order filter, thus making the time constant of the integrator about the same as the output filters. The matrices in Eq. (18) shows the placement of the poles before and after the controller is applied.

$$\begin{bmatrix} 0 \\ -4 \cdot 10^9 \\ -1.13 \cdot 10^5 + 8.67i \cdot 10^5 \\ -1.13 \cdot 10^5 - 8.67i \cdot 10^5 \end{bmatrix} \rightarrow \begin{bmatrix} -5.14 \cdot 10^5 \\ -4 \cdot 10^9 \\ -6.62 \cdot 10^5 + 5.82i \cdot 10^5 \\ -6.62 \cdot 10^5 - 5.82i \cdot 10^5 \end{bmatrix} \tag{18}$$

Since the damped oscillation limits the movement of the integrator, it is to be expected that the LQR will further

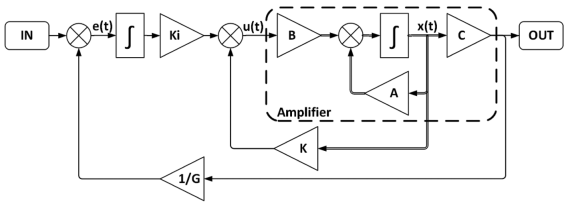

Fig. 5. Amplifier with control. The gain block K consists of the first three elements of K_∞ where each gain is assigned to each state of the amplifier. The last gain in K_∞ is placed after the integrator to set the time constant.

increase the damping of the output filter such that the oscillation will be reduced. All these pole movements generate a growth in the control signal that is limited by the supply voltage. It is important that the control signal does not clip since this would result in the system acting as an open-loop system. To avoid this, the penalty matrix R_2 is increased to emphasize the size of the control signal thereby reducing it. Eq. (19) shows the two penalty matrices. Both matrices are found through hand-tuning of the different penalties.

$$R_1 = \begin{bmatrix} 0.7 & 0 & 0 & 0 \\ 0 & 10^{-3} & 0 & 0 \\ 0 & 0 & 10^{-3} & 0 \\ 0 & 0 & 0 & 10^{11} \end{bmatrix}, \quad R_2 = 30 \qquad (19)$$

By providing a small penalty to the inductor current, the in-rush current is limited thus eliminating any overshoot at the output. Using the obtained model in Eq. (12) and the penalty matrices in Eq. (19) the feedback gains are found using Eqs. (16) and (17). The resulting gains are shown in Eq. (20). Here it is particularly noticeable that the state, describing the current through the speaker, is of next to no interest for the controller. This is probably because the controller focusses on controlling the voltage across the speaker and since the speaker current is a result of the voltage across the speaker, the current does not matter for the control of the amplifier.

$$\begin{aligned} K_\infty &= \begin{bmatrix} K_{ind_I} & K_{spk_I} & K_{spk_V} & -K_i \end{bmatrix} \\ &= \begin{bmatrix} 0.177 & -1.062 \cdot 10^{-5} & 0.056 & -5.774 \cdot 10^4 \end{bmatrix} \end{aligned} \qquad (20)$$

In Eq. (20) the last gain is the negative inverse of the time constant of the integrator, thus the time constant becomes:

$$\tau_i = \frac{1}{-K_i} = 17.321 \mu s \qquad (21)$$

With the feedback gains and the time constant found, the loop can be closed according to the closed system shown in Fig. 5.

An analysis of the closed-loop system can be conducted. Fig. 6a shows the frequency response and Fig. 6b the step response of both the open-loop and the closed-loop system.

The bode plot clearly shows that the damping of the complex conjugated pole pair has been increased since

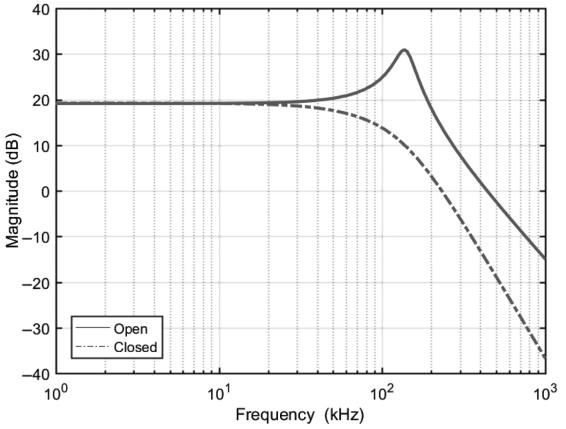

(a) Frequency Response

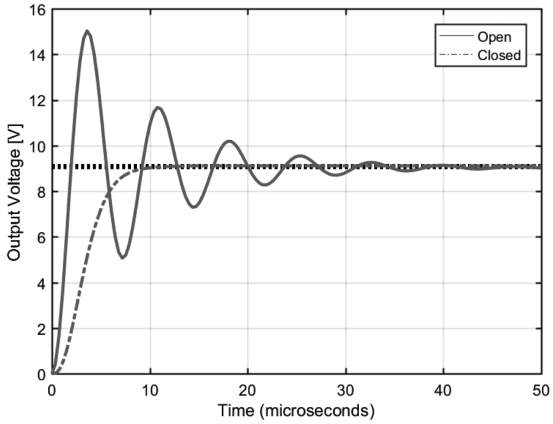

(b) Step Response

Fig. 6. Calculated open and closed-loop step and frequency response for the amplifier

the resonance peak from the open-loop response has completely disappeared. The cutoff frequency of the integrator has moved to approximately 83.8 kHz giving a total bandwidth of the system of 71.3 kHz. This is below the cutoff frequency of the 2nd order filter but still around 3.5 times faster than the minimum requirement for audio at 20 kHz. The step response further confirms that the resonance peak has been eliminated. This can be seen in the closed-loop response that does not have any overshoot or ringing. The step has a rise time of 4.8 μs and a settling time of 8.8 μs.

In order to know the behavior of the remaining states, a simulation of the linear model is made. Fig. 7 shows all the states of the closed-loop system.

Looking at the states, it is seen that the current through the inductor reaches almost 4 A when the step is conducted. This current peak is of no concern because of two reasons. First, the step is made on a single ended model. This results in the speaker resistance only being half of the size it will be in the full bridge due to the conversion made in Sec. 1.1. Due to the reduced resistance size, the current in the model is doubled compared to the implementation. Because of this it is important to remember that the feedback gains for the

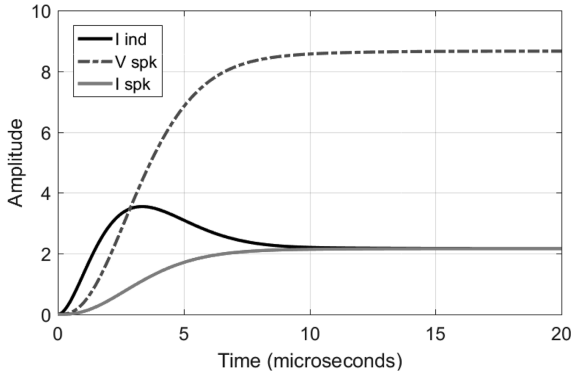

Fig. 7. Calculated step responses for all states

states that describe the currents should be the double of what has been found in Eq. (20). Second, the steps conducted are absolute worst case scenarios. In practice, audio would never make an instantaneous step, thus the overshoot of the current through the inductor would never happen to such extents. The reason why the steps are used are to guarantee robustness of the controller design. If the step response is stable a response to a sinusoid is also guaranteed to be stable.

4 SWITCHING MODEL

To investigate if a switching system will act in the same manner as the linearized system just derived, a non-linear switching Simulink model has been made. This model has the same specifications and component values as the linearized model found in Table 1 and Eq. (8). The switching model implements an AIM modulator [21, 22], propagation delay, dead-time, and non-ideal behaviors of the operational amplifiers. These expansions are made to account for the switching behavior of the system and to determine how switching residuals will affect the controller. Further, the switching model includes a first order low pass filter at the control signal with a cutoff frequency of 550 kHz. The purpose of the filter is to filter out the remaining switching residuals before the control signal enters the modulator without adding additional phase in the audio band. Fig. 9 shows the described Simulink model.

To ensure the equality of the models, an identical step of the open-loop (Fig. 8a) and the closed-loop (Fig. 8b) are conducted for both models.

Fig. 8a clearly shows an identical behavior of the state space model and the switching Simulink model when in open-loop. Here the voltage ripple from the switching is almost non-existing due to the resonance from the filter dominating the signal. On Fig. 8b the switching model overshoots slightly due to the non-ideal behavior of the operational amplifiers. This time, the voltage ripple from the switching is also more visible because the resonance has been eliminated.

These results confirm that a switching system such as a class-D amplifier will follow the same behavior as the linear state space system.

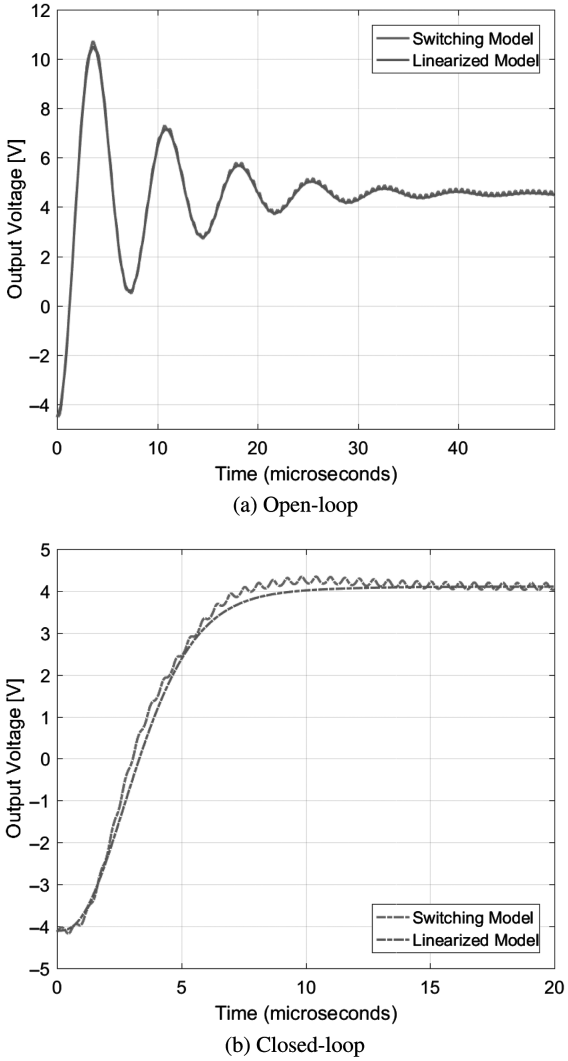

Fig. 8. Open and closed-loop step response for the linearized state space model and the switching simulation

5 IMPLEMENTATION

To assess the true performance of the system with the designed controller a physical implementation is made. The implementation is a 12 V full-bridge class-D amplifier made with the same values as used for the switching and linearized model. The implementation also implements the filter at the controller used in the switching model. Fig. 10 shows a picture of the physical implementation.

In the implementation, the current in the inductor is measured using a lossless equivalent time constant method as proposed in [23, 24]. This method is used since it has a minimal impact on the filter characteristics and has no current sense resistor thus avoiding the resistive loss. For the speaker current, the traditional resistor method is used to measure the current. The physical implementation is compared to the results obtained in Fig. 8 by conducting the same step on the input in open and closed-loop. The

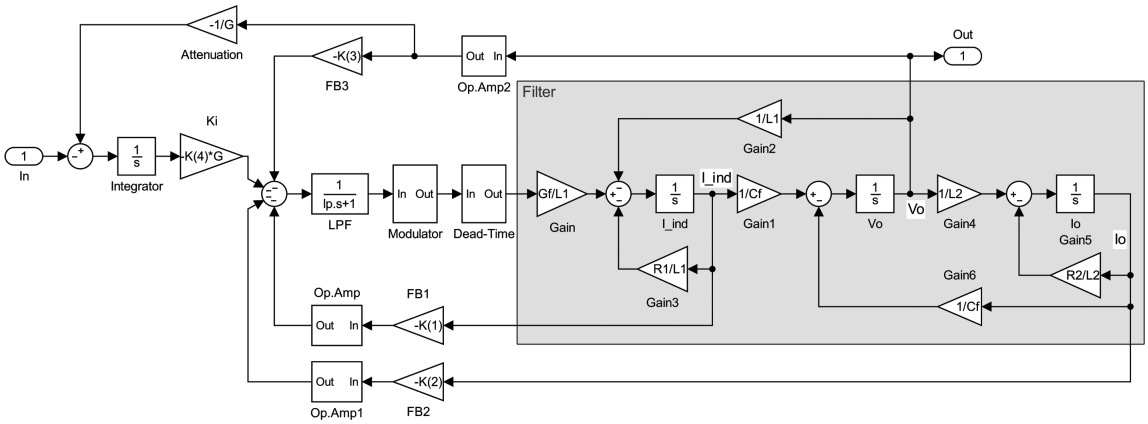

Fig. 9. Simulink model used for simulating the switching behavior of the system

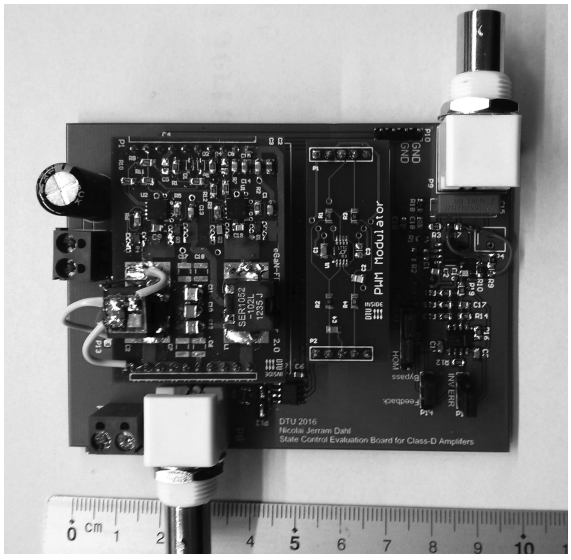

Fig. 10. Prototype of the class-D amplifier and control loop

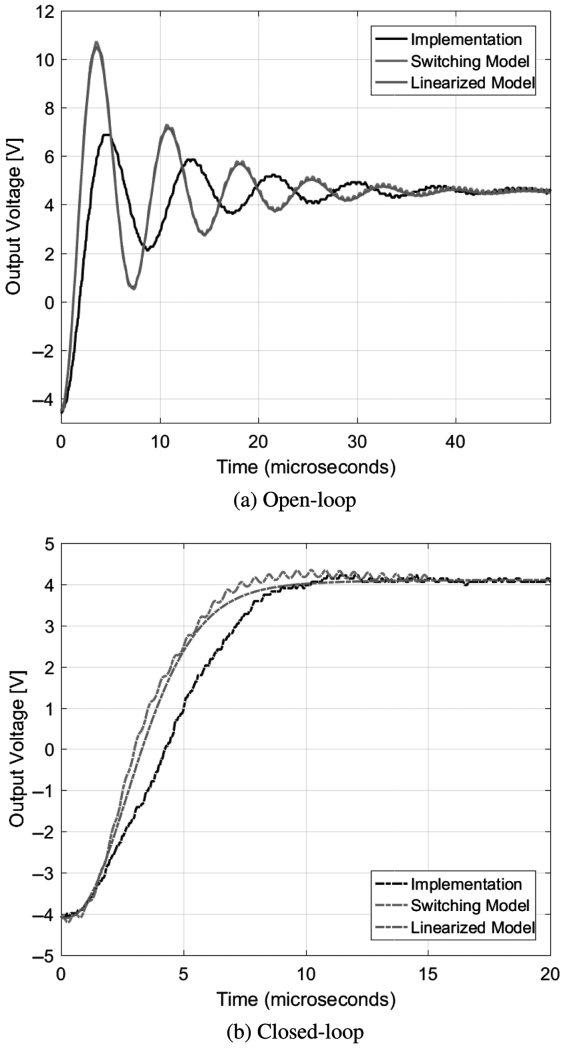

Fig. 11. Open and closed-loop step response for the physical implementation, the linearized and switching simulation

implementation is tested into an 8 Ohm resistor. Thus the inductance of the load is assumed to be close to zero. Fig. 11a shows the step response of all the systems.

From the step response in Fig. 11a it can be seen that the measured step of the implementation deviates slightly from the models. The implementation shows both more damping and an oscillation at a slightly lower frequency. The reason for this deviation is probably because the Equivalent Series Resistance (ESR) of the capacitors in the output filter have not been modeled in the models. The ESR takes energy out of the system thus reducing the overshoot. Since the implementation has more damping than the models, it would be possible to design a controller that is able to track harder than what is possible with the models. This is because the increased damping of the system results in less control effort to move the poles of the filter, thus more control effort could be dedicated to the speed of the integrator.

6 RESULTS

Fig. 11b shows the closed-loop step response of the implementation and the models. The implementation reaches the final value at the same time as the models but with a slightly different trajectory. The difference in the trajectory is due to the ESR in the capacitor that results in a slightly slower response than expected. However, since the final value is reached at the same time, the difference in the trajectory only has a small impact on the performance.

Measurements of the Total Harmonic Distortion plus Noise (THD+N) determine the performance of the system when playing audio. Fig. 12a to 12c shows the measured THD+N for the physical implementation for the three frequencies: 100 Hz, 1 kHz, and 6.6 kHz, with and without the controller connected. The frequency 6.6 kHz provides a worst-case THD measurement as it is the highest frequency before the third harmonic falls out of the audio spectrum. At low power, where the noise is dominant, the closed-loop is able to suppress the noise better than the open-loop due to the control structure reducing the noise variance. Fig. 12d presents the THD+N for the three closed-loop measurements. Here it is seen that the THD+N measurements at 1 kHz and 6.6 kHz are decreasing until 0.01 W where the non-linearities starts to become dominant. The 100 Hz THD+N measurement is able to decrease until 1.5 W, where clipping starts to occur. The reason for the improved THD+N at 100 Hz is the larger bandwidth available resulting in the integrator being able to suppress the non-linearities more. Overall the closed-loop THD+N measurements consistently reach down to 0.02% and below 0.01% for the 100 Hz measurement yielding up to a 30 times improvement in the THD+N compared to open-loop. These results place this solution on a par with state-of-the-art such as [25, 26] from 2012 and 2016. In [25] THD+N measurements down to just below 0.02% at 1 kHz and 0.08% at 6.6 kHz were obtained. In [26] the obtained THD+N measurements go down to 0.01% at 1 kHz and fluctuates around 0.06% at 6.6 kHz. Thus the presented amplifier delivers similar THD+N at 1 kHz, but noticeable lower and more consistent THD+N results at 6.6 kHz.

7 CONCLUSION

This paper presented the fundamentals of modern control and used them in conjunction with class-D amplifiers. Here filter transformation and state space modeling were used to construct a linear model of a high-frequency class-D amplifier with a large resonance peak. An optimal linear full state integral controller based on the state space model was designed, using the LQR method, and verified on a linear and switching model. Finally, measurements on a class-D amplifier with the implemented controller showed step responses and THD+N measurements that aligned well with the theory. The THD+N measurements showed an overall improvement with up to 30 times reduction in the THD+N compared to the amplifier without the controller as well as lower noise through the amplifier. The results obtained are on pair with current solutions with an overall

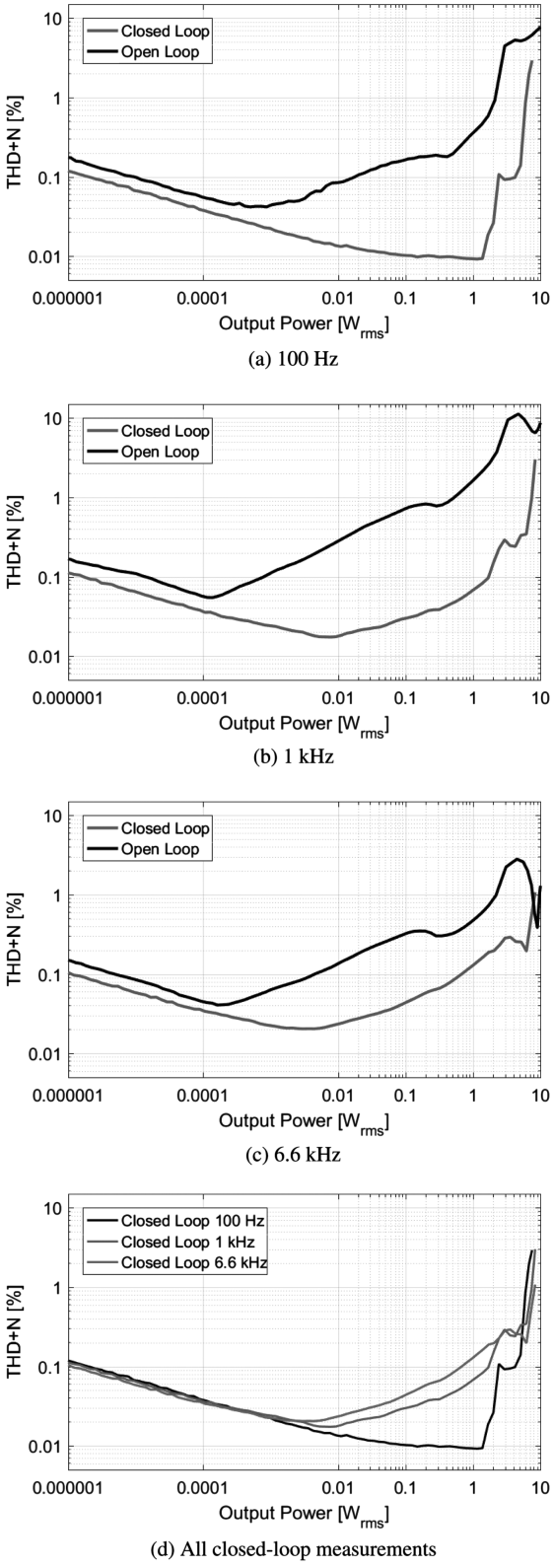

Fig. 12. THD+N vs. Output power measured on the implemented amplifier for the three frequencies: 100 Hz, 1 kHz and 6.6 kHz

improvement in the THD+N at 6.6 kHz. This proves that the principals of modern control achieve good performance in class-D amplifiers, even when the output filter has a large resonance.

8 FUTURE WORK

The i ntegration term needs to be heavily emphasized in the penalty matrix to acquire the desired gain and response of the amplifier. This results in a large control effort that gets limited by the possible output swing of the operational amplifiers and the input range of the modulator. Thus, investigation of alternative cost functions for the control loop should be done to reduce the current size of the integrator as well as reducing the control effort making it more feasible to add an additional global control loop.

9 REFERENCES

[1] K. Nielsen, "*Audio Power Amplifier Techniques with Energy Efficient Power Conversion*," Technical University of Denmark, Ph. D. Thesis (1998 Apr.).

[2] M. Duraij, N. E. Iversen, L. P. Petersen, and P. Boström, "Self-Oscillating 150 W Switch-Mode Amplifier Equipped with eGaN-FETs," presented at the *139th Convention of the Audio Engineering Society* (2015 Oct.), convention paper 9378.

[3] B. Putzeys, "Simple Self-Oscillating Class D Amplifier with Full Output Filter Control," presented at the *118th Convention of the Audio Engineering Society* (2005 May), convention paper 6453.

[4] S. Poulsen and M. A. Andersen, "Simple PWM Modulator Topology with Excellent Dynamic Behavior," presented at the *Applied Power Electronics Conference and Exposition, 2004. APEC'04. Nineteenth Annual IEEE*, vol. 1, pp. 486–492 (2004), https://doi.org/10.1109/APEC.2004.1295852.

[5] J. Lu and R. Gharpurey, "A Self Oscillating Class D Audio Amplifier with 0.0012% THD+ N and 116.5 dB Dynamic Range," presented at the *Custom Integrated Circuits Conference (CICC), 2010 IEEE*, pp. 1–4 (2010), https://doi.org/10.1109/CICC.2010.5617615.

[6] N. Dahl, N. E. Iversen, A. Knott, and M. A. Andersen, "Comparison of Simple Self-Oscillating PWM Modulators," presented at the *140th Convention of the Audio Engineering Society* (2016 May), convention paper 9562.

[7] S. Poulsen and M. A. E. Andersen, "Self Oscillating PWM Modulators, a Topological Comparision," presented at the *Power Modulator Symposium, 2004 and 2004 High-Voltage Workshop. Conference Record of the Twenty-Sixth International*, pp. 403–407 (2004), https://doi.org/10.1109/MODSYM.2004.1433597.

[8] R. Selva Kumar, V. Karthick, and D. Arun, "A Review on Dead-Time Effects in PWM Inverters and Various Elimination Techniques," *Int. J. Emerg. Technol. Adv. Eng.*, vol. 4, no. 1, pp. 385–387 (2014).

[9] T. Ge, J. S. Chang, and W. Shu, "Power Supply Noise in Bang-Bang Control Class D Amplifier," presented at the *Circuits and Systems, 2007. ISCAS 2007. IEEE International Symposium on*, pp. 701–704 (2007), https://doi.org/10.1109/ISCAS.2007.377905.

[10] M. C. Høyerby and M. A. Andersen, "Carrier Distortion in Hysteretic Self-Oscillating Class-D Audio Power Amplifiers: Analysis and Optimization," *IEEE Transactions on Power Electronics*, vol. 24, no. 3, pp. 714–729 (2009), https://doi.org/10.1109/TPEL.2008.2007956.

[11] S.-H. Jung, N.-I. Kim, and G.-H. Cho, "Class D Audio Power Amplifier with Fine Hysteresis Control," *Electronics Letters*, vol. 38, no. 22, pp. 1302–1303 (2002), https://doi.org/10.1049/el:20020936.

[12] W. Polivka, P. Chetty, and R. Middlebrook, "State-Space Average Modelling of Converters with Parasitics and Storage-Time Modulation," presented at the *Power Electronics Specialists Conference, 1980. PESC. IEEE*, pp. 119–143 (1980), https://doi.org/10.1109/PESC.1980.7089440.

[13] C. Nwosu and M. Eng, "State-Space Averaged Modeling of a Nonideal Boost Converter," *Pacific J. Science and Tech.*, vol. 2, no. 9, pp. 1–7 (2008).

[14] M. R. Modabbernia, F. K. Khoshkbijari, R. Fouled, and S. S. Nejati, "The State Space Average Model of Buck-Boost Switching Regulator including all of the System Uncertainties," *Int. J. Computer Science and Engineering*, vol. 5, no. 2, p. 120 (2013).

[15] K. Chan, "Design of Differential Filter for High-Speed Signal Chains," Texas Instruments Application Report (2010).

[16] E. Hendricks, O. Jannerup, and P. H. Sørensen, *Linear Systems Control: Deterministic and Stochastic Methods* (Springer Science & Business Media, 2008), https://doi.org/10.1007/978-3-540-78486-9.

[17] W. Klippel, "Adaptive Stabilization of Electrodynamic Transducers," *J. Audio Eng. Soc.*, vol. 63, pp. 154–160 (2015 Mar.), https://doi.org/10.17743/jaes.2015.0011.

[18] B. Merit and A. Novak, "Magnet-Only Loudspeaker Magnetic Circuits: A Solution for Significantly Lower Current Distortion," *J. Audio Eng. Soc.*, vol. 63, pp. 463–474 (2015 Jun.), https://doi.org/10.17743/jaes.2015.0051.

[19] N. E. Iversen, N. J. Dahl, A. Knott, M. A. E. Andersen, "Towards Higher Power Density Audio Amplifiers" (2017).

[20] S. A. Lindiya, K. Vijayarekha, and S. Palani, "Deterministic LQR Controller for dc-dc Buck Converter," presented at the *Power and Energy Systems: Towards Sustainable Energy (PESTSE), 2016 Biennial International Conference on*, pp. 1–6 (2016), https://doi.org/10.1109/PESTSE.2016.7516450.

[21] B. J. G. Putzeys, "Power amplifier" (2006 Sep. 26), US Patent 7,113,038.

[22] A. Knott, G. R. Pfaffinger, and M. Andersen, "A Self-Oscillating Control Scheme for a Boost Converter Providing a Controlled Output Current," *IEEE Transactions on Power Electronics*, vol. 26, no. 9, pp. 2707–2723 (2011), https://doi.org/10.1109/TPEL.2011.2126600.

[23] LinFinity, "A Simple Current-Sense Technique Eliminating a Sense Resistor," Application Note (1998).

[24] H. P. Forghani-Zadeh and G. A. Rincon-Mora, "Current-Sensing Techniques for DC-DC Converters," presented at the *Circuits and Systems, 2002. MWSCAS-2002. The 2002 45th Midwest Symposium on*, vol. 2, pp. II–II (2002), https://doi.org/10.1109/MWSCAS.2002.1186927.

[25] T. Instruments, "TPA3116D2 15-W, 30-W, 50-W Filter-Free Class-D Amplifier Family with AM Avoidance" (2012).

[26] M. Høyerby, J. K. Jakobsen, J. Midtgaard, and T. H. Hansen, "A 2 x 70 W Monolithic Five-Level Class-D Audio Power Amplifier In 180 nm BCD," *IEEE J. Solid-State Circuits*, vol. 51, no. 12, pp. 2819–2829 (2016), https://doi.org/10.1109/JSSC.2016.2600251.

[27] N. E. Iverson and A. Knott, "Small Signal Loudspeaker Impedance Emulator," *J. Audio Eng. Soci.*, vol. 62, pp. 676–682 (2014 Oct.), https://doi.org/10.17743/jaes.2014.0036.

[28] N. E. Iversen, A. Knott, and M. A. Andersen, "Relationship between Voice Coil Fill Factor and Loudspeaker Efficiency," *J. Audio Eng. Soc.*, vol. 64, pp. 241–252 (2016 Apr.), https://doi.org/10.17743/jaes.2016.0006.

THE AUTHORS


Nicolai J. Dahl


Niels Elkjßr Iversen


Arnold Knott


Michael A. E. Andersen

Nicolai J. Dahl is an electrical engineering student at Technical University of Denmark where he started in 2013. His main focuses in his studies are: control theory, audio electronics, and signal processing; and he has since early 2014 continuously worked with class D amplifiers and their power supplies. Currently Nicolai is working on his M.Sc. degree specializing in control theory for automation.

•

Niels Elkjær Iversen is a Ph.D student at the electronics group at the Technical University of Denmark, Kongens Lyngby, Denmark. He received his M.Sc degree in December 2014. His research interests include electrical aspects of audio such as switch-mode power audio amplifiers, measurement techniques, and transducer modelling. The Audio Engineering Society has appointed his research the "Student Technical Papers Award" on two occasions, at the 136th convention in Berlin and at the 139th convention in New York both later published in the *AES Journal* [27, 28].

•

Arnold Knott received the Diplom-Ingenieur (FH) degree from the University of Applied Sciences in Deggendorf, Germany, in 2004. From 2004 until 2009 he has been working with Harman/Becker Automotive Systems GmbH in Germany and USA, designing switch-mode audio power amplifiers and power supplies for automotive applications. In 2010 he earned the Ph.D. degree from the Technical University of Denmark, Kongens Lyngby, Denmark, working on a research project under the title "Improvement of Out of Band Behaviour in Switch-Mode Amplifiers and Power Supplies by Their Modulation Topology." From 2010 to 2013 he was Assistant Professor and since 2013 Associate Professor at the Technical University of Denmark. His interests include switch-mode audio power amplifiers, power supplies, integrated circuit design, transducers, radio frequency electronics, and electromagnetic compatibility.

•

Michael A.E. Andersen received the M.Sc.E.E. and Ph.D. degrees in power electronics from the Technical University of Denmark, Kongens Lyngby, Denmark, in 1987 and 1990, respectively. He is currently a Professor of power electronics at the Technical University of Denmark. Since 2009, he has been Deputy Head of Department at the Department of Electrical Engineering. He is the author or coauthor of more than 200 publications. His research interests include switch-mode power supplies, piezoelectric transformers, power factor correction, and switch-mode audio power amplifiers

D

Multilevel tracking power supply for switch-mode audio power amplifiers

In IEEE APEC, San Antonio, March 4-8, 2018.

Multilevel tracking power supply for switch-mode audio power amplifiers

Niels E. Iversen[1], Vladan Lazarevic[2], Miroslav Vasic[2], Arnold Knott[1], Michael A.E. Andersen[1] and Jose A. Cobos[2]

[1]Technical University of Denmark, Department of Electrical Engineering, 2800, Kgs. Lyngby, Denmark.
[2]Universidad Politecnica de Madrid, Centro de Electronica Industrial - CEI, Madrid, Spain.
Email: neiv@elektro.dtu.dk

***Abstract*—Switch-mode technology is the common choice for high efficiency audio power amplifiers. The dynamic nature of real audio reduces efficiency as less continuous output power can be achieved. Based on methods used for RF amplifiers this paper proposes to employ envelope tracking techniques to the power supply in order to improve efficiency. A 100 W prototype system was designed. Measured results show that systems employing envelope tracking can improve system efficiency from 2% to 12%, i.e. a factor of 6. The temperature rise is strongly reduced, especially for the switching power MOSFETs where it is halved from 100 °C to 50 °C.**

I. Introduction

Switch-mode power audio amplifiers, also know as class-D amplifiers, have become the conventional choice for audio amplifications as they have excellent audio performance with very low distortion [1]–[3] and superior efficiency compared to linear amplifiers such as class-A and class-AB [4]. However the measurement technique for measuring the efficiency normally utilizes sine waves. Sine waves are fundamentally different from dynamic music signals and therefore do not represent real audio signals very well [5], [6]. Real audio signals is much more dynamic and have a high peak-to-rms ratio, also known as the Crest Factor (CF). Fig. 1 shows the amplitude distribution of 183 audio tracks provided by [6].

It is observed that amplitude distribution between audio and sine waves are fundamentally different and that real audio signals in fact is much more dynamic compared to sine waves. This highly dynamic nature of audio signals causes a degradation of efficiency as less continuous output power can be achieved. The dominant losses in the amplifier at low output power are switching losses which directly relate to the supply voltage level. Low efficiency is a challenge as it indicates an excessive loss within the amplifier which can cause thermal stress on power stage components, increase the size of required heat sink and act as a limiting factor for play back time in battery driven systems.

A similar challenge exists for Radio Frequency (RF) power amplifiers where highly dynamic radio signals cause low efficiency [7]–[9]. To overcome this challenge within RF power amplifiers several methods have been proposed including Envelope Tracking (ET) and Envelope Elimination and Restoration (EER) [10]–[13]. This work aim to apply a multilevel level ET power supply to a 100 W class-D audio amplifier

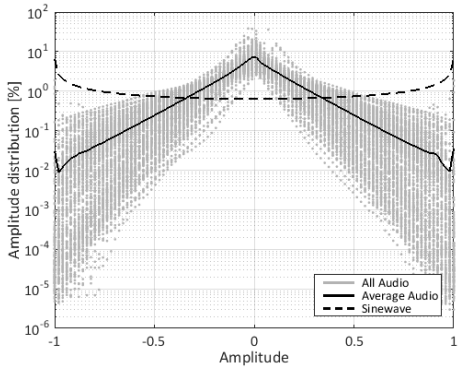

Fig. 1. Amplitude distribution of 183 audio tracks and sine wave [6].

in order to optimize efficiency and operating temperature when playing dynamic audio signals. This technique is not to be confused with conventionally class-H and class-G topologies as those are characterized by having a linear amplifier power stage, opposed to the switch-mode of class-D [14].

II. Proposed Solution

This section present the operating principle of the proposed ET power supply for the class-D amplifier along with relevant equations to estimate the expected impact on the system efficiency.

The core concept of the ET power supply is to supply the power amplifier with just the needed supply voltage so that the amplifier works correctly and does not produced excessive distortion due to clipping. For dynamics signals this will lower the switching losses significantly as they follow the simplified formula:

$$P_{sw} = \frac{1}{2} C_{ds} V_S^2 f_{sw} \tag{1}$$

Where C_{ds} is the parasitic capacitance of the amplifier switching device, V_S is the supply voltage and f_{sw} is the switching frequency. As seen from (1) the losses follows the supply voltage squared meaning that the magnitude of this voltage has great impact of the amount of switching losses.

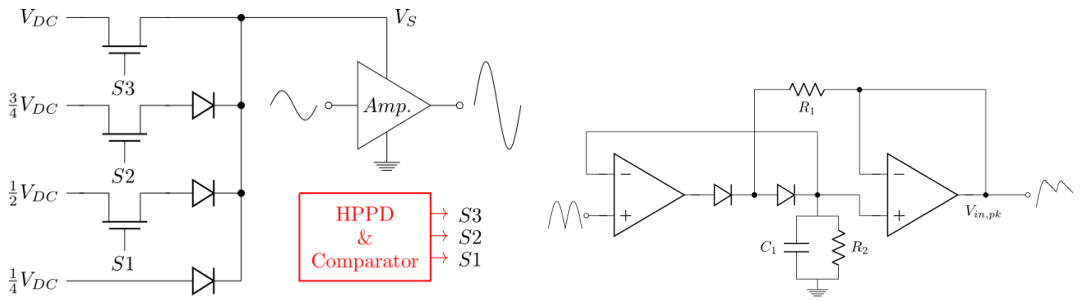

(a) Analog multiplexer.

(b) HPPD circuit.

Fig. 2. Concept of proposed ET power supply consisting of a four level analog multiplexer and a High Precission Peak Detector (HPPD tracking circuit).

This paper proposes to implement the ET utilizing an analog multiplexer which selects the amplifier supply voltage, V_S , from four evenly spaced predefined voltage levels. This selection is performed based on an analysis of amplitude of the audio input which ensures that the amplified audio output generated by the amplifier is never clipped to the supply voltage. Fig. 2(a) shows a simplified schematic of the analog multiplexer. The control signals, $S1-S3$, is generated from an analog High Precision Peak Detection (HPPD) circuit, shown in Fig. 2(b), which tracks the rectified audio input signal. The output of the HPPD, $V_{in,pk}$, is fed to three comparators with hysteresis and individual thresholds, v_{th1-3}. The control signals, $S1-3$, are enabled when the audio input triggers these thresholds:

$$V_{in,pk} > v_{th1-3} \tag{2}$$

The speed of the tracking is set by the time constant formed by $C1$ and $R2$. The tracking speed does not need to very be fast to generate efficiency improvements as depicted in Fig. 3 which shows the predicted behaviour of the switching. Excessive switching in the multiplexer should be avoided as this will generate losses. Tracking speed is therefore a trade-off and a variable that can be optimized in future work. The

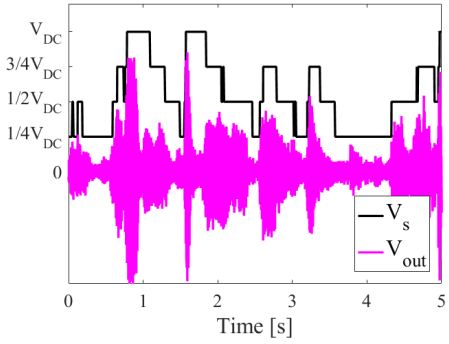

Fig. 3. Estimated Envelope Tracking (ET) power supply voltage, V_S, and amplifier output in case dynamic audio signal.

impact on efficiency the proposed system can be theorised by using a loss model, P_{loss}, based on common equations for switch- and conduction-losses available from previous work [15], [16].

$$P_{loss} = P_{gate} + P_{cond} + P_{sw} + P_{reverse} + P_{Lf} \tag{3}$$

Where P_{gate} is gate-, P_{cond} is conduction-, P_{sw} is switching-, $P_{reverse}$ is reverse body diode conduction- and P_{lf} is filter-losses. The loss model should be evaluated for all desired operating points and supply voltage levels so that it can be formalized as a two dimensional array.

$$P_{loss} = \begin{pmatrix} p_{1,1} & p_{1,2} & \cdots & p_{1,d} \\ p_{2,1} & p_{2,2} & \cdots & p_{2,d} \\ \vdots & \vdots & \ddots & \vdots \\ p_{n,1} & p_{n,2} & \cdots & p_{n,d} \end{pmatrix} \tag{4}$$

where n is the voltage level and d is the operating point specifying a specific duty cycle. Equally the duty cycle distribution, ϕ, of the amplifier power stage can be formalized as:

$$\phi = \begin{pmatrix} \phi_{1,1} & \phi_{1,2} & \cdots & \phi_{1,d} \\ \phi_{2,1} & \phi_{2,2} & \cdots & \phi_{2,d} \\ \vdots & \vdots & \ddots & \vdots \\ \phi_{n,1} & \phi_{n,2} & \cdots & \phi_{n,d} \end{pmatrix} \tag{5}$$

The duty cycle distribution can be translated directly from the amplitude distribution of the audio signal, as long as the amplifier has a linear transfer function. The total loss can be described as the product between the loss model and the duty cycle distribution.

$$P_{tot} = \sum_{n=1}^{N} \kappa_n \cdot \phi_n \cdot P_{loss,n} \tag{6}$$

Where N is the total number of supply voltage levels and κ_n is an array containing the level distribution, i.e. the percentage spent on the n'th supply voltage level.

$$\kappa = \begin{pmatrix} \kappa_1 \\ \kappa_2 \\ \vdots \\ \kappa_n \end{pmatrix} \tag{7}$$

III. Implementation

A prototype system was designed consisting of the ET power supply, equipped with analog multiplexer and the HPPD/comparator tracking circuit, and a 100 W switch-mode power amplifier, designed conventionally in accordance with [17]. Four fixed voltage levels was provided to the multiplexer circuit evenly spaced from 0 to 50 V, i.e. 12.5 V, 25 V, 37.5 V and 50 V. The time constant of the HPPD was set 12 seconds. The amplifier utilizes a synchronous buck topology in a full bridge configuration and has a gain of 32 dB, i.e. 40 V/V. Fig. 4(a) shows the simplified schematic of the amplifier power stage. The input signal range of the amplifier is +/-1 V. The thresholds, v_{th1-3} , of the HPPD/comparator tracking circuit were set to 0.2 V, 0.4 V and 0.6 V respectively, meaning that the multiplexer provides 50 V when the input signal exceeds +/-0.6 V. These thresholds were selected to ensure some headroom to the supply voltage levels thus avoiding significant distortion on the amplified audio signal. Fig. 4(b) shows the implemented system.

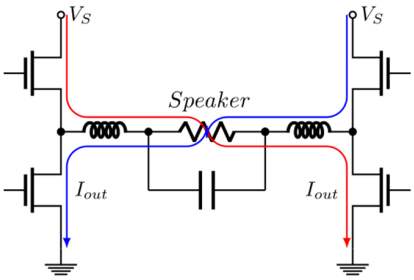

(a) Synchronous buck power stage.

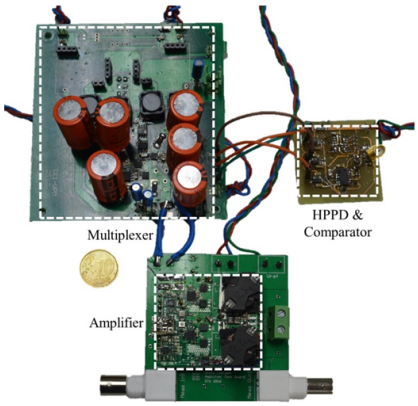

(b) Implemented system.

Fig. 4. Designed system consisting of audio amplifier using a synchronous buck topology and the proposed ET power supply consisting of analog multiplexer and HPPD/comparator tracking circuit.

IV. Results

A series of measurements has been conducted in order to evaluate the impact on the system efficiency and its operating temperature. This includes measurements of system efficiency, using both conventional sine waves and dynamic audio signals

Fig. 7 shows the efficiency of the amplifier with and without the tracking power supply measured conventionally when driven by a sine wave. The input and output power is then measured using digital multi meters, Agilent 34401A. The measured efficiency is compared to predicted values obtained using (6). A good correlation between expectations and measurements is noticed. Especially for lower output powers. Moreover it is observed that the efficiency is greatly improved in the low power region when the tracking power supply is used. The low power efficiency is very important as the most probable power level lies in this range when playing real audio signals instead of sine waves. At 1 W the efficiency is improved from 30% to 65%. For high output levels the efficiency of the system with tracking supply has slightly lower efficiency as the additional circuitry in tracking power supply implementation add some losses. In addition to that the calculated predictions overestimates the efficiency 5 to 7% at higher output powers. This can be explained as a consequence of inaccurate modelling since the loss model does not account for the temperature and voltage dependent nature of the parasitic components of the switching device, e.g parasitic capacitance and on-resistance.

In order to evaluate the efficiency performance using real audio, three audio tracks from different genres have been selected. They have different dynamics as their peak-to-rms ratio, aka. Crest Factor, varies from 8.9 dB to 20.4 dB as seen in Table I.

In order to ensure that the tracks are perceived equally loud they have been loudness normalized in accordance with the EBU- R128 recommendation [18], [19]. For measurement reasons only the first twenty seconds of each track have been considered. Five loudness levels have been selected going from low volume up to clipping, i.e. maximum power. The

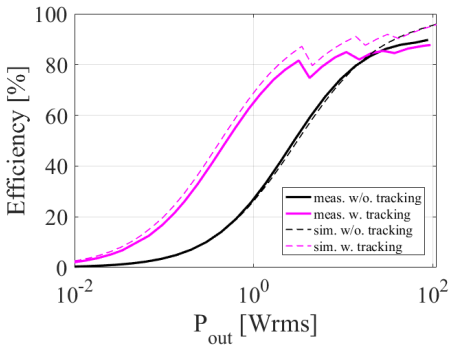

Fig. 5. Simulated and measured efficiencies with and without tracking.

corresponding rms output power can be found in Table II. A DPO3014 oscilloscope from Tektronix equipped with high precision current and voltage probes was used to capture the highly dynamic input and output voltages/currents. With a record length of 10 million points this oscilloscope ensures a sufficient sampling frequency when considering a 20 second audio signal. Fig. 6 shows the measured supply voltage as well as amplifier output playing Daft Punk - Get Lucky at loudness level 5. Though the tracking speed is slow it is clear that the proposed method ensures that supply voltage is vastly lowered for the majority of the audio signal. This will inevitably lower the losses in the power stage. Fig. 7(a) shows the measured and simulated efficiency of each track for the different loudness levels. The simulated results are based on the expected losses obtained using (6). There is a good correlation between the measured and expected results. It is observed that for all tracks and loudness levels the efficiency of the designed system is improved when the tracking power supply is enabled. Especially for low loudness levels the efficiency were improved. That is from 2 to 5% without tracking to 12 to 20% with tracking across the different tracks, i.e. up to a factor 6 improvement. In terms of power losses they were cut down from 2.5 W to only 0.5 W. The efficiency improvement is less significant for higher loudness levels but still a clear improvement is observed. That is from 32 to 53% without tracking to 59 to 76% with tracking across the different tracks. The highly dynamic jazz track, "*Cant we be friends*" marked by "○" in the figures, experiences the greatest efficiency improvement over all loudness levels. The influence of the tracking speed is also investigated. Fig. 7(b) shows the measured and simulated efficiency of the jazz track when the HPPD time constant is lowered from 12 to 3 seconds, resulting in a faster tracking. As expected the efficiency is increased for higher loudness levels but at the price of the signal quality as faster switching produces noise at the amplifier output.

The operating temperatures, in case of a 12 seconds HPPD time constant, were measured using a thermal camera. Fig. 8 shows the measured operating temperature of the audio amplifier with and without the tracking power supply in idle and for the selected audio tracks at loudness level 5. It is observed that in general the operating temperature is greatly reduced. Especially for the four switching MOSFETs

TABLE I
CREST FACTORS OF SELECTED AUDIO TRACKS.

	Name	Artist	Genre	CF
1	Can't We Be Friends	Ella & Louis	Jazz	20.4 dB
2	Redneck	Lamb of God	Metal	8.9 dB
3	Get Lucky	Daft Punk	Pop	13.0 dB

TABLE II
CORRESPONDING OUTPUT POWER FOR DIFFERENT LOUDNESS LEVELS.

Loudness level vs. output power					
Loudness level	1	2	3	4	5
First 20 seconds					
Ella & Louis	0.06 W	0.20 W	0.56 W	0.80 W	1.20 W
Lamb of God	0.08 W	0.25 W	0.71 W	1.00 W	1.50 W
Daft Punk	0.14 W	0.47 W	1.34 W	1.90 W	2.80 W
Full track					
Ella & Louis	0.10 W	0.33 W	0.93 W	1.3 W	1.96 W
Lamb of God	0.14 W	0.46 W	1.32 W	1.86 W	2.77 W
Daft Punk	0.18 W	0.59 W	1.69 W	2.38 W	3.56 W

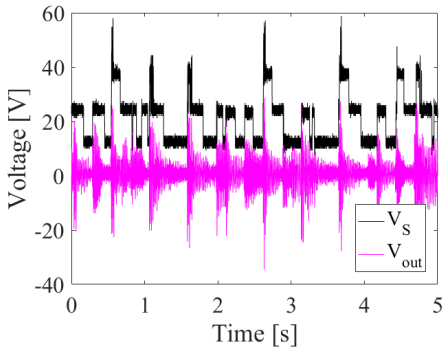

Fig. 6. Multilevel supply voltage and amplifier output in case of Daft Punk Get Lucky.

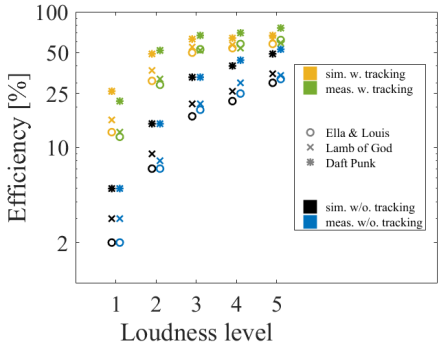

(a) Efficiency of implemented system.

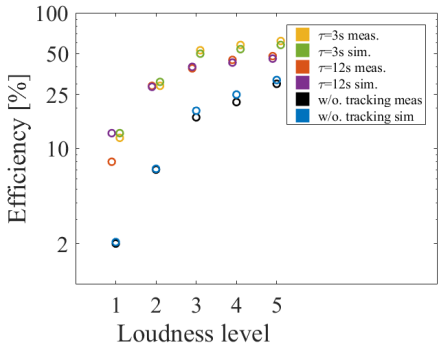

(b) Impact from faster tracking.

Fig. 7. Simulated and measured efficiencies for first 20 seconds of audio tracks. The corresponding output power for each track and loudness level is shown in Table II.

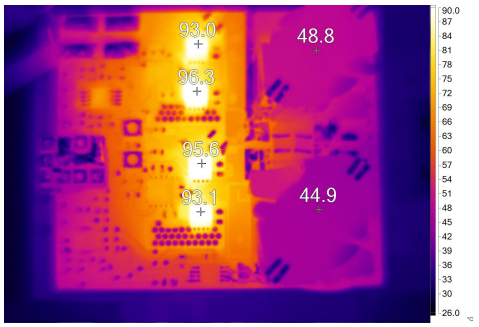

(a) Idle - Without tracking.

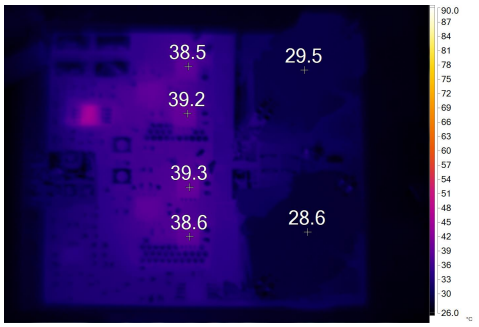

(b) Idle - With tracking.

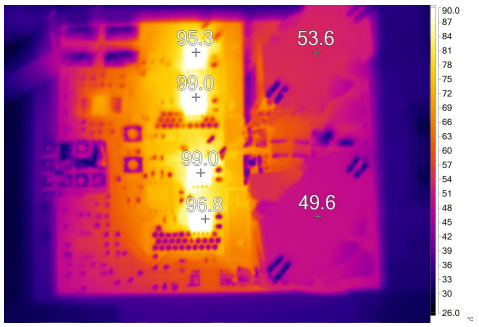

(c) *Ella & Louis* - Without tracking.

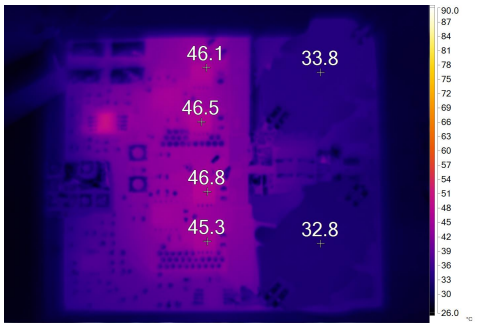

(d) *Ella & Louis* - With tracking.

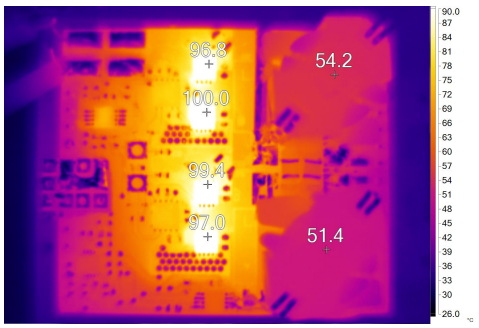

(e) *Lamb of God* - Without tracking.

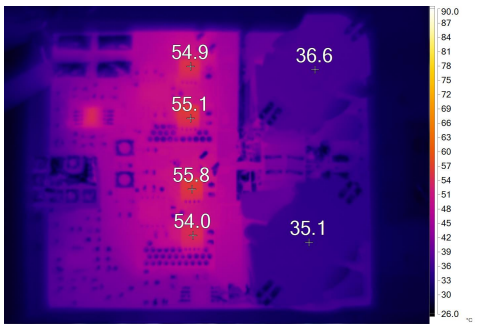

(f) *Lamb of God* - With tracking.

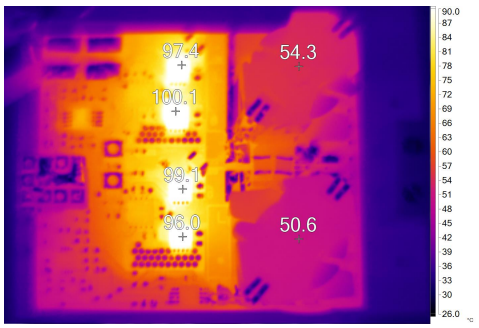

(g) *Daft Punk* - Without tracking.

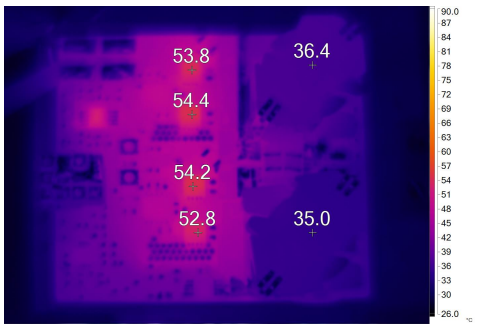

(h) *Daft Punk* - With tracking.

Fig. 8. Measured temperatures of amplifier with- and with-out tracking at loudness level 5.

in the amplifier power stage where the temperature is halved from approximately 100 °C to 50 °C across all tracks. In the same manner the inductor temperature is reduced from approximately 50 °C to 35 °C. A summary of the measured operating temperatures is presented in Table III. This great reduction in MOSFET operating temperature is obtained as the switching losses are greatly reduced. The reduction of the temperature in the filter inductor is related to a smaller ripple current when the supply voltage is low thus causing less AC winding- and core-losses.

Finally crude listening test where performed to evaluate audio quality when the tracking power supply is enabled. From these listening sessions it is clear that the level-shifting, introduced by the tracking power supply, generates undesired audible clicks and therefore it has a negative effect on the audio performance. This can be solve either by having a higher power supply rejection ratio in the amplifier or a lower slew rate in the analog multiplexer. It remains future work to overcome this challenge.

V. Conclusion

The work presented in this paper proposes that tracking power supplies can provide similar efficiency improvements when applied to switch-mode power audio amplifiers as shown for RF amplifiers in previous work. To demonstrate this hypothesis a prototype system was designed consisting of a 100 W power audio amplifier and a tracking power supply based on an analog multiplexer. Measured results show that systems using a tracking power supply achieve significantly higher efficiencies. Especially for low loudness levels the efficiency were improved up to a factor of 6. That is from approximately 2 to 5% without tracking to 12 to 20% with tracking across different music genres. In terms of power losses they were cut down from approximately 2.5 W to only 0.5 W. In addition to that it is observed that the amplifier operating temperature is strongly reduced, especially for the switching power MOSFETs where it has been halved from 100 °C to 50 °C. Moreover measured results show that the efficiency can be further improved for high loudness levels, by increasing the tracking speed.

VI. Future work

Future work includes an implementation using a switch-cap circuit to generate the fixed voltage levels as proposed in [9]. In addition to this the control signals, $S1 - S3$, may be implemented on an audio DSP instead of the HPPD/comparator circuit, as audio DSPs is a typical component in audio systems [21]. Finally good audio quality must be ensured. That means no audible artefacts on the amplified audio signal. This can be achieved either by having high power supply rejection ratio in the amplifier or a lower slew rate in the analog multiplexer, meaning that the jump in supply voltage level happens slower.

TABLE III
Summary of temperature measurements shown in fig. 8

Mean temperatures				
	w/o. tracking		w. tracking	
Input	MOSFETs	Ind.	MOSFETs	Ind.
Idle	94.5 C°	46.9 C°	37.2 C°	29.1 C°
Ella & Louis	97.5 C°	51.6 C°	46.2 C°	33.3 C°
Lamb of God	98.3 C°	52.8 C°	55.0 C°	35.9 C°
Daft Punk	98.2 C°	52.5 C°	53.8 C°	35.7 C°

References

[1] B. Putzeys, "Simple Self-Oscillating Class D Amplifier with Full Output Filter Control", in *118th Audio Engineering Society convention*, Barcelona, May 28-31, 2005.

[2] S. Poulsen, M.A. Andersen, "Simple PWM modulator topology with excellent dynamic behavior", in IEEE APEC, 2004.

[3] M. C. W. Hyerby and M. A. E. Andersen, "Carrier Distortion in Hysteretic Self-Oscillating Class-D Audio Power Amplifiers: Analysis and Optimization", IEEE Transactions on Power Electronics, 2009.

[4] K. Nielsen, "Audio Power Amplifier Techniques With Energy Efficient Power Conversion", Ph.D. thesis, Volume 1, Technical University of Denmark 1998.

[5] R. A. R. van der Zee and A. J. M. van Tuijl, "Test Signals for Measuring the Efficiency of Audio Amplifiers", in *102nd Audio Engineering Society convention*, Amsterdam, May 16-19, 1998.

[6] N. E. Iversen, A. Knott and M. A. E. Andersen, "Efficiency of Switch-Mode Power Audio Amplifiers - Test Signals and Measurement Techniques", in *140th Audio Engineering Society convention*, Paris, 4-7 June, 2016.

[7] Q. Jin, M. Vasic, O. Garcia, P. Alou and J. A. Cobos, "Optimized design of Gan switching capacitor based envelope tracking power supply for satellite applications", in *APEC 2016*. DOI: 10.1109/APEC.2016.7468203.

[8] M. Vasic, O. Garcia, J. A. Oliver, P. Alou, D. Diaz and J. A. Cobos, "Envelope amplifier based on switching capacitors for high-efficiency RF amplifiers", *IEEE Trans. Power Electronics*, vol. 27, no. 3, pp. 1359-1368, March 2012. DOI: 10.1109/TPEL.2011.2163646.

[9] V. Lazarevic, M. Vasic, O. Garcia, Q. Jin, P. Alou, J. A. Oliver and J. A. Cobos, "A comparative analysis of two approaches in EER based envelope tracking power supplies", in *APEC 2017*. DOI: 10.1109/APEC.2017.7931163

[10] Z. Wang, Envelope tracking power amplifiers for wireless communications, Artech House, Boston, 2014.

[11] M. Vasic, O. Garcia, J. A. Oliver, P. Alou, D. Diaz and J. A. Cobos, "Multilevel power supply for high-efficiency RF amplifier", *IEEE Trans. Power Electronics*, vol. 25, no. 4, pp. 1078-1089, April 2010. DOI: 10.1109/TPEL.2009.2033186.

[12] V. yousefzadeh, E. Alarcon and D. Maksimovic, "Three-level buck converter for envelope tracking applications", *IEEE Trans. Power Electronics*, vol. 21, no. 2, pp. 549-552, March 2006. DOI: 10.1109/TPEL.2005.869728.

[13] Leonard R. Kahn, Single-Sideband Transmission by Envelope Elimination and Restoration, *Proceedings of IRE*, vol. 40, no. 7, pp. 803-806, 1952. DOI: 10.1109/JRPROC.1952.273844.

[14] J. Angus, "Ultra efficienct linear amplifiers", in *142nd Audio Engineering Society convention*, Berlin, May 20-23, 2017.

[15] N. E. Iversen, N. J. Dahl, A. Knot. M. A. E. Andersen, Towards high power density audio amplifiers, *submitted to IEEE Trans. Consumer Electronics*, October 2017.

[16] Erickson and Maksimovic, *Fundamentals of Power Electronics*, Second Edition, Kluwer Academic Publishers.

[17] Application Report, "Design Considerations for Class-D Audio Power Amplifiers", Texas Instruments, 1999.

[18] EBU Technical Recommendation R 128: Loudness normalisation and permitted maximum level of audio signals.

[19] EBU Tech Doc 3343: Practical Guidelines for Production and Implementation in accordance with EBU Technical Recommendation R 128.

[20] EBU Tech Doc 3343: Practical Guidelines for Production and Implementation in accordance with EBU Technical Recommendation R 128.

[21] F. Rumsey, "DSP in Loudspeakers", *in J. Audio Eng. Soc.*, vol. 56, no. 1/2, pp. 65-72, January 2008.

E

Efficiency of switch-mode power audio amplifiers - Test signals and measurement techniques

In 140th Audio Engineering Soceity convention, Paris, June 4-7, 2016.

Audio Engineering Society

Convention Paper 9499

Presented at the 140th Convention
2016 June 4–7, Paris, France

Efficiency of Switch-Mode Power Audio Amplifiers - Test Signals and Measurement Techniques

Niels Elkjær Iversen[1], Arnold Knott[1], and Michael A. E. Andersen[1]

[1]*Technical University of Denmark - DTU, Kongens Lyngby, 2800 Denmark*

Correspondence should be addressed to Niels Elkjær Iversen (neiv@elektro.dtu.dk)

ABSTRACT

Switch-mode technology is greatly used for audio amplification. This is mainly due to the great efficiency this technology offers. Normally the efficiency of a switch-mode audio amplifier is measured using a sine wave input. However this paper shows that sine waves represent real audio very poorly. An alternative signal is proposed for test purposes. The efficiency of a switch-mode power audio amplifier is modelled and measured with both sine wave and the proposed test signal as inputs. The results show that the choice of switching devices with low on resistances are unfairly favoured when measuring the efficiency with sine waves. A 10% efficiency improvement was found for low power outputs. It is therefore of great importance to use proper test signals when measuring the efficiency.

1 Introduction

Switch-mode technology has during the last decade become the conventional choice in audio where they are known as Class-D amplifiers. This is due to the superior efficiency this technology offers, which theoretically can reach 100%, and the good performance with very low distortion as shown in [1] and [2]. The theoretcally 100% efficiency is not possible but efficiencies ranging well above 90% have been presented in previous work for a wide range of applications, for example in renewable energy systems [3]. Also in audio applications efficiencies in the vicinity of 90% have been achieved [4], [5]. High efficiency is crucial for especially battery driven sound systems. When specifying the performance of the amplifier the complexity of the audio system is often simplified for test purposes. For example the loudspeaker impedance is often simplified as a pure ohmic resistance as discussed in [6]. Also for amplifier efficiency specification conventional measurement techniques involves driving the amplifier with a sine signal. However sine waves are not a good representation of real music signals. Real music signals has great dynamics as described in [7], [8] and [9]. This has the consequence that the effective RMS output power of the amplifier is much lower when playing real music signals compared when playing sine waves as discussed in [10] and [11]. For this reason the amplifier efficiency obtained in previous work, [4], [5], is not representative for the intended amplifier operation, i.e. when it is playing real music signals. In addition to this the choice of the switching devices, e.g. MOSFETs, could easily be mismatched to favour sine wave efficiency instead of real audio efficiency.

This paper describes the fundamental operation of switch-mode power audio amplifiers and examine the losses generated in the power stage and output filter

of the amplifier. Moreover this paper investigates the dynamics of audio signals and use this information to make a more representative test signal than sine waves. Finally experimental examples illustrates how the choice of the switching devices is dependent on the used test signal.

2 Switch-mode power audio amplifiers

Switch-mode power technology is well describe in literature [12]. However this section will present the basic operation principles. Moreover an elaborated description of the power stage will be presented. This includes an analysis of the switching voltages and currents in the power stage and the inherent loss mechanisms of the power stage.

2.1 Basic operation

A switch-mode power audio amplifier can be split into three essential blocks. They are:

- Modulator
- Power stage
- Output filter

Figure 1 shows a simplified block diagram. Conventional modulators uses Pulse Width Modulation

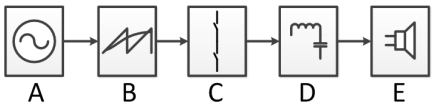

Fig. 1: Block diagram of switch-mode power audio amplifier. A) is audio input, B) is modulator, C) is power stage, D) is output filter and E) is loudspeaker.

(PWM) where the audio signal is modulated with a high frequency carrier waveform. Typically this waveform will have a triangle or sawtooth shape. Normally the modulation is performed by comparing the audio input with the carrier which generates a pulse train at a given frequency, the switching frequency f_{sw}, with varying pulse lengths as shown in figure 2. The length or on-time of the pulses are also known as the duty cycle, D, of the PWM signal. The power stage is where the amplification takes place and it consists of

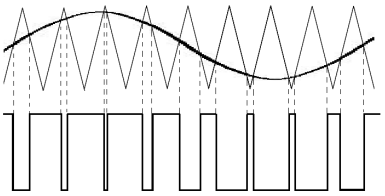

Fig. 2: Modulation of audio signal using triangular carrier resulting in a Pulse Width Modulated (PWM) representation of the audio signal.

switching devices which are switched on and off using the PWM signal. This means that the power stage actually amplifies the PWM signal. The most common switching device for switch-mode power applications is the Metal Oxide Field Effect Transistor (MOSFET). The power stage are typically using a buck topology described in [12]. This topology can be realized either in a half- or full-bridge configuration. The half bridge requires a dual voltage supply while the full bridge only requires a single supply. The component count in the full bridge is twice the component count in the half bridge. This topology is very attractive for audio applications due to an ideally linear transfer function which minimizes the distortion:

$$V_{out} = (2D-1)\,V_{DD} \tag{1}$$

Where V_{out} is the output voltage, D is the duty cycle and V_{DD} is the rail to rail voltage, i.e. V_+ to V_- in half bridge configuration and V_+ to ground in full bridge configurations. In battery driven systems the full bridge configuration is the conventional choice. Figure 3 shows the half bridge buck which includes the output filter formed by the inductor, L_f, and the capacitor, C_f. The switching devices are driven by the PWM signals, V_{gs1} and V_{gs2}, which are 180° out of phase. The output filter is a low pass filter which removes the high frequency PWM representation and restores the audio audio signal which is fed to the load, i.e. the loudspeaker.

2.2 Power stage waveforms

In this section the switching voltages and currents in the half bridge buck power stage will be examined under different switching conditions. In order to do that a more detailed representation of the switching device is necessary. Figure 4 shows the switching device, e.g.

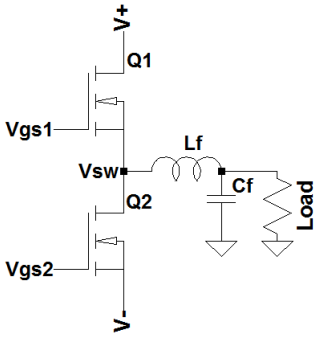

Fig. 3: Half bridge buck topology.

a MOSFET, including its' parasitic components. That is the parasitic capacitances, C_{oss}, C_{gs} and C_{gd}, the on resistance $R_{ds(ON)}$ and the drain to source body diode which will have a given forward voltage drop. As mentioned the gates of the switching devices will be driven 180° out of phase with the PWM signal. To prevent an undesired short circuit through the half bridge some dead time, t_{dt}, between the gate signals should be implemented. Too much dead time can however generate distortion as shown in [13]. This should be taken into account when investigating the switching voltages and currents of the power stage. There exists four different switching conditions which are relevant in order to estimate the losses in the power stage.

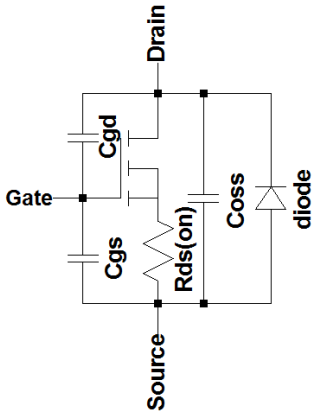

Fig. 4: Switching device, e.g. MOSFET, including the parasitic on resistance, $R_{ds(ON)}$, the drain source capacitance, C_{oss}, the gate capacitances, C_{gs} and C_{gd} and the drain to source body diode.

1. Hard switching occurs when the parasitic drain source capacitance, C_{oss}, of the switching device can not be charged or discharged by the inductor current, I_L, during the dead time period. This can either be due to a very small dead time period, a large parasitic capacitance or an insufficient inductor current. The switching node voltage, V_{sw}, will ramp up and down together with the drain current, I_D, in the switching device, causing some switching losses. Moreover the parasitic capacitances will be charged or discharged very fast during turn on/off and this energy is dissipated as an additional loss.

2. Soft switching, or Zero Voltage Switching (ZVS), on the other hand occurs when the parasitic drain source capacitance of the switching device can be completely charged or discharged by the inductor current during the dead time period. This eliminates the switching losses in theory.

3. When the ripple in the inductor current is larger than the output current, $\Delta i_L > |I_{out}|$, a situation can occur where the parasitic drain source capacitance is charged or discharged beyond the rail to rail voltage, V_{DD}. In this situation the body diode of the switching device start conducting which causes some losses in the switching device due to the forward voltage drop of the body diode.

4. Finally when the output current is larger than the ripple in the current, $|I_{out}| > \Delta i_L$, the body diode of the switching device will continue conducting after turn off causing additional losses.

Figure 5 a) to d) shows the waveforms for the four described switching condition.

Since the power stage is intended for audio use the duty cycle of the PWM signal driving the switching devices will vary according to the audio input. This means that power stage most likely will undergo all four switching conditions.

2.3 Loss mechanisms

This section will focus on the losses in the power stage and the output filter. The main loss mechanisms will

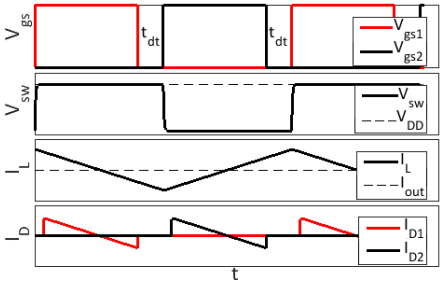

(a) Hard switching

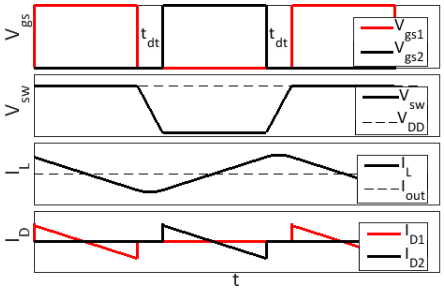

(b) Zero Voltage Switching (ZVS).

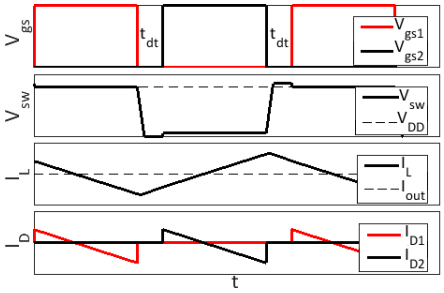

(c) Body diode conduction ($|I_{out}| < \Delta i_L$).

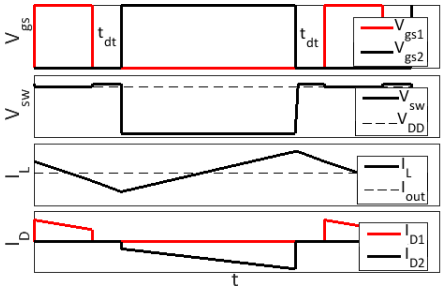

(d) Body diode conduction ($|I_{out}| > \Delta i_L$).

Fig. 5: Waveforms in the Buck power stage for different switching conditions

be described and equations for estimating the losses presented. The equations listed throughout this section is for the half bridge buck shown in figure 3.

1. Gate losses are generated by charging and discharging the gate capacitances, C_{gd} and C_{gs}, of the switching device, e.g. transistor. The needed charge is normally specified in transistor data sheet as the total gate charge, Q_g. The gate losses can be determined knowing the gate source voltage of the switching device, V_{gs}, and the switching frequency.

$$P_{gate} = 2 \cdot Q_g \cdot V_{gs} \cdot f_{sw} \tag{2}$$

2. Conduction losses are generated when the switching transistor is in its' on state. During its' on state a current, I_D, is running causing some power to be dissipated in the on resistance of the transitor.

$$P_{cond} = I_D^2 \cdot R_{ds(ON)} \tag{3}$$

3. Switching losses occur during the switching events between the transistors on and off states. As mentioned a current is running in its' on state while no current runs in the off state. This current will ramp up and down together with the fast voltage transients from rail to rail, causing some power to be dissipated. Moreover the parasitic capacitance, C_{oss}, will be charged and discharged by these transients causing additional losses. However these losses can be minimized if the parasitic capacitances of the transistor is charged/discharged by the inductor current, I_L, in the dead time period.

$$P_{sw} = I_D \cdot \left(V_{DD} - \frac{t_{dt} \cdot I_L}{2C_{oss}} \right) \cdot \frac{t_{rise} + t_{fall}}{2} \cdot f_{sw} \tag{4}$$

$$P_{oss} = C_{oss} \cdot f_{sw} \cdot \left(V_{DD} - \frac{t_{dt} \cdot I_L}{2C_{oss}} \right) \tag{5}$$

where t_{rise} and t_{fall} are the transistor rise- and fall-time, typically available from data sheets.

4. Reverse conduction losses occur in the situation where the body diode in the transistor starts or continue conducting the current, I_D. Due to a small forward voltage drop in the diode some power will be dissipated.

$$P_{reverse} = t_{cond} \cdot f_{sw} \cdot I_D \cdot V_f \tag{6}$$

5. The loss in the output filter are related to the inductor current, I_L, and the resistance of the inductor wire. For low frequency signals, e.g. 0 to 20 kHz, the resistance can be assumed to be negligible. However at higher frequencies, around the switching frequency, losses are expected due to the fact that the resistance increases with the frequency in the inductor. The AC resistance is often denoted the Equivalent Series Resistance (ESR) and can typically be found in data sheet for the inductor or measured with an impedance analyser. The losses can be estimated to be:

$$P_f = I_L^2 \cdot \mathrm{ESR} \tag{7}$$

Finally the total losses can be expressed as the sum of the different loss components:

$$P_{tot} = P_{gate} + P_{cond} + P_{sw} + P_{oss} + P_{reverse} + P_f \tag{8}$$

Normally the conduction losses, P_{cond}, the switching losses, P_{sw}, and the filter losses, P_f, will be the dominant losses. However in idle operation, or close to idle operation, where the output power is small, the losses related to the parasitic capacitances becomes significant, i.e. P_{gate} and P_{oss}. The reverse conduction losses are normally quite small, due to the fact that the forward voltage drop of the body diode in many cases is rather small.

2.4 Efficiency

The efficiency is simply the ratio between the output- and input-power.

$$\eta = \frac{P_{out}}{P_{in}} \tag{9}$$

In order to secure good efficiency one must choose the switching devices carefully. Looking at the equations for the losses presented above it seems obvious that to ensure good efficiency one should choose switching devices with tiny parasitic capacitances and a small on resistance. However this is not possible due to the fundamentals of transistor design [15]. If a transistor is to be designed with a low on resistance, this would require a highly conductive path between the drain and source terminals of the transistor when in its' on state. A highly conductive path is made by making the conductive channel between the drain and source terminals wider, thus increasing the overall conductive area. An increment of the area will equally increase the parasitic capacitances. Therefore transistors with tiny on resistances would normally have large parasitic capacitances and vice versa. Figure 6 shows the modelled efficiency vs. the output power for a 12 V switch-mode power audio amplifier driven with a sine wave input for two types of transistors with different specifications. The figure shows that a low on resistance makes it possible to achieve an efficiency above 80% for a large range of output powers, reaching the vicinity of 90% just before clipping, while low parasitic capacitances improves the idle losses on the cost of a poor peak efficiency.

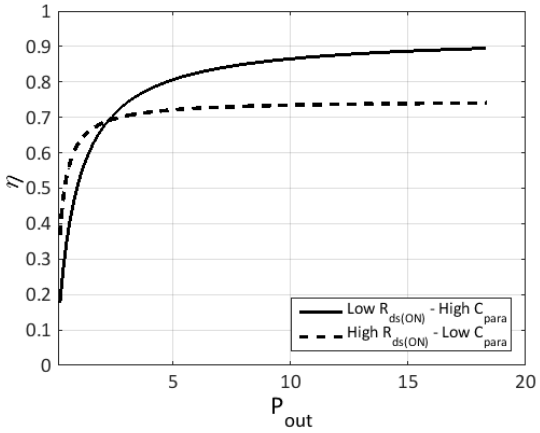

Fig. 6: Modelled efficiency of 12 V switch-mode power audio amplifier driven with a sine wave input for two types of transistors.

3 Audio Dynamics

From the loss analysis performed above and efficiency curves showed in figure 6 it seems obvious to choose transistors with low on resistances to ensure good amplifier efficiency. However a consumer will rarely listen to sine waves and therefore it is relevant to investigate the dynamics of real audio signals.

A music library consisting of 183 audio tracks from a vast selection of genres have been analysed in terms of amplitude distribution and crest factor. The crest factor is the ratio between the peak- and the RMS-value of the signal and is normally given in decibels. Figure 8 a) shows the amplitude distribution of a sine wave and the audio tracks from the music library. The figure shows that there exists a fundamental difference between real

audio signals and sine waves. The amplitude distribution of real audio is centred around an amplitude close to zero. For higher amplitudes the distribution decreases. The amplitude distribution for sine waves is almost the opposite of the audio signals with peaks at the maximum amplitudes and a minima around zero. Moreover the crest factor of sine wave is 3 dB where it ranges from approximately 7 to 25 dB for the audio tracks with a mean value of 15 dB. Keeping this in mind it seems futile that sine waves are among the preferred test signals for audio amplifier applications.

The IEC-268 standard [9] presents a test signal which basically is filtered pink noise. Figure 8 b) shows the amplitude distribution including the IEC-268 filtered pink noise and this signal is found to represent the audio tracks much better and has a crest factor of 12 dB. However this signal is not like a sine wave due to the fact that it is a noise signal and thereby does not have a fundamental frequency. Since many test procedures for specifying amplifier performances, such as frequency responses and THD measurements, uses a frequency sweep with constant amplitude, it is relevant to construct an alternative test signal which represent audio tracks but also have a fundamental frequency like sine waves. This is also relevant when measuring efficiency, making it easier to tell when the signal starts to distort just by looking at the waveform with an oscilloscope. An alternative test signal has been constructed by distorting a normal sine wave and it can be expressed mathematically as:

$$f(t) = \left(\frac{0.5+K\cdot sin(\omega t)-(1-(0.5+K\cdot sin(\omega t)))}{(0.5+K\cdot sin(\omega t))\cdot(1-(0.5+K\cdot sin(\omega t)))} \right)^{\frac{1}{4}} \qquad (10)$$

Where $K = 0.49995$ is a constant and $\omega = 2\pi f$. Figure 7 shows the proposed test signal peak normalized to 1, and figure 8 c) shows the amplitude distribution. It is seen that the proposed test signal represents audio signals well. Its' crest factor is approximately 14 dB.

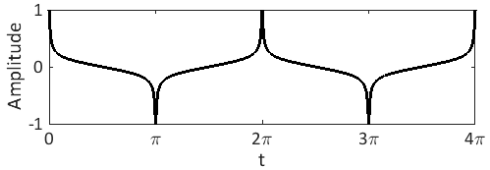

Fig. 7: Proposed test signal peak normalized to 1.

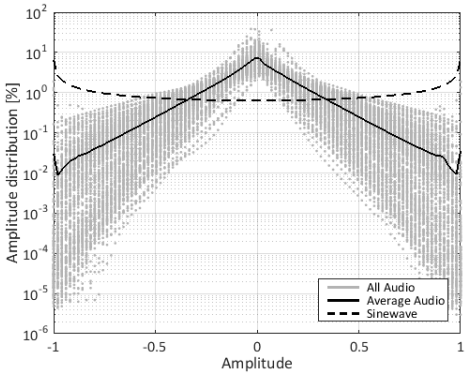

(a) Amplitude distribution of audio and sine.

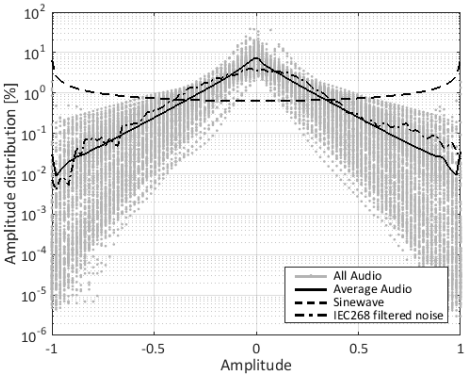

(b) Amplitude distribution of audio, sine and IEC-268 filtered noise.

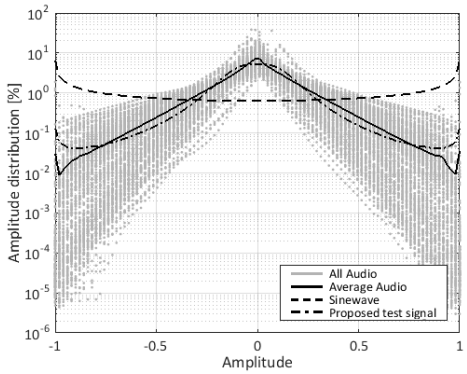

(c) Amplitude distribution of audio, sine and proposed test signal.

Fig. 8: Amplitude distribution of signals.

3.1 Revised efficiency

As mentioned above the average crest factor for the audio signals is approximately 15 dB causing the maximum RMS output power of the switch-mode power audio amplifier to be significantly smaller when playing real audio signals instead of sine waves. This actually means that the duty cycle distribution is significantly different when playing audio compared to sine waves. Since the Buck topology has a linear transfer function as shown in eq. 1 the duty cycle distribution will be directly proportional with the amplitude distribution. Figure 9 shows the duty cycle distribution for the audio tracks, the sine wave and the proposed test signal. Knowing the duty cycle distribution of real audio signals enables modelling of the efficiency for the switch-mode power audio amplifier when playing an audio representing signal, e.g. the proposed test signal. As in section 2.4 the efficiency is modelled for a 12 V switch-mode power audio amplifier for the two types of transistors used in the previous examples. Figure 10 shows the results. First of all the figure shows that the maximum RMS output power of the amplifier is significantly lower compared to the sine wave operation from figure 6. Moreover the figure shows that the amplifier efficiency benefits more from low parasitic capacitances than from a small on resistance when using an actual audio representing signal. When looking at figure 6, which shows the efficiency for the sine wave operation, one could easily be led to believe that a low on resistance would be preferable for good amplifier efficiency however this is not the case.

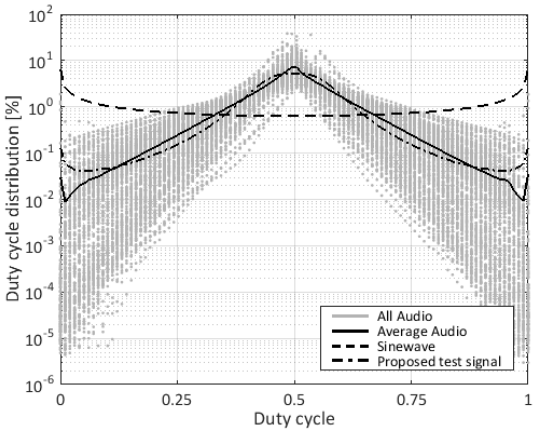

Fig. 9: Duty cycle distribution of audio, sine and proposed test signal.

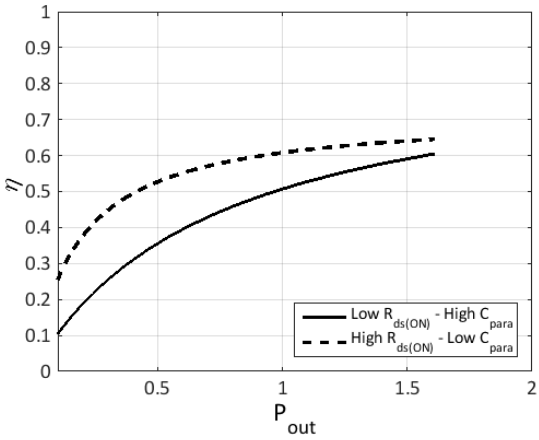

Fig. 10: Modelled efficiency of 12 V switch-mode power audio amplifier driven with an audio representing input signal for two types of transistors.

4 Measurements and results

A series of efficiency measurements have been performed on a 12 V switch-mode power audio amplifier. The implemented test-amplifier uses a full bridge buck topology which enables it to operate from a single voltage supply, e.g. a battery. This also means that it has four switching devices, implemented as MOSFETs in its' power stage. Figure 11 shows the implemented test amplifier. The efficiency has been measured with

Fig. 11: Implemented 12 V test amplifier.

the amplifier driven by a sine wave and the proposed test signal as input. Moreover the efficiency has been measured for two types of MOSFETs, one with low on resistance and high parasitic capacitances and one with high on resistance and low parasitic capacitances. The used MOSFETs are the FDD3672 from Fairchild Semiconductors and the IRLR110PbF from International Rectifier and their key parameters are listed in table 1. It should be mentioned that both MOSFETs are in the same kind of package (D-PAK). The efficiency was

Name	Q_g	$R_{ds(ON)}$	C_{oss}
FDD3672	24 nC	24 mΩ	247 pF
IRLR110PbF	6.1 nC	540 mΩ	80 pF

Table 1: Key parameters for MOSFETs used in power stage

measured by measuring the input and output voltages and currents with a digital multimeter, similar to the Agilent 34401A models [16], for a range of increasing input signals. The measurements continued until the amplified signal was clearly distorted. Figure 12 shows the measured results. Figure 12 a) shows the measured efficiency when the amplifier is driven with a sine wave input while b) shows the measured efficiency when driven with the proposed test signal. The efficiency measurements shows that the FDD3672 MOSFET is preferable for sine wave amplification while the IRLR110PbF is preferable for audio amplification. It is seen that the low power efficiency is approved approximately 10% when using the IRLR110PbF power MOSFET. In this way the results shows the same tendency as shown in the theoretically analysis above. That is that the efficiency of the amplifier benefits more from low parasitic capacitances than from a low on resistance when used for audio. This is due to the fact that the power drawn from the amplifier when playing audio is significantly lower than when playing sine waves and at low power the switching losses are dominating. In addition to this it can be mentioned that the end user will listen to music at background levels most of the time according to [17], lowering the power drawn even more. However no general conclusion or rule on which kind of MOSFETs to choose can be made from this study due to the fact that the presented results only are valid for the 12 V test amplifier. However the importance of using proper test signals when specifying the amplifier efficiency is clearly shown.

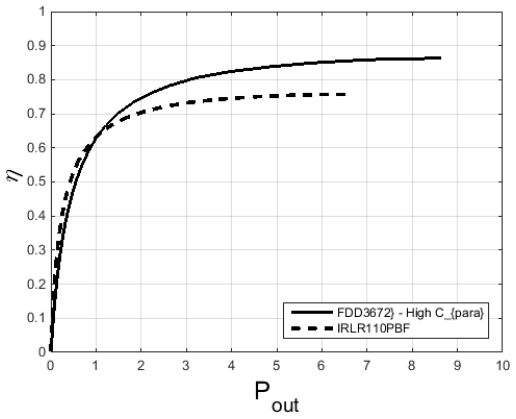

(a) Efficiency measured with sine wave as input signal.

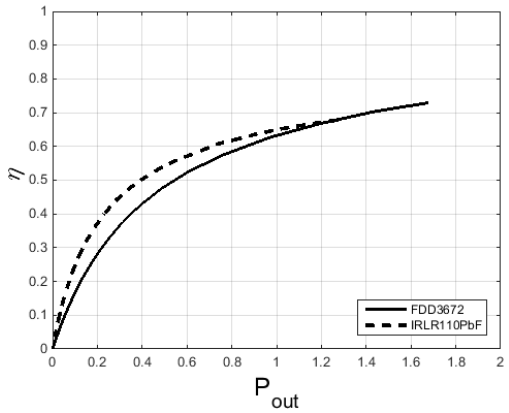

(b) Efficiency measured with alternative test signal as input.

Fig. 12: Measured efficiencies for the amplifier using different input signals.

5 Conclusion

This paper has presented the fundamental principles of switch-mode power audio amplification. This include an overview of the different switching conditions the amplifier can undergo when used for audio amplification. A detailed analysis of the inherent loss mechanisms of the amplifier has been presented in order to model the efficiency. It was found that the properties of the switching devices have great impact on what kind of losses there can be expected. Switching devices with low on resistances and high parasitic capacitances will have higher idle losses but can achieve higher efficiencies at high output powers than switching devices

with high on resistances and low capacitances. It has been shown that high output powers are easily reached when the amplifier is driven with a sine wave input thus favouring switching devices with low on resistances. However a thorough investigation of the amplitude distribution of 183 audio tracks has shown that sine waves are a very poor representation of real audio signals. A better audio representing signal is the IEC-268 filtered noise signal however this signal does not have a fundamental frequency like sine waves. Therefore an alternative test signal has been constructed which also represents audio signals very well. It was found that the crest factor of audio signals are much greater than that of sine waves thus lowering the RMS output power requirements of the amplifier significantly. This increases the importance of the losses related to the parasitic capacitances of the switching device. A series of efficiency measurements were conducted on a 12 V test amplifier equipped with two types of switching devices. The efficiency was measured when the amplifier was driven by a sine wave and when it was driven with the proposed test signal. The results correlated well with the expectations from the theoretical analysis meaning that measuring the efficiency with a sine wave input signal favours switching devices with low on resistances unfairly. Therefore it is of great importance to measure amplifier efficiency with a proper test signal. In addition to this it was shown that the low power efficiency could be improved approximately 10%.

6 Acknowledgements

The authors would like to thank post doc. Henrik Schneider from the Electronics Group at the Technical University of Denmark, for many good discussions on the subject of efficiency in switch-mode audio amplifiers. In addition to this the authors would like to thank the two master students Ruben Bjerregaard and Anders Madsen, also from the Electronics Group, for their assistance in implementing the test amplifier.

References

[1] B. Putzeys, "Simple Self-Oscillating Class D Amplifier with Full Output Filter Control", in AES Convention 118th, Barcelona, May 28-31, 2005.

[2] S. Poulsen and M. A. E. Andersen , "Simple PWM modulator topology with excellent dynamic behaviour", in Applied Power Electronics Conference and Exposition, 2004.

[3] M. Carmen, Z. Zhang, A. Knott and M. Andersen, "Power Flow Control of a Dual-Input Interleaved Buck/Boost Converter with Galvanic Isolation for Renewable Energy Systems ", Applied Power Electronics Conference 2015.

[4] K. Nielsen, "Audio Power Amplifier Techniques With Energy Efficient Power Conversion", Ph.D. thesis, Volume 1, Technical University of Denmark 1998.

[5] M. Duraj, N. E. Iversen, L. P. Petersen and P. Boström, "Self-oscillating 150 W switch-mode amplifier equipped with eGaN-FETs", in AES Convention 139th, New York, October 29-November 1, 2015.

[6] N. E. Iversen and A. Knott, "Small Signal Loudspeaker Impedance Emulator", JAES Volume 62 Issue 10 pp. 676-682, October 2014.

[7] M. Mijić, D. Mašović, M. Petrović and D. Šumarac-Pavlović , "Statistical Properties of Music Signals", in AES Convention 126th, Munich, Germany, May 7-10, 2009.

[8] P. J. Chapman, "Programme material analysis", in AES convention 100th, Coopenhagen, May 11-14, 1996.

[9] International Electrotechnical Commission, "IEC 268-1 Sound System Equipment, Part 1: General", Second edition 1985.

[10] N. E. Iversen, H. Schneider, A. Knott and M. A. E. Andersen, "Efficiency Investigation of Switch-Mode Power Audio Amplifiers Driving Low Impedance Transducers", in AES Convention 139th, New York, October 29-November 1, 2015.

[11] R. A. R. van der Zee and A. J. M. van Tuijl, "Test Signals for Measuring the Efficiency of Audio Amplifiers", in AES Convention 102th, Amsterdam, May 16-19, 1998.

[12] Erickson and Maksimovic, "Fundamentals of Power Electronics", Second Edition, Kluwer Academic Publishers.

[13] F. Koeslag and T. Mouton, "Accurate characterization of pulse timing errors in class-D audio amplifier output stages", In AES 37th International Conference, Hillerœd, Denmark, August 28-30, 2009.

[14] A. Knott, T. Stegenborg-Andersen, O. C. Thomsen, D. Bortis, J. W. Kolar, G. Pfaffinger and M. A. E. Andersen, "Modeling Distortion Effects in Class-D Amplifier Filter Inductors", in AES 128th Convention, London, May 22-25, 2010.

[15] T.C. Carusone, D.A. Johns and K. Martin, "Analog Integrated Circuit Design", Second Edition, John Wiley and Sons (2012).

[16] Agilent Technologies, "Agilent 34401A Multimeter", User's guide.

[17] A. Yamauchi, H. Schneider, A. Knott, I. H. H. Jørgensen and M. A. E. Andersen , "Investigation of Energy Consumption and Sound Quality for Class-D Audio Amplifiers using Tracking Power Supplies", in AES Convention 138th, Warsaw, Poland, May 7-10, 2015.

F

Low impedance voice coils for improved loudspeaker efficiency

In 139th Audio Engineering Soceity convention, New York, October 29-1 November, 2015.

AES139th Convention Best Student Technical Paper Award Winner

Audio Engineering Society

Convention Paper 9389

Presented at the 139th Convention
2015 October 29–November 1 New York, USA

Low Impedance Voice Coils for Improved Loudspeaker Efficiency

Niels Elkjær Iversen[1], Arnold Knott[1], and Michael A. E. Andersen[1]

[1] *Technical University of Denmark - DTU, Kongens Lyngby, 2800 Denmark*

Correspondence should be addressed to Niels Elkjær Iversen (neiv@elektro.dtu.dk)

ABSTRACT

In modern audio systems, utilizing switch-mode amplifiers, the total efficiency is dominated by the rather poor efficiency of the loudspeaker. For decades voice coils have been designed so that nominal resistances of 4 to 8 Ω is obtained, despite modern audio amplifiers, using switch-mode technology, can be designed to much lower loads. A thorough analysis of the loudspeaker efficiency is presented and its relation to the voice coil fill factor is described. A new parameter, the drivers mass ratio, is introduced and it indicates how much a fill factor optimization will improve a driver's efficiency. Different voice coil winding layouts are described and their fill factors analysed. It is found that by lowering the nominal resistance of a voice coil, using rectangular wire, one can increase the fill factor. Three voice coils are designed for a standard 10" woofer and corresponding frequency responses are estimated. For this woofer it is shown that the sensitivity can be improved approximately 1 dB, corresponding to a 30% efficiency improvement, just by increasing the fill factor using a low impedance voice coil with rectangular wire.

1. INTRODUCTION

A system designed for high quality audio reproduction involves many different blocks. These often include power supply, Digital Signal Processing (DSP), pre-amplifier, amplifier, cross-over network, loudspeaker enclosure and transducer. However all these blocks can be boiled down to three essential blocks which are:

- Power supply
- Amplifier
- Transducer

Modern power supplies and amplifiers are widely utilizing switch-mode power technology which is described in [1]. This is due to the high efficiency this technology offers, which theoretically can reach 100%. In practice the theoretical efficiency cannot be reached but it is possible to reach efficiencies above 90% for audio applications [2] and [3]. Moreover switch-mode power audio amplifiers delivers excellent audio performance with Total Har-

monic Distortion (THD) beneath 0.005% [4]. The transducer of the sound system is the loudspeaker driver which normally is mounted in a carefully designed enclosure. Loudspeaker drivers and their enclosures are well described in literature [5], [6], [7]. The impedance of the driver consist of an acoustical-, a mechanical and an electrical-part and is carefully described in [8] and [9]. The nominal resistance of the driver is characterized by the voice coil resistance. This resistance is also know as the DC resistance, corresponding to the resistance at 0 Hz. For decades it has been widely accepted to aim for voice coil DC resistances between 3 and 8 Ω. However modern switch-mode power audio amplifiers can easily be designed to deliver power to lower load resistances. A reduction of the load resistance leads to a downgrade of the amplifier's voltage rail requirement for a given output power as discussed in [10]. In [11] it is shown that a low rail voltage can benefit the efficiency of the switch-mode power audio amplifier due to lower switching losses. In addition to this the switch-mode power supply can be spared in battery driven systems, such as portable and automotive sound systems, when the DC resistance becomes so low, that the battery voltage is sufficient for generating a desired sound pressure level. On the transducer side a lower voice coil DC resistance can be obtained using rectangular or foil windings resulting in higher fill factors which can benefit the efficiency of the transducer, as discussed in [12].

This paper will focus on the design of low impedance voice coils for loudspeaker drivers and how these designs can benefit the efficiency of the driver and thereby the whole sound system.

2. LOUDSPEAKER EFFICIENCY

Conventional loudspeaker drivers are known to have very poor efficiency, typically in the range 0.2-2% depending, among others, on the magnet system, diaphragm size and weight and driver type. The overall efficiency for a system, from electrical input to acoustical output, is simply the product of the efficiencies of the subsystems. For a system consisting of a power supply, an audio amplifier and a loudspeaker the total efficiency becomes:

$$\eta_{tot} = \eta_{supply} \cdot \eta_{amp} \cdot \eta_{spk} \tag{1}$$

Since the efficiency of the amplifier and the power supply is much higher than the efficiency of the loudspeaker, it is clear that the overall efficiency for such systems normally will be dominated by the poor efficiency of the loudspeaker. One method to compensate for the poor efficiency of the driver is to improve the impedance match between the driver diaphragm and the air load. This can be done by using various types of acoustical horns [7]. For low frequency drivers, horn speakers tend to increase the overall size of the speaker significantly and therefore they will not be discussed further in this paper.

The efficiency of a loudspeaker driver is simply the ratio between the acoustic power emitted from the diaphragm, P_A, and the electrical power flowing into the voice coil, P_E.

$$\eta_0 = \frac{P_A}{P_E} \tag{2}$$

A more common measure is the loudspeaker driver's sensitivity, where the Sound Pressure Level (SPL) is measured in dB at a given distance with a given input power. The SPL can be expressed as:

$$SPL = 10 \log \left(\frac{P_E \frac{\eta_0}{A}}{P_o} \right) \tag{3}$$

Where $P_o = 10^{-12}$ W/m^2 is the reference acoustic sound power and A is the area of the sound surface at a given distance from the driver. Normal sensitivity measurements are measured at 1W@1m with the driver mounted in an infinite baffle, thus playing into a half sphere environment. A half sphere environment corresponds to $A = 2\pi r^2$, where r is the radius of the half sphere. With $r = 1$ meter we get a 8 dB reduction in sensitivity. The Sound pressure level at 1W@1m can then be expressed as:

$$SPL_{1W@1\text{m}} = 10 \log \left(\frac{\eta_0}{P_o} \right) - 8\text{dB} \tag{4}$$

The sensitivity is normally in the range 85-95 dB. In literature [7] the efficiency is expressed as a function of the force factor, Bl, the diaphragm area, S_D, the DC resistance of the voice coil, R_E, and the total mass of the diaphragm when attached to the voice coil, M_{ms}:

$$\eta_0 = \frac{\rho_0 (Bl)^2 S_D^2}{2\pi c R_E M_{ms}^2} \tag{5}$$

Where $\rho_0 = 1.18$ kg/m^3 is the density of air and $c = 345$ m/s is the speed of sound in air. The force

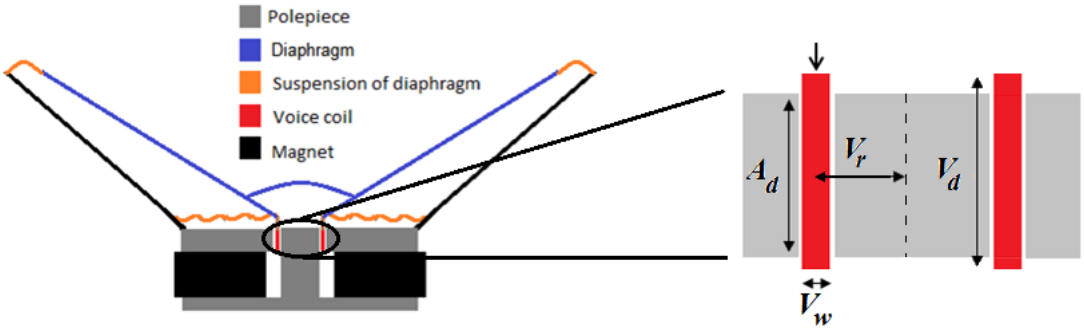

Fig. 1: Loudspeaker driver and voice coil winding area.

factor is the product between the the static magnetic field strength of the permanent magnet and the length of the wire in the air gap. From eq. 5 it seems obvious that for a given driver with a specific diaphragm area and magnet system, one can increase the efficiency by lowering the DC resistance or by increasing the force factor. However these two solutions cancels each other out. This can be shown when considering how the DC resistance and force factor are related to the winding area of the loudspeaker driver. A conceptual model of a loudspeaker driver and its voice coil is shown in fig. 1. V_d is the winding depth, V_w is the winding width, A_d is the air gap depth and V_r is the radius of the voice coil. Normally the winding depth will be bigger than the air gap depth to compensate for non linearities caused by the displacement [13] resulting in an overhung voice coil design.

Assuming that the entire winding area can be filled with wire the force factor and DC resistance can be written as follows:

$$\begin{aligned} R_E &= \frac{l_w}{\sigma A_{wire}} = \frac{NV_o}{\sigma \frac{V_w V_d}{N}} = \frac{N^2 V_o}{\sigma V_w V_d} \\ Bl &= Bl_w \frac{A_d}{V_d} = BNV_o \frac{A_d}{V_d} \end{aligned} \tag{6}$$

Where l_w is the total length of the wire, A_{wire} is the cross sectional area of the wire, $V_o = 2\pi V_r$ is the circumsphere of the voice coil, N is the number of turns and σ is the conductivity of the conductor. For copper the conductivity is $\sigma_{Cu} = 5.96 \cdot 10^7\ S/\mathrm{m}$.

Considering eq. 5 we find the ratio between the force factor squared and the DC resistance to be constant.

$$\begin{aligned} \frac{(Bl)^2}{R_E} &= \frac{B^2 N^2 V_o^2 \left(\frac{A_d}{V_d}\right)^2}{\frac{N^2 V_o}{\sigma V_w V_d}} \downarrow \\ \frac{(Bl)^2}{R_E} &= \frac{B^2 V_o V_w A_d^2 \sigma}{V_d} = \textbf{constant} \end{aligned} \tag{7}$$

Due to this constant ratio the efficiency is theoretically also a constant for a given driver with a given magnet system. However the above expression is only valid if one assumed that the entire available winding area is filled with conducting copper, which in practice is not possible. Therefore one have to consider the fill factor of the voice coil, i.e. the ratio between the area of the conducting copper and the total winding area:

$$\kappa = \frac{A_{Cu}}{A_w} \tag{8}$$

Taking the fill factor into account we get:

$$\begin{aligned} R_E &= \frac{N^2 V_o}{\sigma V_w V_d \kappa} \\ \frac{(Bl)^2}{R_E} &= \frac{B^2 V_o V_w A_d^2 \sigma \kappa}{V_d} \neq \textbf{constant} \end{aligned} \tag{9}$$

Moreover the total moving mass of the driver, M_{ms}, can also be expressed as a function of the fill factor:

$$\begin{aligned} M_{ms} &= M_{d+cf} + M_{vc} \\ M_{d+cf} &= M_d + M_{cf} \\ M_{vc} &= V_d V_w V_o \rho_{wire} \kappa \end{aligned} \tag{10}$$

Where M_d is the mass of the diaphragm, M_{cf} is the mass of the coil former, M_{vc} is the mass of the voice coil wire and ρ_{wire} is the density of the wire material. Now it is possible to express the efficiency of the loudspeaker driver as a function of the fill factor by substituting eq. 9 and eq. 10 into eq. 5:

$$\eta_0(\kappa) = \frac{\rho_0 S_D^2 B^2 V_o V_w A_d^2 \sigma \kappa}{2\pi c V_d \left(M_d + M_{cf} + V_d V_w V_o \rho_{wire} \kappa\right)^2} \quad (11)$$

From eq. 11 it is seen that the efficiency, expressed as a function of the fill factor, is a ratio between a linear function and and a second order polynomial of the simplified form of:

$$\eta_0(\kappa) = \frac{\kappa}{(a + b \cdot \kappa)^2} \quad (12)$$

Where a and b are constants. Considering positive values of κ we find the efficiency to have a shape as shown in fig. 2. In this particular example it is seen that the maximum of efficiency is found at a theoretical fill factor of 50%. In general the fill factor corresponding to the maximum efficiency, can be found by solving for the derivative of the efficiency function. In the simplified expression from eq. 12 we find:

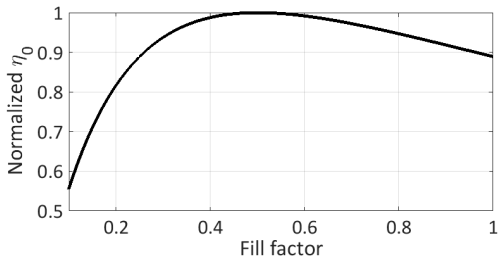

Fig. 2: The efficiency as a function of the fill factor

$$\eta_0'(\kappa) = \frac{1}{(a+b\cdot\kappa)^2} - \frac{2b\cdot\kappa}{(a+b\cdot\kappa)^3}$$

$$\eta_0'(\kappa) = \frac{1}{(a+b\cdot\kappa)^2} - \frac{2b\cdot\kappa}{(a+b\cdot\kappa)^3} = 0 \downarrow \quad (13)$$

$$\kappa_{optimal} = \frac{a}{b}$$

Applying this solution to eq. 11 yields:

$$\eta_0'(\kappa) = 0 \downarrow$$

$$\kappa_{optimal} = \frac{M_d + M_{cf}}{V_d V_w V_o \rho_{wire}} \quad (14)$$

However this is only true for cases where:

$$M_d + M_{cf} \geq V_d V_w V_o \rho_{wire} \quad (15)$$

This is due to the fact that the theoretical maximum fill factor is $\kappa = 1$, i.e. 100%. Therefore we will redefine eq. 14 by introducing a new parameter: The driver's mass ratio:

$$M_{ratio} = \frac{M_d + M_{cf}}{V_d V_w V_o \rho_{wire}} \quad (16)$$

It is seen that the mass ratio is the ratio between the mass of the diaphragm plus the coil former and the maximum mass of the actual wire within the voice coil. It is quite common that typical drivers will have a mass ratio above one. For these cases the optimal fill factor is $\kappa = 1$, meaning that these drivers' efficiencies would benefit from a fill factor optimization. However the impact on the efficiency achieved by this fill factor optimization is dependent on how far above one the mass ratio is. This is shown on fig. 3 where the efficiency is normalized around a fill factor of 50%, which is not an uncommon fill factor for voice coil designs. From the figure it is seen that the impact on the efficiency becomes greater for higher mass ratios.

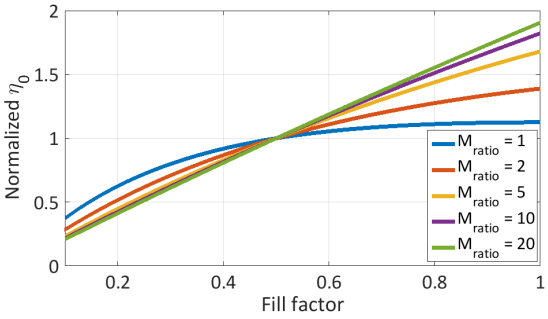

Fig. 3: Impact on efficiency for different mass ratios

3. SMALL-SIGNAL PARAMETERS

The small-signal parameters are well described in litterature, [5], [6], [7], and is also referred to as Thiele-Small parameters. This section will focus on the small-signal parameters known as the quality factors of the loudspeaker driver. That is the electrical-, the mechanical-, and the total-quality factor, Q_{ES}, Q_{MS} and Q_{TS}. These parameters determine the

frequency response of the driver and therefore it is relevant to investigate how they are affected by the fill factor of the voice coil.

3.1. Electrical quality factor

From literature, [7], the electrical quality factor can be expressed as:

$$Q_{ES} = \frac{R_E}{(Bl)^2}\sqrt{\frac{M_{ms}}{C_{ms}}} \tag{17}$$

Where C_{ms} is the mechanical compliance of the diaphragm suspension, which normally is given in the data sheet for a given driver. In eq. 9 it was shown that the relationship between the force factor, Bl and the DC resistance, R_E, could be expressed as a function of the fill factor. Similar it was shown in eq. 10 that the total moving mass, M_{ms}, also could be expressed as a function of the fill factor. Applying these two equations to eq. 17 yields:

$$Q_{ES}(\kappa) = \frac{\frac{N^2 V_o}{\sigma V_w V_d \kappa}}{\left(BNV_o\frac{A_d}{V_d}\right)^2}\sqrt{\frac{M_{d+cf}+V_d V_w V_o \rho_{wire}\kappa}{C_{ms}}} \downarrow$$

$$Q_{ES}(\kappa) = \frac{Vd}{\sigma V_o V_w B^2 Ad^2 \kappa}\sqrt{\frac{M_{d+cf}+V_d V_w V_o \rho_{wire}\kappa}{C_{ms}}} \tag{18}$$

From eq. 18 it is seen that when the fill factor increases the electrical quality factor decreases.

3.2. Mechanical quality factor

The mechanical quality factor is given by:

$$Q_{MS} = \frac{1}{R_{ms}}\sqrt{\frac{M_{ms}}{C_{ms}}} \tag{19}$$

Where R_{ms} is the mechanical resistance of the diaphragm suspension, normally provided in loudspeaker driver data sheets. Similar to the electrical quality factor we can express the mechanical quality factor as a function of the fill factor by substituting eq. 10 into eq. 19:

$$Q_{MS}(\kappa) = \frac{1}{R_{ms}}\sqrt{\frac{M_{d+cf}+V_d V_w V_o \rho_{wire}\kappa}{C_{ms}}} \tag{20}$$

From eq. 20 it is seen that the mechanical quality factor increases with the fill factor.

3.3. Total quality factor

The total quality factor of a loudspeaker driver is simply the combination of the electrical- and mechanical-quality factor:

$$Q_{TS} = \frac{Q_{MS}Q_{ES}}{Q_{MS}+Q_{ES}} \tag{21}$$

The total quality factor determines the frequency response of the driver. This is evident from the pressure transfer function of the loudspeaker driver which is given by:

$$p = \frac{\rho_0}{2\pi}\frac{Ble_g}{S_d R_E M_{as}}G(s) \tag{22}$$

Where $\rho_0 = 1.18$ kg/m^3 is the density of air, e_g is the electrical input to the voice coil, S_d is the diaphragm area, $M_{as} = M_{ms}/S_D^2$ is the acoustic mass of the diaphragm and air load, and finally $G(s)$ is the second order high pass transfer function related to the total quality factor.

$$G(s) = \frac{(s/\omega s)^2}{(s/\omega s)^2 + (1/Q_{TS})(s/\omega s)} \tag{23}$$

Where $\omega_s = 2\pi f_s$ and f_s is the resonance frequency of the driver given by:

$$f_S = \frac{1}{2\pi\sqrt{M_{ms}C_{ms}}} \tag{24}$$

For an optimal flat response the total quality factor should be approximately 0.7. For lower values we get a reduction in the low frequency content and for higher values we get a ripple, boosting the lower frequencies. The transfer function from eq. 22 is only valid for low frequencies. For higher frequencies a roll off is expected due to the self inductance of the voice coil, however this effect can be minimized using a copper cap in the magnetic design. An expression for the total quality factor as a function of the fill factor can be obtained by substituting eq. 18 and 20 into eq. 21:

$$Q_{TS}(\kappa) = \frac{(M_{d+cf}+V_d V_w V_o \rho_{wire}\kappa)V_d}{C_{ms}\sqrt{\frac{M_{d+cf}+V_d V_w V_o \rho_{wire}\kappa}{C_{ms}}}(\sigma V_o V_w B^2 Ad^2\kappa + R_{ms}V_d)} \tag{25}$$

From eq. 25 it is seen that the total quality factor decreases with the fill factor.

4. FILL FACTOR OF VOICE COIL LAYOUTS

This section presents an analysis of the fill factor for conventional voice coil layouts using round wire and an unconventional layout using rectangular wire.

4.1. Round winding layout 1

Conventional voice coil designs utilize round wire in two layers. The concept of the winding layout is shown in fig. 4. It is evident that the round

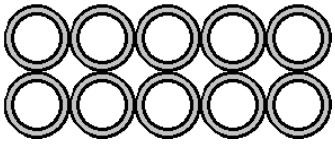

Fig. 4: Round winding layout 1.

shape causes some air gaps to exist between the wire. For this winding layout the maximum fill factor becomes:

$$\kappa_{round,1} = \frac{A_{Cu}}{A_w} = \frac{\pi r_w^2}{(2r_w)^2} = \frac{\pi}{4} \approx 0.79 \qquad (26)$$

Where r_w is the radius of the wire. Taking the insulation of the wire into account the fill factor will be even lower.

$$\kappa_{round,1} = \frac{A_{Cu}}{A_w} = \frac{\pi \left(r_w - \frac{t_{iso}}{2}\right)^2}{(2r_w)^2} \qquad (27)$$

Where t_{iso} is the total insulation thickness on both sides of the wire. In conventional voice coil designs using this winding layout DC resistances between 3 and 8 Ω are quite normal.

4.2. Round winding layout 2

During production of voice coils with round wire in two layers, the windings are often squeezed together as shown in fig. 5. It is seen that the round shape

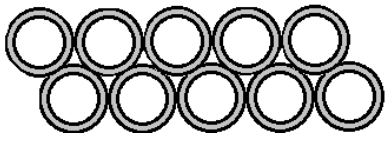

Fig. 5: Round winding layout 2.

still causes some tiny air gaps to exist. However the size of the air gaps are reduced compared to the layout from fig. 4. This leads to an increment of the maximum fill factor:

$$\kappa_{round,2} = \frac{A_{Cu}}{A_w} = \frac{\pi r_w^2}{\left(2+\sqrt{3}\right) r_w^2} = \frac{\pi}{\left(2+\sqrt{3}\right)} \approx 0.84 \qquad (28)$$

With insulation the fill factor of this winding layout becomes:

$$\kappa_{round,2} = \frac{A_{Cu}}{A_w} = \frac{\pi \left(r_w - \frac{t_{iso}}{2}\right)^2}{\left(2+\sqrt{3}\right) r_w^2} \qquad (29)$$

4.3. Rectangular winding layout

Considering an unconventional voice coil winding layout utilizing rectangular wire, as shown in fig. 6, it is possible to achieve a higher fill factor.

$$\kappa_{rec} = \frac{A_{Cu}}{A_w} = \frac{(W_w - t_{iso})(W_t - t_{iso})}{W_w W_t} \qquad (30)$$

Where W_w is the winding width and W_t is the winding thickness. In this winding layout there exist no

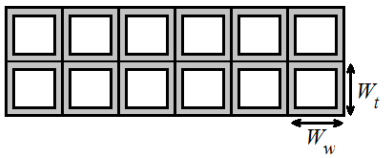

Fig. 6: Winding layout utilizing rectangular wire.

air gap between the wires and therefore the theoretical maximum fill factor is $\kappa_{rec} = 1$, i.e. 100%. In order to fill out the entire winding area, the width of the rectangular wire will change as a function of the DC resistance of the voice coil. For lower DC resistances less turns is required, resulting in a greater wire width and thereby higher fill factor. For this reason the fill factor can be increased by lowering DC resistance and thereby the number of turns. Knowing the voice coil width, V_w, the air gap depth, A_d, the voice coil circumsphere V_o and the winding depth, V_d, one can determine the exact number of turns for a given DC resistance and insulation thickness. This is done by realizing that for a given voice coil geometry the DC resistance is only dependent

Name	Parameter	Value
Voice coil width	V_w	0.45 mm
Voice coil radius	V_r	13.5 mm
Voice coil circumsphere	V_o	84.8 mm
Voice coil depth	V_d	12 mm
Air gap depth	A_d	8 mm
Magnetic field strength	B	1 T
Mass of diaphragm and coil former	M_{d+cf}	21 g
Compliance of diaphragm suspension	C_{ms}	0.7 mm/N
Resistance of diaphragm suspension	R_{ms}	0.75 Kg/s
Diaphragm Area	S_D	332 cm^2

Table 1: Parameters and geometry for 10" woofer

on the number of turns and the insulations thickness which can be assumed to be a given value.

$$R_E = \frac{lw}{\sigma A} = \frac{NV_o}{\sigma W_{t,cu}(W_w - t_{iso})} = \frac{NV_o}{\sigma W_{t,cu}\left(\frac{V_d}{0.5N} - t_{iso}\right)} \tag{31}$$

Where $W_{t,Cu} = W_t - t_{iso}$ is the actual thickness of the copper in the wire. By solving for the number of turns N in eq. 31 we get:

$$N = \frac{-R_E W_{t,Cu} t_{iso}\sigma + \sqrt{R_E^2 W_{t,Cu}^2 t_{iso}^2 \sigma^2 + 8R_E V_o V_d W_{t,Cu}\sigma}}{2V_o} \tag{32}$$

From this the actual width of the copper in the wire can be determined as:

$$W_{w,Cu} = W_w - t_{iso} = \frac{Vd}{0.5N} - t_{iso} \tag{33}$$

This is valid for voice coil with two layers. When the number of turns becomes equal to one, $N = 1$, only one layer exist and a theoretical filling factor of 100% is obtained. In this case the voice coil becomes a one layer solid ring of conducting material. However the DC resistance will be very small, close to zero, which will make it difficult to drive, even with modern switch-mode audio power amplifiers.

4.4. Comparison of winding layouts

Fig. 7 shows a comparison between the different voice coil winding layouts. Note that the x-axis has the relative scale t_{iso}/d_w, where d_w is the diameter of the wire or, for the rectangular wire, the thickness, W_t. It is seen that the voice coil layout using rectangular wire can achieve a higher fill factor than that of the layouts using round wire. For the rectangular wire the decrement rate of the fill factor as the insulation thickness increases, is dependent on the shape of the wire. For high ratios of W_t/W_w there will be a fast decrement rate of the fill factor and for low ratios there will be a slower decrement rate.

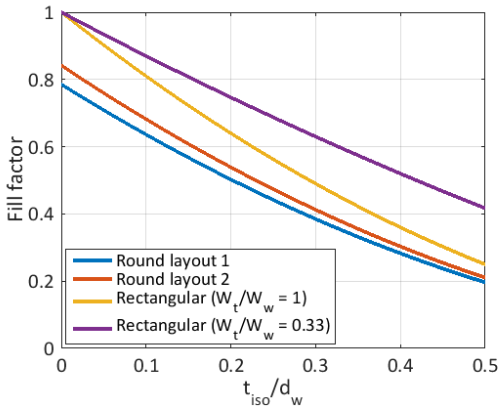

Fig. 7: Fill factor comparison of different winding layouts.

5. VOICE COIL DESIGN

This section presents the voice coil designs for a 10" woofer using the two voice coil layouts for round wire and the voice coil layout for rectangular wire with a low DC resistance of 0.5 Ω. The frequency responses of the three designs are evaluated, compared and discussed. The relevant parameters for the 10" woofer are listed in table 1. It is assumed that the insula-

Design	N	R_E	Bl	κ	η_0	Q_{ES}	Q_{MS}	Q_{TS}	*SPL 1W@1m*
Round layout 1	107	5.2Ω	6.04 T·m	58%	0.77%	0.82	7.71	0.74	90.9 dB
Round layout 2	100	4.1Ω	5.95 T·m	64%	0.83%	0.75	7.75	0.68	91.2 dB
Rectangular layout	39	0.5Ω	2.20 T·m	82%	1.00%	0.61	7.87	0.56	92.0 dB

Table 2: Driver parameters for each design

tion thickness is the same for all three designs and has the value of $t_{iso} = 31$ μm, [14], and that all the voice coil designs utilizes regular copper wire. For this driver the mass ratio, M_{ratio}, is calculated to be:

$$M_{ratio} = \frac{M_{d+cf}}{V_d V_w V_o \rho_{wire}} \approx 5.1 \tag{34}$$

For this mass ratio we will expect to see some improvement of the efficiency when optimizing the fill factor according to fig. 3.

5.1. Design with round winding layout 1

This design utilizes the winding layout shown in fig. 4. The diameter of the whole wire and the actual copper inside is found to be:

$$\begin{aligned} W_d &= \tfrac{1}{2} V_w = \underline{\underline{0.225\text{mm}}} \\ W_{d,Cu} &= W_d - t_{iso} = \underline{\underline{0.194\text{mm}}} \end{aligned} \tag{35}$$

From this the number of turns can be calculated:

$$N = \frac{2V_d}{W_d} \approx \underline{\underline{107}} \tag{36}$$

Now the length of the wire can be calculated:

$$l_w = V_o N \approx \underline{\underline{9.08\text{m}}} \tag{37}$$

Now we can use eq. 4, 6, 11, 18, 20, 25 and 27 to find the DC resistance, the force factor, the fill factor, the efficiency, the quality factors and the sensitivity of the driver. The results are listed in table 2.

5.2. Design with round winding layout 2

This voice coil uses the winding layout shown in fig. 5. The diameter of the wire and the conducting copper can be found using:

$$\begin{aligned} W_d &= \tfrac{2}{2+\sqrt{3}} V_w = \underline{\underline{0.241\text{mm}}} \\ W_{d,Cu} &= W_d - t_{iso} = \underline{\underline{0.210\text{mm}}} \end{aligned} \tag{38}$$

Then the number of turns and the length of the wire can be calculated:

$$\begin{aligned} N &= \tfrac{2V_d}{W_d} \approx \underline{\underline{100}} \\ l_w &= V_o N \approx \underline{\underline{8.48\text{m}}} \end{aligned} \tag{39}$$

Again we can use eq. 4, 6, 11, 18, 20, 25 and 29 to find the parameters of interest which are listed in table 2.

5.3. Design with rectangular winding layout

This design utilizes the winding layout from fig. 6. For this particular design the DC resistance is simply chosen to be:

$$R_E = 0.5\ \Omega \tag{40}$$

The thickness of the wire and the actual conductor can now be found:

$$\begin{aligned} W_t &= \tfrac{1}{2} V_w = \underline{\underline{0.225\text{mm}}} \\ W_{t,Cu} &= W_t - t_{iso} = \underline{\underline{0.194\text{mm}}} \end{aligned} \tag{41}$$

The number of turns can be calculated using eq. 32.

$$\begin{aligned} N &= \tfrac{-R_E W_{t,cu} t_{iso} \sigma + \sqrt{R_E^2 W_{t,cu}^2 t_{iso}^2 \sigma^2 + 8 R_E V_o V_d W_{t,cu} \sigma}}{2V_o} \downarrow \\ N &= \underline{\underline{39}} \end{aligned} \tag{42}$$

Now the width of the wire and the actual conducting copper can be calculated using eq. 33:

$$\begin{aligned} W_w &= \tfrac{Vd}{0.5N} = \underline{\underline{0.616\text{mm}}} \\ W_{w,Cu} &= W_w - t_{iso} = \underline{\underline{0.585\text{mm}}} \end{aligned} \tag{43}$$

Now the length of the wire can be calculated:

$$l_w = V_o N \approx \underline{\underline{3.31\text{m}}} \tag{44}$$

Finally the parameters of interest are found using eq. 4, 6, 11, 18, 20, 25 and 30. The results are listed in table 2.

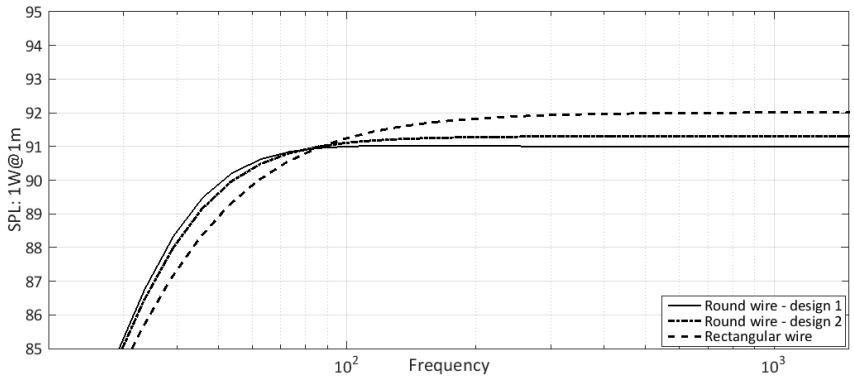

Fig. 8: Frequency response of the three woofer designs.

5.4. Frequency responses

From table 2 we can see that when the fill factor increases the efficiency/sensitivity of the woofer increases as well. Moreover it is seen that the total quality factor decreases when the fill factor is improved. From this the frequency response is expected to gain higher sound pressure levels for midrange frequencies but a slight dampening of the low frequency content when the fill factor is optimized.

We can plot the frequency of the three designs using the pressure transfer function from eq. 22. The electrical input voltage is set so that a rms power of 1 watt is obtained:

$$e_g = \sqrt{1\ \mathrm{W} \cdot R_E} \tag{45}$$

This ensures that the frequency responses of the different designs can be compared properly. Fig. 8 shows the frequency responses of the three different designs. It is seen that the frequency responses behave exactly as predicted. The decrement of the total quality factor for the high fill factor design causes a minor attenuation of low frequencies. Moreover the sensitivity increases and the difference between the use of round wire, with low fill factor, and rectangular wire, with high fill factor, is approximately 1 dB, corresponding to approximately 30% efficiency improvement.

6. CONCLUSION

This paper has presented a thorough analysis of the loudspeaker efficiency and its relation to the fill factor of the voice coil. It has been shown that the efficiency can be expressed as a function of the fill factor and the geometry of the magnet system. In addition to this a new parameter, the mass ratio of the driver, was introduced. This parameter indicates how much a given driver will benefit from fill factor optimization. The higher mass ratio the higher impact. Moreover the small-signal parameters related to the frequency response of the driver were analysed, e.g the quality factors. It was found that the total quality factor of driver decreases when the fill factor increases. Different voice coil winding layouts have been described and analysed with respect to their fill factors. It was found that by using rectangular wire to realize voice coils with low DC resistance the fill factor could be increased compared to that of conventional voice coils using round wire. Finally three voice coils were designed for a 10" woofer, using different voice coil winding layouts. The response of the woofer was calculated and it showed that the sensitivity for the woofer could be increased up to 1 dB just by optimizing the fill factor using low impedance voice coils realized with rectangular wire. This corresponds approximately to an astonishing 30% efficiency improvement. Since the efficiency of the driver dominates that of an entire audio system consisting of power supply, amplifier and loudspeaker, this efficiency improvement is

valid for the whole audio system. More over this improvement could be even better if the woofer was designed to have a higher mass ratio. In addition to this the total quality factor of the driver could also be designed so that a maximum flat response is obtained, meaning that the low frequencies would not be attenuated.

7. FUTURE WORK

Future work includes a practical realization of a loudspeaker driver using a fill factor optimized-, low impedance-voice coil with rectangular wire. In addition to this measurements of the actual response of a fill factor optimized driver should be compared to the theoretically calculated. Audio power amplifiers capable of handling low impedance drivers are to be developed but with the use of switch-mode technology this should be possible. The authors encourage the development of a new loudspeaker design, with high fill factors, high mass ratios and low DC resistance. This could allow for a series of high efficiency drivers.

8. ACKNOWLEDGEMENTS

The authors would like to thank Carsten Thingaard and Morten Halvorsen from PointSource Acoustics for their many good advices and their know-how on loudspeaker design and in particular voice coil design. Moreover the authors would like to thank Henrik Schneider from the Electronics Group, in the Department of Electrical Engineering, at the Technical University of Denmark, for many good discussions on the subject of voice coil designs.

9. REFERENCES

[1] Erickson and Maksimovic, "Fundamentals of Power Electronics", Second Edition, Kluwer Academic Publishers.

[2] K. Nielsen, "Audio Power Amplifier Techniques With Energy Efficient Power Conversion", Ph.D. thesis, Volume 1, Technical University of Denmark 1998.

[3] A. Yamauchi, A. Knott, I. H. H. Jørgensen and M. A. E. Andersen , "Frequency dependent loss analysis and minimization of system losses in switch-mode audio power amplifiers", in AES Convention 137th, Los Angeles October 9-12, 2014.

[4] S. Poulsen, "Simple PWM modulator topology with excellent dynamic behavior", Applied Power Electronics Conference and Exposition, 2004.

[5] R. H. Small, "Closed-box loudspeaker systems", J. Audio Eng. Soc., vol 20 pp. 383-395 (June 1972).

[6] A. N. Thiele, "Loudspeakers in vented boxes, Parts I and II", J. Audio Eng. Soc., vol. 19 pp. 382-392 (May 1971); pp. 471-483 (June 1971).

[7] W. Marshall Leach, Jr. "Introduction to Electroacoustics and Audio Amplifier Design", Kendall/Hunt Publishing Company, 2003.

[8] H. F. Olson, "Acoustical Engineering", Proffesional Audio Journals, Inc.

[9] N. E. Iversen and A. Knott, "Small Signal Loudspeaker Impedance Emulator", JAES Volume 62 Issue 10 pp. 676-682, October 2014.

[10] N. E. Iversen, H. Schneider, A. Knott and M. A. E. Andersen , "Efficiency Investigation of Switch-Mode Power Audio Amplifiers Driving Low Impedance Transducers", in AES Convention 139th, New York October 29th-1st November, 2015.

[11] A. Yamauchi, H. Schneider, A. Knott, I. H. H. Jørgensen and M. A. E. Andersen , "Investigation of Energy Consumption and Sound Quality for Class-D Audio Amplifiers using Tracking Power Supplies", in AES Convention 138th, Warsaw May 7-10, 2015.

[12] S. Poulsen and M. A. E. Andersen , "Practical considerations for integrating switch mode audio amplifiers and loudspeakers for a higher power efficiency", in AES Convention 116th, Berlin May 8-11, 2004.

[13] Wolfgang Klippel, "Loudspeaker Non linearities. Causes, Parameters, Symptoms", Klippel GmbH, Dresden, Germany.

[14] Elektrisola, "Technical data for enamelled copper wire, based on IEC 60317", Elektrisola.

G

Design of efficient sound systems for low voltage battery driven applications

In 141st Audio Engineering Soceity convention, Los Angeles, September 29-2 October, 2016.

Audio Engineering Society

Convention Paper

Presented at the 141st Convention
2016 September 29 – October 2, Los Angeles, CA, USA

Design of Efficient Sound Systems for Low Voltage Battery Driven Applications

Niels Elkjær Iversen[1], Rien Oortgiesen[2], Arnold Knott[1], Michael A. E. Andersen[1], and Mikkel Høyerby[2]

[1]*Technical University of Denmark - DTU, Kongens Lyngby, 2800, Denmark*
[2]*Merus Audio, Herlev, 2730, Denmark*

Correspondence should be addressed to Niels Elkjær Iversen (neiv@elektro.dtu.dk)

ABSTRACT

The efficiency of portable battery driven sound systems is crucial as it relates to both the playback time and cost of the system. This paper presents design considerations when designing such systems. This include loudspeaker and amplifier design. Using a low resistance voice coil realized with rectangular wire one can boost the efficiency of the loudspeaker driver and eliminate the need of an additional power supply. A newly developed switching topology is described which is beneficial to near-idle efficiency (< 2 W), which is crucial for real audio applications in the consumer electronics space. A small sized sound system was implemented using the discussed design considerations. The amplifier efficiency performance was found to be very high with near-idle efficiency reaching a remarkably 88% at 2 W. The average output SPL was estimated to be up to 90 dB in half spheric anechoic conditions. Measured results are compared with current state-of-art and shows a 14% points efficiency improvement.

1 Introduction

The efficiency of consumer electronics is an important performance parameter. Not only due to the environmental challenges the society faces but also due to the extended battery life in portable sound systems that comes with high efficiency. In audio there is an increasing trend towards battery driven and portable sound systems. One of the big challenges for these kind of sound systems is the capability to play sufficiently loud while having a decent play back time. An immediate solution is to use larger batteries. However this will increase the cost and weight of the sound system. The optimal solution is to utilize methods to boost the efficiency of the sound system. This paper presents these methods including the design procedure and implementation of a highly efficient battery driven sound system. That includes special transducer and amplifier design. Measurements of the realized sound systems performance are provided and commented.

2 Sound system efficiency

To make an efficient audio systems the different blocks of which it consists must be considered. This essentially includes the loudspeaker, the amplifier and the power supply.

2.1 Loudspeaker

Loudspeakers are very well described in literature [1], [2], [3]. However the fundamentals of its' operation will be repeated here for convenience. The conventional loudspeaker is the moving coil loudspeaker. It

consist of three essential building blocks which are coupled to one another. That is the voice coil, the magnet system and the diaphragm. Fig. 1 shows the loudspeaker driver with the three blocks highlighted. The voice coil is essentially a piece of wire turned

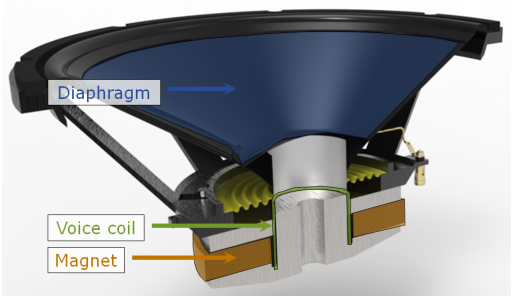

Fig. 1: Cross sectional view on a loudspeaker driver.

many items around the core of the magnet system. This makes it an inductor with a nominal resistance, that is the resistance at 0 Hz. This resistance is also known as the DC resistance, R_E, and conventional loudspeaker drivers have DC resistances ranging from 4-8 Ω. The loudspeaker is operating when the amplified signal from the amplifier is fed into the voice coil terminals. This will generate a current. The current will induce an electromagnetic field in the voice coil, causing a displacement due to the static magnetic field of the permanent magnet. This displacement is transferred to the diaphragm and emitted as sound. To improve the efficiency of the loudspeaker and the sound system a lower voice coil DC resistance is desired. A low DC resistance can increase the fill factor of the voice coil which is beneficial for the loudspeaker efficiency. This is discussed in [4], [5] and [6] where measurements confirms the theory that the fill factor, κ, is approximately proportional with the efficiency, η_0:

$$\eta_0 \propto \kappa \tag{1}$$

A method to obtain a low DC resistance while improving the fill factor is to use rectangular wire for the voice coil windings as it removes the tiny air gaps that exist between conventional round wire as shown in fig. 2.

2.2 Electronics

To boost the efficiency of the electronics in a battery driven sound system, which basically consists of the

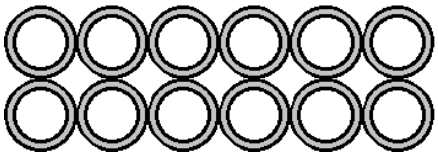

(a) Round winding layout.

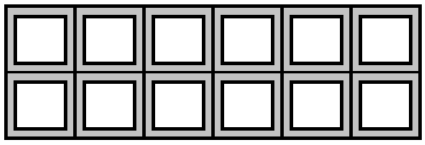

(b) Rectangular winding layout.

Fig. 2: Using a rectangular winding layout increases the fill factor as the tiny air gaps between the conventionl round wires are removed.

power supply and amplifier, one definitely want to utilize switch-mode technology. This technology is widely used in power electronics [7] and theoretically offers an efficiency of 100%. Previous work has shown that practical implementations can achieve efficiencies well above the 90% mark as shown in [8], [9] and [10]. In addition to this switch-mode audio amplifiers can achieve excellent performance with Total Harmonic Distortion (THD) beneath 0.005% [11], [12]. To further improve the efficiency a tracking power supply could be an option as discussed in [13].

However a simpler solution is to completely remove the power supply. This can be done with the use a low impedance load. In a previous study it has been observed that the efficiency of a battery driven sound system can be greatly improved when driving low impedance loads from a low voltage rail [14]. In addition to this it has been shown in [15] and [16] that especially near-idle losses are important for the amplifier when playing real music signals. Typically the output power of the amplifier will be in a range up 2 W when driven from a low voltage supply, that is typically less or equal to 12 V, also observed in [15]. Therefore it is relevant to use an amplifier topology that deals specifically well in this power range.

2.2.1 Amplifier topology

Such an amplifier topology is the newly developed eximo® topology, designed by Merus Audio. This topology achieves the lowest idle power consumption

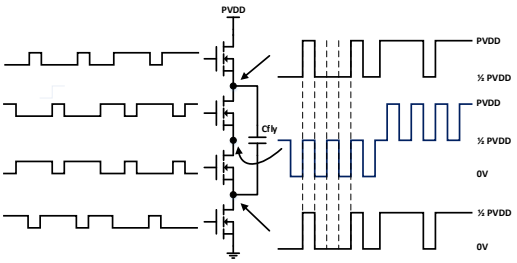

Fig. 3: Multi-level output stage.

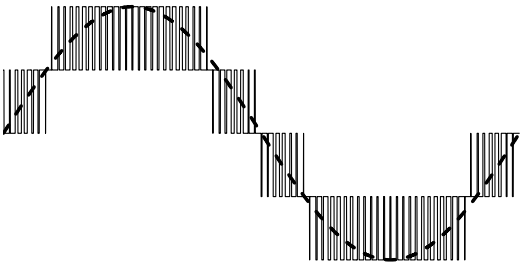

Fig. 4: Full bridge-tied load 5-level output signal when driven by a sinusoid input signal.

normalized to maximum output power [17]. Low near-idle power loss is achieved by employing multi-level switching technology which can establish multiple PWM output levels from a single supply. The half-bridge power stage that is used to establish a multi-level output signal is shown in fig. 3. A total of four MOSFETs is used in each power stage of which each MOSFET is driven by an individual PWM signal. The capacitor (C_{fly}) that is sitting in between the top and the bottom MOSFET functions as an extra supply element. One half-bridge power stage will establish a three level output signal at its switching node: 0V, 1/2PVDD, and PVDD. When combining two half-bridge power stages into a full bridge-tied load (BTL) configuration, up to five levels can be established as seen by a differentially connected speaker load, as shown in fig. 4. Note that an inherent property of a five multi level system is a quadrupling of the switching frequency at the output nodes. As a differentially connected speaker load sees a five level modulated signal it experiences significantly less out-of-band switching residuals. This implies that the amplifier can operate in a filter-less output configuration while maintaining efficiency and reducing EMI and EMC implications. The main advantage in near-

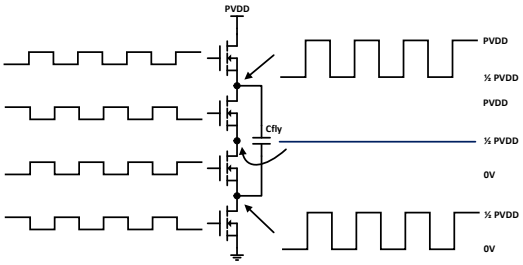

Fig. 5: Multi-level output stage.

idle operation is that the output node of the half-bridge contains close to zero switching activity due to cancellation of the individual switching nodes, as shown in fig. 5. Close to zero switching activity in near-idle operation can significantly reduce power loss in the amplifier through two main mechanisms:

- Elimination of idle conduction losses in the power stage, filter, and speaker. Both conductive and magnetic losses.
- Capacitive switching losses can subsequently be effectively reduced to scale down MOSFET switching frequency.

3 Implementation and measurements

Based on the technological overview presented above a sound system has been designed to be as efficient as possible. The implemented amplifier utilizes the described eximo® switching topology with a five level PWM modulation to boost the efficiency at low power outputs. Moreover the switching topology allows for an implementation without output filter. The system is designed to run from a low voltage supply of approximately 10 V corresponding to the available voltage from three lithium ion battery cells in series which is a typical configuration in small battery packs.

A four inch driver was implemented using a rectangular winding layout for the voice coil to increase the fill factor. The resulting DC resistance was measured to be 1.7Ω. In addition to this the small signal parameters of the implemented driver was measured with a Klippel system [18] and the results are shown in table 1. Note that the nominal sensitivity is rather low, 84 dB, compared to high efficiency drivers which can be

above 90 dB. However this is expected due to the small size of the driver and the low resonant frequency of the driver which is obtained by using a rather heavy diaphragm. The low resonant frequency of the driver

Q_{TS}	V_{AS}	f_S	R_E	$SPL_{1W@1m}$	η_0
0.55	3.9L	61Hz	1.7Ω	83.6dB	0.145%

Table 1: Measured small signal parameters of implemented driver.

is beneficial for the low frequency output of the driver. The frequency response of the driver was measured in anechoic conditions and fig. 6 shows the results. The frequency response of the driver reveals that it is an extended range driver as its' pass band is from approximately 100 Hz to 7500 Hz. To emulate the application

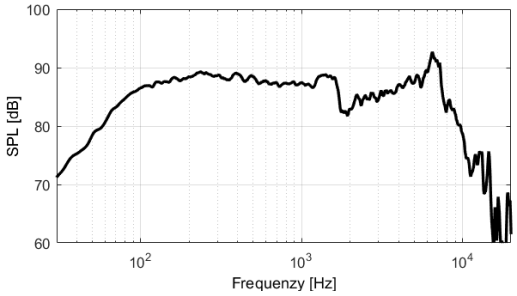

Fig. 6: On axis frequency response of implemented driver at 1.13V@40cm measured in anechoic conditions at a halfsphere environment (2π).

of a portable sound system a small vented box cabinet was designed for the driver. Vented box cabinets are well described in previous work [2], [3] and will not be elaborated here. The cabinet has a small volume of approximately 3.3 litres, making it in the same size range as commercially available portable systems. The Helmholtz resonant frequency of the cabinet is approximately 70 Hz. This boost the frequency response a little bit around 100 Hz. Fig. 7 shows the implemented amplifier, driver and speaker.

3.1 System efficiency

The efficiency of amplifier was measured when playing into the real implemented loudspeaker. The test signal used was a pink noise signal as it represents

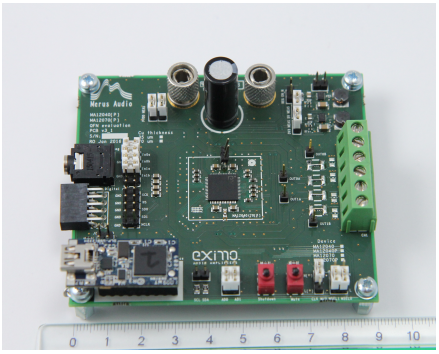

(a) Implemented amplifier using the eximo® switching topology.

(b) Custom made driver with $R_E = 1.7\Omega$ using a rectangular winding layout.

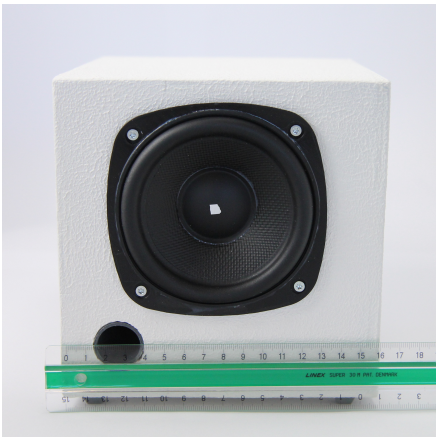

(c) Simple vented box cabinet designed for the custom made driver emulating the complete small battery driven sound system.

Fig. 7: Implemented amplifier, custom driver and final loudspeaker.

real audio much more realistic than sine waves. This is described in [15]. Due to the complex impedance of the loudspeaker normal multi meters could not be used to measure the efficiency as it would generate measurement errors due the lack of phase information. To avoid these errors the efficiency measurements were performed with an oscilloscope where the input and output voltages and currents were measured over a ten second window. From this the input and output power could be calculated for each measured data point. The average input and output was found by integrating over the whole window and from this the efficiency could be calculated. Fig. 8 shows the measured results of the implemented amplifier and a reference amplifier, which is widely used in the industry and considered state-of-the-art. Note that the reference amplifier has an LC output-filter and was measured using a standard measurement setup with multi meters while playing sine waves into a purely resistive load. It is seen that the implemented amplifier performs very well. At 200 mW the efficiency is at 50% and at 2 W it hits a remarkably 88%. In addition to this the results shows that the implemented amplifier performs better than the reference amplifier. At 600 mW the implemented amplifier has 14% points efficiency advantage. Note that the efficiency advantage would be even greater if the reference system used a conventional loudspeaker instead of an approximately 2 Ω load, as it would need an additional power supply to obtain the same output powers. Based on the evaluated sensitivity of the implemented loudspeaker listed in table 1 the Sound Pressure Level (SPL) in the pass band can be evaluated for a the different input powers which allows for a plot of the SPL@1m vs. input power in a half sphere anechoic condition. The SPL can be calculated using:

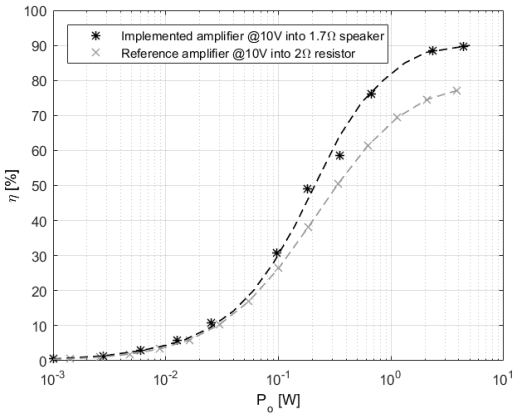

Fig. 8: Amplifier efficiency.

$$SPL = 10\log\left(\frac{P_E \frac{\eta_0}{A}}{P_o}\right) \tag{2}$$

Where P_E is the electrical input power, $P_o = 10^{-12}$ W/m^2 is the reference acoustic sound power and A is the area of the sound surface at a given distance from the driver. A half sphere environment corresponds to $A = 2\pi r^2$, where r is the radius of the half sphere. With $r = 1$ meter we get a 8 dB reduction thus the SPL can be calculated as:

$$SPL = 10\log\left(\frac{P_E \eta_0}{P_o}\right) - 8\text{dB} \tag{3}$$

Fig. 9 shows the results including the estimated SPL for the reference amplifier. It is seen that actually very little power is required to generate a decent SPL of 80 dB for listening levels. Moreover it is seen that the peak output SPL is up to 90 dB which is rather loud. The actual SPL for real operating conditions will be even higher due to the fact that a typical operation will not be anechoic nor in a half sphere environment. Finally it is worth noticing that the implemented amplifier uses less power compared with the reference amplifier for the same SPL, especially at low listening levels.

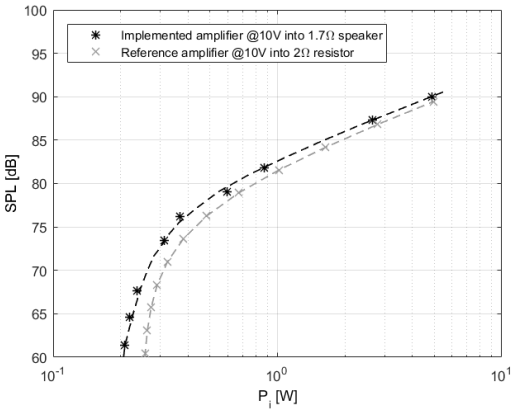

Fig. 9: Estimated output SPL@1m in a half sphere anechoic environment.

4 Conclusion

This paper has described and discussed methods to boost the efficiency in battery driven sound systems. It

was found that the efficiency of the loudspeaker driver could be improve using rectangular wire with a low DC resistance for the voice coil. In addition to this it was argued that the low DC resistance can eliminate the need of a boosting power supply in battery driven applications thus improving the efficiency of the electronics. Moreover the typical output power of the amplifier was discussed and, based on previously work, found to be in the range up to 2 W. For this reason it was relevant to find an amplifier topology performing very well in this range. A new kind of amplifier topology has been described, the eximo®. It utilizes a five level modulation which boost the efficiency performance in near-idle operation.

Based on the analysis a prototype sound system has been implemented. The sound system is designed to a 10 V voltage supply corresponding to the available voltage from three lithium ion battery cells in series which is a typical configuration in small battery packs. A custom loudspeaker driver was implemented using a rectangular winding layout with a low DC resistance of 1.7 Ω for the voice coil design to boost its' efficiency. A small vented box cabinet was build to emulate the whole sound system. An amplifier utilizing the described eximo® switching topology was implemented to boost the near-idle efficiency. Measurements show a very well performing sound system with a near-idle efficiency reaching 88% at 2 W. The average output SPL was estimated to be above 90 dB at 1 meter in the pass band when operating with pink noise in a half sphere anechoic environment. In non anechoic environments this will be even louder. Moreover it was shown that very little power was needed to generate a decent SPL of 80 dB for listening levels. The measured results was compared with a reference amplifier which is widely used in the industry and considered state-of-the-art. The comparison showed that the implemented amplifier has an efficiency advantage up to 14% points and this would be even greater in conventional systems not using the custom designed low impedance speaker as they would be dependent on additional power supplies to generate the same output powers.

5 Acknowledgements

The authors would like to thank Carsten Thingaard and Morten Halvorsen from PointSource Acoustics for their assistance in the process of implementing the custom designed voice coil as well as loudspeaker driver.

References

[1] R. H. Small, "Closed-box loudspeaker systems", J. Audio Eng. Soc., Vol. 20 pp. 383-395, June 1972.

[2] A. N. Thiele, "Loudspeakers in vented boxes, Parts I and II", J. Audio Eng. Soc., Vol. 19 pp. 382-392 (May 1971); pp. 471-483, June 1971.

[3] W. Marshall Leach, Jr. "Introduction to Electroacoustics and Audio Amplifier Design", Kendall/Hunt Publishing Company, 2003.

[4] N. E. Iversen, A. Knott and M. A. E. Andersen , "Low Impedance Voice Coils for Improved Loudspeaker Efficiency", in AES Convention 139th, New York October 29th-1st November, 2015.

[5] S. Poulsen and M. A. E. Andersen , "Practical considerations for integrating switch mode audio amplifiers and loudspeakers for a higher power efficiency", in AES Convention 116th, Berlin May 8-11, 2004.

[6] N. E. Iversen, A. Knott and Michael A. E. Andersen, "Relationship between voice coil fill factor and loudspeaker efficiency", J. Audio Eng. Soc., April 2016.

[7] Erickson and Maksimovic, "Fundamentals of Power Electronics", Second Edition, Kluwer Academic Publishers.

[8] A. Yamauchi, A. Knott, I. H. H. Jørgensen and M. A. E. Andersen, "Frequency dependent loss analysis and minimization of system losses in switch-mode audio power amplifiers", in AES Convention 137th, Los Angeles, October 9-12, 2014.

[9] K. Nielsen, "Audio Power Amplifier Techniques With Energy Efficient Power Conversion", Ph.D. thesis, Volume 1, Technical University of Denmark 1998.

[10] M. Carmen, Z. Zhang, A. Knott and M. Andersen, "Power Flow Control of a Dual-Input Interleaved Buck/Boost Converter with Galvanic Isolation for Renewable Energy Systems ", Applied Power Electronics Conference 2015.

[11] S. Poulsen, M.A. Andersen, "Simple PWM modulator topology with excellent dynamic behavior", Applied Power Electronics Conference and Exposition, 2004.

[12] B. Putzeys, "Simple Self-Oscillating Class D Amplifier with Full Output Filter Control", in AES Convention 118th, Barcelona, May 28-31, 2005.

[13] A. Yamauchi, H. Schneider, A. Knott, I. H. H. Jørgensen and M. A. E. Andersen, "Investigation of Energy Consumption and Sound Quality for Class-D Audio Amplifiers using Tracking Power Supplies", in AES Convention 138th, Warsaw, Poland, May 7-10, 2015.

[14] N. E. Iversen, H. Schneider, A. Knott and M. A. E. Andersen, "Efficiency Investigation of Switch-Mode Power Audio Amplifiers Driving Low Impedance Transducers", in AES Convention 139th, New York, October 29-1 November, 2015.

[15] N. E. Iversen, A. Knott and M. A. E. Andersen, "Efficiency of Switch-Mode Power Audio Amplifiers - Test Signals and Measurement Techniques", in AES Convention 140th, Paris, 4-7 June, 2016.

[16] R. A. R. van der Zee and A. J. M. van Tuijl, "Test Signals for Measuring the Efficiency of Audio Amplifiers", in AES Convention 102th, Amsterdam, May 16-19, 1998.

[17] Mikkel Høyerby, Jørgen Kragh Jakobsen, Jesper Midtgaard, Thomas Holm Hansen, Allan Nogueras Nielsen, Hans Hasselby-Andersen, "A 270W Monolithic Five-Level Class-D Audio Power Amplifier", *2016 IEEE International Solid-State Circuits Conference*, 2016

[18] Wolfgang Klippel, "Loudspeaker Non linearities. Causes, Parameters, Symptoms", Klippel GmbH, Dresden, Germany.

H

Efficiency investigation of switch-mode power audio amplifiers driving low impedance transducers

In 139th Audio Engineering Soceity convention, New York, October 29-1 November, 2015.

Audio Engineering Society

Convention Paper

Presented at the 139th Convention
2015 October 29–November 1 New York, USA

Efficiency Investigation of Switch-Mode Power Audio Amplifiers Driving Low Impedance Transducers

Niels Elkjær Iversen[1], Henrik Schneider[1], Arnold Knott[1], and Michael A. E. Andersen[1]

[1] *Technical University of Denmark - DTU, Kongens Lyngby, 2800 Denmark*

Correspondence should be addressed to Niels Elkjær Iversen (neiv@elektro.dtu.dk)

ABSTRACT

The typical nominal resistance span of an electro dynamic transducer is 4 Ω to 8 Ω. This work examines the possibility of driving a transducer with a much lower impedance to enable the amplifier and loudspeaker to be directly driven by a low voltage source such as a battery. A method for estimating the amplifier rail voltage requirement as a function of the voice coil nominal resistance is presented. The method is based on a crest factor analysis of music signals and estimation of the electrical power requirement from a specific target of the sound pressure level. Experimental measurements confirms a huge performance leap in terms of efficiency compared to a conventional battery driven sound system. Future optimization of low voltage, high current amplifiers for low impedance loudspeaker drivers are discussed.

1. INTRODUCTION

A system designed for high quality audio reproduction involves many different blocks. These often include power supply, Digital Signal Processing (DSP), pre-amplifier, amplifier, cross-over network, loudspeaker enclosure and transducer. However all these blocks can be boiled down to three essential blocks which are:

- Power supply
- Amplifier
- Transducer

Modern power supplies and amplifiers are widely utilizing switch-mode power technology which is described in [1]. This is due to the high efficiency this technology offers, which theoretically can reach 100%. In practice the theoretical efficiency cannot be reached but it is possible to reach efficiencies above 90% for audio applications [2] and [3]. Moreover the switch-mode power audio amplifiers delivers excellent audio performance with Total Harmonic Distortion (THD) beneath 0.005% [4]. The transducer of the sound system, also referred to as the loudspeaker driver, is normally mounted in a care-

fully designed enclosure. Loudspeaker drivers and their enclosures are well described in literature [5], [6], [7]. The impedance of the driver consist of an acoustical-, a mechanical and an electrical-part and is carefully described in [8] and [9]. The nominal resistance of the driver is characterized by the voice coil resistance. This resistance is also know as the DC resistance, corresponding to the resistance at 0 Hz. For decades it has been widely accepted to aim for voice coil DC resistances between 4 Ω and 8 Ω. According to Joules and Ohms laws a reduction of the load impedance leads to a decreased amplifier voltage rail requirement and an increased current requirement for a given output power:

$$U = \sqrt{P \cdot R}, \qquad I = \sqrt{\frac{P}{R}} \tag{1}$$

In traditional sound systems where relatively long cables connect the amplifier to a number of passive loudspeakers the high current requirement would result in high conduction losses or very thick cables which are clear disadvantages. In these systems a load in the range of 4 Ω to 8 Ω is still preferable. In integrated sound systems or active loudspeakers where the amplifier is located in close proximity to the transducer a low impedance load could be advantageous. Modern switch-mode power audio amplifiers can easily be designed to deliver power to lower load impedances. A low amplifier voltage rail requirement will enable the amplifier to be driven directly from a low voltage source such as batteries without the need of an extra power conversion utilizing a switch-mode power supply. In battery powered audio applications this will lead to reduced size, cost and weight as well as increased efficiency. The increased efficiency could either be exploited to prolong the operational time between charging or to reduce the battery size leading to additional cost, size and weight benefits. On the transducer side a lower voice coil DC resistance can be obtained using rectangular or foil windings resulting in higher fill factors which can benefit the efficiency of the transducer, as discussed and shown in [11] and [12].

This paper will focus on the consequences for the power electronics, e.i power supply and audio amplifier, when utilizing low impedance loudspeaker drivers.

2. VOLTAGE RAIL ANALYSIS

Switch-mode power audio amplifiers normally utilizes a Buck topology [1]. This topology can be realized either in a half- or full-bridge configuration. The half bridge requires a dual voltage supply while the full bridge only requires a single supply. However the component count in the full bridge is twice the component count in the half bridge. For battery driven systems the full bridge Buck, shown in fig. 1, is the conventional used topology. The Buck

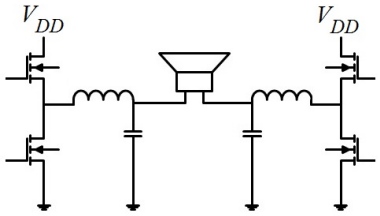

Fig. 1: Full bridge buck topology.

topology has an ideally linear steady state transfer function, enabling low THD, which makes it suitable for audio applications. The steady state transfer function for the full bridge Buck is shown in eq. 2.

$$V_o = (2D - 1)\, V_{DD} \tag{2}$$

Where D is the duty cycle, V_{DD} is the supply rail voltage and V_o is the output voltage. It is seen that when the duty cycle is either 0% or 100% the maximum output voltage is obtained $|V_{o,max}| = |V_{DD}|$. The peak output power is simply:

$$P_{pk} = \frac{|V_{DD}|^2}{R_L} \tag{3}$$

Where R_L is the load resistance which equivalents the transducer impedance. For DC-DC operation the maximum output power can be found using eq. 3. However when operated with dynamic signals one have to take the crest factor (CF) of the signal into account. The crest factor is the ratio between the peak and the rms value of a signal and is normally given in decibels.

$$CF = 20 \log\left(\frac{V_{pk}}{V_{rms}}\right) = 10 \log\left(\frac{P_{pk}}{P_{rms}}\right) \tag{4}$$

For test purposes audio signals are normally estimated with sine waves, which have a crest factor of:

$$CF_{sine} = 20\log\left(\sqrt{2}\right) = 3 \text{ dB} \tag{5}$$

While the peak power remains the same for signals with different crest factor, the maximum continuous output power, e.i the RMS output power, is strongly affected:

$$P_{RMS} = \frac{P_{pk}}{\exp\frac{CF\cdot\ln(10)}{10}} \tag{6}$$

The voltage rail requirement should satisfy eq. 3.

$$V_{DD} = \sqrt{R_L P_{pk}} \tag{7}$$

In order to determine the required rail voltage the crest factor and the maximum RMS output power must be known. These quantities will be examined in the next chapters.

3. CREST FACTOR ANALYSIS

As mentioned sine waves are normally used for test purposes of audio amplifiers. However real music signals are much more dynamic than sine waves. This is described in [13] and [14], where it is also shown that the crest factor depends a lot on the genre of music. In [15] the historic evolution of the crest factor is described. Here it is stated that the crest factor has been decreasing since the nineties due intensive compressor use in the mastering process of an audio recording.

The difference between audio signals and sine waves can be visualized when investigating the actual signal amplitude distribution of audio tracks and sine waves. Fig. 2 shows the signal amplitude distribution of more than 400 different audio tracks and compares it to that of a sine wave. From the figure it is seen that even though the amplitude peaks are the same, the amplitude of the audio tracks is concentrated around zero while the sine signal amplitude is distributed more evenly and actually increases in the outer regions. From fig. 2 it can be easily realized that the RMS value of the audio tracks are significantly smaller than that of the sine wave. Moreover this means that the resulting crest factor of the audio tracks are significantly larger than that of the sine wave. The amplitude bins used in the analysis

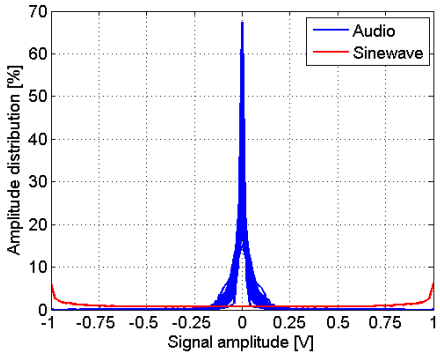

Fig. 2: Amplitude distribution of music compared to a sine wave

were 0.1 V which explains why the amplitude distribution does not reach 0 at high signal amplitude for the sine wave. To get a good estimation of the average crest factor of audio tracks, the crest factors of +400 audio tracks have been analysed. Not only have this analysis been performed on the original audio signals but also on a low pass-, a band pass- and a high pass-filtered version of the original signal. By doing so one obtain an example of crest factors of actual audio signals delivered to a subwoofer, a woofer and a tweeter, as shown in fig. 3, displayed as box plots. From the figure it is evident

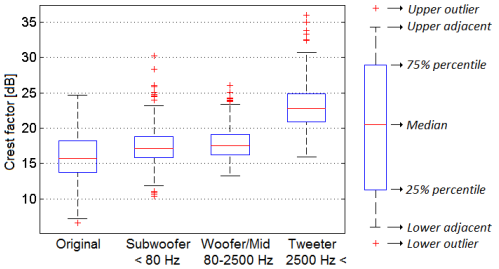

Fig. 3: Calculated crest factor of +400 original and filtered audio signal

that the crest factor span is huge. For the original signal we find crest factors ranging from 5 dB up to 25 dB. However when focussing only on the 25%

Crest factor	Original	Subwoofer	Woofer/Mid	Tweeter
High	18 dB	19 dB	19 dB	25 dB
Medium	16 dB	17 dB	17 dB	23 dB
Low	14 dB	16 dB	16 dB	21 dB

Table 1: Most common crest factor span

percentile to the 75% percentile, e.i the tracks with the most common crest factor value, it is seen that the crest factor ranges approximately from 14 dB to 18 dB with the median value of 16 dB. This result is summarized in table 1.

From fig. 3 it is observed that the crest factor for the subwoofer- and woofer-filtered signals are quite similar to that of the original. The tweeter-filtered signals has, on the other hand, a much higher crest factor. Equal rail voltages may however be utilized for all loudspeaker driver types due to the relative lower power requirement of tweeters [13].

Due to loudness normalization, tracks with different crest factors will sound equally loud when played back over an audio system. However the music with high crest factor will demand power peaks which are greater than that of the music with low crest factor. Higher power peaks equals higher output voltage peaks and in order to deliver these peaks without clipping one must ensure that voltage rail of the amplifier is of sufficient size as shown in fig. 4.

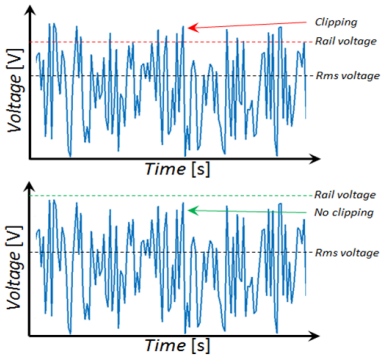

Fig. 4: Music signal gets distorted when rail voltages are insufficient.

4. EXAMPLE OF VOLTAGE RAIL REQUIREMENT

Consider the sound system shown in fig. 5 playing into a half sphere environment. r is the distance from the transducer to the listener in meters, P_{out} is the electrical output power of the amplifier and P_A is the acoustical output power. Assuming that the

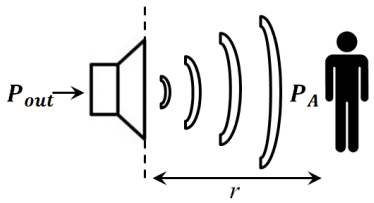

Fig. 5: Sound system with listener at a distance of r away from transducer.

desired maximum continuous sound pressure level (SPL) at the listener's position is 93 dB, which is a rather loud sound pressure level, we can calculate the maximum continuous electrical output power using:

$$P_{RMS} = 10^{\frac{SPL}{10}} P_o A \eta_0^{-1} \tag{8}$$

Where $P_o = 10^{-12}$ W/m^2 is the reference acoustic sound power, $A = 2\pi r^2$ is the area of the sound surface at a given distance from the driver and η_0 is the efficiency of the driver. With the listener placed 1 meter from the transducer, which is a standard loudspeaker driver with an efficiency of 0.61%, corresponding to a loudspeaker sensitivity of 90 dB (1W@1m), we get:

$$\begin{aligned} P_{RMS} &= 10^{\left(\frac{93dB}{10}\right)} 10^{-12} 2\pi 1^2 0.0061^{-1} \\ &= 2 \text{ W} \end{aligned} \tag{9}$$

This is the maximum RMS output power which this system should provide in order to generate the de-

sired sound pressure level. The peak power requirement is 126 W based on equation (4) and a crest factor of 18 dB. This power requirement is most likely overestimated, due to the fact that normal listening conditions are not in perfectly half sphere environment, but in a room. However we can use eq. 7 and the crest factor span from table 1, to obtain an estimate of the requirements to the voltage rail as a function of the DC resistance as seen in fig. 6. This graph simplify the selection of the voice coil DC resistance as a function of a given battery supply.

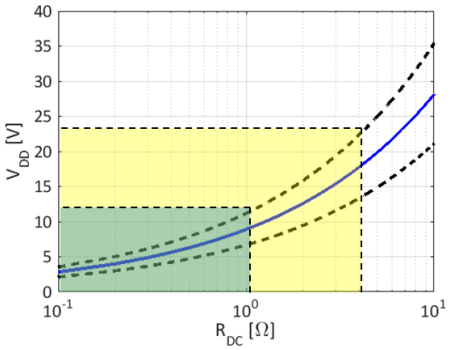

Fig. 6: V_{DD} vs. R_{DC} for an output power of $P_{RMS} = 2$ W including crest factor span of the unfiltered audio tracks. The solid line is for $CF = 16$ dB. For low load resistances, up to 1 Ω, the desired output power can be obtained directly from a 12 V battery supply (the green box). For a typical 4 Ω load a voltage rail of 24 V is required (the yellow box).

5. EXPERIMENTAL RESULTS

Figure 7 shows the hardware used during the experimental work (left: power supply, right: amplifier). The power supply is a 150 W boost converter (based on UC3843 from Texas Instruments) that can handle 10 - 32 V_{DC} on the input and 12 - 35 V_{DC} on the output. The dimensions are 6.5 cm x 4.8 cm x 2.5 cm. The amplifier is a 2 x 50 W class-D amplifier (based on the TPA3116D2 from Texas Instruments) with a working rail voltage of 6.5 V_{DC} to 26 V_{DC}. The dimensions are 8 cm x 7 cm x 2.5 cm.

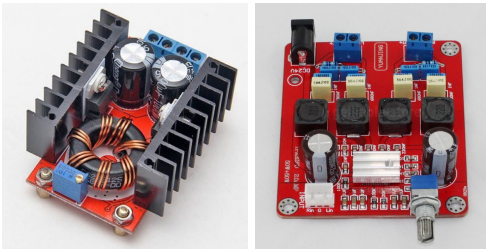

Fig. 7: Power supply (left) and amplifier (right)

5.1. Amplifier Efficiency

To study the consequences of driving a low impedance load with a commercial available class-D amplifier the amplifier efficiency was measured driving a standard 4 Ω load resistance with a rail voltage of 24 V and a 1 Ω load resistance with a rail voltage of 12 V - see figure 8. It is observed that the amplifier efficiency driving a 1 Ω resistive load is greatly improved below 2 W, which was the previously estimated maximum continuous power level. This is due to lower switching losses, [10]. In addition to this the continuous output power level will be below 2 W when the user listens to background music. It is expected that the efficiency of a low voltage and high current amplifier can be further improved since the amplifier under test was not optimized for driving a low impedance. This issue will be addressed in a later discussion.

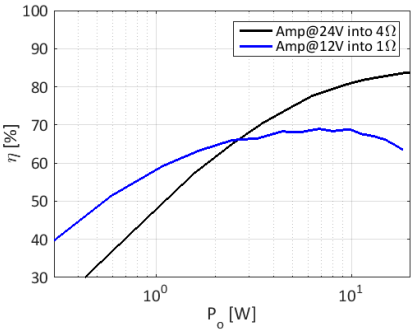

Fig. 8: Efficiency measurements

5.2. Battery Powered Audio Systems

As mentioned before one of the major advantages of a low impedance loudspeaker would be the ability to drive the amplifier and the loudspeaker directly from a low voltage source without the need for an additional power conversion unit such as a switch mode power supply. Figure 9 illustrate the test setup of a conventional battery powered sound system consisting of a battery, a power supply, an amplifier and a 4 Ohm load and the proposed direct drive sound system with a low impedance load simplified by a 1 Ω resistance. The measured efficiency of the two systems are shown in figure 10. Even though the power supply is fairly efficient (see figure 11) the efficiency of the direct drive and low impedance sound system obtain a significant higher efficiency, especially for light loads. As the power increases conduction losses begins to dominate and we see a decrement of the efficiency of the direct drive setup. This is expected due to the fact that the amplifier used is not optimized for high currents. It could be argued that a higher efficiency of the conventional system could be achieved by intelligent on/off control of the power supply as a function of the signal amplitude. But besides an increased control complexity this would still demand a power supply in the system which leads to increased cost, size and weight.

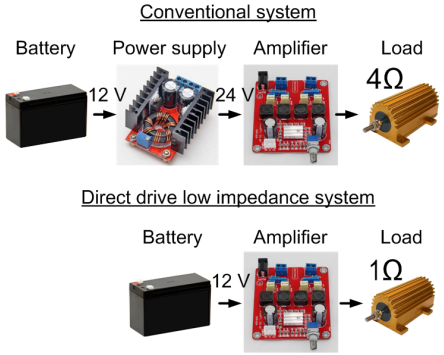

Fig. 9: Measurement setup

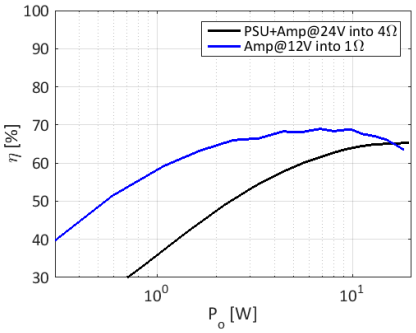

Fig. 10: Efficiency measurements of conventional vs. direct drive sound system

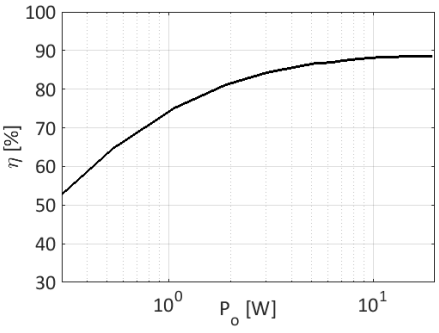

Fig. 11: Efficiency measurements of the power supply

6. DISCUSSION AND FUTURE WORK

The experimental result clearly show an advantage in terms of system efficiency for battery powered low impedance transducers. A further efficiency increase can be obtained by improving the amplifier design. The low voltage rail requirement open up the possibility of using switching devices with a low voltage rating. Table 2 show a small selection of MOSFET's with extreme characteristics chosen for either low drain-source resistance or low gate charge and input capacitance. It is noted that a low drain-source voltage MOSFET offer a lower R_{DS}, Q_G and $Ciss$. Despite the voltage rating, the right balance between these parameters is important to optimize the amplifier efficiency. Amplifiers for driving low impedance transducers where the output current is high would benefit from a low drain source resistance

Part number	Package	V_{DSS}	R_{DS}	Q_G	Ciss
IPT004N03LATMA1	8-PowerSFN	30 V	0.4 mΩ	163 nC	24 nF
PMZ350XN,315	SOT-883	30 V	420 mΩ	0.65 nC	37 pF
IPT015N10N5ATMA1	8-PowerSFN	100 V	1.5 mΩ	211 nC	16 nF
FDMA86108LZ	6-WDFN	100 V	243 mΩ	3 nC	163 pF

Table 2: MOSFET's with extreme characteristics

R_{DS} due to decreased conduction loss. The switching loss which are related to Q_G and $Ciss$ would decrease due to the low voltage rail requirement as investigated in [10]. This effect is also apparent in figure 8 when looking at the low impedance drive situation of 1 Ω. Here the efficiency at lower power levels increase due to decreased switching losses and decrease at higher power levels due to increased conduction losses compared to the 4 Ω drive situation. With an optimized amplifier the efficiency could be improved by the use of different switching devices. Future work should focus on the efficiency optimization of low voltage and high current amplifiers for driving low impedance loudspeakers.

7. CONCLUSION

This work investigate the efficiency of class-D amplifiers driving a low impedance transducer. The motivation is to drive the amplifier and a low impedance transducer directly from a low voltage source such as a battery to obtain a improvement of size, weight, cost and efficiency. An analysis of the peak to RMS voltage of music signals compared to sine wave signals is performed. In combination with a worst case estimation of the power requirement, the DC resistance of the voice coil can be designed given a certain battery voltage. Experimental results on commercial available power supplies and amplifiers demonstrate the advantage of a low impedance transducer in terms of efficiency for battery operated sound systems. Future work will focus on optimization of the amplifier for driving low impedance transducers.

8. REFERENCES

[1] Erickson and Maksimovic, "Fundamentals of Power Electronics", Second Edition, Kluwer Academic Publishers.

[2] K. Nielsen, "Audio Power Amplifier Techniques With Energy Efficient Power Conversion", Ph.D. thesis, Volume 1, Technical University of Denmark 1998.

[3] A. Yamauchi, A. Knott, I. H. H. Jørgensen and M. A. E. Andersen , "Frequency dependent loss analysis and minimization of system losses in switch-mode audio power amplifiers", in AES Convention 137th, Los Angeles October 9-12, 2014.

[4] S. Poulsen, M.A. Andersen, "Simple PWM modulator topology with excellent dynamic behavior", Applied Power Electronics Conference and Exposition, 2004.

[5] R. H. Small, "Closed-box loudspeaker systems", J. Audio Eng. Soc., vol 20 pp. 383-395 (June 1972).

[6] A. N. Thiele, "Loudspeakers in vented boxes, Parts I and II", J. Audio Eng. Soc., vol. 19 pp. 382-392 (May 1971); pp. 471-483 (June 1971).

[7] W. Marshall Leach, Jr. "Introduction to Electroacoustics and Audio Amplifier Design", Kendall/Hunt Publishing Company, 2003.

[8] H. F. Olson, "Acoustical Engineering", Proffesional Audio Journals, Inc.

[9] N. E. Iversen and A. Knott, "Small Signal Loudspeaker Impedance Emulator", JAES Volume 62 Issue 10 pp. 676-682, October 2014.

[10] A. Yamauchi, H. Schneider, A. Knott, I. H. H. Jørgensen and M. A. E. Andersen , "Investigation of Energy Consumption and Sound Quality for Class-D Audio Amplifiers using Tracking Power Supplies", in AES Convention 138th, Warsaw, Poland, May 7-10, 2015.

[11] S. Poulsen and M. A. E. Andersen , "Practical considerations for integrating switch mode

audio amplifiers and loudspeakers for a higher power efficiency", in AES Convention 116th, Berlin May 8-11, 2004.

[12] N. E. Iversen and A. Knott, "Low Impedance Voice Coils for Improved Loudspeaker Efficiency", to be presented at the 139th AES convention in New York, USA, 2015.

[13] H. Schneider, L. C. Jensen, L. P. Petersen, A. Knott and M. A. E. Andersen , "Requirements Specification for Amplifiers and Power Supplies in Active Loudspeakers", in AES Convention 137th, Los Angeles, USA, October 9-12, 2014.

[14] M. Miji, D. Maovi, M. Petrovi and D. umarac-Pavlovi , "Statistical Properties of Music Signals", in AES Convention 126th, Munich, Germany, May 7-10, 2009.

[15] E. Wickers, "The Loudness War: Background, Speculation and Recommendations", in AES 129th Convention, San Francisco, USA, November 4-7, 2010.

Comparison of simple self-oscillating PWM modulators

In 140th Audio Engineering Soceity convention, Paris, June 4-7, 2016.

Audio Engineering Society

Convention Paper 9562

Presented at the 140th Convention
2016 June 4–7, Paris, France

Comparison of Simple Self-Oscillating PWM Modulators

Nicolai J. Dahl, Niels E. Iversen, Arnold Knott, and Michael A.E. Andersen

Technical University of Denmark

Correspondence should be addressed to Niels Iversen (neiv@elektro.dtu.dk)

ABSTRACT

Switch-mode power amplifiers has become the conventional choice for audio applications due to their superior efficiency and excellent audio performance. These amplifiers rely on high frequency modulation of the audio input. Conventional modulators use a fixed high frequency for modulation. Self-oscillating modulators do not have a fixed modulation frequency and can provide good audio performance with very simple circuitry. This paper proposes a new type of self-oscillating modulator. The proposed modulator is compared to an already existing modulator of similar type and their performances are compared both theoretically and experimentally. The result show that the proposed modulator provides a higher degree of linearity resulting in around 2 % lower Total Harmonic Distortion (THD).

1 Introduction

Switch-mode power amplifiers have become the conventional choice for audio applications during the last decade. This is due to the superior efficiency these amplifiers offer, compared with traditional linear amplifiers. For audio applications efficiencies in the vicinity of 90% have been achieved as shown in [1] and [2]. Also in terms of linearity switch-mode power amplifiers have shown great performance with Total Harmonic Distortion as low as 0.001%, [3] and [4]. The switch-mode power amplifier works by modulating the input audio into a high frequency pulse train which drives a power stage, typically equipped with MOSFETs. The linearity of the modulation is important for the overall distortion of the amplifier. Conventionally the modulator modulates the audio input at a fixed high frequency. However this can introduce Electro Magnetic Interference (EMI) issues. Self-oscillating oscillators does not have a fixed modulation frequency and therefore this type of modulator is preferable for EMI reasons [5]. Moreover the circuit complexity is reduced when using this type of modulators.

This paper will describe the fundamental principles of Pulse Width Modulation (PWM) and examine how this can be generated in self-oscillating modulators. A new type of self-oscillating modulator will be presented and compared to an already existing self-oscillating modulator topology. A thorough analysis of both modulators will be presented in order to evaluate their linearity. Finally measured results obtained from implemented test boards will be presented to support the theoretical analysis.

2 Modulator

2.1 Principles

The function of a modulator in a switch mode audio amplifier is to convert a continuous audio signal to a pulse coded signal. Among the different types of

pulse coding the Pulse Width Modulation is the most commonly used for switch mode audio amplifiers [6]. PWM works by changing the percentage of time the output is high compared to the time the output is low. Depending on the current value of the audio signal, the aforementioned percentage will change. This property is called the duty cycle and with PWM it is possible to obtain a unique duty cycle for each unique value of the audio signal. The duty cycles spectrum can further be described with the modulation index which is a value that tells how much of the spectrum the modulation should span over.

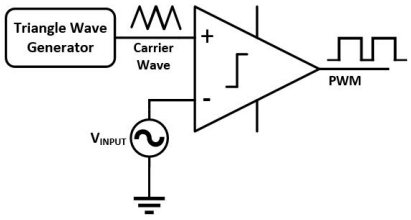

Fig. 1: Concept of a modulator

Figure 1 shows a simple hardware realization. By comparing the audio signal with a triangle signal, also called the carrier waveform, it is possible to create a PWM signal. However, to get a good representation of the audio signal the carrier waveform needs to run at a frequency that is much higher than the highest audible frequency. This is necessary to get a high resolution of the audio signal. The PWM signal is fed to the power stage of the amplifier which amplifies the signal. Finally a lowpass filter removes the high switching frequency thus restoring the original audio signal. The reason a triangle waveform is used as the carrier waveform is that the triangle provides a constant relationship between the audio signal and the corresponding duty cycle. In practice this means that the modulator will not induce any harmonic distortion to the audio signal as long as the amplitude of the audio signal does not exceed the amplitude of the carrier waveform. If the audio signals amplitude exceeds the amplitude of the carrier waveform clipping would happen.

While this method is able to create a great transparent modulation it has some drawbacks. The carrier waveform is run at a fixed frequency which will result in a build-up of spectral energy at the carrier frequency and its harmonics [5]. This can introduce unwanted EMI. Moreover the size of the circuitry is also large compared to other implementations of PWM modulators due to the need of an external triangle generator [12]. One way to address these problems is by using the self-oscillating modulator topology.

2.2 Self-Oscillating Modulators

Self-oscillating modulator are a branch of modulators where the carrier waveform generator circuitry has been merged with the comparator circuitry thus making it possible to reduce the amount of components needed, [7], [8], [9] and [10]. The carrier waveform generation is achieved by feeding back the output of the modulator, through some circuitry, back into the comparator making the modulator oscillate. This also makes the switch frequency dependant of the input signal, ultimately reducing EMI [5]. To ensure that the modulator has a controlled oscillation a 180^{o} phase lag is introduced. This is typically done either by a hysteresis window or a phase shift [11].

2.2.1 Astable Integrating Modulator

One of the simplest self-oscillating modulators is the Astable Integrating Modulator (AIM) as presented in [12] shown in fig. 2.

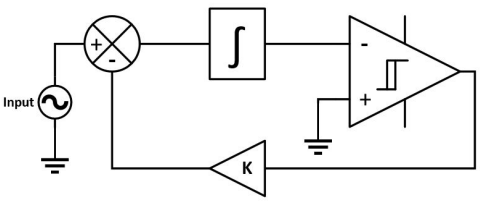

Fig. 2: Concept of the AIM

The AIM works by using its output with the audio input to calculate an error signal. The error signal is integrated to generate a triangle carrier waveform which is sent to a comparator with a hysteresis window. The hysteresis window is used to control the amplitude of the carrier waveform and by doing so it also controls the maximum carrier frequency also called the idle switch frequency. The idle frequency is controlled by

the gain factor K as well which controls the size of the error and therefore the slope of the integration. Figure 3 shows a possible way of implementing the AIM in hardware.

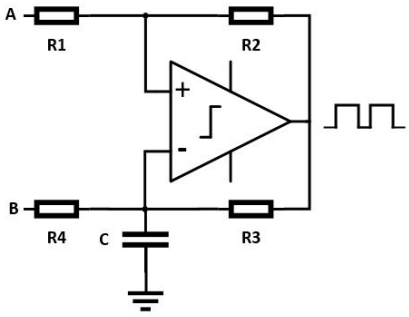

Fig. 3: Implementation of AIM and HOM

In fig. 3 the terminal A is connected to a reference voltage and terminal B is connected to the audio input. The reference voltage is used as the bias voltage for the entire modulator as well as the audio input. The hysteresis window is implemented using the resistors R_1 and R_2 while the error signal integration is realized using R_3, R_4 and C. The integration is implemented as a RC network which operation deviates from an ideal integration. While an ideal integrator generates a slope that is proportional to the error signal, the RC network generates an exponential response. This results in harmonic distortiondue to the fact that the RC network is not able to produce ideal triangles. Figure 4 shows this phenomenon.

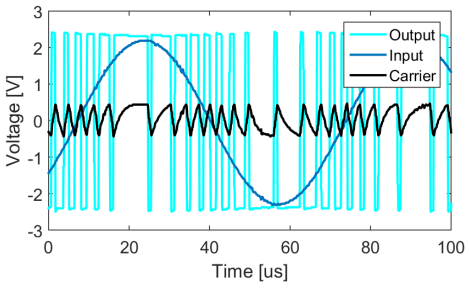

Fig. 4: Input, output and carrier for an AIM

The harmonic distortion can to a certain degree be reduced by reducing the size of the hysteresis window or reducing the modulation index. However, a reduction in the hysteresis window will result in smaller internal signals in the modulator thus making the modulator more sensitive to noise since the signal levels come closer to the noise floor. A reduction in the modulation index will result in a lower efficiency of the amplifier. This renders both solutions undesirable.

2.2.2 Hysteresis Offset Modulator

To address this problem of the AIM this paper proposes an alternative self-oscillating modulator consisting of the same circuitry as the AIM in fig 3. The main difference, between the AIM and the proposed modulator, is that the voltage reference and the audio input is swapped so that the audio signal is connected to terminal A and the voltage reference to terminal B. This makes the input signal offset the hysteresis window and hence it is named 'Hysteresis Offsetting Modulator' shorted HOM. This simple change completely changes the behaviour of the system which can be seen on fig. 5.

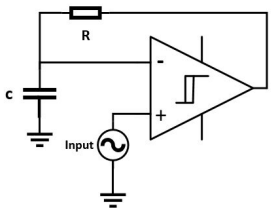

Fig. 5: Concept of the HOM

Unlike the AIM, where the RC network is a drawback for the performance due to the harmonic distortion the HOM actively exploits the properties of the RC network to make the modulation. By using the audio input to change the reference voltage of the comparator, the hysteresis window is constantly being offset. This results in the RC network constantly operating in different zones thus changing the slope more or less as seen on fig. 6.

3 Deriving of Models

To determine which of these two modulators introduces most harmonic distortion, mathematical models need to

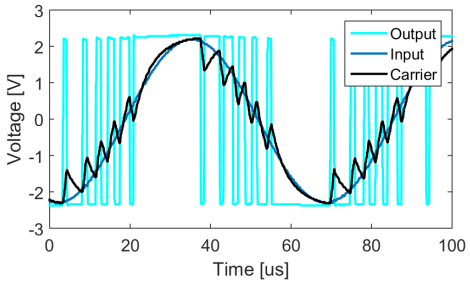

Fig. 6: Input, output and carrier of the HOM

be constructed. A similar approach has been presented in previous work for the AIM modulator [13]. The models will be constructed such that the performance of the modulator can be described by:

- The size of the hysteresis window
- The peak-peak voltage of the audio input
- The reference voltage
- The supply voltage

Since the two modulators share the same circuitry, many parts of the model will be identical. Both modulators generate a PWM output and therefore need an equation for describing the time the output is high as well as an equation to describe the time the output is low. The two states of the output are defined as:

$$v_{out}(t) = \begin{cases} v_H & \forall v_C(t) < v_{hys}(t) \\ v_L & \forall v_C(t) > v_{hys}(t) \end{cases} \quad (1)$$

Where v_H and v_L is the high and low voltage given on the output of the modulator. v_C and v_{hys} is the voltage of the carrier waveform and hysteresis window respectively for any given time.

The hysteresis window works identically for the two modulators. It consists of two resistors R_1 and R_2 which form a voltage divider. The hysteresis window is connected through the resistor R_2 to the output v_{out} and therefore changes instantaneous with the output. The window is centred around the voltage on terminal A which is where R_1 is connected to. From this information the following can be found:

$$v_{hys}(t) = \begin{cases} v_{thh} & \forall v_{out}(t) = v_H \\ v_{thl} & \forall v_{out}(t) = v_L \end{cases} \quad (2)$$

$$v_{thh} = k_1 \cdot (v_H - A) + A \quad (3)$$

$$v_{thl} = k_1 \cdot (v_L - A) + A \quad (4)$$

v_{thh} and v_{thl} is the upper and lower threshold voltage for the hysteresis window and k_1 is the scaling factor given by the resistor network R_1 and R_2 from fig. 3. From v_{thh} and v_{thl} it is possible to calculate the size of the hysteresis window:

$$v_{hw} = v_{thh} - v_{thl} = k_1 \cdot (v_H - v_L) \quad (5)$$

By isolating k_1 in eq. 5 and inserting it in eq. 3 and 4 the threshold voltages can be rewritten to:

$$v_{thh} = v_{hw} \frac{v_H - A}{v_H - v_L} + A \quad (6)$$

$$v_{thl} = v_{hw} \frac{v_L - A}{v_H - v_L} + A \quad (7)$$

These expressions are independable of the component values which is highly desired since it makes it easier to achieve desired design values.

When finding the expression for the carrier waveform v_C, the same method, as for the hysteresis window can largely be used. For the modulators to function properly the carrier voltage must be able to charge and discharge to the value of the hysteresis window as long as the audio input signal stays within the desired voltage span. To ensure that, the lowest voltage, the carrier voltage can have when the output is high, and the highest voltage, it can have when the output is low, is found. These limits are controlled by v_{out} and the signal on port B. The limits can be described as:

$$v_{Ch}(t) = k_2 \cdot (v_H - B) + B \quad (8)$$

$$v_{Cl}(t) = k_2 \cdot (v_L - B) + B \quad (9)$$

Where k_2 is the voltage divider consisting of the resistor network R_3 and R_4 from fig. 3 and v_{Ch} and v_{Cl} is the upper and lower limit the RC network is able to charge and discharge to. From this, the size of the window can be found:

$$v_{Cwin} = v_{Ch} - v_{Cl} = k_2 \cdot (v_H - v_L) \tag{10}$$

To find the limits for a specific input signal size, the following two equations are used to describe the limits of the input signal. Here it is assumed that the input signal is offset by the reference voltage, v_{ref}.

$$v_{inh} = v_{ref} + \frac{v_{span}}{2} \tag{11}$$

$$v_{inl} = v_{ref} - \frac{v_{span}}{2} \tag{12}$$

Where v_{inh} and v_{inl} is the highest and lowest expected input voltage. v_{ref} is the reference voltage which is applied on terminal A for the AIM and on terminal B for the HOM. v_{span} is the expected span of the input signal, i.e. the voltage difference between v_{inh} and v_{inl}. To simplify further calculations, the following is assumed:

$$v_{ref} = \text{mean}(v_H, v_L) \tag{13}$$

For the AIM, the audio input signal is send into terminal B. This means that it is possible to rewrite eq. 8 and 9 by substituting B with eq. 11 for eq. 9 and with eq. 12 for eq. 8. By isolating these for k_2 and inserting the expression for k_2 in eq. 8 and 9 again, an expression for the upper and lower limit of the carrier waveform is found. These equations have the input signal on terminal B as a variable.

$$v_{Ch_{AIM}}(t) = B + \frac{v_{span}(v_H - B) + v_{hw}(v_H - B)}{v_H - v_L + v_{span}} \tag{14}$$

$$v_{Cl_{AIM}}(t) = B + \frac{v_{span}(v_L - B) + v_{hw}(v_L - B)}{v_H - v_L + v_{span}} \tag{15}$$

For the HOM, the audio input signal is send into terminal A. This means that the size of the hysteresis window when it is offset must not exceed v_{Cwin} since it will result in clipping at smaller input signals than intended. To prevent this, the following is stated:

$$v_{Cwin} = v_{hw} \tag{16}$$

Since the audio input is on terminal A, A is substituted with eq. 11 and 12 in eq. 6 and 7 respectively. From this eq. 5, 10 and 16 is used to get:

$$v_{thh} - v_{thl} = k_2 \cdot (v_H - v_L) \tag{17}$$

By isolating k_2 and inserting it in eq. 8 and 9 the following expressions are found:

$$v_{Ch_{HOM}} = \frac{v_H + v_L + v_{hw} + v_{span}}{2} - \frac{v_{hw} v_{span}}{2(v_H - v_L)} \tag{18}$$

$$v_{Cl_{HOM}} = \frac{v_H + v_L - v_{hw} - v_{span}}{2} + \frac{v_{hw} v_{span}}{2(v_H - v_L)} \tag{19}$$

Now all the necessary equations to find the duty cycle for any given input signal both for the HOM and AIM modulator have been derived.

Since both modulators are first order modulators, they can be described using the equation for a RC network. By isolating the time in the equation for a first order RC network, the timings can be found to be:

$$t_{high} = \tau \cdot ln\left(\frac{v_{Ch} - v_{thl}}{v_{Ch} - v_{thh}}\right) \tag{20}$$

$$t_{low} = -\tau \cdot ln\left(\frac{v_{Cl} - v_{thl}}{v_{Cl} - v_{thh}}\right) \tag{21}$$

These timing equations hold true for both modulators. From the equations, it is now possible to calculate the frequency and duty cycle of each modulator's output.

$$f = \frac{1}{t_{high} + t_{low}} \tag{22}$$

$$D = \frac{t_{high}}{t_{high} + t_{low}} \tag{23}$$

4 Theoretical Results

The total harmonic distortion is strongly connected with how linear the relationship, between the input voltage and the duty cycle is. The relationship between the input voltage and the duty cycle can be found by sending a DC voltage into the modulator where after the duty cycle on the output is read. It is possible to do this because the switch frequency is significantly higher than the highest frequency of the audio signal. Therefore, the audio signal can be considered a DC signal when used by the modulator. For the following theoretical results, the values in table 1 have been used:

Table 1: Specifications

v_H	v_L	v_{hw}	v_{span}
1 V	0 V	0.5 V	1 V

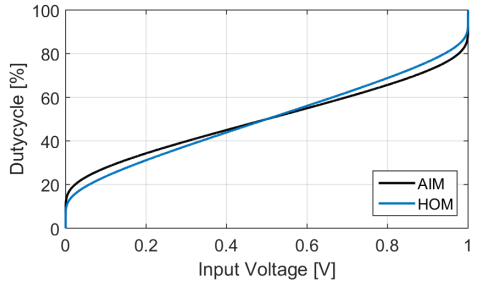

Fig. 7: Theoretical relation between the input voltage and the duty cycle of the output for the AIM and HOM

Figure 7 shows the DC transfer function of both modulators. It seems that the HOM assembles a straight line more and for a longer duration than the AIM. This would mean that the HOM in general is more transparent in the modulation than the AIM and would, due to that, have a lower total harmonic distortion (THD) than the AIM. To get a more precise view, a linear regression is found for the transfer function of each modulator and the correlation coefficient is calculated from that.

$$r^2_{AIM} = 0.9912 \tag{24}$$

$$r^2_{HOM} = 0.9954 \tag{25}$$

This is a clear indication that the transfer function of the HOM assembles a straight line more than the AIM.To further verify these results, a calculation of the theoretical THD of both modulators is performed. Figure 8 shows the theoretical THD found by using a sinusoid at 6.66 kHz with increasing amplitude as input.

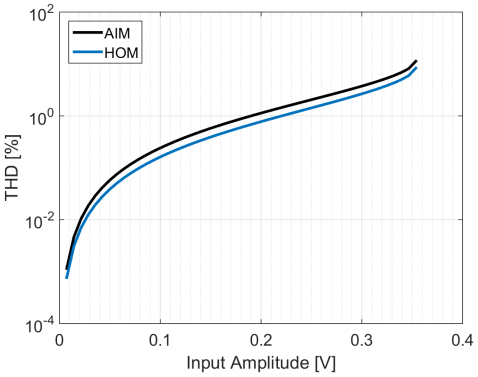

Fig. 8: Theoretical THD of both modulators

The THD calculations support the theory further as it clearly shows that a reduction in THD for the HOM, compared to the AIM, is to be expected.

The switch frequency of the output will change with the input voltage.

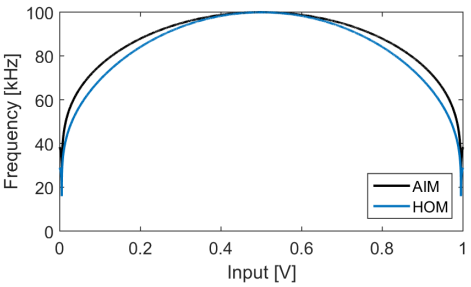

Fig. 9: Theoretical switch frequency of the output of each modulator

Figure 9 shows that the HOM tends to fall in switch frequency a bit faster than the AIM which is an unwanted behaviour. This is due to the fact that the modulator potentially will reach a switch frequency which is too low, for the modulator to operate properly, faster.

5 Measurements

5.1 Measurement Setup

To test the theory in practice, six test boards were made. This was done to ensure a consistency in the theory over multiple configurations. The boards were made in pairs such that one AIM board and one HOM board had the same specifications. All the boards were supplied with 5 V and had a reference voltage of 2.5 V. The comparator on the boards were able to deliver an output voltage from about 0.1 V to 4.85 V. The board specific specifications were the following:

Table 2: Board Specifications

Boards	1 and 2	3 and 4	5 and 6
f_{sw}	300 kHz	600 kHz	500 kHz
v_{hw}	1 V	1.6 V	0.6 V
v_{span}	4.95 V	2.1 V	1.2 V

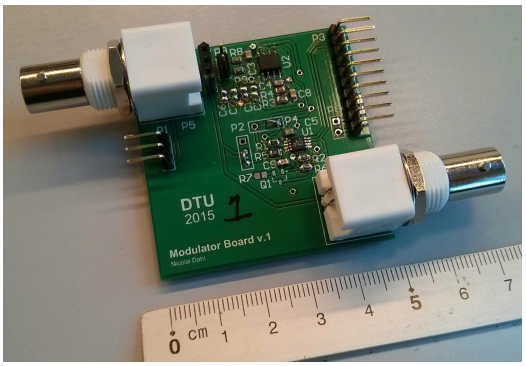

Fig. 10: Picture of test board 1. All the other boards looks similar.

5.2 Measurement results

For each board, three measurements were made; a measurement of the DC transfer function, a measurement of the switching frequency and a measurement of the THD. The measurement of the DC transfer function and the switching frequency was made by reading the duty cycle and frequency of the output when different input voltages were applied. The results of the DC transfer function can be seen on fig. 11a and the results of the switch frequency on fig. 11b. Both results are being compared with what was expected by the theory.

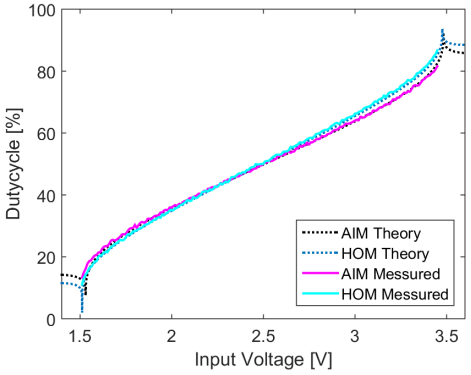

(a) DC transfer function

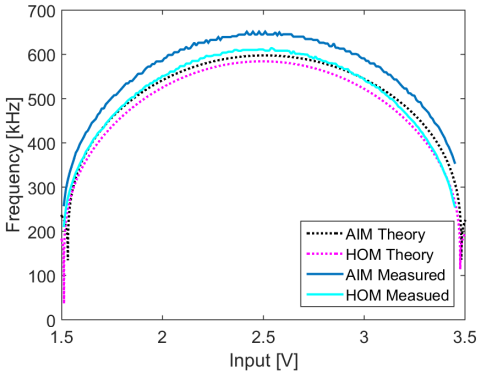

(b) Switch frequency

Fig. 11: Output of board 3 and 4 compared to the expected results

Figure 11a shows the DC transfer function for board 3 and 4 compared to the expected results. It is seen that the measured results and the theoretical results are close to identical. Similar results was obtained with the other boards. This supports the theory and indicates that the measurements of the THD should be close to the theory as well. Regarding the response of the switch frequency on fig. 11b it is possible to see that the measured switch frequency follows the same curve as the theory, however, the measured results are at a higher frequency than expected. This is due to stray capacitance and component tolerances since a small

adjustment in the capacitance in the theory results in a very accurate fit (fig. 12).

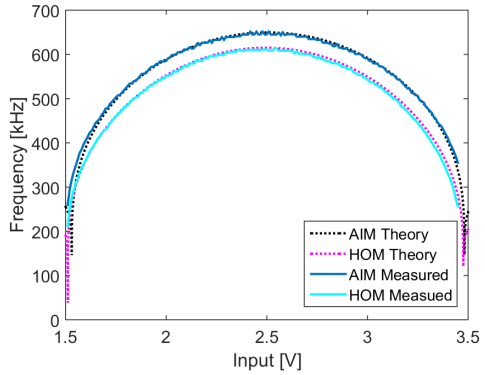

Fig. 12: Switch frequency with adjusted capacitance

The THD measurements were made with an active 2. order lowpass filter on the output of the modulator. The filter had a THD of around 0.5 % across the entire amplitude range which was used for testing.

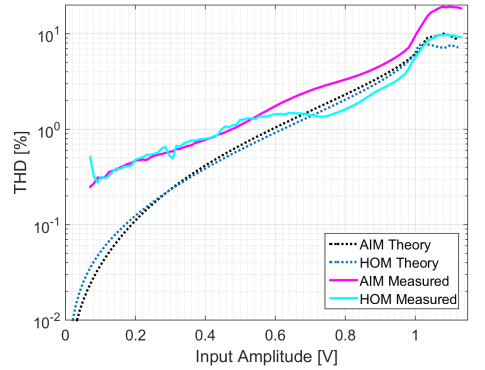

Fig. 13: Measured THD compared to the expected results

Figure 13 shows the measured THD compared to what was expected from the theory. It is seen that the measured results generally have a higher THD than expected yet still clearly follow the trends of the theory as the HOM has a lower THD than the AIM. The higher THD is partially due to the active filter but also due to noise in the circuitry. Especially at lower amplitudes it is possible to see the noise from the modulators from the jitter in the readings. Here it is seen that the HOM modulator seems to have noise problems up to a higher amplitude than the AIM, but this is for further studies. At the amplitude 0.7 V the measured THD of the HOM begins to move below the theoretical possible THD. This is probably due to tolerances in the resistors making the circuit behave a little different from the desired specifications.

6 Conclusion

This paper has presented the fundamental principles of PWM modulation. A thorough analysis of two simple self-oscillating modulators has been presented. That is the AIM modulator and the proposed HOM modulator. The analysis showed that the proposed HOM modulator can provide a more linear modulation than the AIM. This was evident from the modelling of the DC-DC transfer functions and the evaluated THD. Finally experimental results showed very good correlation with the presented theory and it was found that the proposed HOM modulator performs a 5th of a decade better in terms of THD. However the HOM modulator seems to be more susceptible to noise than the AIM. Future work will have to investigate this further.

References

[1] K. Nielsen, "Audio Power Amplifier Techniques With Energy Efficient Power Conversion", Ph.D. thesis, Volume 1, Technical University of Denmark, 1998.

[2] M. Duraj, N. E. Iversen, L. P. Petersen and P. Boström, "Self-oscillating 150 W switch-mode amplifier equipped with eGaN-FETs", in AES Convention 139th, New York, October 29-November 1, 2015.

[3] B. Putzeys, "Simple Self-Oscillating Class D Amplifier with Full Output Filter Control", in AES Convention 118th, Barcelona, May 28-31, 2005.

[4] S. Poulsen and M. A. E. Andersen , "Simple PWM modulator topology with excellent dynamic behaviour", in Applied Power Electronics Conference and Exposition, 2004.

[5] D. Nielsen, A. Knott, G. Pfaffinger and M. A.E. Andersen, "Investigation of switching frequency variations and EMI properties in self-oscillating class D amplifiers", in AES Convention 127th, New York, October 2009

[6] E. Gaalaas, "Class D Audio Amplifiers: What, Why, and How", Analog Devices, June 2006

[7] S. Poulsen, "Global Loop Integrating Modulator", World Intellectual Property Organization, November 2004.

[8] B. Putzeys ,"Power Amplifier", U.S. Patent No.: US 7,113,038 B2, September 2006.

[9] L. Risbo, M. C. W. Hœyerby and M. A. E. Andersen , "A Versatile Discrete-Time Approach for Modeling Switch-Mode Controllers", IEEE PESC, 2008.

[10] M. C. W. Hœyerby, "High-Performance Control in Radio Frequency Power Amplification Systems", Ph.D. Thesis, Technical University of Denmark, 2008.

[11] S. Poulsen and M. A.E. Andersen, "Self-Oscillating PWM Modulators, A Topological Comparison", in IPMHVC 26th, 2004

[12] S. Poulsen, "Towards Active Transducers", Ph.D. thesis, Technical University of Denmark, 2004

[13] A. Knott, G. Pfaffinger and M. A. E. Andersen , "A Self-Oscillating Control Scheme for a Boost Converter Providing a Controlled Output Current", IEEE transactions on Power Electronics, January 2009.

J

Optimal modulator with loudspeaker parameter inclusion

In 143rd Audio Engineering Soceity convention, New York, October 18-21, 2017.

Audio Engineering Society

Convention Paper 9824

Presented at the 143rd Convention
2017 October 18–21, New York, NY, USA

Optimal Modulator with Loudspeaker Parameter Inclusion

Nicolai J. Dahl[1], Niels E. Iversen[1], and Arnold Knott[1]

[1] *Technical University of Denmark*

Correspondence should be addressed to Nicolai Dahl (nicolai@jerram.dk)

ABSTRACT

Today, most class-D amplifier designs are able to deliver high efficiency and low distortion. However, the effect of parasitic components and speaker dynamics are not taken into account, resulting in a degradation of the performance. This paper proposes a new PWM modulator which is able to capture an arbitrary amount of dynamics through optimization based design methods. This makes it possible to include the parasitic components in the amplifier and the loudspeaker parameters in the design, thus creating a more linear response.

1 Introduction

Today class-D amplifiers are a common pick of choice when high efficiency and power are needed in an application. The high efficiency is achieved by using a switching power stage meaning the output is either fully on or fully off [1, 2]. This results in a reduction of the losses in the amplifier thus minimizing the power dissipation. The switching signal in the class-D amplifier is generated by the modulator. The audio signal enters the modulator which generates a pulse coded signal, which usually is Pulse Width Modulated (PWM). The modulated output is amplified and then sent through a 2nd order low-pass filter before leaving the amplifier. The low-pass filter ensures that the switching transients are attenuated leaving only the amplified audio signal.

Today, multiple modulator topologies exist which can be used with just as many different control strategies. Among the different topologies for modulators, and the control hereof, it seems to be the ones that incorporate the power stage, and sometimes also the output filter, that perform the best [3, 4, 5]. Class-D amplifiers with Total Harmonic Distortion (THD) as low as 0.0012% have been achieved proving that both low distortion and high efficiency can be obtained [4, 6].

A common limitation for today's class-D amplifiers is that the designs are based around obtaining a low THD on the output voltage of the amplifier. This results in the dynamics of the loudspeaker often being neglected in the design process and thus replaced by a purely ohmic resistance. This approach is not optimal since the loudspeaker introduces uncontrolled non-linear dynamics, thus increasing the THD with sereval orders of magnitude before the sound reaches the ears of the listener. [7, 8]. The design methods also tend to assume that the output filter is ideal, resulting in the effect of the parasitic components being neglected thus increasing the uncertainty of the design.

In this paper, a self-oscillating modulator topology for class-D amplifiers is proposed. This modulator is designed from an arbitrary sized state space model, enabling the inclusion of parasitic components as well as loudspeaker parameters directly in the design. This is achieved by generalizing the design problem by

applying optimization procedures to find satisfactory solutions. The result of this is the possibility to include feedback signals from the speaker directly back into the modulator which helps flatten the frequency response and reducing the non-linearities of the speaker.

2 State Space Modelling

A class-D amplifier is, like any switch mode power amplifier, a piecewise continuous system which can be modelled as a Linear Time Invariant (LTI) model using the state space average model [9]. This method has been widely used as it provides an internal model of the system, thus making it suitable for describing the small signal transfer properties of the system [9, 10]. In the model, each state of the system is modelled separately for every switching state the system can assume. The models are then averaged with a weight based on the duty cycle of a selected linearization point. The duty cycle is a measure for the percentage of time the switching output is high in a switching period. For a half-bridge class-D amplifier only two switching states on a single signal need to be considered. This makes the modelling of the amplifier so simple that it is often beneficial to model full-bridge class-D amplifiers as half-bridge by applying a filter transformation [11]. Equation 1 shows the two switching states of a half-bridge class-D amplifier.

$$V_{sw} = \begin{cases} V_{cc} & \forall\, dT_{sw} \\ -V_{cc} & \forall\, \bar{d}T_{sw} \end{cases} \tag{1}$$

Since audio is an AC signal, the linearization point will usually be selected to be in the center of the AC signal. For a class-D amplifier, this would result in the linearization point where the duty cycle is $d = 0.5$. This linearization point has the nice property of making the averaged state space model equivalent to the standard state space model. Equation 2 shows the state evolution of the standard state space description for a LTI system and Equation 3 shows the corresponding output.

$$\dot{x}(t) = Ax(t) + Bu(t) \tag{2}$$
$$y(t) = Cx(t) \tag{3}$$

When constructing the state space model, all the dominant internal states must be modelled. This makes the minimum order of the model to be at least equal to the order of the output filter of the amplifier. Naturally, it is desirable to include more dynamics to the model to get a better description of the amplifier. Besides modelling the amplifier, the model can be extended to also include loudspeaker parameters or a crossover network if desired. This will result in the possibility of linearizing the loudspeaker, hence reducing the harmonic distortion introduced by its non-linearities. One should keep in mind that all the states selected for the model must be measurable in some way if only an analog controller is desired. Equation 4 shows the states selected for this paper which are: The capacitor voltage, the speaker current and the inductor current. The capacitor voltage and inductor current are used to model the 2nd order output filter and are the most suitable choice as both states are easily measured. The speaker current is used to model the inductance of the voice coil in the loudspeaker. This limited amount of states are selected to avoid the need for a digital controller. Figure 1 shows a diagram of the modelled circuit.

$$x(t) = \begin{bmatrix} I_{ind} \\ I_{spk} \\ V_c \end{bmatrix} \tag{4}$$

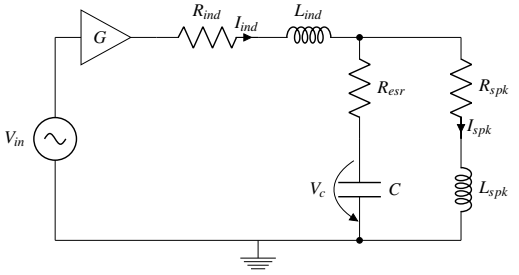

Fig. 1: The circuit modelled in the state space model. Multiple parasitics are considered

Here G is the open-loop gain of the comparator and will usually be in the tens of thousands. The output of G, however, is limited by the supply voltage V_{cc} placing a bound on the signal. Writing up the circuit equations and doing the linearization, the system matrix A and the input matrix B is found (Eq. 5).

$$A = \begin{bmatrix} -\frac{R_{ind}+R_{esr}}{L_{ind}} & \frac{R_{esr}}{L_{ind}} & -\frac{1}{L_{ind}} \\ \frac{1}{L_{spk}} & -\frac{R_{spk}+R_{esr}}{L_{spk}} & \frac{1}{L_{spk}} \\ \frac{1}{C} & -\frac{1}{C} & 0 \end{bmatrix} \quad B = \begin{bmatrix} \frac{G}{L_{ind}} \\ 0 \\ 0 \end{bmatrix} \tag{5}$$

The output matrix C is usually selected to be the last state the signal propagates through. In this case, it is the speaker current I_{spk} which is also evident from Figure 1. Equation 6 shows the output matrix.

$$C = \begin{bmatrix} 0 & 1 & 0 \end{bmatrix} \tag{6}$$

3 System Design

Using the state space description of the class-D amplifier, the feedback for both the modulator and control can be calculated.

3.1 Self-Oscillating Modulator

Self-oscillating modulators are a family of modulators where the generation of the carrier waveform, used for the oscillation, is embedded into the modulator. These modulators have the benefits of lower EMC and increased system bandwidth compared to fixed frequency modulators [12]. The self-oscillation is achieved by feeding back a filtered version of the modulators own output to itself while preventing the modulator from reaching a stable state. The stable state is prevented by either using a hysteresis window [13, 3] or introducing 180° of phase-shift in the feedback signal [6]. The filter can be realized in multiple ways where some common methods are: to use an RC-network directly from the output of the modulator [13] or to use the ripple current I_Δ through the output filter inductor L_{ind} [5]. The last mentioned method will be used here to create a hysteresis based modulator.

When designing a self-oscillating modulator, it is desired to control two key parameters: The idle switching frequency f_{idle} of the modulator and the gain through the modulator. These parameters can be controlled through the feedback gains to the modulator allowing for the two parameters to be designed independently. Figure 2 shows the modulator with the feedback gains k_1 and k_2 coming from the inductor current and capacitor voltage as specified in Figure 1. These two feedback signals form the carrier signal $V_{car}(t)$ which is used for driving the modulator. The size of the hysteresis window V_{hys} is specified by the two resistors R_1 and R_2 by conventional means.

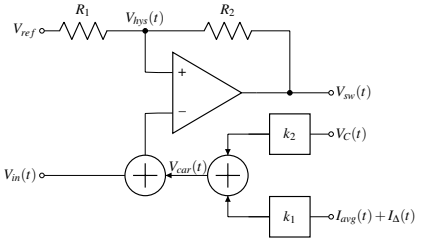

Fig. 2: Modulator with the feedback signals for the carrier waveform generation

The idle switching frequency is the switching frequency when no signal is applied to the amplifier. This simplifies the design as the output voltage will be approximately zero resulting in only the inductor current needing consideration. The current in the inductor is the first state in the state space description, making it easy to isolate. Thus the evolution of the state can be easily determined. Equation 7 shows the system matrix A where the inductor current state has been isolated in the upper left corner (A_{11}).

$$A = \left[\begin{array}{c|cc} -\frac{R_{ind}+R_{esr}}{L_{ind}} & \frac{R_{esr}}{L_{ind}} & -\frac{1}{L_{ind}} \\ \hline \frac{1}{L_{spk}} & -\frac{R_{spk}+R_{esr}}{L_{spk}} & \frac{1}{L_{spk}} \\ \frac{1}{C} & -\frac{1}{C} & 0 \end{array}\right] \tag{7}$$

With the inductor current state isolated, the evolution of the state can easily be found through Equation 8.

$$I_{ind}(t) = \int_0^\infty \mathrm{e}^{A_{11}(t-\tau)} B u(t)\,\mathrm{d}\tau \tag{8}$$

$$= -\frac{V_{cc}\left(\mathrm{e}^{-\frac{R_{ind}+R_{esr}}{L_{ind}}t} - 1\right)}{R_{ind}+R_{esr}} \tag{9}$$

Equation 9 shows the resulting exponential function describing the state evolution of the inductor current. Here the gain, G, from the input matrix B is in its saturated state, hence being the supply voltage V_{cc}. Multiplying with the feedback gain k_1 and isolating the time

t, the idle frequency can be determined as the time it takes to charge from the lower threshold of the hysteresis window to the upper threshold of the hysteresis window. Equation 10 shows the function for the idle switching frequency.

$$f_{idle} = \frac{1}{(t_{high} - t_{low}) \cdot 2} = -\frac{R_{ind} + R_{esr}}{2L_{ind} \ln\left(\frac{4k_1 V_{cc}}{2k_1 V_{cc} + V_{hys}(R_{ind}+R_{esr})} - 1\right)} \tag{10}$$

Since it is the feedback gain k_1 that needs to be determined, k_1 in Equation 10 is isolated. Equation 11 shows the equation to determine k_1 based on a desired switching frequency, hysteresis window size, inductor size and parasitics.

$$k_1 = \frac{V_{hys}(R_{ind} + R_{esr}) \coth\left(\frac{R_{ind}+R_{esr}}{4L_{ind} f_{idle}}\right)}{2V_{cc}} \tag{11}$$

The feedback signal from the inductor through k_1 will provide a voltage measurement of the scaled ripple current which is used as the carrier voltage for the modulator. However, the average current, I_{avg}, due to the audio signal is also contained within the feedback signal. This is undesirable as only the carrier voltage is needed. To avoid the average current, another feedback path from the capacitor voltage is included. The capacitor voltage will at low frequencies be in phase and proportional with the current in the inductor. Thus the carrier voltage can be isolated by subtracting the scaled capacitor voltage from the scaled inductor current. Equation 12 shows how the feedback gain k_2 can be found for the capacitor voltage. Here the proportionality between the current through the amplifier and the voltage across the capacitor when the system is saturated is used.

$$k_2 = -k_1 \frac{I_{sat}}{V_{sat}} \tag{12}$$

The inclusion of an additional feedback path also has the advantage of helping to suppress possible carrier distortion since an offset due to distortion would create a change in the capacitor voltage which would be feedback and thus suppressed. With the two modulator feedback gains designed, a closed-loop description can be obtained for use with the controller design. Equation 13 shows the closed-loop description.

$$A_{mod} = A - BK_{mod} \quad K_{mod} = \begin{bmatrix} k_1 & 0 & k_2 \end{bmatrix} \tag{13}$$

3.2 Linear Quadratic Regulator

The Linear Quadratic Regulator (LQR) is a special type of full state feedback controllers where the control problem is solved as an optimization problem [14]. This allows for an optimal selection of feedback gains and thus an optimal closed-loop response of the system. The LQ-controller is significantly different from the commonly used PID-controller in the fact that it uses feedback from each state in the system. This makes it possible for the controller to act quicker to possible changes, but more importantly, it makes it possible to change the dynamics of the system without increasing the order hereof [15, 14]. This enables the controller to flatten the response in the audio band through the entire system, thus also improving the audio properties of the loudspeaker. It is also common to see a significant reduction of the noise propagating through the system, resulting in an increase in the signal to noise ratio and the power supply rejection ratio [11]. This, however, comes with the drawback that complete state knowledge must be acquired, resulting in the potential need of an observer in cases where the states cannot be measured.

When designing a LQ-controller, a cost function needs to be made. This cost function specifies the control objective which the controller will need to minimize. Equation 14 shows a scalar cost function designed for amplifiers.

$$J(u) = \lim_{t\to\infty} \int_0^t \left(u(t) - \frac{y(t)}{G_{cl}}\right)^2 \mathrm{dt} \tag{14}$$

Inspecting Equation 14 it can be seen that the design goal is to minimize the difference between the control signal $u(t)$ and the output of the system $y(t)$ which is amplified by the closed-loop system gain G_{cl}. This will result in the controller trying to maintain the gain G_{cl} while minimizing any resonances in the system as these will increase the cost. To find the optimal solution to the cost function, the control problem needs

to be reformulated as a Ricatti equation from where an optimal solution K_∞ is obtained [14].

In cases where high order state space models are used to model the loudspeaker, see [16], it will not be possible to measure every single state, thus an observer must be implemented to estimate the remaining states. Observers are usually implemented on microcontrollers for practical reasons meaning that an analog-digital combined control loop needs to be made. Here all the measurable states will have their own analog feedback and only the estimated states will have a digital feedback.

3.3 System Merging

The feedback path of the modulator feedback and the LQR feedback both require the inductor current and the capacitor voltage to function properly. For the inductor current, the modulator uses the ripple current I_Δ to create the carrier voltage $V_{car}(t)$ used for the self-oscillation. On the other hand, the LQR is only designed to work with linear continuous signals thus the performance is degraded by the ripple current being superimposed on the control signal. This seems to impose two conflicting demands to the property of the measured inductor current. To clarify the situation, Figure 3 shows the modulator with the LQR feedback entering from the left side along with the audio input forming the control signal $u(t)$, and the modulator feedback entering from the right side creating the carrier voltage $V_{car}(t)$. Only the relevant LQR feedback signals are shown.

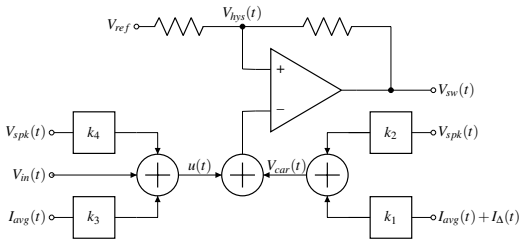

Fig. 3: Modulator with the feedback from the LQ-controller and the modulator gains

A classical solution to accommodate these conflicting demands of the inductor current would be to introduce a low-pass filter for the signal going to the LQR as this would attenuate the ripple current. However, this would increase the complexity of the system and it would be hard to obtain a desirable attenuation without introducing a phase shift in the audio band, potentially making the control less efficient or unstable. Due to these drawbacks, a novel solution is proposed which is based around merging the feedback structure of the LQR and the modulator. Looking at Figure 3, the equation for describing the signal on the negative input terminal of the comparator V_{in-} can be constructed. Equation 15 shows this equation with the time dependency omitted.

$$\begin{aligned} V_{in-} &= V_{car} + u \\ &= V_{spk}(k_2+k_4) + I_{avg}(k_1+k_3) + I_\Delta k_1 + V_{in} \end{aligned} \tag{15}$$

From Equation 15 it is evident that it is possible to add the gains from the same measurement to create a new gain with the same properties as the individual gains had. Unfortunately, by doing this the inductor ripple current becomes isolated which is just as problematic to realize as it was the other way around with the average inductor current. However, if it turns out that the LQR procedure always will set k_3 close to zero, a possibility for further reduction is created. Equation 16 shows the case where k_3 is approaching zero.

$$\lim_{k_3 \to 0} V_{in-} = V_{spk}(k_2+k_4) + (I_{avg}+I_\Delta)k_1 + V_{in} \tag{16}$$

Equation 16 clearly shows that if the assumption about k_3 is correct, the conflicting goals of the inductor current can be eliminated and a full integration of the linear quadratic regulator into the amplifier can be obtained. This would be very beneficial as it would allow for a less complex design and a simple method to include potential speaker measurements for regulation directly into the class-D amplifier. Further, the integration of the LQR also removes the constraints of the control signal, making it possible to design the controller without worrying about potential clipping of the audio signal. In short, an Optimal Modulator with Embedded Control (OMEC) could be realized. To validate the assumption about k_3, the cost function of the LQR and the modulator design method needs to be reviewed. The cost function (Eq. 14) focusses on obtaining a specific gain through the system while reducing the resonances in

the system. Thus, if the feedback gain for the modulator k_1 ensures well damped poles for the 2nd order low-pass filter, the LQR design routine will generate a small k_3 as the inductor current state will not be important to achieve the design goal. To see if k_1 results in a sufficient damping of the 2nd order low-pass filter, the filter is written in its simplest form where all the parasitics are ignored and the gain k_1 included. Equation 17 shows the transfer function of the filter and equation 18 shows the resulting damping factor ζ.

$$H(s) = \frac{\omega_c^2}{\omega_c^2\left(1+\frac{Gk_1}{R_{spk}}\right)+s\left(\frac{1}{R_{spk}C}+\frac{Gk_1}{L_{ind}}\right)+s^2} \quad (17)$$

$$\zeta = \frac{\frac{1}{R_{spk}C}+\frac{Gk_1}{L_{ind}}}{2\omega_c} \quad (18)$$

Since G is the open-loop gain of the comparator, it is evident from equation 18 that even extremely small positive values of k_1 will result in an overdamped filter, thus it can be concluded in general that k_3 will be close to zero, resulting in Equation 16 being valid.

By injecting the LQR control loop directly into the modulator, as done with the proposed method, the size of the control signal will not induce any limitations for additional control loops. This results in an overall improvement in the performance regarding linearity, noise, and power supply rejection, without imposing any limitations on the remaining system.

4 Example System

To evaluate the performance of the OMEC class-D amplifier, a switching model for simulation has been constructed in Simulink. Table 1 shows a table with the specifications of the amplifier used in the simulation. Equation 19 and 20 show the corresponding system and input matrix. These matrices have the same structure as the previously shown, hence both the capacitor's ESR and the inductance of the loudspeaker's voice coil are included. Please note that while the first element in B has an exact description, it can in practice be selected to be any large number because of the gain of the comparator.

Cutoff Frq (f_c)	35	kHz
Damping factor (ζ)	0.1	
Idle Switch Frq (f_{sw})	500	kHz
Rail Voltage (V_{cc})	$\pm$40	V
Maximum Power (P_{max})	200	Wrms
Speaker resistance (R_{spk})	4	Ω
Speaker inductance (R_{ind})	20	μH

Table 1: Class-D Amplifier Specifications

$$A = \begin{bmatrix} -6185 & 2748.9 & -1.3744\cdot 10^5 \\ 1000 & -2.01\cdot 10^5 & 50000 \\ 1.7593\cdot 10^5 & -1.7593\cdot 10^5 & 0 \end{bmatrix} \quad (19)$$

$$B = \begin{bmatrix} 6.8722\cdot 10^{12} \\ 0 \\ 0 \end{bmatrix} \quad (20)$$

First the modulator feedback gains K_{mod} are found using Equation 11 and 12. The resulting closed-loop description is then used to find the controller feedback gains K_∞ using the LQR method. Equation 21 shows the combined feedback gains for the class-D amplifier. The order of the gains corresponds to the order of the state vector (Eq. 4).

$$K = K_{mod} + K_\infty = \begin{bmatrix} 0.090946 & -0.12381 & 0.11691 \end{bmatrix} \quad (21)$$

The controller feedback gains have been selected such that a sufficient bandwidth of the closed-loop system is achieved. This, however, results in a low gain of the system. A frequency analysis is carried out to evaluate the system's performance. Figure 4 shows the bode plot of the system before and after the LQR control is applied. Here it is seen that the achieved bandwidth of the system after the LQR control is applied is 22.2 kHz and thus sufficient for audio applications. This bandwidth has come with the cost of a lower gain through the system compared to without the LQR. The gain is only 7.6 dB equivalent to a times 2.4 amplification from input to I_{spk}. This equals a voltage amplification of 19.7 dB or a 9.6 times amplification.

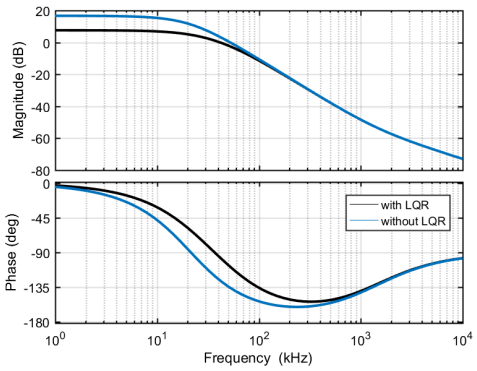

Fig. 4: Calculated frequency response of the closed-loop system from input to I_{spk}

The reason why it is hard to obtain better system performance than what has been found is that the output is chosen to be the current through the voice coil. This introduces additional dynamics to the system, thus slowing down the response. This also shows that a high bandwidth for the speaker voltage does not necessarily imply that a sufficient bandwidth is achieved in the speaker. To accommodate this, an increase of the cutoff frequency of the output filter and the switch frequency should be considered.

5 Results

Two simulations are conducted using the switching model. The first simulation is with zero input on the amplifier to verify that the idle switching frequency is as expected. Figure 5 shows the simulated carrier waveform when no input is applied. Measuring the time period shows that the idle switching frequency is exactly 500 kHz but in practice some deviation due to component tolerances is to be expected. Simulations also show that the response of the switching frequency to the input voltage have the known behaviours of hysteresis based self-oscillating modulators, meaning that the switching frequency will decrease as the amplitude of the input is increased [13, 12]. Figure 6 shows the second simulation. Here the system is given an input signal resulting in the amplifier delivering 50% of its maximum output (Fig. 6a) and 95% of its maximum output power (Fig. 6b). Both simulations are compared with the linearized model. The input signal is a sine wave with a frequency of 6.6 kHz which is the highest possible frequency before the third harmonic falls out of the audio band.

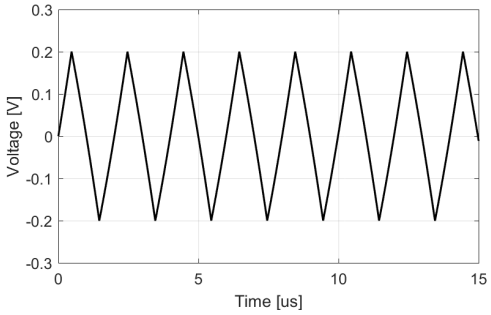

Fig. 5: Simulated carrier signal at 500 kHz with no input applied

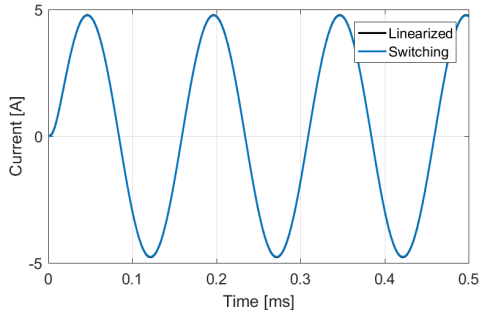

(a) Sinusoid at 50% output power. Hardly any distortion on the waveform

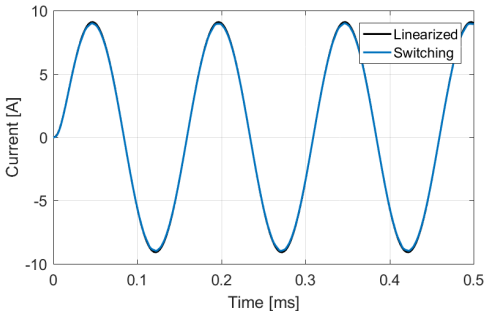

(b) Sinusoid at 95% output power. Distortion is just visible at the peaks

Fig. 6: Simulated sinusoid with a frequency of 6.66 kHz at 50% and 95% of total output power.

From Figure 6b it is seen that the modulator introduces some harmonic distortion when the system is close to clipping. To get a better idea of the total harmonic distortion (THD) a 10 round Monte Carlo simulation at 6.6 kHz with different amplitudes are conducted and the resulting THD+N averaged. Figure 7 shows the THD+N versus the output power of the amplifier. Two Gaussian white noise sources are included for these simulations to get more realistic results. The first noise source simulates input noise and has the distribution $N(0, 10^{-9})$. The second noise source simulates noise from the power supply and has the distribution $N(0, 0.01)$.

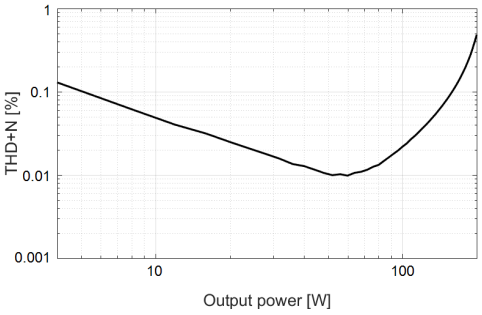

Fig. 7: Simulated THD+N from 4 W to 200 W output at 6.6 kHz

From Figure 7 it is seen that this specific OMEC modulator in theory is able to deliver harmonic distortion lower than 0.01% and no higher than 0.48%. It is possible to further reduce the THD by adding a global feedback loop around the system in the form of a PID or a $\mathscr{H}_2$ loop [15].

6 Summary

In this paper, a method for integrating a LQR control loop into a class-D amplifier has been presented. Methods for designing the feedback gains for the modulator and linear quadratic controller from state space models have been shown. By merging the feedback gains for the controller and the modulator, a simpler design was achieved while the performance of both feedback loops were preserved. The merge of the loops also resulted in the removal of constraints in the design process of the control loop and made it possible to include speaker parameters into the amplifier. Hereby, all the advantages of the control loop was retained e.g. better linearity, power supply rejection, and noise reduction, while the disadvantages was avoided. To verify the theory, simulations were made on a stochastic switching system model. These simulations showed that the properties of the class-D amplifier were preserved, thus agreeing with the theory. Lastly, theoretical THD+N measurements were made which showed that the simulated amplifier in average had THD+N lower than 0.01% and would never exceed 0.48%.

References

[1] Nielsen, K., "Audio power amplifier techniques with energy efficient power conversion," *Technical University of Denmark, Ph. D. Thesis April*, 1998.

[2] Duraij, M., Iversen, N. E., Petersen, L. P., and Boström, P., "Self-oscillating 150 W switch-mode amplifier equipped with eGaN-FETs," in *Audio Engineering Society Convention 139*, Audio Engineering Society, 2015.

[3] Poulsen, S. and Andersen, M. A., "Simple PWM modulator topology with excellent dynamic behavior," in *Applied Power Electronics Conference and Exposition, 2004. APEC'04. Nineteenth Annual IEEE*, volume 1, pp. 486–492, IEEE, 2004.

[4] Lu, J. and Gharpurey, R., "A self oscillating class D audio amplifier with 0.0012% THD+ N and 116.5 dB dynamic range," in *Custom Integrated Circuits Conference (CICC), 2010 IEEE*, pp. 1–4, IEEE, 2010.

[5] Poulsen, S. and Andersen, M. A. E., "Self oscillating PWM modulators, a topological comparision," in *Power Modulator Symposium, 2004 and 2004 High-Voltage Workshop. Conference Record of the Twenty-Sixth International*, pp. 403–407, IEEE, 2004.

[6] Putzeys, B., "Simple self-oscillating class D amplifier with full output filter control," in *Audio Engineering Society Convention 118*, Audio Engineering Society, 2005.

[7] Klippel, W., "Tutorial: Loudspeaker nonlinearities—Causes, parameters, symptoms," *Journal of the Audio Engineering Society*, 54(10), pp. 907–939, 2006.

[8] Bjerregaard, R., Madsen, A. N., Schneider, H., Agerkvist, F. T., and Andersen, M. A., "Accelerometer Based Motional Feedback Integrated in a 2 3/4" Loudspeaker," in *Audio Engineering Society Convention 140*, Audio Engineering Society, 2016.

[9] Polivka, W., Chetty, P., and Middlebrook, R., "State-space average modelling of converters with parasitics and storage-time modulation," in *Power Electronics Specialists Conference, 1980. PESC. IEEE*, pp. 119–143, IEEE, 1980.

[10] Nwosu, C. and Eng, M., "State-space averaged modeling of a nonideal boost converter," *The pacific journal of science and Technology*, 2(9), pp. 1–7, 2008.

[11] Dahl, N. J., Iversen, N. E., and Knott, A., "Optimal Control of a High Frequency Class-D Amplifier," Unpublished, 2017.

[12] Nielsen, D., Knott, A., Pfaffinger, G., and Andersen, M. A., "Investigation of switching frequency variations and EMI properties in self-oscillating class D amplifiers," in *Audio Engineering Society Convention 127*, Audio Engineering Society, 2009.

[13] Dahl, N., Iversen, N. E., Knott, A., and Andersen, M. A., "Comparison of Simple Self-Oscillating PWM Modulators," in *Audio Engineering Society Convention 140*, Audio Engineering Society, 2016.

[14] Hendricks, E., Jannerup, O., and Sørensen, P. H., *Linear systems control: deterministic and stochastic methods*, Springer Science & Business Media, 2008.

[15] Skogestad, S. and Postlethwaite, I., *Multivariable feedback control: analysis and design*, volume 2, Wiley New York, 2007.

[16] Madsen, F. S., Thorsen, S., Iversen, N. E., and Knott, A., "Model for Evaluation of Power Consumption of Vented Box Loudspeakers," in *Audio Engineering Society Convention 142*, Audio Engineering Society, 2017.

K

Self-oscillating 150W switch-mode amplifier equipped with eGaN-FETs

In 139th Audio Engineering Soceity convention, New York, October 29-1 November, 2015.

Audio Engineering Society

Convention Paper 9378

Presented at the 139th Convention
2015 October 29–November 1 New York, USA

Self-oscillating 150 W switch-mode amplifier equipped with eGaN-FETs

Martijn Duraij[1], Niels Elkjær Iverson[1], Lars Press Petersen[1], and Patrik Boström[2]

[1] *Technical University of Denmark, Kongens Lyngby, Denmark*

[2] *Bolecano Holding AB, Helsingborg, Sweden*

Correspondence should be addressed to Martijn Durij (m.duraij@gmail.com)

ABSTRACT

Where high-frequency clocked system switch-mode audio power amplifiers equipped with eGaN-FETs have been introduced the past years, a novel self-oscillating eGaN-FET equipped amplifier is presented. A $150\,W_{RMS}$ amplifier has been build and tested with regard to performance and efficiency with an idle switching frequency of 2 MHz. The amplifier consist of a power-stage module with a self-oscillating loop and an error-reducing global loop. It was found that an eGaN-FET based amplifier shows promising potential for building high power density audio amplifiers with excellent audio performance. However care must be taken of the effects caused by a higher switching frequency.

1. INTRODUCTION

Enhancement mode Gallium-Nitride FETs (eGaN-FETs) are getting more attention these days in power conversion applications due to their superior Figure of Merit (FOM) compared to regular silicon type MOSFETs [1]. eGaN-FETs' low parasitic capacitances, low gate-source voltage, small package and low $R_{DS_{ON}}$ make these devices suitable for high switching frequencies. A high switching frequency in switch-mode power electronics can lead to smaller output filters. Combined with the small eGaN-FET packages the road opens for high power density converters and amplifiers.

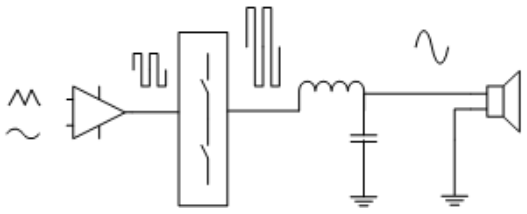

Fig. 1: A topological review on class D amplification.

Class D audio amplification modulates the audio input signal by comparing it to a high frequency triangular carrier waveform using a comparator (Fig.

1). The two-state output is a Pulse Width Modulated (PWM) signal where the width of each pulse in the pulse-train is directly proportional the input audio information. This PWM signal is amplified by switching between the power supply rails of an amplifier. This switching will be handled by eGaN-FETs in the designed amplifier. After the switching stage the audio signal is reconstructed by a demodulation filter. The carrier signal can be generated externally, where a self-oscillating system generates this signal using feedback.

The goal of the research is to investigate eGaN-FETs potential to create smaller and more powerful amplifiers without suffering in performance. Previous research [2,3] showed a promising performance in audio amplifiers, but all used a clocked system. In this research a single channel self-oscillating class D amplifier with a high idle switching frequency is introduced using eGaN-FET devices.

The specifications for this amplifier are summed up in Table 1.

2. THE POWER STAGE

The specifications mentioned in Table 1 are used to design a power stage equipped with eGaN-FETs in a self-oscillating system. For an output power of 150 W in to 4 Ω the voltage supply rails (V_S) have been set to $+/-40$ V. This is slightly higher than is required for the specified output power to create a headroom. Since the switching frequency is much higher than for a regular silicon based class D amplifier the bandwidth can also be increased. Noise and distortion measurements should give results what can be expected from a high performance amplifier. A higher switching frequency could suggest higher switching losses could be involved but because of the eGaN-FETs low parasitic capacitances similar losses to that of a silicon based amplifier are expected. The power stage losses can be divided into: gate losses (P_{gate}), output charge losses ($P_{C_{OSS}}$), switching losses (P_{SW}) and conduction losses (P_{cond}). The effect of dead-time on the losses (P_{dt}) will be taken into account as a conduction loss.

$$P_{gate} = C_{ISS} \cdot f_{SW} \cdot V_{GS}^2 \tag{1}$$

$$P_{Coss} = C_{OSS} \cdot f_{SW} \cdot V_{DS}^2 \tag{2}$$

$$P_{SW} = \hat{\mathrm{I}}_{ripple} \cdot V_{DS} \cdot \frac{T_{rise} + T_{fall}}{2 \cdot T_{sw}} \tag{3}$$

$$\begin{aligned} P_{cond} &= P_{cycle} + P_{dt} \\ &= I_{D_{RMS}}^2 \cdot R_{DS_{ON}} + \hat{\mathrm{I}}_{ripple} \cdot 2 \cdot f_{SW} \cdot t_{dt} \cdot V_{fd} \end{aligned} \tag{4}$$

$$P_{Semi} = P_{gate} + P_{cond} + P_{Coss} + P_{SW} \tag{5}$$

,where V_{DS} the drain-source voltage, V_{GS} the gate-source voltage, V_{fd} the reverse conduction path voltage drop, $I_{D_{RMS}}$ the RMS drain current, $\hat{\mathrm{I}}_{ripple}$ the peak ripple inductor current, $R_{DS_{ON}}$ the eGaN-FET on resistance, C_{ISS} is the input capacitance, C_{OSS} the output capacitance, f_{SW} the switching frequency, t_{dt} the dead-time, T_{rise} and T_{fall} are the respective rise and fall times of the switching node and T_{sw} is the total switching cycle time interval.

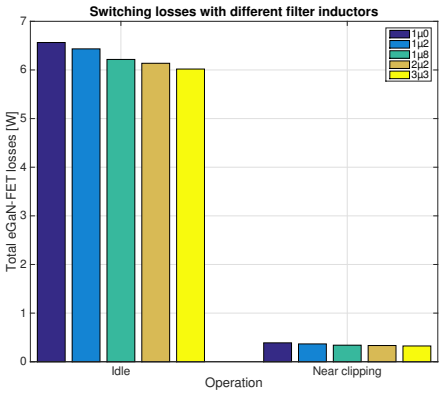

Fig. 2: The eGaN-FET switching losses for different output filter inductor values for both idle and near clipping operation. Results are showed for the dissipated power per eGaN-FET.

The output charge losses are depended on the supply rail voltages where the switching losses are depended on the turn-on and -off time as well. During the dead-time the filter inductor current does not change direction. This current charges/discharges the switch-node capacitance (can be seen later in Fig. 15)

Parameter	Minimal	Typical	Maximum	Unit
Output power		300 150		W_{peak} @ 4Ω W_{RMS} @ 4Ω
Gain		26		dB
Bandwidth	10 - 100000			Hz
f_{SW}			2	MHz
THD			0.01%	1kHz at $P_{max}/8$ @ 4Ω
Efficiency	95			%

Table 1: The set amplifier specifications.

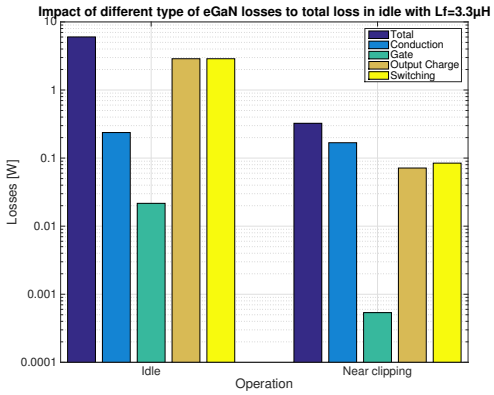

Fig. 3: Contribution of switching losses type to total eGaN-FET switching losses for both idle and near clipping operation.

. The output filter inductor stores energy where the inductor current can not change rapidly during the switching cycle where where the current is the integral of the voltage across the inductor. The eGaN-FET output charge is either charged or discharged by this inductor current. Where the switch-node voltage transients the inductor current it at is maximum or minimum (the ripple current peaks).

The total eGaN-FET losses differ over different inductor ripple currents in idle operation (Fig. 2). It was also found that gate losses are not significant compared to the other losses of these devices as can be observed in Fig. 3. Also the effect of the dead-time conduction losses add up to a large amount of the total losses in the power stage. The results where obtained using the modulator behaviour discussed later.

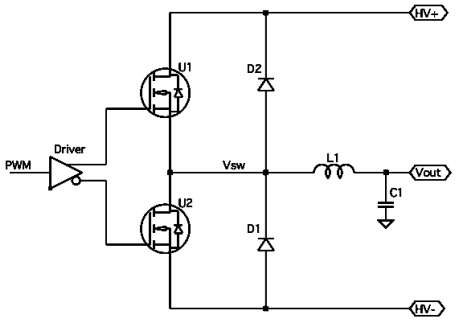

Fig. 4: The researched half-bridge power stage equipped with eGaN-FETs.

To prevent a shoot-trough in the power stage a small dead-time t_{dt} is added to the PWM signal in the order of nano seconds. During a dead-time event the output inductor current first charges/discharges the output charge of the eGaN-FETs, where-after a reverse conduction path (or freewheeling path) is required. eGaN-FETs do not have a physical body diode, however a reverse conduction path is present [4]. This is the reason a "diode" is represented in the eGaN-FET symbol as shown in Fig. 4. The drawback of this reverse conduction in eGaN-FETs is that the voltage drop is higher than for their MOSFET counterparts (approx. 2.5 V for eGaN compared to approx. 0.7 V for silicon) but reverse recovery charge is absent. Using the body diode in a MOSFET design requires a reverse recovery charge which is not present in eGaN-FETs which means a eGaN-FET can conduct current in the reverse direction directly. This means the power loss during dead-time for an eGaN-FET is higher than for a

MOSFET design. Adding two fast diodes with a low V_{fd} (Schottky type) in the half-bridge from Fig. 4 introduce an alternative current path during dead-time with a decreased voltage drop and therefore decreased losses as can be seen in Fig. 5. The losses near clipping due to dead time are larger because the output current is larger in near clipping events.

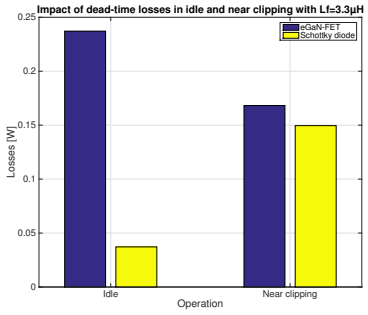

Fig. 5: Effect of the reverse conduction path on dead-time losses.

eGaN-FETs have a lower $R_{DS_{ON}}$ and lower parasitic capacitances (C_{OSS} and C_{ISS}) than regular MOSFETs. When the switching frequency increases, the eGaN-FET brings up limitations in the switching losses in the same way as for MOSFETs. The $R_{DS_{ON}}$ of the eGaN-FET is not the main priority for class-D audio amplifiers, especially at a higher switching frequency. The limiting factor to achieve a high efficiency are the parasitic capacitances where a eGaN-FET with a slightly higher $R_{DS_{ON}}$ but lower parasitic capacitances would be desired. One could state that eGaN-FETs lower parasitic losses are compromised by having a higher switching frequency. A lower switching frequency would compromise the power density of the amplifier. If loudspeaker impedance goes down towards 2 Ω or lower the $R_{DS_{ON}}$ should be given more attention.

3. MODULATION

Different topologies of self-oscillating systems with and without output filter control have been introduced before [5,6]. This research has been done using traditional silicon based semiconductor devices. eGaN-FETs allow a higher switching frequency which may be used in these existing topologies. Increasing the switching frequency means that the output filter inductor can be reduced in size. A smaller output inductor can reduce a large cut of the costs of amplifier modules. A drawback of higher switching frequencies may be the increasing factor of dead-time since the ratio between dead-time and switching cycle becomes larger. Dead-time can increase distortion since no direct control over the switch node is available during this time interval.

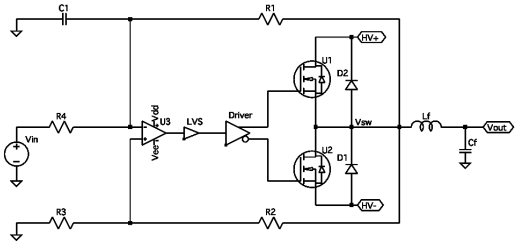

Fig. 6: The implemented AIM modulator with eGaN-FETs.

3.1. AIM

To generate a high frequency PWM signal a very fast comparator is used. A PWM signal can be created by applying a hysteresis positive feedback and a integrating negative feedback. This circuit (Fig. 6) is called an Astable Integrating Modulator (AIM), introduced in the 1970's [7] and has been widely used.

The AIM modulator can be constructed around the eGaN-FET output stage as seen in Fig 6. The switching-node is used for both the hysteresis and integrator feedback to run the modulator. The integrator feedback with R1 and C integrates the switch-node voltage in a triangular waveform until it hits the hysteresis window set by R2 and R3. This flips the output signal state and therefore the switch-node voltage towards the other rail causing the system to oscillate. The output filter (or demodulation filter) is constructed by a inductor (Lf) and capacitor (Cf) circuit where the output voltage is reconstructed.

An AIM modulator topology has a larger gain in the feed back loop if one would compare with a clocked system. This means that when a global loop is applied there is more signal gain available for error

reduction of the output voltage. In other words, distortion will be lower. There are however certain drawbacks of using an AIM modulation scheme. For any self-oscillating amplifier loop the switching frequency is depended on the modulation index (or duty cycle of the PWM signal) which is directly proportional to the audio input information. The frequency drops when the modulation index becomes larger for higher output levels [8]:

$$f_{SW} = \frac{V_S}{4} \cdot \frac{1 - M^2}{\tau_{int} \cdot V_{hyst} + \frac{1}{2} \cdot t_d \cdot V_S(1 + M^2)} \quad (6)$$

,where V_S is the supply rail voltage, V_{hyst} the hysteresis window in volt, M the modulation index, τ_{int} is the integrator time constant and t_d the total delay trough the power stage.

When reaching higher power levels the switching frequency of the amplifier is reduced meaning that there are less switching transitions during a given time period. This means the switching losses are lower for a maximum modulation index. However when the modulation index reaches $M = 1$ the switching frequency is 0 Hz where the amplifier clips towards one of the supply rails.

The bandwidth of the AIM modulator is depended on the integrating negative feedback, which is the only pole in the system [8]. This means the bandwidth of the modulator is limited towards the placement of this pole. Since the carrier is generated using a resistor and capacitor circuit the feedback only behaves as an integrator for frequencies above the pole frequency. For lower carrier frequencies, which are modulation index depended, carrier distortion may occur resulting in output signal distortion.

3.2. Loop filter

Setting the gain and the bandwidth of the complete amplifier can be done by a global loop. The global loop compares the output signal to the referenced input signal creating a error signal to drive the modulator.

Placing the output filter cut-off frequency f_{LC} at a higher frequency, more bandwidth is available for the transition bandwidth (Fig. 7). In the loop filter , the bandwidth between the high gain in the audible bandwidth and the required attenuation at

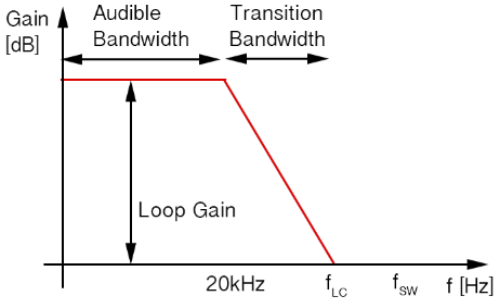

Fig. 7: The placement of the output filter frequency compared to the audible bandwidth and the switching frequency.

switching frequencies can be used for this transition. The output filter cut-off frequency can be placed at a higher frequency because the switching frequency of the eGaN-FETs is much higher. As a rule of thumb the filter cut-off freqnecy should be placed a decade below the switching frequency, in this case around 200 kHz. This creates a larger bandwidth for the transition region, which can make room for a higher gain in the audible bandwidth. A higher gain in the audible bandwidth means a lower distortion of the output signal.

In this paper a two stage PI controller global loop is implemented (Fig. 8 and 9). The first PI controller creates the summing node. A zero is added in the feedback from the output voltage using C_Z around the filter cut-off frequency to create some phase margin. The placement of the poles can be optimized using $R2 + C2$ and $R7 + C3$ where they are implemented around 6 kHz and 1.5 kHz. The gain of the amplifier is set by $R1$ and $R3$ to a total of approx. 28dB. If improvements should be made to reduce distortion, the loop gain can be increased with an higher order loop. Future work could also conclude an active THD shaping filter [9].

4. IMPLEMENTATION

A very fast LT1711 comparator from Linear Technology is used with a propagation delay time of 4 ns and very fast rise- and fall times. Since the comparator outputs a signal between the +5 V supply

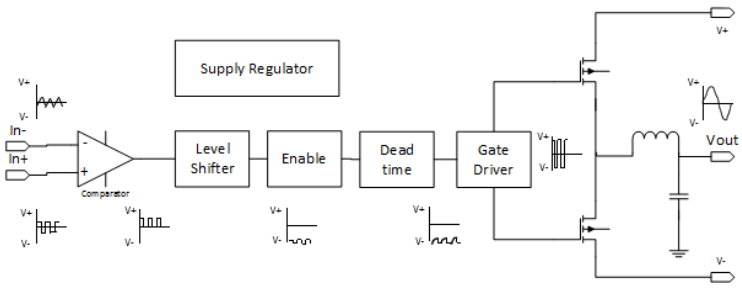

Fig. 10: The building blocks of the common power stage module.

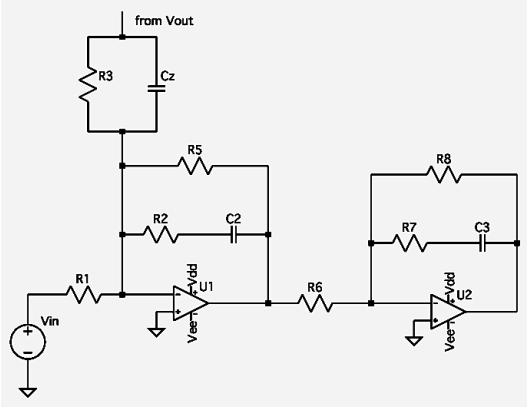

Fig. 8: Two PI controllers in series form the global loop filter.

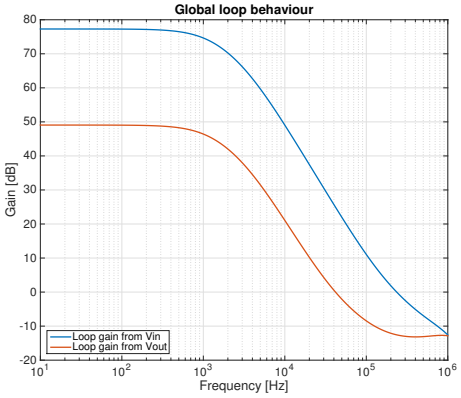

Fig. 9: The global loop open-loop gain simulated.

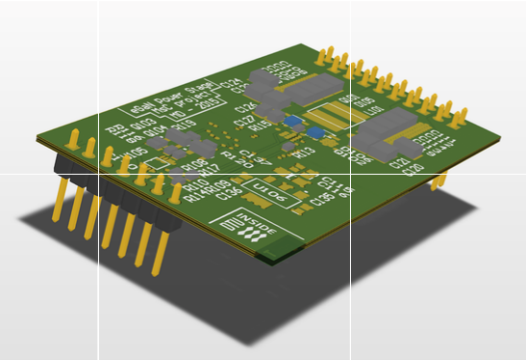

Fig. 11: The designed power stage as a plug-in module.

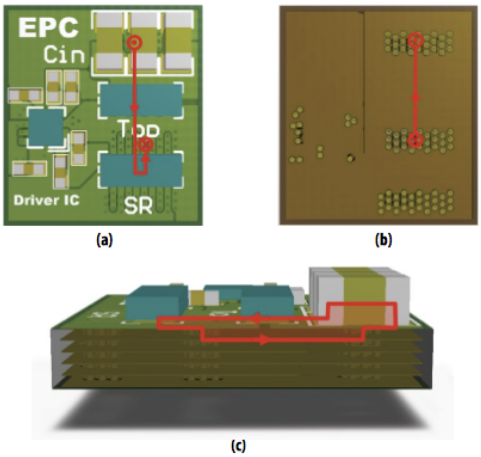

Fig. 12: Suggested optimal power loop by EPC in [13]. The top view in (a) with component placement and the first inner layer in (b) show the switching current loop in red. A side view is given in (c). Figures from [13].

rail and the reference ground and the gate driver expects an input signal where the driver is referenced to the negative supply rail a level shifter is required. This level shifter has to be very fast to decrease the delay trough the loop and has to be stable over heavy switching ripple on the negative supply rail. It was found that an bipolar PNP transistor based level shifter performs best in these circumstances. By applying an AND gate after the level shifter the PWM signal can be buffered. Dead-time control is implemented using a simple dead-time control circuit with a resistor, capacitor and diode as used in [2]. The gate driver is an LM5113 type from Texas Instruments driving the eGaN-FETs.

To reduce the current loop size and area in the switching stage the output filter is incorporated close to the power stage improving noise immunity, switch-node behaviour (over- and undershoot) and EMC/EMI. The output filter can be equipped with footprints optimized for use of different inductors values from the XAL6030-XXX series or the XAL7030-XXX series from Coilcraft [10,11] with values ranging from $1\,\mu H$ to $4.7\,\mu H$. The output filter capacitance can be configured by a capacitor bank using up to 8 1210 SMD size film type capacitors. The total output capacitance can be adjusted together with the output filter inductor to optimize bandwidth, switching frequency attenuation and stability.

4.1. Layout

A modular power-stage Printed Circuit Board (PCB, Fig. 11) was designed and build to test an amplifier with an AIM modulation topology. Having created a plug-in module more modulation topologies and applications can be tested in the future with the same module. This PCB holds a comparator, level-shifter, dead-time circuit, enable/disable circuit, gate driver, switching eGaN-FETs and output filter on a footprint of 35 mm times 70 mm rating a $150\,W_{RMS}$ amplifier in to $4\,\Omega$. This results in a power density of $15.66\,W/cm^3$. Layout can be optimized to decrease the PCB area and increase the power density of the amplifier to around $20\,W/cm^3$.

Layout is a very important issue when working with high frequencies and very large dv/dt and di/dt values. As illustrated in [12,13,14] a small inductance in the switching loop can have a large effect on the switching behaviour. Overshoot, decreasing efficiency, accidental gate triggering voltages, thermal behaviour and therefore overall performance are compromised when layout has been given insufficient attention. As suggested in [13] (for reference in Fig. 12) an optimized PCB layout for the power stage is a combination of a lateral and vertical switching

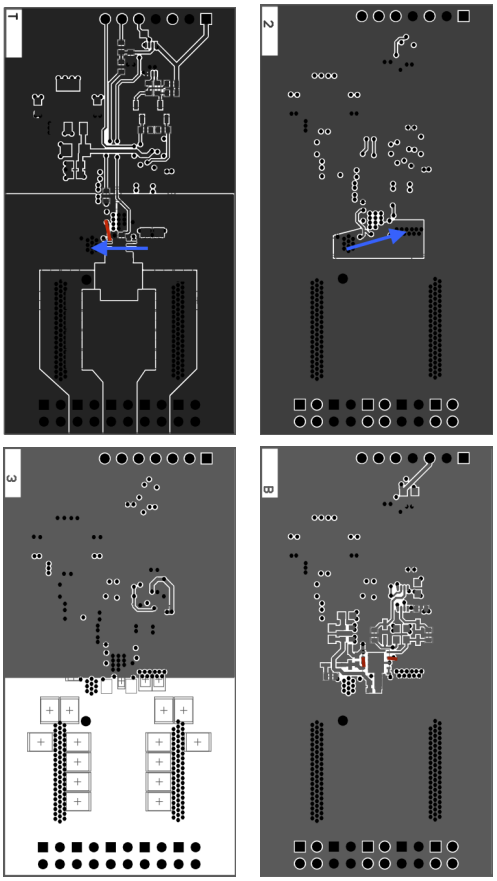

Fig. 13: Layout of the 300W eGaN-FET based power stage module. From top to bottom: Top layer, Inner layer 1, Inner layer 3 and Bottom layer. The images are on a 1:1 scale. The gate switching loops are emphasized in red where the switching current loop is highlighted in blue.

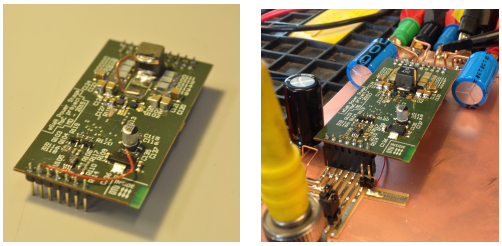

Fig. 14: The designed power stage plug-in module and the measurement set-up.

current loop over a 4 layer board (Fig. 13). By doing so a self cancelling field loop is created where no shield layer is required. To provide very fast switching transients decoupling capacitors in between the supply rails are placed very close to the switching eGaN-FETs.

5. MEASUREMENTS

The plug in module is used on a test board with the global feedback added. Decoupling capacitors are placed on the test board to provide a stable power supply and eliminate supply noise as seen in Fig. 14.

The switch node transients are very fast and the delay trough the power stage module very small. The delay consists of the circuit delay and the dead-time adding up to a total of 62 ns with a dead time of 14 ns. As can be seen in Fig. 15 the switching-node transients are very fast. The total rise and fall time (including dead-time) take approx. 22 ns, where the maximum dv/dt is reaching 29.7 V/ns.

Total Harmonic Distortion (THD) is measured using an Audio Precision at 3 different frequencies. The plot in Fig. 16 shows that a decent performance can be achieved at 100 Hz in blue and 1 kHz in red. At 6.6 kHz in yellow the distortion is larger. The minimum is found at a test signal frequency of 100 Hz at 7 W output power where THD is 0.0034%. To attenuate unwanted behaviour of the 6.6 kHz harmonics sufficient gain in the global loop is required at 3 times this frequency (approx. 20 kHz). The loop filter can be adjusted to create a larger gain up to 20 kHz to decrease output voltage distortion, however one must keep the stability criteria in mind.

The measured distortion at 1 kHz at $1/8^{th}$ of the output power is within the specification. Where the

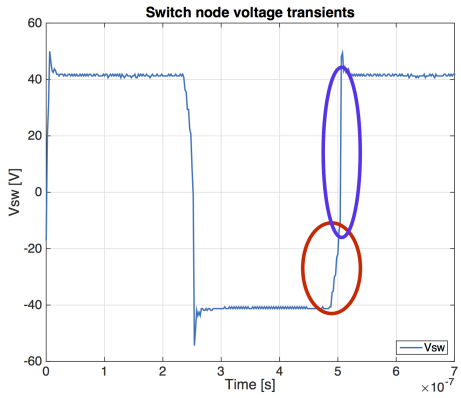

Fig. 15: The measured transients at the switch-node. Not the charging of C_{OSS} with the slow transient during dead-time highlighted in red where after a high dv/dt is seen where the top eGaN-FET switches on highlighted in blue.

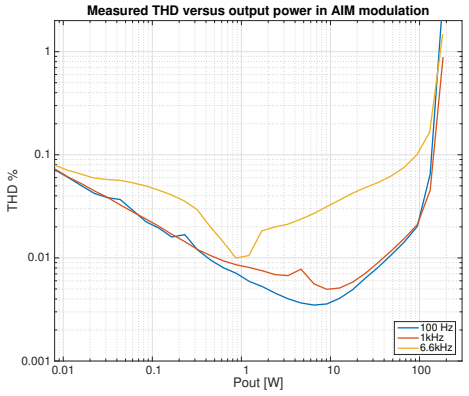

Fig. 16: The AIM modulated eGaN-FET power stage distortion versus output power.

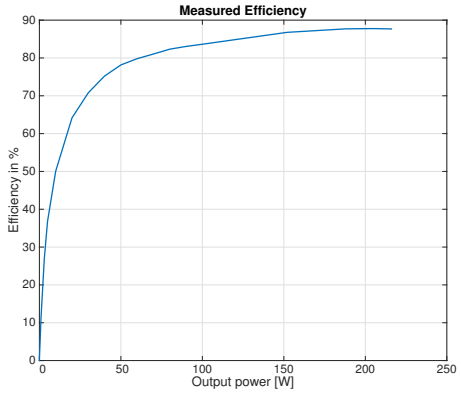

Fig. 17: The eGaN-FET equipped amplifier efficiency.

specification was 0.01% at 27 W, the measured distortion is 0.008%. The loop filter has yet to be optimized where the wider transition bandwidth can be used fully and create a higher gain in the audible bandwidth. A design improvement goal would include lowering the distortion of the measured 6.6 kHz response.

The efficiency of the amplifier has yet to be improved as can be seen from Fig. 17, although it must be said the figure is based on an estimating measurement set up and does not have a high accuracy. However, it can be found that an efficiency around 86% at 1% THD generates excessive losses.

On a thermal picture of the power stage module in Fig. 18 it can be seen that the diodes and eGaN-FETs heat up to the higher temperature on the PCB at around 82.6°C in idle operation. It has also been observed that after a longer running time in idle mode the output filter inductor heats up significantly. This could point out a large AC copper resistance is present in the inductor coil, which is larger at high frequencies. There is also a large amount of switching losses which can be decreased by decreasing dead-time. For eGaN-FET usage a dead-time period of 14 ns is considered to be long. Since the required dead-time is depended on the turn-on and -off time of the eGaN-FETs next steps need to be taken optimizing the switching cycle using [4].

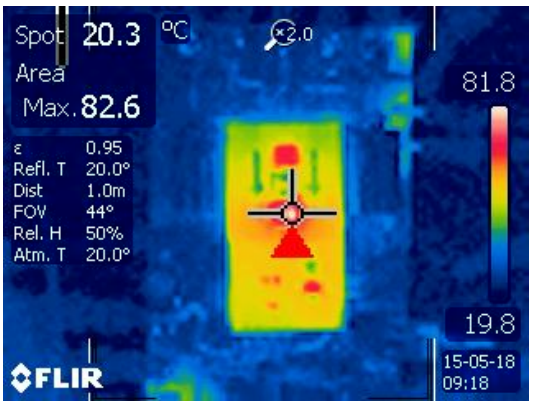

Fig. 18: Thermal behaviour of the eGaN-FET power stage.

6. CONCLUSION

Promising results are shown for a self-oscillating system using eGaN-FETs. The performance of the built amplifier is good with a lowest point measured distortion of 0.0034% at 7 W of the output power. Higher switching frequencies do provide a design stress relief on the loop filters where a wider transition bandwidth is available between gain in the audible band and required attenuation for switching frequencies. At the same time these higher switching frequencies make layout and inductor design very critical. The results show excellent performance when kept in mind only a second-order loop filter was used, a higher order would increase the performance. Improvements have to be made in optimizing efficiency.

7. FUTURE WORK

The switching cycle has to be optimized for all possible output currents and voltages to improve efficiency, optimize dead-time and prevent shoot-trough. Also the output filter inductor has to be tuned accordingly and thermal behaviour needs to be optimized. Improving distortion measurements can be done by optimizing the loop filter to a higher order with more gain and a sharper roll-off. Also THD shaping loop filters can be studied.

8. REFERENCES

[1] A. Lidow, "GaN Transistors for Efficient Power Conversion" 2015

[2] R.Ploug, "GaN Power Stage for Switch-mode Audio Amplification," presented at the AES 138th convention, Warchaw, Poland, May 2015.

[3] J. Lee, H.Kim, K. Cho and H. Park "The Audio Performance Comparison and Method of Designing Switching Amplifiers using GaN FET" presented at the AES 135th convention, New York, NY, USA, October 2013

[4] J. Strydom and D. Reusch, "Dead-Time Optimization for Maximum Efficiency" EPC white paper 2013

[5] B. Putzeys, "Simple Self-Oscillating Class D Amplifier with Full Output Filter Control" presented at the AES 118th convention, Barcelona, Spain, May 2005.

[6] S. Poulsen and M.A.E. Andersen, "Simple PWM modulator topology with excellent dynamic behavior" Applied Power Electronics Conference and Exposition, 2004.

[7] Geelen, P. Self-Oscillating PWM Amplifier. Elektor 5.9 (1979): 946-948. Print.

[8] Poulsen, Sren., and Technical University of Denmark. rsted-DTU. "Towards Active Transducers". rsted-DTU, Technical University of Denmark, 2004. Print.

[9] K.S. Meyer "Minimizing distortion in self-oscillating switching amplifiers" MSc Thesis at Oersted DTU Department for Electric Power Engineering, Kngs Lyngby, Denmark, July 2006.

[10] Datasheet Shielded Power Inductors XAL6030, Coilcraft, 2012

[11] Datasheet Shielded Power Inductors XAL7030, Coilcraft, 2012

[12] A. Lidow, J. Strydom, "eGaN FET drivers and layout considerations" EPC white paper 2012

[13] D. Reusch, "Optimizing PCB layout" EPC white paper 2014

[14] D. Reusch, "Impact of parasitics on performance" EPC white paper 2013

L

Loudspeaker impedance emulator for multi resonant systems

In 138th Audio Engineering Soceity convention, Warsaw, April 26-29, 2014.

Audio Engineering Society

Convention Paper 9289

Presented at the 138th Convention
2015 May 7–10 Warsaw, Poland

Loudspeaker impedance emulator for multi resonant systems

Niels Elkjær Iversen[1], and Arnold Knott[1]

[1] *Technical University of Denmark - DTU, Kongens Lyngby, 2800 Denmark*

Correspondence should be addressed to Arnold Knott (akn@elektro.dtu.dk)

ABSTRACT

Specifying the performance of audio amplifiers is typically done by playing sine waves into a pure ohmic load. However real loudspeaker impedances are not purely ohmic but characterised by its electrical, mechanical and acoustical properties. Therefore a loudspeaker emulator capable of adjusting its impedance to that of a given loudspeaker is desired for measurement purposes. An adjustable RLC based emulator is implemented with switch controlled capacitors, air gap controlled inductors and potentiometers. Calculations and experimental results are compared and show that it is possible to emulate the loudspeaker impedance infinite baffle-, closed box- and the multi resonant vented box-loudspeaker by tuning the component values in the proposed circuit. Future work is outlined and encourage that the proposed impedance emulator is used as part of a control circuit in a switch-mode based impedance emulator.

1. INTRODUCTION

Specifying the performance of switch-mode audio power amplifiers and audio amplifiers in general normally includes measurements of the Gain, Total Harmonic Distortion (THD), Intermodulation Distortion (IMD), Signal to Noise Ratio (SNR) and other parameters such as power supply pumping, crosstalk and efficiency [1], [2], [3]. These measurements are typically used as indicators on how well the amplifier performs. Normally these measurements are performed when the amplifier is playing sine waves into a load, typically a power resistor of 4 to 8 Ω. However a real loudspeaker impedance is not purely resistive as a power resistor as discussed in [4], [5] but characterized by the resonance frequency of the driver and the acoustical properties of the enclosure.

Specifying the performance of audio amplifiers using a real loudspeaker as load involves several challenges due to the fact that the amplified sine waves in many cases will generate sound pressure levels beyond legal limits for working environments. In addition to this, the impedance will vary for different kinds of loudspeakers, making it difficult to obtain a simple test bench.

Several studies, [3], [6], [7], within this field have al-

ready been done showing that the type of load used when measuring the performance of audio amplifier has great influence on the measured results. In [6] it has been shown that the power supply pumping in a switch-mode audio power amplifier was reduced in an actual loudspeaker load compared with the pure resistive load of a power resistor. In [3] the concept of active loads for audio amplifiers is proposed for amplifier efficiency measurements purposes. In [7] a small signal loudspeaker impedance emulator was implemented. Result show that it was possible to adjust a resonance frequency by tuning two resistors. However the proposed small signal impedance emulator from [7] was limited to single resonant systems. Single resonant systems are valid for drivers in free air, infinite baffle and closed box configurations. However, when a driver is mounted in a vented box enclosure, an additional resonance frequency form. Therefore it is relevant to investigate the possibilities for a loudspeaker impedance emulator capable of emulating and impedance with up to two resonance frequencies.

2. LOUDSPEAKER MODELLING

2.1. Basic loudspeaker operation

Loudspeaker operation is well described in [8] but is briefly repeated here for convenience. A loudspeaker works by converting an electrical signal into motion of its diaphragm, creating pressure differences in air which we perceive as audio. Fig. 1 shows the conceptual elements of a loudspeaker unit. The signal

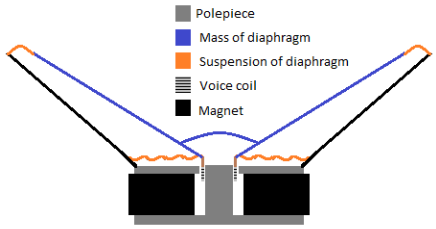

Fig. 1: Conceptual loudspeaker driver

enters the voice coil causing a current to flow. This current generates a magnetic field causing a displacement of the voice coil due to the static magnetic field of the permanent magnet. This displacement is transferred to the diaphragm and emitted as sound. We can split the loudspeaker into three different domains:

- Electrical domain
- Mechanical domain
- Acoustical domain

The electrical domain is characterised by the voice coil with a given DC resistance and self-inductance, R_e and L_e. The strength of the coupling from the electrical to the mechanical domain is determined by the force factor Bl, which is the product of the magnetic field strength of the static magnet in the voice coil gap, B, and the length of the voice coil in the static magnetic field, l.

The mechanical domain is characterised by the mass, M_{MD}, of the diaphragm, the compliance, C_{MS}, of its suspension and a mechanical damping, R_{MS}. The mass and the compliance will introduce a resonance frequency, f_S, which is dampened to some level due to the mechanical damping. This means that the resonance will have a given Quality factor, Q_{MS}, known as the mechanical Q-factor. At the resonance frequency the driver will reach its maximum impedance. The electrical domain is also characterised by a Q-factor, Q_{ES} which is dependent on Bl, R_e, M_{MD} and C_{MS}. Combining the mechanical and electrical Q-factors results in a total Q-factor known as Q_{TS}. The strenght of the coupling from the mechanical to the acoustical domain is related to the area of the driver diaphragm, S_D.

The acoustical domain is characterised by the acoustical impedance in front, Z_{AF}, and behind , Z_{AB}, the diaphragm. Typically the impedance in front of the diaphragm will be dependent on the acoustical properties of the room the driver plays into while the impedance behind the diaphragm will be dependent of the acoustical properties of the enclosure which the driver is mounted in. Normally a loudspeaker will be mounted in some kind of enclosure and therefore a parameter known as the volume compliance, V_{AS}, is introduced. The volume compliance corresponds to the equivalent volume of air which, when compressed by a piston having the same area as the driver diaphragm, will have the same compliance as

the mechanical compliance of the driver suspension C_{MS}.

The above described parameters are known as Thiele-Small parameters and are well described in literature, [9] and [10] and are listed in table 1. These parameters are normally given in datasheets for drivers and are used when designing enclosures for the loudspeaker driver, eg. cabinets.

Symbol	Parameter
R_e	DC resistance of voice coil
L_e	Self inductance of voice coil
Bl	Force factor
M_{MD}	Mass of diaphragm
C_{MS}	Compliance of suspension
R_{MS}	Mechanical damping
f_S	Resonance frequency
Q_{MS}	Mechanical quality factor
Q_{ES}	Electrical quality factor
Q_{TS}	Total quality factor
S_D	Area of diaphragm
V_{AS}	Equivalent volume

Table 1: Thiele-Small parameters

2.2. Loudspeaker modelling

There exist many different kinds of loudspeaker models which have different focuses and purposes. This paper aims at an impedance emulator and therefore the only criteria to the models presented in this paper is that they can emulate the impedance of a given loudspeaker in a simple enclosure. These enclosures are:

- Infinite baffle
- Closed box
- Vented box

2.2.1. Infinite baffle and closed box loudspeaker

The infinite baffle loudspeaker can be modelled with the circuit shown in fig. 2. L_{ces} models the compliance of the driver's diaphragm, C_{mes} models the mass of the diaphragm and R_{es} models the mechanical damping. Combined these three components models the mechanical characteristics of the driver.

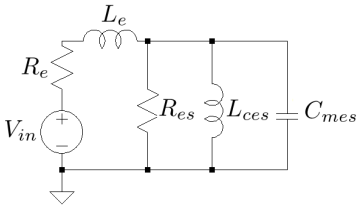

Fig. 2: Equivalent circuit for driver mounted in infinite baffle

L_e and R_e model the self inductance and DC resistance of the voice coil respectively. Combined they represent the electrical character of the voice coil. The impedance of this circuit is seen to be:

$$\begin{aligned} Z_{in} &= R_e + sL_e + \frac{1}{\frac{1}{R_{es}} + \frac{1}{sL_{ces}} + C_{mes}s} \\ Z_{in} &= R_e + sL_e + \frac{sL_{ces}R_{es}}{s^2 C_{mes}L_{ces}R_{es} + sL_{ces} + R_{es}} \end{aligned} \tag{1}$$

Where s is the Laplace operator equal to the complex angular frequency $\omega j = 2\pi f \cdot j$. The resonance frequency, the mechanical- and electrical-quality factors for this circuit can be calculated using:

$$Q_{ES} = 2\pi f_S C_{mes} R_E \tag{2}$$

$$Q_{MS} = 2\pi f_S C_{mes} R_{es} \tag{3}$$

$$f_S = \frac{1}{2\pi\sqrt{C_{mes}L_{ces}}} \tag{4}$$

When the loudspeaker driver is mounted in an enclosure the acoustical load on each side of the diaphragm is unequal and therefore the acoustical part must be taken into account. The volume of the enclosure, V_{AB}, works as an acoustical compliance. The acoustic compliance of the enclosure can be modelled as an inductor, L_{ceb}. This inductor will be in parallel with the inductor modelling the mechanical compliance. Fig. 3 shows the electrical equivalent model. A new parameter known as the compliance ratio, α, is introduced. α is the ratio between the mechanical and acoustical compliances.

$$\alpha = \frac{V_{AS}}{V_{AB}} = \frac{L_{ces}}{L_{ceb}} \tag{5}$$

The two inductors, L_{ces} and L_{ceb} can be modelled as one equivalent compliance inductor, L_{eq}.

$$L_{eq} = \frac{L_{ces}L_{ceb}}{L_{ces} + L_{ceb}} \tag{6}$$

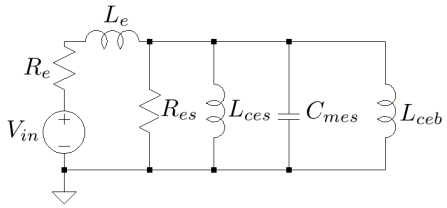

Fig. 3: Equivalent circuit for closed box loudspeaker

Note that the value of L_{eq} cannot be larger than the L_{ces}. This leads to the consequence that the resonance frequency, f_C, and quality factor, Q_{TC}, of a closed box system will be shifted upwards compared to the infinite baffle system.

$$f_C \approx \sqrt{1+\alpha} f_S \tag{7}$$

$$Q_{TC} \approx \sqrt{1+\alpha} Q_{TS} \tag{8}$$

The impedance of the closed box loudspeaker has the same form as for the infinite baffle loudspeaker impedance from eq. 1 however L_{ces} is substituted with L_{eq}.

2.2.2. Vented box loudspeaker

Vented box loudspeakers uses an additional resonance frequency to increase the low frequency output. The vent and the volume of the enclosure is in fact a Helmholtz resonator, and its resonance frequency, f_B, is known as the Helmholtz resonance. The mass of the air in the vent will resonate with acoustical compliance of the volume of the enclosure, modelled by L_{ceb}. The mass of the air in the vent can be modelled as a capacitance, C_{mep}. The Helmholtz resonance frequency, formed by C_{mep} and L_{ceb}, is dampened due to air leaks of the enclosure which can be modelled with a resistance, R_{el}. The Helmholtz resonance frequency and its quality factor are given by:

$$f_B = \frac{1}{2\pi\sqrt{C_{mep} L_{ceb}}} \tag{9}$$

$$Q_L = \frac{1}{2\pi f_B C_{mep} R_{el}} \tag{10}$$

Fig. 4 shows the electrical model for the vented box circuit.

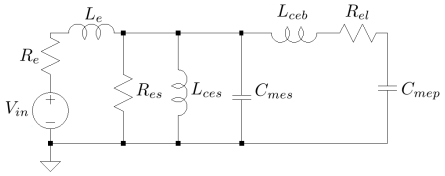

Fig. 4: Equivalent circuit for vented box loudspeaker

The impedance of the electrical equivalent circuit is seen to be:

$$Z_{in} = R_e + sL_e + \frac{1}{\frac{1}{R_{es}} + \frac{1}{L_{ces}s} + C_{mes}s + \frac{1}{R_{el} + L_{ceb}s + \frac{1}{C_{mep}s}}} \tag{11}$$

Vented box cabinets are designed to comply with a specific alignment. For a given driver there will be an optimal alignment. The alignment ultimately determines the enclosure volume, the compliance ratio and the Helmholtz resonance frequency. Conventional alignments are the 4th order Butterworth (B4), the 3rd order Quasi butterworth (QB3) and the Chebyshew equal ripple (C4). How these alignments are calculated and can be used to design optimal vented box cabinets is explained in [8].

2.2.3. Accuracy of loudspeaker models

To verify the accuracy of the loudspeaker models a real loudspeaker was designed and built for measurements purposes. The Thiele-Small parameters for the driver used are listed in table 2.

A vented box cabinet was designed using the technique described in [8]. The material used for the cabinet was foam core board which was glued together. This material is good for fast prototyping. However it does cause air leakage losses and therefore the quality factor of the enclosure was chosen to be rather low, $Q_L = 5$ when designing. The optimal alignment was found to be a chebyshew equal ripple alignment with a Helmholtz resonance frequency at $f_B = 79$ Hz and cabinet volume of $V_{AB} = 3$ litres. The realized loudspeaker is shown in fig. 5.

Due to imperfection during implementation the actual volume was measured to be $V_{AB} = 2.6$ litres, the Helmholtz resonance to be $f_B = 66$ Hz and the quality factor of the enclosure was estimated to be $Q_L = 2.5$. From this the component values needed

Symbol	R_e	L_e	f_S	Q_{MS}	Q_{ES}	Q_{TS}	V_{AS}
Value	6.4 Ω	110 μH	124 Hz	12.3	0.69	0.65	0.54 L

Table 2: Thiele-Small parameters for a 2.5" woofer used in implementation

Symbol	R_e	R_{es}	R_{el}	L_e	L_{ces}	L_{ceb}	C_{mep}	C_{mes}
Value	6.4 Ω	108 Ω	9 Ω	110 μH	11.3 mH	54.2 mH	107.3 μF	146.4 μF

Table 3: Component values needed for vented box model emulating the impedance of the designed speaker

Fig. 5: Realized speaker

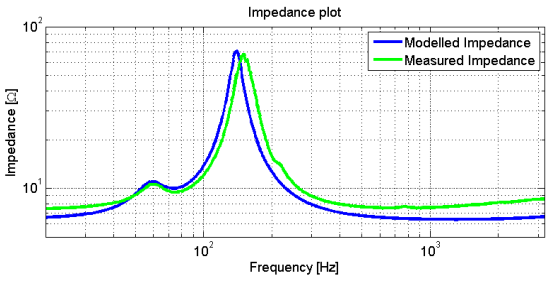

Fig. 6: Comparison of measured and modelled impedance

for the vented box loudspeaker model, from fig. 4, could be found by using eq. 2, 3, 4, 5, 9 and 10. The resulting component values are shown in table 3. The impedance of the actual speaker was measured by applying a psuedo random noise signal to the speaker which was connected in series with a 33 Ω resistor. Then the input voltage and the loudspeaker voltage was measured and from this the impedance could be calculated as:

$$Z_{spk} = -33\Omega \frac{\left(\frac{V_{in}}{V_{spk}}\right)^{(-1)}}{\left(\frac{V_{in}}{V_{spk}}\right)^{(-1)} - 1} \tag{12}$$

The measured and modelled impedances are shown in fig. 6. It can be seen that the modelled impedance fits the measured impedance very well. However the DC resistance and the upper resonant frequency is slightly off. This is assumed to be due to tolerances.

3. RANGE OF COMPONENT VALUES

In order to realize a loudspeaker impedance emulator for any driver in either an infinite baffle, closed box or vented box, it is desired to make an estimate of which range the component values should be within. Therefore a database, [11], containing the Thiele-Small parameters of more than 2000 drivers has been analysed. The database includes drivers from well known brands such as, Monacor, JBL, Vifa, Fostex etc. and the size ranges from 1.5" to 30". The author of [11] has collected the data with the help from people who have reported Thiele-Small parameters from various drivers on-line. This also means that there is no guarantee that all data in the database correlates with the parameters provided by the manufacturer. However after picking random samples in the database and compared the parameters from the samples to the ones provided by the manufacturers, without finding major mismatches, the data in the database is assumed to be valid.

By using eq. 2, 3, 4, 5, 9 and 10 on each driver in the database the range in component values needed to implement infinite baffle, closed box and vented box can be estimated. Fig. 7 shows the results using box plots.

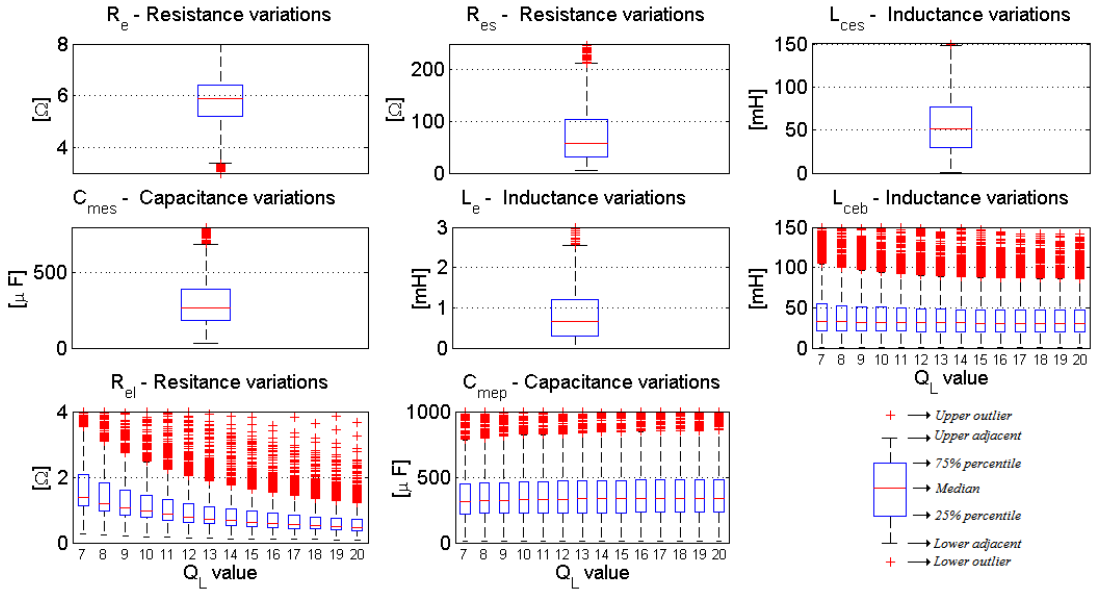

Fig. 7: Box plots showing variations of component values based on analysis of the dataset

	R_e	R_{es}	R_{el}	L_e	L_{ces}	L_{ceb}	C_{mep}	C_{mes}
Up ADJ	2Ω	215Ω	3.6Ω	2.5mH	150mH	110mH	850μF	700μF
Low ADJ	3.4Ω	5Ω	90mΩ	-	1mH	1mH	13.5μF	30μF
75%	6.5Ω	105Ω	0.4Ω	1.2mH	80mH	55mH	440μF	390μF
25%	5Ω	30Ω	2Ω	0.3mH	5mH	25mH	220μF	190μF

Table 4: Summary of boxplot data from the database analysis

Choosing a focus area from the lower to the upper adjacent (95% of the data) it is observed that for the components modelling the electrical properties of the driver we have variations for R_e from approximately 3.4 to 8 Ω and L_e from some μH to 2.5 mH. For components modelling the mechanical properties of the driver we have variations for R_{es} from approximately 5 to 215 Ω, L_{ces} from approximately 1 to 150 mH, C_{mes} from approximately 30 to 700 μF. For the components modelling the properties of the vented enclosure we have variations for L_{ceb} from approximately 1 to 110 mH, C_{mep} from approximately 13.5 to 850 μF and R_{el} from approximately 0.09 to 3.6 Ω. Note that for R_{el} is clearly reduced as Q_L increases corresponding to lower air losses. Moreover it is observed that if the focus area is changed to be from the 25 to 75% percentile, corresponding to 50% of the most common drivers, the component value span is strongly reduced. Table 4 summarizes the analysis.

4. IMPLEMENTATIONS AND RESULTS

4.1. Implementation

To keep an implementation of the loudspeaker impedance emulator as simple as possible but still capable of adjusting its impedance to the different loudspeaker configurations, switch controlled capac-

itors and air gap controlled inductors were used.

Switch controlled capacitors utilizes the fact the equivalent capacitance of capacitors in parallel is simply the sum of the capacitances. This makes it possible to construct an array of N capacitors in parallel and control the resulting capacitance by switching the capacitors in and out. An additional benefit from this type of implementation is that the parasitic series resistance will tend to be rather small due to the parallel connection of the capacitors. The concept is shown in fig. 8 The equivalent capacitance

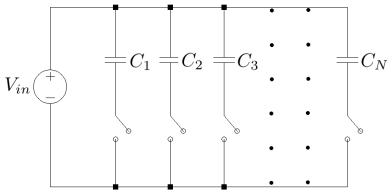

Fig. 8: Concept of switch controlled capacitors

of this circuit, assuming all switches are closed will simply be:

$$C_{eq} = C_1 + C_2 + C_3 + \cdots + C_N \tag{13}$$

An adjustable inductor can be implemented the same way as the switch controlled capacitors. The only difference is that the inductors in such an inductor array should be in series instead of in parallel. However this is difficult to implement elegantly and therefore it will be more convenient to adjust the inductance by controlling the air gap in the inductor.

According to [12] the inductance of inductors can be determined knowing the effective permeability of the inductor, μ_e, the effective magnetic length, l_e, and the magnetic cross section, A_e.

$$\begin{aligned} \mu_e &= \frac{1}{1+\mu_r \cdot \frac{l_g}{l_c}} \\ l_e &= l_c + l_g \\ L &= \frac{\mu_e \mu_0 N^2}{\frac{l_e}{A_e}} \end{aligned} \tag{14}$$

Where $\mu_0 = 4\pi \cdot 10^{-7}$ H·m^{-1} is the permeability of air, μ_r is the relative permeability of the core, l_c is the magnetic length of the core, l_g is the length of the air gap of the inductor and N is the number of turns. From this it is evident that when increasing the air gap for a core with given relative permeability, then the effective permeability will decrease and thus also the inductance. The inductor can be adjusted by having some kind of mechanical displacement control in the air gap. This was implemented so that the air gap could be controlled with a screw driver. The schematic of the implemented loudspeaker impedance emulator is shown in. fig. 9. As seen from the schematic the self inductance of the voice coil has not been considered in this implementation. The switch, *S1*, on the schematic determines

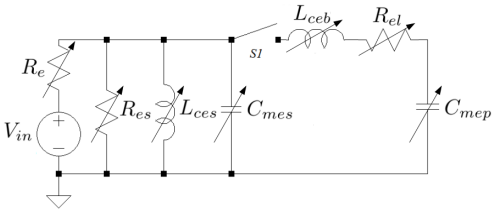

Fig. 9: Schematic of realized loudspeaker impedance emulator

whether the impedance emulator should emulate an infinite/closed box- or a vented box-impedance. The component used in the implementation has been chosen, keeping in mind the expected component variations, presented in section 3. So the resistors were implemented with potentiometers adjustable from 0 to 500 Ω. The capacitors was implemented using arrays of 6 +/-% electrolytic capacitors. The capacitance could be adjusted from approximately 10 to 630 μF with a resolution of 10 μF. The inductors are winded on ETD-49 un-gapped cores. A custom made accessory for the core allows the user to adjust the air gap with a screw driver. The inductance of can be adjusted from approximately 5 to 40 mH. The parasitic series resistance of the inductors was measured to be approximately 0.6 Ω. The power this circuit is able to handle is limited to the maximum ratings of the components used. Moreover this power is wasted and turned into heat. Fig. 10 shows the realized loudspeaker impedance emulator.

4.2. Measurements and results

During the measurements the 2.5" woofer with Thiele-Small parameters listed in table 5 was con-

Symbol	R_e	L_e	f_S	Q_{MS}	Q_{ES}	Q_{TS}	V_{AS}
Value	3.45 Ω	71 μH	114 Hz	12	0.55	0.53	0.61 L

Table 5: Thiele-Small parameters for given 2.5" woofer

	R_e	R_{es}	R_{el}	L_{ces}	L_{eq}	L_{ceb}	C_{mep}	C_{mes}
Inf. Baffle	3.45 Ω	75 Ω	-	8.8 mH	-	-	-	223 μF
Closed box	3.45 Ω	75 Ω	-	-	5 mH	-	-	223 μF
Vented box	3.45 Ω	75 Ω	1.11 Ω	8.8 mH	-	20.61 mH	167 μF	223 μF

Table 6: Component values needed for loudspeaker emulator implementation

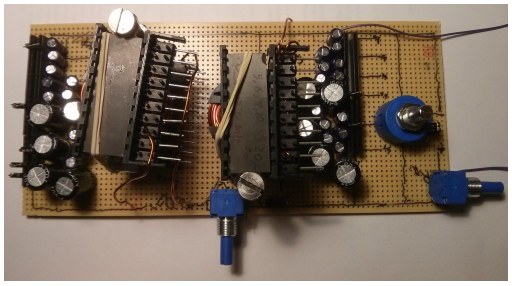

Fig. 10: Realized implementation of loudspeaker impedance emulator

sidered in three different configurations. They are:

- The 2.5" woofer in infinite baffle
- The 2.5" in closed box with 0.82 litres volume
- The 2.5" in vented box

The optimal vented box alignment was found to be a C4 alignment with:

$$\begin{aligned} \alpha &= 0.424 \\ f_B &= 85.6\text{Hz} \end{aligned} \tag{15}$$

The corresponding loudspeaker impedance emulator component values can be found using eq. 2, 3, 4, 5, 6, 9 and 10 and are listed in table 6.

The measurements was conducted the same way as in section 2.2.3. Fig. 11 shows the measured and calculated impedance of the 2.5" woofer in infinite baffle configuration. The component values of the loudspeaker impedance emulator was adjusted to match the values of R_e, R_{es}, L_{ces} and C_{mes} listed in table 6. The measured impedance corresponds very well with the expected one in terms of resonance frequency. However the peak impedance is lower than expected and this is due to the parasitic resistances in the capacitance and the inductance. Including the series resistance of approximately 0.6 mΩ of the inductor in the calculation of the impedance, a better correlation between measurement and theory is obtained.

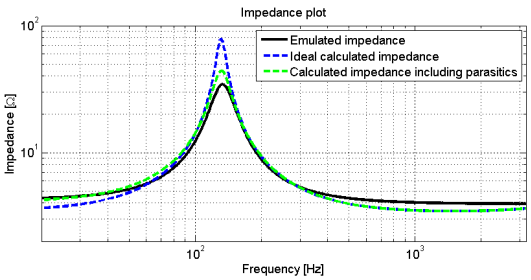

Fig. 11: Measurements of emulated and calculated impedance for the 2.5" woofer in infinite baffle

Fig. 12 shows the measured and calculated impedance of the 2.5" woofer in a closed box with 0.82 litres volume. The component values of the loudspeaker impedance emulator was adjusted to match the values of R_e, R_{es}, L_{eq} and C_{mes} listed in table 6. Again it is seen from the plot that the impedance is as expected, especially when taking the parasitic resistance of into account.

Finally fig. 13 shows the measured and calculated impedance of the 2.5" woofer in a vented box config-

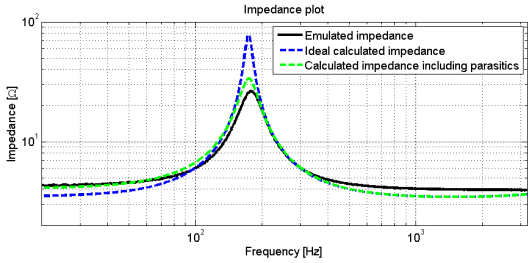

Fig. 12: Measurements of emulated and calculated impedance for the the 2.5" woofer in closed box

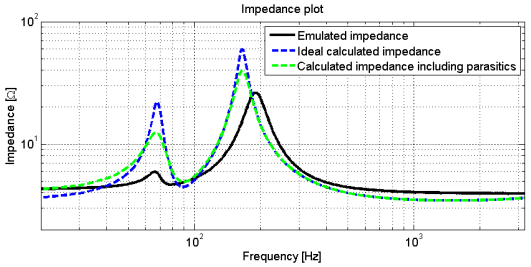

Fig. 13: Measurements of emulated and calculated impedance for the 2.5" woofer in vented box

uration. The component values of the loudspeaker impedance emulator was adjusted to match R_e, R_{es}, R_{el}, L_{ces}, L_{ceb}, C_{mes} and C_{mep} listed in table 6. From the plot we can see that the impedance is close to the expected impedance in terms of resonance frequencies. However the peak impedance of the Helmholtz resonance (the resonance around 70 Hz) is lower than expected, also when the parasitics of the inductors are taken into account. This is properly due to the fact that the potentiometer used for the implementation of R_{el} must be very accurate for low resistance values and this was not the case. This has the consequence that the resistance value of R_{el} becomes higher than intended, thus reducing the quality factor of the Helmholtz resonance. Moreover it is seen that the resonance frequency of the woofer in the cabinet enclosure also has a lower peak impedance that the expected one, even with the parasitic of the inductors included. Again this is due to the not optimal implementation of R_{el}. A higher resistance than expected of R_{el} will not only affect the Helmholtz resonance but also the driver's resonance.

5. CONCLUSION

This paper has presented a thoroughly analysis of loudspeaker models and loudspeaker drivers in general. Based on this a RLC based loudspeaker impedance emulator, utilizing switch controlled capacitors, air gap controlled inductors and potentiometers to adjust its impedance, was implemented.

Based on the work done in this paper it can be concluded that measurements of performance parameters for audio amplifiers measured in pure ohmic loads are not equivalent to that measured on frequency dependent loads such as loudspeakers. Moreover it can be concluded that the impedance of infinite baffle-, closed box- and vented box-loudspeakers can be modelled using electrical equivalent models, consisting of resistors, capacitors and inductors. A comparison of a measured impedance and the corresponding modelled one showed that the accuracy of the electrical equivalent loudspeaker model is good. In addition to this it was shown that the component values needed to implement the electrical equivalent models varies from 2 to 105 Ω, 0.3 to 80 mH and 190 to 440 μF for the most common drivers. Finally it can be concluded that loudspeaker impedance emulators may be implemented using switch controlled capacitors and air gapped control inductors. Results show good correlation between measured and modelled impedances.

6. FUTURE WORK

The future work involves includes further investigation of potential loudspeaker impedance emulators, especially of emulators capable of handling more power. Such an impedance emulator may be implemented using switch-mode technology. Using switch-mode technology the power drawn from the DUT may also be redistributed back to the grid. A switch-mode adjustable AC load has already been implemented by [13]. However this implementation only works for a static input frequency meaning that conventional performance parameters such as THD, IMD and crosstalk can not be measured. This may be corrected by using the proposed loudspeaker impedance from this paper as a part of the control network for a switch-mode based solution.

Moreover the proposed loudspeaker impedance emu-

lator should be improved in terms of precision. The switch controlled capacitors could be improved using digital logic. The resistances could be implemented with transistors, where the gate source voltage will determine the resistance values. The air gap in the inductors could be controlled more accurately with an electrical stepper motor. This could lead to more automated control which may increased the speed of the adjustment process. Finally the parasitic resistances of the inductors should be minimized in order to improve the loudspeaker impedance emulator's performance.

The author would also like to encourage a more elaborate description of loudspeaker impedance for different kinds of loudspeakers in future work. That include description of the impedance for transmission lines, horns, balanced armatures and so on, but also a cross-over's influence on the impedance in a loudspeaker system. In addition to this more reliable database of Thiele-Small parameters is desired.

7. REFERENCES

[1] J. Mønster, L. Crone, J. Pedersen, A. Knott. "Debugging of Class-D Audio Power Amplifiers" presented at the AES 132th convention, Budapest, Hungary, 2012 April 26-29. Convention paper 8630.

[2] N. E. Iversen, T. H. Birch, R. O. Ploug, A. Knott. "Investigation of Crosstalk in Self Oscillating Switch-mode Audio Amplifier" presented at the AES 132th convention, Budapest, Hungary, 2012 April 26-29. Convention paper 8631.

[3] H. Dymond, P. H. Mellor. "An Active Load for Evaluating the Efficiency of Audio Amplifiers" presented at the AES 125th convention, San Francisco, USA, 2008 October 2-5. Convention paper 7572.

[4] K. Thorborg, A. D. Unruh, C. J. Struck. "An Improved Electrical Equivalent Circuit Model for Dynamic Moving Coil Transducers" presented at the AES 122th convention, Vienna, Austria, 2007 May 5-8. Convention paper 7063.

[5] R. Aiken. "Designing A Reactive Speaker Load Emulator". 2006.

[6] A. Knott, L. P. Petersen "Comparison of Power Supply Pumping of Switch-mode Audio Amplifiers with Resistive and Loadspeakers as Loads" presented at the AES 134th convention, Rome, Italy, 2013 May 4-7. Convention paper 8838.

[7] N. E. Iversen, A. Knott, "Small signal loudspeaker impedance emulator". Technical University of Denmark, Kgs. Lyngby, Danmark. Presented at the AES 136th convention, Berlin, Germany, 2014 April 26-29. Convention paper 9053.

[8] W. M. Leach, Jr. "Introduction to Electroacoustics and Audio Amplifier Design", Kendall/Hunt Publishing Company, 2003.

[9] A. N. Thiele, "Loudspeakers in vented boxes, Parts I and II", J. Audio Eng. Soc., vol. 19 pp. 382-392 (May 1971); pp. 471-483 (June 1971),

[10] R. H. Small, "Closed-box loudspeaker systems", J. Audio Eng. Soc., vol 20 pp. 383-395 (June 1972).

[11] http://petoindominique.fr/

[12] D. K. Cheng, "Field and Wave Electromagnetics", Addison Wesley Publishing company, 1989. ISBN 0-7923-7270-0.

[13] I. W. Jeong, M. Slepchenkov, K. Smedley and F. Maddaleno, "Regenerative AC Electronic Load with One-Cycle Control", Dept. of Electrical Engineering and Computer Science, University of California, Irvine, USA.

M

Design and Implementation of a High Efficiency Subwoofer

Accepted for 144th Audio Engineering Soceity convention, Milan, May 23-26, 2018.

Audio Engineering Society

Convention Paper

Presented at the 144th Convention
2018 May 23 – 26, Milan, Italy

Design and Implementation of a High Efficiency Subwoofer

Sebastian Tengvall[1], Niels E. Iversen[1], and Arnold Knott[1]

[1] *Technical University of Denmark*

Correspondence should be addressed to Arnold Knott (akn@elektro.dtu.dk)

ABSTRACT

The demand for battery driven loudspeakers is increasing but the challenge of efficient low frequency reproduction remains. An alternative approach to the conventional 4th order bandpass enclosure design for a subwoofer to achieve a high peak in the passband and increase voltage sensitivity is investigated. The response is corrected with DSP to ensure a flat response in the passband. The results proved that this approach can increase the voltage sensitivity dramatically, reaching an average sensitivity of over 100dB in the passband from 45Hz to 90Hz. It also showed that the design is sensitive to construction errors. Precise assembling is required to achieve satisfactory results, while small errors can ruin the purpose of the design.

1 Introduction

Enjoying music is no longer limited to sitting in a chair in your living room and playing back your favourite tunes. People are starting to bring their music with them when moving outdoor and socialising with friends and want to share their music with the people around them in this growing lifestyle fashion[1]. This has made the loudspeaker industry grow from big power demanding loudspeaker in a living room to small and efficient battery driven loudspeakers that you can bring along as portables. However, high performance is still desired. This creates an exceptional challenge for audio engineers, as physical limits to what is possible with traditional loudspeaker designs, are met. With modern technology like Class D audio amplifiers and Digital Signal Processing (DSP) new ways, such as slave bass and using dynamic bass, to optimise low frequency performance in small cabinets are appearing.

One of the biggest challenges is how to achieve powerful SPL in small designs at low frequencies. One problem is the physical limitations; if high SPL is desired, a lot of air needs to be moved. The second problem is that low frequencies require more power than high frequencies, thus efficiency is a problem at low frequencies, when using traditional closed or vented boxes as described in [2]. An approach to reduce the power needed at low frequencies is investigated in [3]. By exploiting the speakers high efficiency around its resonance point, the overall efficiency is improved. This is also investigated in [4]. The proposed design was with a standard vented box and with small loudspeaker drivers and concluded that if used in larger outdoor systems (greater than 20 litres) that runs of battery, it will benefit from this alternative design approach.
This paper builds on the research conducted in [3] of driving the loudspeaker around its resonant frequency to increase efficiency, but by using a different type of enclosure and with a bigger loudspeaker driver. The enclosure type used is the 4th order bandpass enclosure, which pushes the second impedance peak towards a higher frequency, where the vented enclosure usually has one above 20 Hz and the second one at a much

lower frequency.

The goal is to see if pushing the lower end impedance peak to a higher frequency, and thereby drive the speaker between the two impedance peaks can increase the voltage sensitivity compared to a traditional vented enclosure.

This paper will briefly present the 4th order bandpass cabinet and the most important design parameters and how they have been used in this research case.
The difference from the conventional 4th order bandpass design will be shown and the potential that it could prove is demonstrated.
Selection of the driver and cabinet tuning is presented next, along with simulation results of a small signal model of the configuration.
The measuring setups and results of the measurements are shown and held against the simulated results and discussed upon.
Finally concluding remarks, based on the discussion, are presented to summarise the paper.

2 Methods

In this paper the desired specifications are:

- 15 ” driver
- Passband response between 45 Hz to 90 Hz
- 2.83 V (at speaker terminals) sensitivity of minimum 98 dB SPL
- Maximum volume size of 150 L

2.1 Cabinet design

Fig. 1 shows the 4th order bandpass enclosure. It is named this due to a high pass and low pass roll of, which characterise a 2nd order slope. This yields a bandpass between the two impedance peaks, which is where the subwoofer will be driven. Depending on the rear chamber and front chamber size, along with the tuning frequency of the vent, different passband parameters can be acquired. The first parameter is the passband, which is defined from the -3 dB low cut to the -3 dB high cut. The cuts are defined when the response has dropped -3 dB compared to the response in the middle of the passband.

The second parameter is the passband gain, which is the additional decibels gained compared to what the

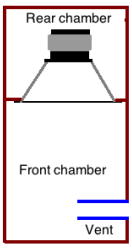

Fig. 1: Overview of 4th order bandpass design.

driver is measured to in free space. This is achieved through different tuning of the enclosure and vent.

The last parameter is the passband ripple, which is defined as the difference between the highest and lowest point in the passband.

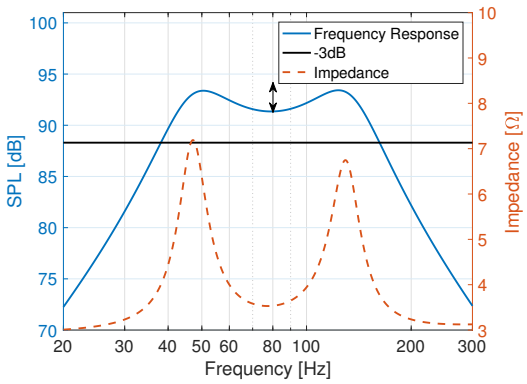

Fig. 2: The passband parameters in a conventional 4th order bandpass design.

These three parameters allows the designer to tune the response to a specific application. As with all loudspeaker designs, the three parameters pull in separate directions; increasing the gain in the passband reduces the actual passband width. Allowing a bigger ripple in the passband can again help to achieve a wider passband. Thus, a compromise between the three design parameters must be made.

Due to these characteristics, this design is mostly suitable for low frequency applications, like a subwoofer, because of the defined passband and that it uses the vent to play through. Previous work on bandpass loudspeakers is presented in[5] and another one researching the

specific use for subwoofers is presented in [6]. Additional research about the bandpass cabinet is conducted and findings concluded in [7], [8] and [9].

Fig. 2 shows that the impedance is lowest in the middle of the passband, and a lot of current will be drawn from the amplifier at this point. In this example, the response is not great at this point, so a lot of current will be needed, but a higher SPL will not be achieved, compared to the edges of the passband.

However, if the enclosure is built and tuned to achieve a very high gain in the passband instead of a flat passband or with a ripple (dip), a DSP can be used to flatten the passband, and a lot of current can be saved and thereby power effectively increasing the efficiency of the loudspeaker.

This will be the approach for the 4$^{\text{th}}$ order bandpass enclosure.

2.2 Driver selection

Due to this type of enclosure design, there are no general guidelines or recipes defined to guarantee acceptable results with specific drivers. However the general design rules for a closed box and vented box can still be applied to some extent. These are that drivers with high values of Q_{ts} are well suited for closed box designs, whereas drivers with low Q_{ts} are better suited for vented box designs [10].

Selecting a driver which performs well in a closed enclosure is considered more important than one for a vented enclosure. This is because the vent in the vented enclosure gives some tuning possibilities, whereas the closed enclosure only depends on the volume of the box. Selecting a driver with a high Q_{ts} is therefore prioritised.

To achieve high output levels at low frequencies, the driver should also have a high sensitivity rating and a low resonant frequency, f_s.
A 15 inch (38 cm), 4 Ω nominal driver was selected for the application. The full product name is DCS380-4 [11]. This driver was selected because it had a high quality factor, of $Q_{ts} = 0.483$ and a low resonance frequency of $f_s = 21.5Hz$, with a nominal sensitivity of 93.6 dB measured at 2.83 V at 1 m.

2.3 Cabinet tuning

To ensure a high gain performance in the passband of the design, the closed box resonance frequency should be at the centre frequency of the passband. Using the vent in the vented enclosure to tune the Helmholtz frequency to the same as the closed box resonance ensures a high gain at the center frequency of the passband. Increasing the volume of the vented enclosure, will increase the peak of the Helmholtz frequency, but the impedance created by it will also start dominating, so that the impedance of the closed box will diminish. Good results are achieved, when the two impedance peaks are of equal size.

2.4 Simulation

A SPICE small signal simulation model using the model given by [2] was made to simulate the behaviour of the driver in the enclosure. Fig. 3 shows the small signal model.

Many different box sizes and vent tunings were simulated to see which gave the best performance. The best performance was achieved with a rear chamber of 30 L, front chamber of 110 L and a vent tuning of 70 Hz. However, due to the driver taking up some of the volume in the rear chamber, a 40 L enclosure was used instead.

Fig. 4 shows the simulated response and impedance.

The peak is seen to appear slightly to the right in the passband. The best case would be to have it centered, so that it would be exactly between the two impedance peaks. Lowering the rear chamber volume would achieve this, and since the actual volume seen by the driver is lower than 40 L, which was used in the simulation, this should not be a problem. Another solution would be to increase the size of the front chamber, but this would increase the overall size of the subwoofer, which is not desired. Lowering the Helmholtz frequency, would require to also increase the volume of the vented enclosure in order to achieve a peak in the passband.

Thus, this simulated design was deemed the best possible solution and was the one to be built and assembled.

The enclosure is built using 22 mm Medium Dense Fiberboard (MDF) and the edges are glued together

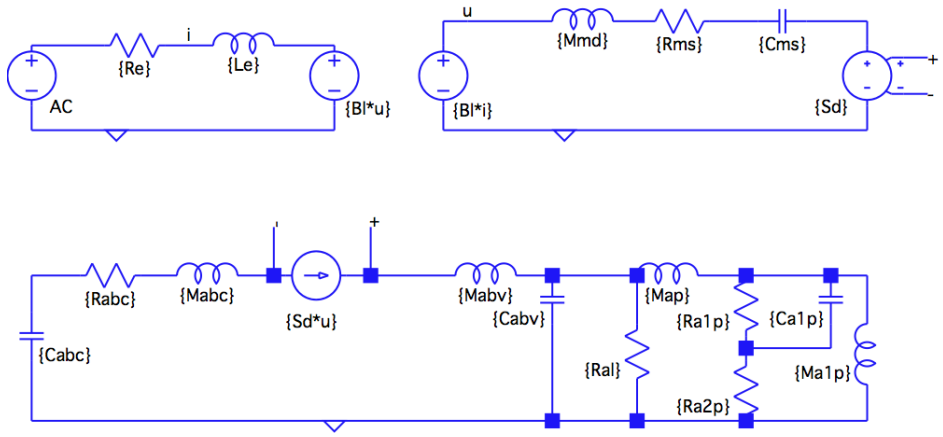

Fig. 3: Spice model simulation separated into an electric, mechanic and acoustic equivalence. The model includes radiation impedance in front of the vent as well.

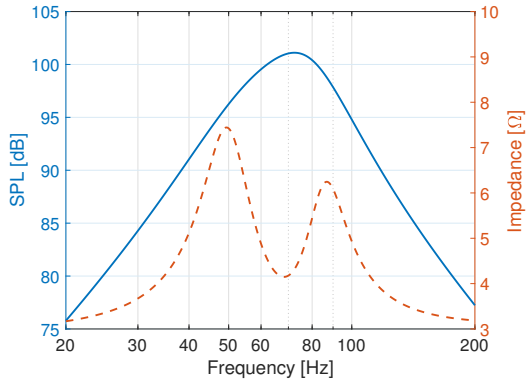

Fig. 4: Pressure response and impedance simulated with spice model. 2.83 V at 1 meter in a 2π environment.

to proper seal the enclosure and tightened with screws. Polyvinyl chloride (PVC) pipes with a diameter of 7 cm are used for vents. 4 vents with a length of 3.3 cm must be used to achieve the target Helmholtz frequency of 70 Hz. This was found through equation (1), which is given by [2].

$$L_p = \left(\frac{c}{2\pi f_b}\right)^2 \frac{S_p}{V_{abv}} - 1.462\sqrt{\frac{S_p}{\pi}} \qquad (1)$$

The subtraction in equation (1) is due to end correction. Due to a small amount of air mass which moves in front of the vent at either end, the vent will act longer than it physically is, thus a subtraction has to be made. The vent will be flanged in one end and unflanged in the other, and a subtraction factor of 1.462 equals this configuration [2].

Since 4 vents are used to cover the total area required, S_p, the end correction gets much more complicated, because the air masses in front of each vent will affect each other depending on placement. How they affect each other have not yet been documented properly. However, using equation (1) to model the four vents as one big vent, and changing the end correction to just account for one of the vents was deemed to be a reasonable compromise. The equation is thus changed to:

$$L_p = \left(\frac{c}{2\pi f_b}\right)^2 \frac{S_p}{V_{abv}} - 0.731\sqrt{\frac{S_p}{\pi}}$$

This yielded a vent length of 3.3 cm. It must be noted, that this is a simple approximation of the true end correction when using multiple vents. Fig. 5 shows the assembled subwoofer.

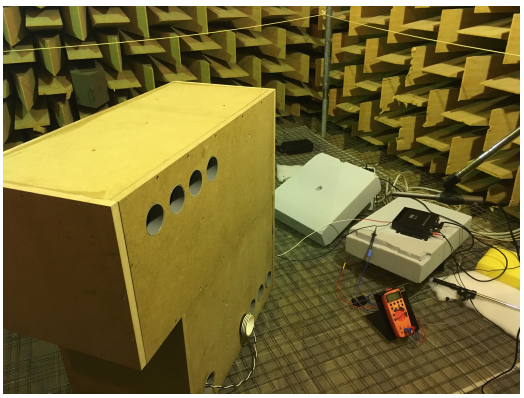

Fig. 5: The assembled subwoofer with the 4 vents facing the microphone.

2.5 Measuring Setup

Three different measurements were made. A frequency response, apparent power consumption and impedance measurement. They were performed according to the following descriptions.

2.5.1 Frequency Response

The frequency response measurement was conducted in an anechoic chamber. The chamber is approximately 60 m^3 and has a lower frequency limit of about 100 Hz. This means that reflections of frequencies below 100 Hz might occur and affect the response. To reduce the reflections, the measurement was conducted with a 0.5 m distance between the subwoofer and microphone, thus increasing the relative distance to the walls compared to the measuring distance. This does however not comply with standard measurements, which are made at 1 m distance. Referring to [12], which presents the pressure equation for a monopole (recited in equation (2)), where p is the pressure, Q is the volume velocity and ω is the radial frequency. This is a good approximation for low frequency reproduction, and it is seen that halving the measuring distance, r, leads to doubling the pressure, p.

$$p = \frac{\rho \omega Q}{4\pi r} \tag{2}$$

On the logarithmic scale a factor of 2 equals approximately 6 dB.

$$20\log 10(2) \approx 6dB$$

A subtraction of 6 dB to the measurement was applied later to emulate a distance of 1 m. This setup should attenuate the reflections below 100 Hz compared to the direct sound wave that the microphone measures.

The measurement was performed with a logarithmic sweep signal from 20 Hz to 200 Hz using Room Equalization Wizard (REW) and the UMIK-1 microphone by MiniDSP. The measuring voltage was set at 2.83 V.

A second frequency response with a DSP was also made. The DSP applied a high frequency cut at 45 Hz and a low pass cut at 95 Hz along with a parametric equalisation to make the passband response as flat as possible.

2.5.2 Power Consumption

Apparent power consumption was found by measuring the current running into the subwoofer and the voltage across its terminals during a 10 second logarithmic sweep from 20 Hz to 200 Hz. A TELEDYNE LECROY MSO 104MXS-B was used to perform this measurement, with a AP015 current probe.

Information about the phase difference between the voltage and current could not be obtained this way, thus only the apparent power [VA] can be accurately found through this measurement. However, through the SPICE simulation an approximation of the impedance phase can be used to calculate the real power consumption. This is done and explained in the discussion section. The product of the current and voltage during the sweep was calculated to find the apparent power consumption in the sweep.

The apparent power consumption was also measured when the DSP was applied as described in the frequency response measurement.

2.5.3 Impedance Measurement

Fig. 6 shows the measuring setup for the impedance. The impedance was found from the loudspeaker voltage, V_1 and the reference voltage V_2. Assuming that the loudspeaker impedance is much smaller than the 1 kΩ resistance, the current in both cases can be assumed to be the same. Thus the impedance is calculated through equation (3).

$$Z_L = 3.3\frac{V_1}{V_2} \tag{3}$$

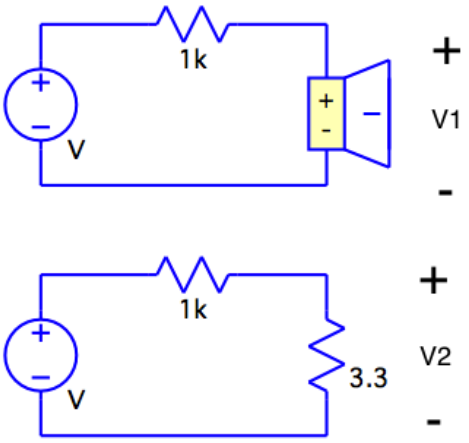

Fig. 6: Measurement setup for impedance.

3 Results

Fig. 7 shows the frequency response along with the impedance measurement. The passband is seen to be from approximately 50 Hz to 90 Hz but the desired peak in the middle of the passband is not seen, as Fig. 4 shows in the simulation. It is also observed that the response is a bit higher around 80 Hz compared to the rest of the passband, which could indicate that the peak occurs at 80 Hz instead of the target design of 70 Hz. The peak is also not as high as desired. Also, the impedance peaks does not appear at the edges of the passband, but are shifted slightly to the left of what was expected.

Fig. 8 shows the apparent power consumption measured with and without DSP applied along with the pressure response. The parametric equalisation applied with the DSP was a -6 dB attenuation at 70 Hz with a quality factor of 1. Additionally a 8^{th} order high pass cut at 45 Hz and a low pass cut at 90 Hz was applied with the DSP.
The power consumption is as expected, lowest at the edges of the passband, as this is where the impedance is the highest. In the middle of the passband, the power consumption is highest. This was also the expectation. Naturally the power consumption is quite large outside of the passband, but the subwoofer is not intended to be used outside the passband and is corrected with the DSP.

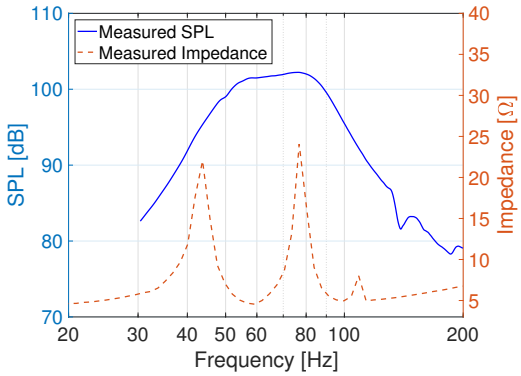

Fig. 7: Frequency response and Impedance at 2.83V at 1 meter distance.

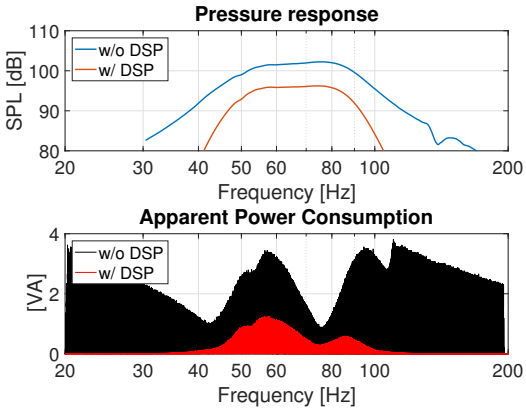

Fig. 8: Response and apparent power with and without DSP filters. Performed with a 10 s logarithmic sweep from 20 Hz to 200 Hz. RMS voltage at terminals without DSP is 2.83 V. RMS voltage as a result of the applied DSP in the passband from 45 Hz to 90 Hz is 1.42 V.

Even though a peak in the passband was not acquired, the parametric equalisation still achieves to flatten out the passband response, achieving a nice flat response across the passband.
There is clearly an advantage of using a DSP to attenuate frequencies outside of the passband, as this reduces the overall power consumption a lot. In the passband, the power consumption is also lower as a result of the parametric filter applied by the DSP, thereby reducing the RMS voltage in the passband

from 2.83 V to 1.42 V.

The design goals listed in the beginning of this paper correlates well with these results, even though the exact simulated results was not achieved. The passband stretches approximately from 48 Hz to 90 Hz, which is very close to the design goals of 45 Hz to 90 Hz. The measurement without DSP applied is seen to reach just above 100 dB in the passband at a RMS voltage of 2.83 V, which is well above the listed voltage sensitivity of 98 dB at 2.83 V.
Because the impedance phase was not measured, an accurate representation of the real power consumed could not be made. However, an approximation can be made by using the impedance phase found in the SPICE simulation. This is done and evaluated in the discussion section.

4 Discussion

The measured results do not completely match the simulation, but still mostly manages to meet the requirements specified in the introduction. The mismatch between simulation and reality could be due to several factors, which were investigated by fitting the simulation to the actual measurements. Fig. 9 shows the results of aiming to fit the response curve to the measured curve.

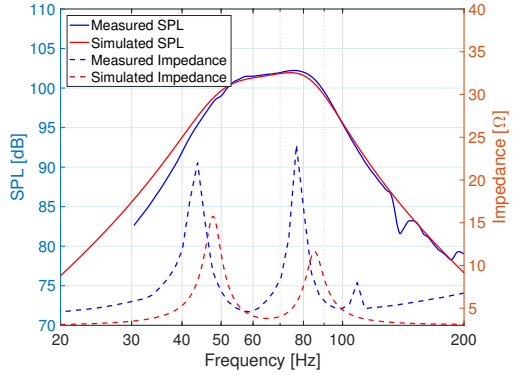

Fig. 9: Measured result VS simulated fit with response without any DSP and a RMS voltage of 2.83 V.

This simulated fit was achieved by lowering the radiation impedance in front of the vents and shifting the vent tuning frequency to 80 Hz as seen in the measurement. This clearly indicates that modelling the radiation impedance when using multiple vents is much more complex than simply having one vent. It clearly shows that depending on the position of the vents and how close they are to each other, they will interact with each other in different ways. If placed close to each other, each individual vent will no longer radiate in a half space, but something less, due to its neighbouring vents, thereby reducing the overall radiation impedance[2]. This is why lowering the radiation impedance in the simulation yields a response curve closer to the measured response curve.

It is also seen that the vent tuning frequency is actually higher than the target of 70 Hz, which is why changing this in the simulation, also helps shaping the curve closer to what is measured. The shift in tuning frequency is most likely due to the simplification of the end correction, which was discussed during the method chapter. The higher tuning frequency actually shows that the end correction should be even lower, than what was approximated. This can be seen in equation (1). From these observations it is seen that the radiation impedance and end correction is closely related. This was not investigated further, as it is not in the scope of this paper.

The SPL level of the fitted simulation also aligns nicely with what was measured. The sensitivity requirement was met, however, based on the simulations it is thought that an even higher sensitivity is possible if the desired peak in the passband, as shown by Fig. 4, was achieved. This would have caused a higher response in the passband and possibly also a wider passband response. This hypothesis is left for future work and research.

Because the vent tuning is different from the target tuning, reducing acoustic losses in the simulation doesn't increase the peak as would be expected. This shows how important the vent tuning is for the 4^{th} order bandpass design, in order to achieve the high peak in the passband as desired.

Even with a fitted response curve, the impedance does not match the measured impedance. The peaks are shifted slightly to the left and are bigger than simulated. Although the simulation shows that the left peak should be higher than the right, the measured impedance shows the opposite.
Fig. 10 shows the result of trying to fit the simulated impedance to the measured impedance. It is seen that it changes the response curve to have a peak at the

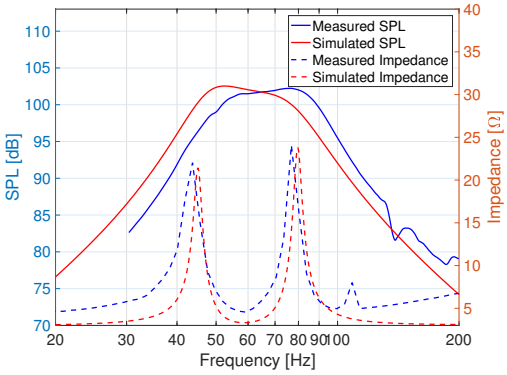

Fig. 10: Measured result vs simulated fit with impedance.

lower end of the passband instead. One possible conclusion for the appearance of the difference in impedance could be due to leakage between the closed box and vented box designs. For simplicity this leakage was not included in the simulation. A thorough analysis of leakage and losses in a 4th order bandpass design is researched and explained further in [13] and it is concluded that leakage losses between the two enclosures are the most important one for these types of design and can change the expected response curve dramatically if not accounted for in simulation. Fig. 7 clearly illustrates this phenomena, as the impedance curve is very much different to that showed in Fig. 4. Another important statement, is that these leakage losses affect the response even more, when the design is not symmetrical, as is very much the case in the design presented in this article.

If more research is to be conducted on this design approach, using a simulation with included leakage between the closed and vented enclosure should be prioritised. Proper assembling of the enclosure should also be ensured to reduce leakages.

By using the simulation model where the impedance was fitted to match the measurement, an approximation of the real power consumed can be made, based on the impedance phase in the fitted simulation.

Fig. 11 shows the impedance and phase from the simulation. The second plot shows the power factor. The power factor was calculated as the cosine of the impedance phase, $\cos\phi$.

The power factor goes toward unity at places where the slope of the impedance is flat and the real part of the impedance dominates. When the slope of the impedance is steep, the imaginary part of the impedance dominates and the power factor is thereby reduced.

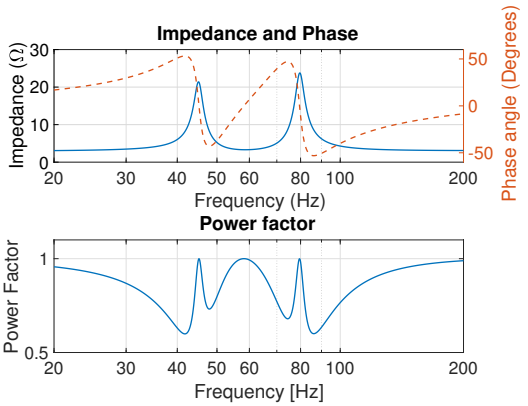

Fig. 11: SPICE simulated Impedance and phase along with the power factor as calculated from the impedance phase.

Multiplying the power factor with the apparent power measurement for each frequency, then yields an approximation of the real power consumed. Fig. 12 shows the results of the power consumption with and without DSP with the same voltages as stated earlier in the result chapter. For comparison the apparent power is also displayed.

The average values of the real power and apparent power shows that the real power is only slightly lower than the apparent power. Even though this is an approximation from the impedance achieved through the SPICE simulation it can still be used as an estimation of the real power consumption.

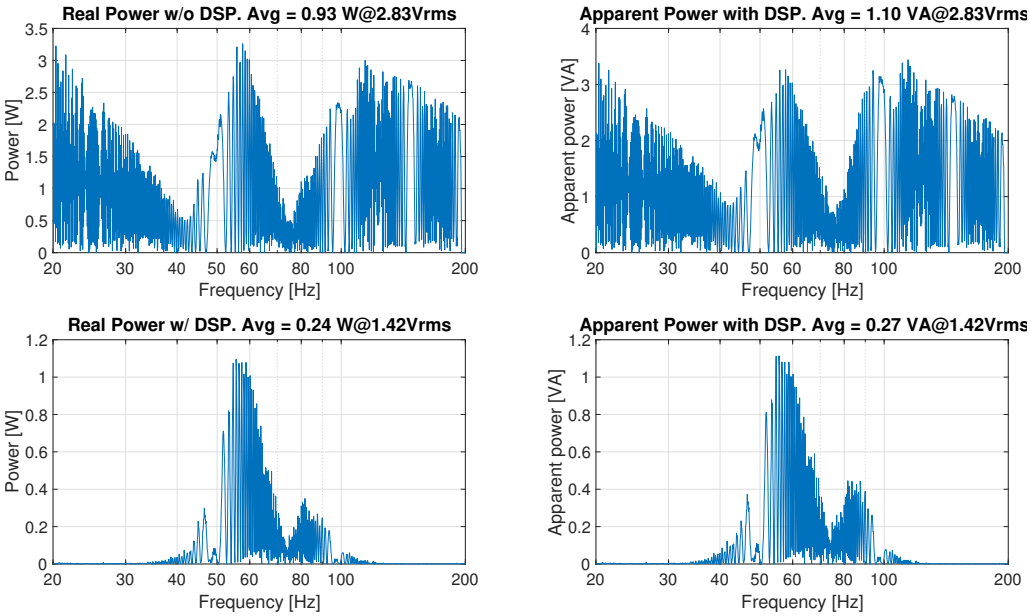

Fig. 12: Approximated real power and apparent power consumption during a 10 s logarithmic sweep. The displayed average power is only for the passband limit of 45 Hz to 90 Hz.

5 Summary and Conclusion

Even though the actual design did not match the simulation perfectly, it is still shown that it is possible to increase the voltage sensitivity in a subwoofer by the use of a 4th order bandpass design. The results show that the design is very sensitive to small errors during the construction phase of the enclosure. Small mistakes in the building process can lead to changes of the expected response curve compared to the simulation, which will critically affect the performance of the subwoofer.
Correct tuning of the vent is also extremely important. If this is just slightly of the design target it will lead to a much lower gain in the passband and also at the wrong frequency, which will ruin the concept of the design idea.

If precise assembling of the enclosure is possible and thus reducing the acoustic leakage between the enclosures, the peaky behaviour in the middle of the passband is still considered to be achievable. And with the implementation of a DSP, a nice and flat passband response is obtained with very low power consumption, making it an efficient alternative to low frequency reproduction in battery driven application.

References

[1] Tiwari, R., "Bluetooth Speakers Market Worth $7 Billion by 2019," *PRNewswire*, 2014.

[2] W. Marshall Leach, J., *Introduction to Electroacoustics and audio amplifier design*, Kendall Hunt, 4th edition, 2010, ISBN 978-0-7575-7286-9.

[3] Thydal, T., "Efficiency Investigation of Subwoofer Driven Around Resonance Frequency," 2016.

[4] Zuccatti, C., "Direct-radiator loudspeaker efficiency at fundamental resonance," *AES: Journal of the Audio Engineering Society*, 53(4), pp. 307–312, 2005, ISSN 15494950.

[5] Geddes, E. R., "Correction to -An Introduction to Band-Pass Loudspeaker Systems-," *Journal of the Audio Engineering Society*, 42(3), pp. 152–152, 1994, ISSN 00047554.

[6] Thiele, N., "Bandpass subwoofer design," *AES: Journal of the Audio Engineering Society*, 62(3), pp. 145–160, 2014, ISSN 15494950.

[7] Nieuwendijk, J. and Philips Consumer Electronics, "Bandpass Loudspeaker Enclosure with Long Port," 1993.

[8] Fincham, L. R., "A Bandpass Loudspeaker Enclosure," *AES: Journal of the Audio Engineering Society*, 1979.

[9] D'Appolito, J., "Designing Symmetric Response Bandpass Loudspeakers," *Audio Engineering Society Convention 91*, 1991.

[10] Dickason, V., *The Loudspeaker Design Cookbook, 7th Edition*, volume 106, 2006, ISBN 1-882580-47-8, doi:10.1121/1.428228.

[11] Dayton Audio, "DCS380-4 15" Classic Subwoofer 4 Ohm," *Dayton Audio*, 2015.

[12] Jacobsen, F., Poulsen, T., Rindel, J. H., Gade, A. C., and Ohlrich, M., *Fundamentals of Acoustics and Noise Control*, 31200, 2010, ISBN 9781905209255, doi:10.1002/9780470612439.

[13] Andrzej, D., "The Influence of Losses on the Frequency Response of the Band-Pass Loudspeaker Systems," *Audio Engineering Society*, 2002.

N

Efficiency Investigation of Subwoofer Driven Around Resonance Frequency

In 142nd Audio Engineering Soceity convention, Berlin, May 20-23, 2016.

Audio Engineering Society

Convention Paper

Presented at the 142nd Convention
2017 May 20–23, Berlin, Germany

Efficiency Investigation of Subwoofer Driven Around Resonance Frequency

Tobias Thydal[1], Niels Elkjær Iversen[1], and Arnold Knott[1]

[1] *Technical University of Denmark*

Correspondence should be addressed to Tobias Thydal (Tobiasthydal@gmail.com)

ABSTRACT

The need for efficient portable speaker systems has increased tremendously over the past 10 years. The batteries, amplifiers and filtering has all seen great improvements in efficiency leaving the speakers units as the most inefficient part of the system, mainly due to the large amounts of current drawn that ends up being dissipated as heat in the voice coil.
This paper will look at how you can design a speaker system to take advantage of the resonance of a speaker unit, since that is where the unit is most efficient and draws the least current. A subwoofer speaker system will be designed with focus on only driving the speaker units near their resonance frequency.
The tests found that with modern DSP it was rather simple to design a speaker system that operate in a very narrow frequency band around the speaker units' resonance frequencies, which in turn ensured a very small current draw. This greatest drawback of this method is the increase in components needed, which drives up cost and complexity.

1 Introduction

Portable speaker system sales continue to increase [1], and so demand for efficient speaker systems that can last longer on a single battery charge increases.

Looking at the individual parts of a portable speaker system it can most often be summed up into the battery, the amplifier, filtering and the speaker(s).
Batteries generally increase in size and weight, whenever you want to increase the amount of energy storage. To ensure portability the battery size and weight must be kept down. So in order for the system to be able to play music for longer periods of time the rest of the system must be optimized.
The development of class D amplifiers has made it possible to design amplifiers with an efficiency of up to 90-95% [2, 3, 4], which makes them near perfect for use in portable speaker system. Moreover they provide great audio performance with very low distortion [5, 6].
The filtering of the signal going from the amplifier to the speaker units is often handled by a digital signal processing unit (DSP), which means a small physical footprint, fine tuning of the frequency response and a low power consumption [7].
This leaves the speaker unit, which is incredibly inefficient compared to the other parts of the system. Most speakers have an efficiency of 0.5-2% [8, 9], meaning that only 0.5-2% of the power send into the speaker unit's voice coil (VC) will generate pressure waves. The rest of the power is converted to heat in the voice coil. Since the nominal impedance of most speaker units is between 2-8 Ω a lot of current is

needed to achieve high sound pressure levels (SPL). This combined with the fact that most portable speaker systems are used outdoors where the sound escapes more easily means that the battery drains fast.

One way to reduce the need for current is to increase the impedance, since

$$P = I^2 \cdot R$$

Looking at an impedance plot for any dynamic speaker unit you will find that the impedance of the VC increase tremendously around the resonance frequency of the driver. This behaviour is what will be used to design a speaker system that draws less current

This paper will investigate the possibility of designing a speaker system where each speaker unit only operates near its resonance frequency to take advantage of the higher impedance.
A speaker system consisting of two different speaker units together covering the frequency band from 65-110 Hz will be designed and assembled. The reason for the frequency band is because of how much content most modern music contains in that frequency band and because it is in the lower frequencies the most current is needed to produce a satisfactory SPL. The SPL at 1W@1m when driven with pink noise will be measured along with the current and voltage needed to produce said SPL. As real music is dynamic pink noise is used because it more closely resembles the energy distribution of music compared to white noise [10, 11, 12, 13].

2 Methods

2.1 Design Choices

2.1.1 Speaker Units

The two units used in this project are a 2 inch sub woofer unit and a 3 inch sub woofer unit, both off the shelf speaker units. The main reason for choosing these two unit was the very high impedance rise near the units' resonance frequencies, which are 75 Hz and 55 Hz respectively. This makes the drivers very suitable for the purpose of this paper.
The 2 inch driver is a Tang Band W2-2040S with a peak impedance of 70 Ω as seen in 1. The sensitivity of this speaker unit approximately 74 dB, which means that it will output a SPL of 74 dB at 1 m with 1 W of input power.

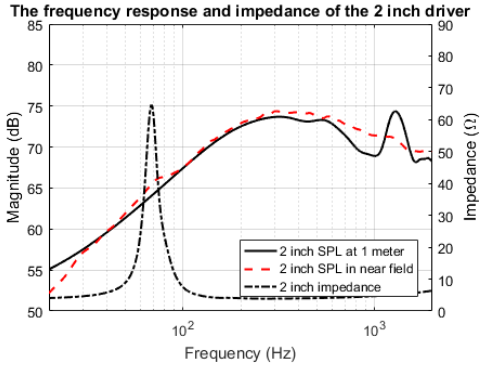

Fig. 1: Frequency response and impedance of the W2-2040S

The 3 inch driver is a Tang Band W3-1876S with a peak impedance of about 25 Ω as seen in 2. The sensitivity of this speaker unit is approximately 77 dB.

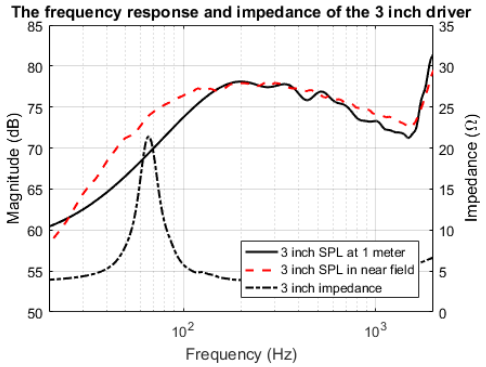

Fig. 2: Frequency response and impedance of the W3-1876S

The sensitivity of both speaker units is rather low compared to most regular high fidelity (Hi-Fi) speaker units that usually have a sensitivity of 83-89 dB [14]. This does not say as much about the final design however, as we will find the total SPL of the two speakers playing together, which will increase the sensitivity. Placing the speaker units in cabinets will also increase the sensitivity, and so the choice of speaker cabinets will help ameliorate this [15].

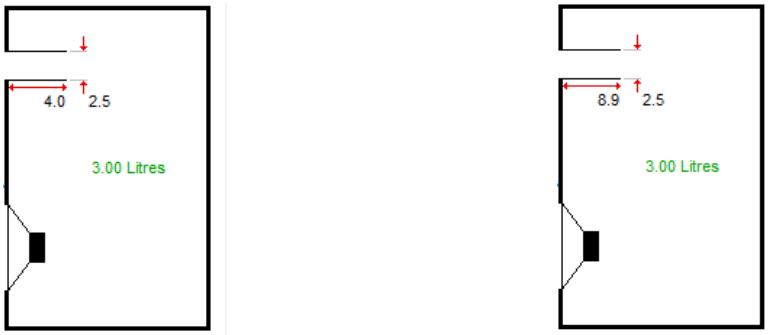

(a) Cabinet dimensions for the 2 inch speaker unit **(b)** Cabinet dimensions for the 3 inch speaker unit

Fig. 3: Dimension of the two cabinets simulated in FINEBox

2.1.2 Cabinets

When designing the cabinet certain requirements had to be met, since this project looks at efficiency improvements in portable set-ups. The speaker units are sub woofer units intended for reproducing the lower frequencies, and so it was decided that the frequency response of speaker set-up had to cover 65-100 Hz at an SPL of at least 85 dB at 1W/1m in order to keep the system competitive with commercially available speaker system. This had to be achieved while keeping the total internal volume under 6 L, so that the setup was still somewhat portable.

With the previously stated requirements in mind and looking at the speaker units' specifications, especially the total Q factor, Q_{ts} (0.26 and 0.43 for 2 inch and 3 inch speaker units respectively), it was decided that a vented box design would be the most suitable for the job [8, 16]. By using a vented box, we could achieve a higher SPL in the same frequency band as the vent allows for a higher SPL at the lower frequencies. Using FINEBox from Loudsoft the internal volumes of the two cabinets were found along with the dimension of the vents, which can be seen in figure 3. To achieve a high SPL in the frequency band specified we took advantage of the output of the vent, which is why you observe such a peaky behavior in figure 4. This will be used, when designing the crossover. Also, the 3 inch is about 3 dB lower in SPL, but this will be boosted via DSP. See section 2.1.3.

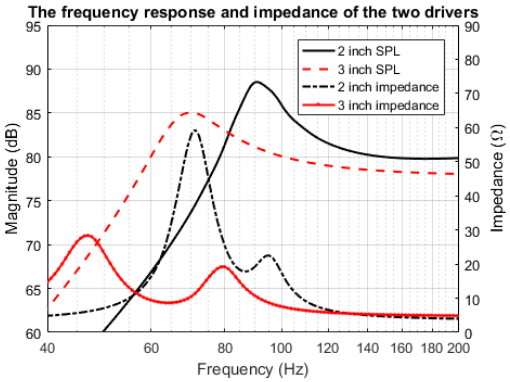

Fig. 4: Frequency response and impedance of the two speaker units in FINEBox

The frequency response and impedance of the two speaker units in their individual cabinet were simulated in FINEBox and can be seen in figure 4.
It is seen in figure 4 that the SPL of the 2 inch speaker unit is 3 dB higher than that of the 3 inch speaker unit. This is a consequence of having the 3 inch speaker reproduce lower frequencies with the same cabinet volume. To achieve a more even combined frequency response we can either attenuate the output of the 2 inch or boost the output of the 3 inch. Attenuating is not desirable, since we would lose max SPL. Looking at the excursion of the VC of the 3 inch in figure 5 we can see that diaphragm is hardly moving in the frequency band we wish to drive it in. Looking at the specifications of the 3 inch speaker unit we can see that Xmax (maximum excursion of the VC) is 5 mm, which

means that we can boost the output of the 3 inch via DSP (Digital Signal Processing) without risking the VC overextending.

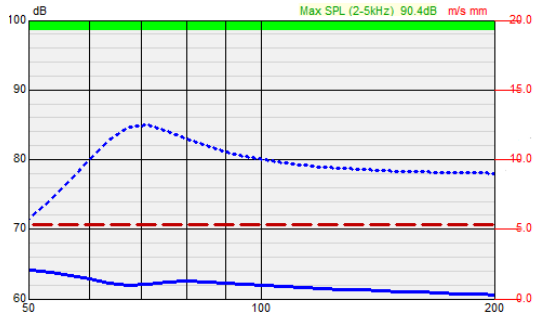

Fig. 5: Excursion of the VC (solid line) versus the frequency response (dashed line) of the 3 inch speaker unit

2.1.3 Crossover

The crossover between the two speaker units was chosen so that they would operate ± 3 dB around their highest SPL output. This means that the 3 inch speaker unit has to operate between 65-85 Hz and the 2 inch speaker unit has to operate from 85-110 Hz, see figure 4. Since the two speaker units operate in such narrow bands and so close to each other that very steep slopes are needed, i.e. -48dB/oct. It was quickly decided against passive components as it would involve too many components that would take up too much space, introduce large losses while being more difficult to achieve.
The next possibility was active components, i.e. Sallen-Key filters. Active filters was also decided against again due to filter complexity, when going for such a high slope.
The final option was to use DSP. This would allow for the very steep slopes required along with easier fine tuning of the frequency response by using parametric equalization. The DSP chosen was a miniDSP [17], which is a DSP package that handles analog-to-digital conversion, performs the crossovers and equalization and then performs digital-to-analog conversion. Using the GUI the crossovers were quickly setup with the required slopes and frequency bands.

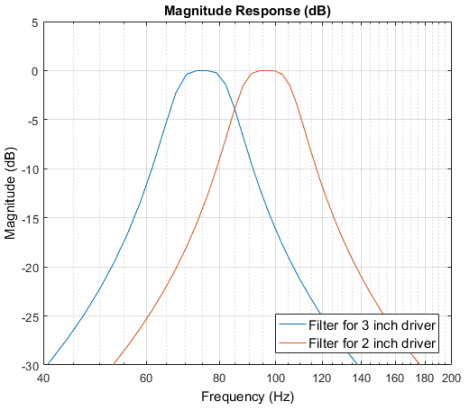

Fig. 6: The crossover of the two speaker units implemented via a miniDSP

2.2 Measuring Setup

Fig. 7: The two speakers as measured

2.2.1 Frequency response

The frequency response is measured in an anechoic chamber at Technical University of Denmark. The room is approx. 60 m^3 and with a limiting lower frequency of about 100 Hz. This makes the room less than

perfect for measuring the lower frequencies; however, the distances to the walls, celling and floor are more than 1.5 times longer than to the microphone, and while the room does not eliminate the reflection below 100 Hz completely they are still attenuated compared to the direct wave, making the room usable for measuring the frequency response. The frequency response is measured by performing a sweep from 1-200 Hz using Room Equalization Wizard (REW) along with a Umik-1 microphone from miniDSP.

2.2.2 Power Draw

To measure the current, voltage and power drawn by the individual speaker a Teledyne Lecroy MSO 104MXs-B is used. The current running into the speaker unit is measured using a AP015 current probe griping the positive wire attached to the positive terminal of the speaker unit. The voltage is measured using a differential voltage probe attached to the positive and negative wires connected to the positive and negative terminals of the speaker unit respectively. The total power drawn by each of the speaker units is found by $P = V \cdot I$.
The input signal used when measuring the power draw is pink noise, since it contains an equal amount of energy in each octave band. This gives a better representation of how music is perceived by the human ear compared to using white noise, which is why it is often used to fine tune speaker systems [12].

2.2.3 Sound Pressure Level

The SPL is measured in the same room as the frequency response using REW and the Umik-1 with pink noise as the input signal. The microphone is placed 1 meter away from the speaker system and amplifier outputs one watt into each of the speaker units.
The SPL is measured using pink noise. The SPL is measured over 30 seconds to ensure that the measured SPL is not a local low or high due to the randomness of the input signal. The measured SPL is then averaged over the period to obtain the average SPL output of the speaker system.

3 Results

3.1 Frequency Response

Figure 8 shows the frequency response of the speaker system, which has the desired output from 65-110 Hz with all other frequencies attenuated heavily. The SPL matches the simulated SPL of the two speaker units seen in figure 4 somewhat. The simulated responses are without crossovers applied, hence output shown at higher frequencies, whereas the measured response shows the total frequency response of the two speakers combined with crossover applied.

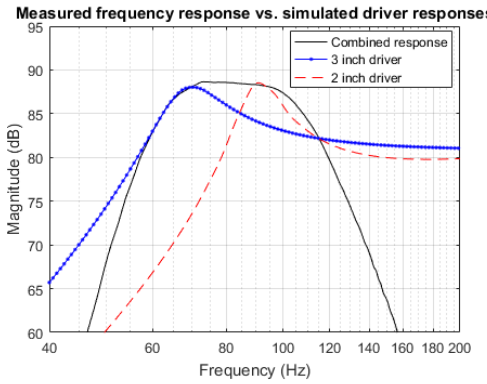

Fig. 8: Total frequency response of the speaker system

3.2 Sound Pressure Level

Figure 9 shows the SPL of the speaker system, if the speaker system was driven with 1 W. Comparing the SPL while playing pink noise with the frequency response in figure 8, which is normalized to 1W@1m, we see a good correlation and such they help to validate each other.

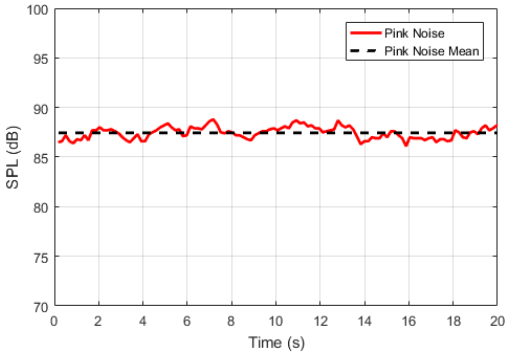

Fig. 9: The SPL of the speaker system while playing pink noise at 1W

What is most interesting and the main subject of this paper is the current drawn by the speaker units while playing. Figure 10 shows the current drawn by the speaker system and the individual speaker units. These measurements were done when the amplifier was outputting 0.01 W into the speaker system. The reason for the low output is due to an unexplainable attenuation of the signal in the miniDSP when using pink noise. The behavior was not observed when using sine waves or music. What is most interesting about this plot is the difference in current drawn by the 2 inch speaker unit and the 3 inch speaker unit. The 2 inch draws quite a bit less current than the three inch with the units drawing on average 13.1 mA and 21.7 mA respectively. Looking at the impedance plots in 4 we see that the impedance of the 2 inch is substantially greater in the 2 inch's passband (85-110 Hz) compared to the 3 inch's impedance in its passband (65-85 Hz), which explains the need for less current. This is while both drivers are outputting the same SPL at the same voltage, helping to confirm that speaker units with a high impedance can be relevant when designing portable speaker systems.

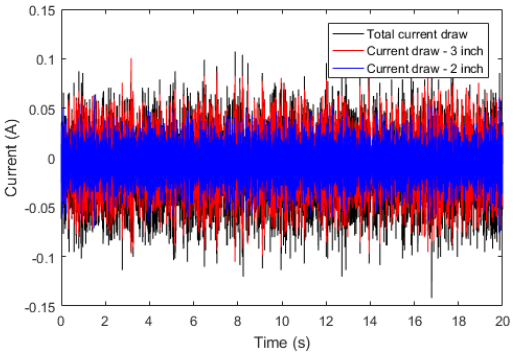

Fig. 10: The current drawn by the speaker system while playing pink noise at 10 mW

4 Discussion

It is fairly clear from the results seen in figure 10 that there are advantages to driving the speaker near its resonance frequency. Due to the great increase in the speaker unit's impedance the current required to drive the speaker unit is greatly reduced. At the same time the speaker unit does not have to work very hard as it is primarily the port that provides the SPL, which means that less VC excursion is required, see figure 5 and thus we can push the speaker unit to produce even higher SPL without VC leaving the motor.
However, it is not all good as there are some disadvantages, especially if the speaker unit is to be used in a portable setup. Because the impedance increases so much at the resonance, up to 34 Ω, the voltage required to drive the unit also increases greatly. This can pose a problem, since most batteries are either 12 V or 24 V. This problem can be bypassed somewhat by using boost converters and other circuitry to increase the voltage. Another problem is the narrow band at which the unit operates most efficiently. If you want the speaker system to cover the lower frequencies from, say, 50-150 Hz, since that is where the most current is usually spent, you will need at least 4+ speaker unit similar to the speaker units used in this paper, if you want them to operate in the narrow frequency band where they are the most efficient. This adds cost, complexity and size, which are all negatives when building portable setups. However, if custom speaker units were to be designed for a system such as the one used in this paper, then it might be possible to reduce the negative effects. Since the speaker units only have to cover a narrow frequency band less time is needed for optimizing the frequency response of the speaker units as you only have to focus on the narrow frequency band the speaker units need to cover. Also, the requirements for expensive materials that behave well across a wide frequency band diminishes, which can help to reduce the costs and complexity further.

The results also raise the question of why speaker units always aim for nominal impedances of 2-8 Ω, when there are clear advantages to higher impedance speaker units, especially for portable systems. Headphones have generally been designed with impedances ranging from 32-600 Ω, which makes you wonder even more why regular speaker units have to be designed with such a low impedance.
Looking at the benefits we see that we can reduce the amount of current needed to drive the speaker unit considerably, which prolongs battery life and it can have the added benefit of less distortion as well [18]. Again, this will still require the amplifier to be able to raise the voltage considerably in order to be able to drive the speaker system to a satisfactory SPL.

5 Summary

It is clear that building a speaker system that utilizes the efficiency of the speaker units when driven near the resonance does have some merit, especially when you are concerned about battery life. It is key to acknowledge that battery life is the main motivational factor for designing such a speaker system however, since the negative sides can easily outweigh the benefits. Because we have to use several drivers to cover any appreciable frequency band the size, complexity and price of the design increases substantially and so it might quickly loose its appeal for smaller portable speaker systems. Outdoor, battery-driven portable systems on the other hand might not be as restricted in regards to the size of the system, and so a setup similar to the one described in this paper with multiple speaker units might be an attractive option.

If you opt for a design such as the one investigated in this paper, there are certain factors that should be considered when designing the speaker units. First up would be to design the speaker unit with a high impedance; however, whether this should be across the full frequency band like in a headphone or around the resonance frequency depends on how the speaker is thought to be used. Driving the unit only at resonance has the advantage of voice coil needing to move very little, but also means that the usable frequency band is quite narrow and increases the need for high order filters. Choosing to go with a high impedance across the frequency band increases the usable frequency band and so reduces the number of speaker units required and might lower the crossover slopes needed. Next thing will be to design the unit, so that it performs the best in the cabinet design chosen. Whether a closed box or a box with a vent/passive radiator is used is up to the individual as they both have advantages and disadvantages. Lastly, the designer has to ensure that the amplifier can handle the high impedance, i.e. that it can output a high enough voltage to produce an appreciable SPL.

This paper has proven that a speaker system designed around the resonance frequency of the speaker units does have its advantages, especially in portable setups where current draw is a consideration. However, it comes with some caveats that need to be overcome. So it is up to the designer to weigh the pros and cons, when choosing which direction to go.

6 Future Work

A comparison with a more traditional design, i.e. a single driver subwoofer, needs to be done to see how big a reduction of the current draw one can achieve. For such a comparison there are certain requirement however. The design will have to cover the same frequency band with an SPL equal to that of the design used in this paper as a minimum. For it to be a proper comparison the cabinet volume cannot exceed the total volume of the design described in this paper, which is 6 L.
It would also be interesting to have a speaker unit designed with a overall higher impedance to allow for a single driver design. This would both reduce complexity of the entire setup, while benefiting from a reduced current draw.

References

[1] R. Tiwari, "Bluetooth Speakers Market Worth $7 Billion by 2019", 2014, *Date Accessed: 2016-12-03*.

[2] J. Honda, "Application Note AN-1071", International Rectifier, 2005.

[3] K. Nielsen, "Audio Power Amplifier Techniques With Energy Efficient Power Conversion", Ph.D. thesis, Volume 1, Technical University of Denmark 1998.

[4] M. Duraj, N. E. Iversen, L. P. Petersen and P. Boström, "Self-oscillating 150 W switch-mode amplifier equipped with eGaN-FETs", in AES Convention 139th, New York, October 29-November 1, 2015.

[5] B. Putzeys, "Simple Self-Oscillating Class D Amplifier with Full Output Filter Control", in AES Convention 118th, Barcelona, May 28-31, 2005.

[6] S. Poulsen and M. A. E. Andersen , "Simple PWM modulator topology with excellent dynamic behaviour", in Applied Power Electronics Conference and Exposition, 2004.

[7] I. Garcia, "TMS320C6412 Power Consumption Summary", Texas Instruments, 2005.

[8] W. Marshall Leach, Jr. "Introduction to Electroacoustics and Audio Amplifier Design", Kendall/Hunt Publishing Company, 2003.

[9] N. E. Iversen, A. Knott and Michael A. E. Andersen, "Relationship between voice coil fill factor and loudspeaker efficiency", J. Audio Eng. Soc., May 2016.

[10] P. J. Chapman, "Programme material analysis", in AES convention 100th, Copenhagen, May 11-14, 1996.

[11] R. A. R. van der Zee and A. J. M. van Tuijl, "Test Signals for Measuring the Efficiency of Audio Amplifiers", in AES Convention 102th, Amsterdam, May 16-19, 1998.

[12] Sweetwater, "Pink Noise Versus White Noise", 2000, http://www.sweetwater.com/insync/pink-noise-versus-white-noise/, *Date Accessed:2016-12-05*.

[13] International Electrotechnical Commission, "IEC 268-1 Sound System Equipment, Part 1: General", Second edition 1985.

[14] F. E. Toole, "Sound Reproduction: Loudspeakers and Rooms", Taylor & Francis, 2008.

[15] J. Borwick, *Loudspeakers and Headphone handbook*, CRC Press, 2012.

[16] A. N. Thiele, "Loudspeakers in vented boxes, Parts I and II", J. Audio Eng. Soc., Vol. 19 pp. 382-392 (May 1971); pp. 471-483, June 1971.

[17] *miniDSP 2x4 box*, miniDSP, 2016.

[18] Wolfgang Klippel, "Loudspeaker Non linearities. Causes, Parameters, Symptoms", Klippel GmbH, Dresden, Germany.

O

Model for evaluation of power consumption of vented box loudspeakers

In 142nd Audio Engineering Soceity convention, Berlin, May 20-23, 2016.

Audio Engineering Society

Convention Paper

Presented at the 142nd Convention
2017 May 20–23, Berlin, Germany

Model for evaluation of power consumption of vented box loudspeakers

Filip Sommer Madsen[1], Søren Thorsen[1], Niels Elkjær Iversen[1], and Arnold Knott[1]

[1]*Technical University of Denmark - DTU, Kongens Lyngby, 2800 Denmark*

Correspondence should be addressed to Filip Sommer Madsen (Filip_S_Madsen@outlook.dk)

ABSTRACT

In the design of mobile sound systems an estimation of power consumption must be made in order to choose a battery of appropriate size and cost. However poor methods for power estimation tend to result in large and costly batteries. This paper aims to present a more precise method for estimating power consumption for a vented box sound system. Instead of simplifying a loudspeaker system as a purely ohmic resistance, its mechanical and acoustic parameters are used to create a state space model. Despite deviations at high frequencies, the state space model is at least twice as accurate at estimating the power consumption than simplifying the speaker as a resistor.

1 Introduction

Power consumption is an important consideration in most mobile electronic systems. This is no exception in mobile sound systems, where high efficiency is needed to play at a loud level for an extended period of time [1]. Larger batteries ensures longer play time but increases both cost, size and weight. It will therefore always be a trade-off when deciding how large batteries should be used with a given sound system. Finding an appropriate trade-off requires an estimation of the power consumption [2]. The typical approach to estimate the power consumption in sound systems however relies on two major simplifications. First of all speakers are often modelled as purely ohmic resistances [3]. In reality speakers have a frequency varying impedance caused by its mechanical nature and its acoustic surroundings. At frequencies, where the speaker has a high impedance, less current and power will be drawn from the amplifier. This leads to the other simplification which lies in the signal. Music signals consists of a wide range of frequencies and is known to often have a large dynamic range [4], [5]. However the used signals for testing power consumption are often sinusoids [6]. Because of the frequency dependent nature of speakers, testing with single frequency signals will result in very inaccurate estimations. This paper presents a model to ensure more precise modelling of the power consumption in a sound system. The model is based on the state space representation, which allows the use of complex input signals. This is in contrast to the laplace transform, which can only evaluate sinusoidal signals. By using the state space representation the output current of the amplifier can be estimated, which allows for easy calculation of the average power. The modelled sound system consists of an amplifier driving a speaker placed in a vented box. Vented box speakers are commonly used when small size, large bass response or high efficiency is desired [7]. This is usually the case for mobile sound system, which is the reason for making model a vented box speaker. The model does not take the losses of the amplifier into account, and therefore only the

output power of the amplifier is modelled.

2 Theory

To create a model of a vented box loudspeaker as precise as possible, the fundamental principles of a loudspeaker and how its acoustic surroundings affect it must be considered.

2.1 Fundamentals of loudspeakers

The most typical loudspeaker is the moving coil loudspeaker, which is well described in literature [8], [9], [10]. It is an electro-acoustic transducer, that converts electrical energy into mechanical energy and which is then converted into acoustic energy. In other words the loudspeaker has both electrical, mechanical and acoustic parameters, which should be taken into account when trying to describe its behaviour. Conveniently both the mechanical and the acoustic nature of the speaker can be modelled as electrical circuits, which figure 1 shows.

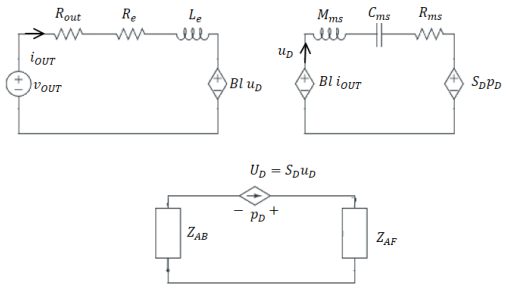

Fig. 1: Equivalent electrical circuit for a speaker

The electrical circuit for a speaker in figure 1 is simplified as being linear. However in real speakers a number of nonlinearities in e.g. the voice coil inductance exists, making the state space model more complex [11]. This is out of the scope of this paper.

The electrical parts of a speaker are coupled to the mechanical ones with the force factor, Bl. The mechanical parts are then coupled to the acoustic one with the effective area of the diaphragm, S_D.

The electrical parameters consist of the dc-resistance in the coil, R_e, along with the inductive behavior of the voice coil, L_e. The mechanical parameters consists of the mechanical mass, M_{ms}, compliance, C_{ms} and dampening, R_{ms}, in the loudspeaker. These parameters are modelled as an electric inductor, spring and resistance respectively. This forms a second order bandpass filter, which determines the resonance frequency of the speaker given by:

$$f_S = \frac{1}{2\pi\sqrt{M_{ms}C_{ms}}} \tag{1}$$

When an output voltage, v_{OUT}, is generated from an amplifier, this gives rise to an electrical current, i_{OUT}. This current creates a mechanical force, $f_D = Bl \cdot i_{OUT}$, which in turn creates a voice coil velocity, u_D. The movement of the coil is translated to the diaphragm, which creates a volume velocity, U_D. The sound pressure, p_D, generated across the diaphragm is then given as follows:

$$p_D = U_D\left(Z_{ab} + Z_{af}\right) \tag{2}$$

In the equation above Z_{ab} and Z_{af} are the acoustical impedances at the back and front of the diaphragm respectively. Loudspeakers are sometimes simplified as being mounted in an infinite baffle, where the back and front are isolated. In that case the loudspeaker can be modelled by consisting of only its electric and mechanical parameters.

2.2 State space model of loudspeaker

To create a model of the speaker system which can evaluate complex input signals a state space model can be used. The state space representation is a way to mathematically describe dynamic systems in the time domain. The model made up of coupled first-order ordinary differential equations expressed in the following form:

$$\mathrm{x}'(\mathrm{t}) = \mathbf{F}\mathrm{x}(\mathrm{t}) + \mathbf{G}\mathrm{u}(\mathrm{t}) \tag{3}$$

Here $\mathrm{x}(\mathrm{t})$ is the state vector describing the current state of the system and $\mathrm{x}'(\mathrm{t})$ is its derivative. $\mathbf{F}$ describes the system dynamics and is called the state matrix. $\mathbf{G}$ is the input matrix describing how the input affects the state variables. A state space model of a loudspeaker has been found in [12] which has been rearranged into:

$$\mathbf{x(t)} = \begin{bmatrix} i_{OUT} \\ x_D \\ u_D \end{bmatrix} \mathbf{G} = \begin{bmatrix} -\frac{1}{L_e} \\ 0 \\ 0 \end{bmatrix} \tag{4}$$

Here x_D is the displacement in the mechanical spring.

$$\mathbf{F} = \begin{bmatrix} -\frac{R_e}{L_e} & 0 & -\frac{Bl}{L_e} \\ 0 & 0 & 1 \\ \frac{Bl}{M_{ms}} & -\frac{1}{C_{ms}M_{ms}} & -\frac{R_{ms}}{M_{ms}} \end{bmatrix} \tag{5}$$

Note that in the state space model above the acoustic impedances Z_{af} and Z_{ab} are assumed to be only acoustic masses, which are included in the mechanical mass, M_{ms}. Placing the speaker in a vented box increases the significance and complexity of the acoustic system, which will be examined next.

2.3 Effects of a vented box

Mounting a loudspeaker in a box has several advantages. It prevents the back of the speaker, which radiates 180 °out of phase, from causing destructive interference at the front. This increases the bass response. However it also adds an acoustic volume, which acts as an extra mechanical spring increasing the resonance frequency of the system. If lower bass response, small size or higher efficiency is needed a vented box can be used. Figure 3 shows the electrical model of the vented box system. This adds an acoustical mass, M_{ap}, which together with the acoustic volume, V_{ab}, forms a second order band pass filter. The phase delay from the back to the front will then be $180° + 180° = 360°$, which makes it radiate in phase with the speaker, boosting the output.

2.3.1 Impedance of a vented box

Figure 2 shows the frequency dependent impedance of a loudspeaker in a vented box. The minimum impedance is found at 0 Hz as the voice coil DC-resistance. At high frequencies the impedance is seen to rise which is due to the inductive behavior of the voice coil. In reality the voice coil also has a lossy behavior [8], which due to simplification will not be examined in this paper.

Two peaks are present. The higher one is due to the mechanical nature of the speaker. The lower one is caused by the vent, and the null between is the resonance frequency of the vent and the acoustic volume. By ohms law it is clear that the speaker will draw the less power at these impedance peaks.

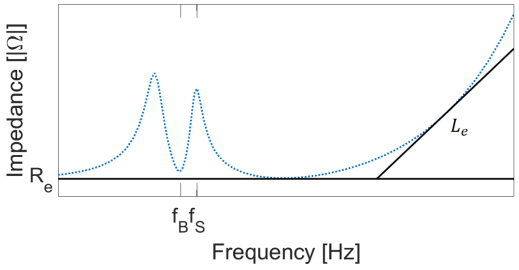

Fig. 2: Impedance of a speaker in a vented box

2.3.2 Electrical equivalent circuit of a vented box

The equivalent electrical for a speaker in figure 1 can be expanded to include the acoustic parameters of a vented box, which is shown in figure 3.

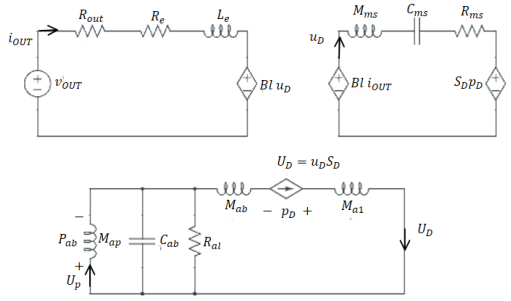

Fig. 3: Electrical equivalent circuit for a speaker in a vented box

The resistance R_{al} in figure 3 models the air-leakage through the box. M_{a1} and M_{ab} model the radiation impedance on the front and in the box respectively. This is somewhat a low frequency simplification, and a more precise modelling of radiation impedance can be implemented in future work. Doing so will cause the size of the state space model to increase significantly.

2.3.3 State space model of vented box

By placing the speaker in a vented box the state space model presented in section 2.2 is no longer valid. There-

fore a new state space model is to be made in order to describe the expanded system.

The state variables in x(t) from equation 3 are found by analyzing all energy storing elements in figure 3. For capacitors the state variable will be the voltage and for inductors it will be current. The found state vector is:

$$\mathrm{x(t)} = \begin{bmatrix} i_{OUT} \\ x_D \\ u_D \\ p_{ab} \\ U_p \end{bmatrix} \tag{6}$$

Here U_p is the volume velocity in the port. p_{ab} is the sound pressure in the acoustic volume, which is equivalent to the voltage across a capacitor. U_D, which is stored in M_{ab} and M_{a1}, is not needed to take account for because it is equal to $u_D S_D$. Now the derivative to each state variable must be expressed by the other state variables. $\frac{di_{OUT}}{dt}$ and $\frac{du_D}{dt}$ can be solved for in equation 7 and 8 respectively, which are found from using Kirchhoff's voltage law in the electric and mechanical circuit.

$$v_{OUT} = i_{OUT}R_e + L_e\frac{\mathrm{d}i_{OUT}}{\mathrm{d}t} + Blu_D \tag{7}$$

$$Bli_{OUT} = u_D R_{ms} + M_{ms}\frac{\mathrm{d}u_D}{\mathrm{d}t} + x_D\frac{1}{C_{ms}} + p_D S_D \tag{8}$$

The derivative of the mechanical displacement, x_D, is simply the mechanical velocity:

$$\frac{\mathrm{d}x_D}{\mathrm{d}t} = u_D \tag{9}$$

The derivative of the volume velocity through the port can be found from the relation between voltage change in current in an inductor. Translating acoustic pressure into voltage and volume velocity into current it can be shown that:

$$p_{ab} = M_{ap}\frac{\mathrm{d}U_p}{\mathrm{d}t} \tag{10}$$

Lastly the derivative of the pressure in the box can be found from using Kirchhoff's current law along with the relation for voltage change and current in a capacitor:

$$u_D S_D - U_p - \frac{p_{ab}}{R_{al}} = C_{ab}\frac{\mathrm{d}p_{ab}}{\mathrm{d}t} \tag{11}$$

Solving for the derivatives of each state variable in equation 7, 8, 9, 10 and 11, the state matrix can now be found as:

$$\mathbf{F} = \begin{bmatrix} -\frac{R_e}{L_e} & 0 & -\frac{Bl}{L_e} & 0 & 0 \\ 0 & 0 & 1 & 0 & 0 \\ \frac{Bl}{M_{tot}} & -\frac{1}{C_{ms}M_{tot}} & -\frac{R_{ms}}{M_{tot}} & 0 & -\frac{S_D}{M_{tot}} \\ 0 & 0 & 0 & 0 & \frac{1}{M_{ap}} \\ 0 & 0 & \frac{S_D}{C_{ab}} & -\frac{1}{C_{ab}} & -\frac{1}{R_{al}C_{ab}} \end{bmatrix} \tag{12}$$

In the state matrix above the term M_{tot} is equal to $(M_{a1} + M_{ab})S_D^2 + M_{ms}$.

The only state variable depending on the input, v_{OUT}, is i_{OUT}. Solving for $\frac{\mathrm{d}i_{OUT}}{\mathrm{d}t}$ in equation 7 makes it straightforward to set up the input vector, **G**.

$$\mathbf{G} = \begin{bmatrix} \frac{1}{L_e} \\ 0 \\ 0 \\ 0 \\ 0 \end{bmatrix} \tag{13}$$

2.4 Speaker model for estimation of average input power

By using the established state space model it is now possible to estimate the output current, $i_{OUT}(t)$, when exciting the speaker with an arbitrary voltage signal, $v_{OUT}(t)$. The instantaneous power is achieved by multiplying $i_{OUT}(t)$ and $v_{OUT}(t)$. The instantaneous power contains both the real and reactive parts of the power, but when evaluating power consumption, only the real power is of interest. Since the reactive power simply moves back and forth between energy storing elements, this part will approximately be reduced to zero when integrating over a long period of time. To find the average input power the one must simply divide by the period. The measured average output power can therefore be calculated as:

$$P_{out,avg} = \frac{1}{t_2 - t_1} \int_{t_1}^{t_2} i_{OUT}(t) v_{OUT}(t) \mathrm{d}t \tag{14}$$

This model will for the future be referred to as the speaker model.

2.5 Simple resistor model

For the sake of comparison a simple model has been made to simulate the power consumption when the loudspeaker is modelled as a purely ohmic resistance. This model simply estimates the output current by:

$$i_{OUT} = \frac{v_{OUT}}{R_e} \tag{15}$$

Hereafter the average input power is again calculated using equation 14. This model will for the future be referred to as the resistor model.

3 Implementation

In this section the specific speaker and vented box used in the measurements are described. Also the test setup is explained along with the method for measuring the average output power. Furthermore it explains how the average output power is to be estimated through simulations.

3.1 Calculation of component values

The values of the components in the circuit shown in figure 3 are a mix of calculated and found. The electric and mechanic values are obtained directly from the Thiele Small parameters of the loudspeaker [13], which are shown in table 1. For higher precision these values can be measured [14]. The speaker is a small 3" low frequency driver with a free air resonance frequency of 55 Hz.

The only parameter in table 1, which is not taken directly from the datasheet, is the mechanical dampening R_{ms}. This has been estimated from:

$$R_{ms} = \frac{1}{Q_{ms}} \sqrt{\frac{M_{ms}}{C_{ms}}} \tag{16}$$

The speaker has been placed in a custom made vented box. The acoustic values have been calculated based of the dimensions of the box and the vent and using formulas from [8]. The box size, V_{ab}, is approximately 3.2 liters, which gives the following acoustic compliance of the box:

Table 1: Thiele Small parameters for the loudspeaker used

Parameter	Value	Unit
R_e	3.6	Ω
L_e	0.19	mH
M_{ms}	9.98	g
C_{ms}	737.67	μm/N
R_{ms}	1.16	Kg/N
Bl	5.28	Tm
S_D	0.0027	m^2
Q_{ms}	3.17	

$$C_{ab} = \frac{V_{ab}}{\rho_0 c^2} = 22.48 \cdot 10^{-9} \mathrm{m}^5/\mathrm{N} \tag{17}$$

The acoustic mass in the port, M_{ap}, is found from the cross section area, S_P, and the length of the port, L_P by:

$$M_{ap} = \frac{\rho_0}{S_P} \left(L_P + 1.462 \sqrt{\frac{S_P}{\pi}} \right) = 261.73 \mathrm{Ns}/\mathrm{m}^5 \tag{18}$$

To calculate the acoustical dampening, R_{al}, coming from air leakage in the box, a value for the vented box quality factor, Q_L, must be found. Because the volume of the box is quite small, a high Q_L value of 20 is assumed [8]. This gives an acoustical dampening of:

$$R_{al} = \frac{1}{Q_L} \sqrt{\frac{M_{ap}}{C_{ab}}} = 2.17 \mathrm{Ns}/\mathrm{m}^5 \tag{19}$$

The radiation impedance on the front of the diaphragm, M_{a1}, is a low frequency simplification and found by:

$$M_{a1} = \frac{8\rho_0}{3\pi^2 a} = 11.1 \mathrm{kg}/\mathrm{m}^4 \tag{20}$$

Here a is the effective radius of the diaphragm given by:

$$a = \frac{\sqrt{S_D}}{\sqrt{\pi}} \tag{21}$$

Lastly the acoustic mass of the air in the box, M_{ab} is found by:

$$M_{ab} = \frac{B\rho_0}{\pi a} = 8.5\text{kg/m}^4 \quad (22)$$

Here the mass loading factor, B, is assumed to be 0.65 [8].

3.2 Test setup

The test setup is shown in figure 4, and consists of a power supply, a class-D amplifier and the vented box loudspeaker. Figure 5 shows the actual setup.

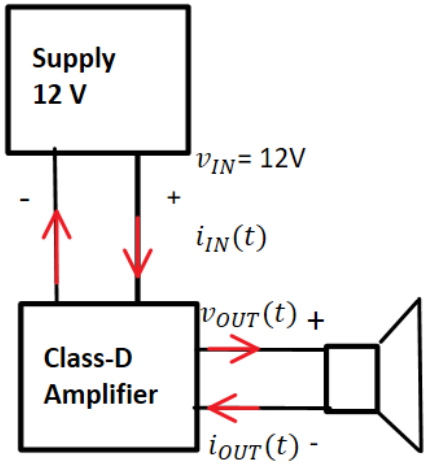

Fig. 4: Block diagram of test setup

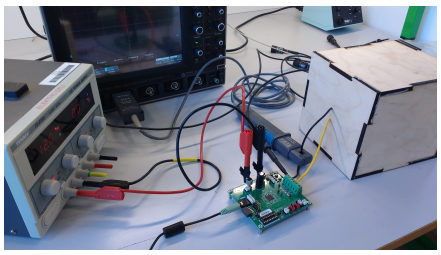

Fig. 5: Test setup

Both conduction and idle losses are present in the amplifier, but by measuring $i_{OUT}(t)$ and $v_{OUT}(t)$, these losses are not relevant for calculating the output power.

For the test setup in figure 5 the MA12040P amplifier chip from Merus Audio was used [15].

The goal of the measurement is verifying the average output power found in the simulations, defined in equation 14 can be used to predict the power consumption more accurately than the simple resistor model.

The measurements are carried out on a LeCroy WaveSurfer 104MXs-B oscilloscope by tracing the current with current probes, as well as measuring the voltage. Since the oscilloscope works by taking samples in the discrete time domain the average output power can be found by:

$$P_{out,avg} = \frac{1}{T}\sum_{n=0}^{N} v_{OUT}[n] \cdot i_{OUT}[n] \quad (23)$$

Where N is the number of samples used, and T is the period the measurement is taken over.

Since the audio files being played through the speaker has a sample rate of 44.1kHz, the oscilloscope needs to have a sample rate, f_s, equal to or higher than this. The specific scope used can store 1 million samples at a time. Choosing a sample rate of 50 kHz the measurement period is found to be 20 seconds, using equation 24.

$$\frac{N}{f_s} = T \quad (24)$$

If a larger time interval would be chosen, aliasing would occur at higher frequencies, and the results would come up incorrect.

4 Results

To verify the validity of the represented state space model, measurements have been made. These measurements have been compared to simulations of both the speaker and the resistor models.

4.1 Measurements with sinusoid signals

Theory predicts that the frequency varying loudspeaker impedance will cause the average input power to vary as well. However if modelled as a resistor, the average input power will be constant for all frequencies. To examine which model is most precise a number of measurements with sinusoids of 12 V peak at different frequencies has been made. Figure 6 shows the results. No measurements were made below 45 Hz, fearing that this would damage the speaker unit.

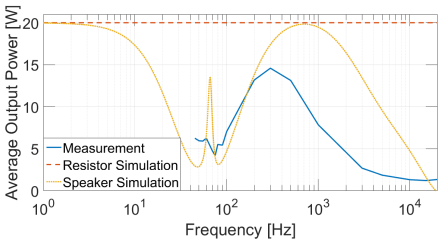

Fig. 6: Comparison between simulations and measurements at different frequencies

What is first to notice in figure 6 is that the measured average input power varies quite a lot. The simulation of the resistor model however is constant and does at all frequencies predict a larger power consumption. This is expectable since the highest current draw will occur when the loudspeaker impedance equals its dc-resistance. Especially at frequencies above 1 kHz the resistor model is very inaccurate. The loudspeaker model however generally does a better job predicting the measured average input power. Around the port and driver resonances the simulation is quite close compared to the resistor model. However the loudspeaker simulation generally predicts larger variations. Also in the range from 100 Hz to 300 Hz the two slopes seems to be offset by around 30 Hz. This could very well be because of imprecise speaker parameters from the datasheet. For instance a higher compliance or smaller mass will move the driver resonance up in frequency. However it should be stated that all formulas used to calculate the acoustical parameters are approximations, which might have lead to deviations. The largest deviation for the speaker simulation starts at above 500 Hz. This is most likely due to imprecise modelling of the self inductance in the voice coil. Predicted from the datasheet value of L_e, the voice coil impedance should start rising above 1 kHz. However from the impedance plot of the speaker in free air in from the datasheet, the impedance starts rising above 300 Hz [13]. This corresponds very nicely with the measured result, and a much more precise speaker model above 300 Hz would be expected, if the modelling of the voice coil inductance were more precise. To examine the accuracy of the simulations further, the deviation of the measurement and the simulations has been calculated in percentage. The deviation in percent is found by:

$$\text{Deviation} = \frac{\text{Simulated result} - \text{Measured result}}{\text{Measured result}} 100\% \qquad (25)$$

Using the above formula for both simulations, the deviations in figure 7 are obtained. The frequency axis is limited to go up to 500 Hz, which is because at higher frequencies large deviations occur due to the imprecise modelling of the self inductance. Also since the driver is a low frequency driver, the higher frequencies are irrelevant since a low pass filter would be used with the speaker.

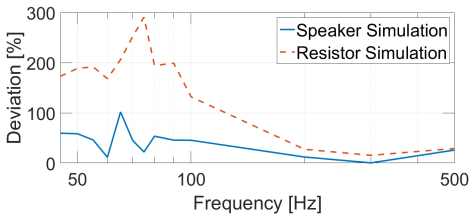

Fig. 7: Deviation between simulations and measurement at different frequencies

Figure 7 shows that the speaker model at all frequencies is more precise than the resistor model. While the resistor model goes up to maximum of 300 %, the speaker model mostly stays under 50 %. The largest deviation of the speaker model is around 65 Hz, which is close to the port resonance. This deviation is most likely due to the acoustic system being simplified, neglecting more complex acoustic phenomenons and the non ideal speaker implementation. However at around 300 Hz, where the speaker draws a lot of power, the speaker model is very accurate. At 75 Hz the speaker model deviates with only 22 %, while the resistor deviates 290 %. In other words at this frequency the speaker model is more than 10 times more accurate than the resistor model. This is a big improvement, especially because of the fact, that the speaker is a low frequency driver typically operating around this frequency.

4.2 Measurements with complex signals

One of the major advantages of using the state space representation for modeling the speaker is, that complex signals can be used as inputs. It is therefore important to verify how correctly the model can predict the average input power for such signals. To do this the white and pink noise signals along with the IEC 268-5 signal have been sent through the speaker. The IEC 268-5 signal is a measuring signal based on pink noise, but with roll off at low and high frequencies [16], which gives it more characteristics of a music signal. The three signals have also been used as inputs to both the resistor model and speaker model. Table 2 shows the results of this along with the measured average input power. Due to the fact that the amplitude of the three signals varied a bit, a peak normalization has been made in the simulations. This can lead to deviations.

Table 2: Average output power for speaker and resistor simulations along with measured data

	White Noise	**Pink Noise**	**IEC**
Measured[W]	0.41	0.35	0.94
Speaker[W]	0.83	0.44	1.56
Resistor [W]	15.81	0.95	2.00

Both the simulation of the speaker and the resistor generally predicts higher power consumption than measured. However for all three measurements the simulation of the speaker is closer than it is for the simulation of the resistor. Especially for inputs of white noise the resistor does a poor job predicting the correct average input power. This has most likely something to do with the resistor simulation giving large deviations at high frequencies. As both pink noise and the IEC 268-5 signal has a roll off at high frequencies, the deviation is much smaller for these signals.

Table 3: Percentage deviations between both simulations and the measurements

	White Noise	**Pink Noise**	**IEC**
Speaker [%]	102.44	25.71	65.96
Resistor [%]	3756.09	171.43	112.76

In table 3 the percentage deviations for the same measurements are shown. Here it is even clearer to see that with simulation a resistor overall gives poor results. This is especially true for signals containing high frequency content. The state space model for the speaker however is down to 25.71 % deviation for the pink noise signal, which is more than six times less than for the resistor model, which is at 171.43 %. For the IEC 268-5, where the resistor model performs its best with a deviation of 112.76 %, the speaker model still has an accuracy almost twice as good. Though the deviations for the speaker model could be smaller it should be kept in mind the large amount assumptions and approximation that have been made when creating the model. Apart from calculations of the acoustic parameters, this includes assuming datasheet parameters to be correct. It was also found that numerical errors would appear at above 10 kHz. This along with the poorly simulated voice coil inductance is most likely the main reason why the loudspeaker model performs better with pink noise and IEC 268-5 than white noise.

4.3 Simulation with music signals

The model was also simulated using real music, in this case, the top 50 tracks from Billboard Hot 100[1] as of 15/12/16, were loaded into the simulation with a peak amplitude of 12 V.

Table 4: Average input power for speaker and resistor simulations for music

	Billboard
Speaker [W]	1.34
Resistor [W]	2.49

This continues the trend of the resistor using more power than the real speaker, According to [6] the average audio signal has a characteristics comparatively close to that of the IEC 268-5 signal, and comparing table 2 and 4 their power consumption are fairly similar.

The results generally show that the state space model of the vented box loudspeaker is much more precise than by approximating the speaker as a resistor. At all frequencies the loudspeaker model estimates a lower power consumption than the resistor model does. In other words when estimating minimum requirements for batteries in a given sound system, one would always end out with a smaller and cheaper solution. One could argue that due to the fact that the loudspeaker

[1] http://www.billboard.com/charts/hot-100

model at some frequencies underestimates the power consumption, a safety margin of a few watts should be added. Because the model at all three test signals overestimates the power consumption, this should not be necessary, however if a different driver with more reliable parameters, and a better implemented cabinet were to be used, this might be an issue to address.

5 Conclusion

Power consumption is generally a big concern in mobile sound systems, as it decides the size and price of batteries. When modelling a loudspeaker as a purely ohmic resistance, the result is an overestimation of power consumption. This leads to larger and more expensive batteries. In an attempt to avoid this, this paper has presented a state space model of a loudspeaker in a vented box. Measurements of the average input power for sinusoid signal with different frequencies were performed. These were compared to simulated values for the state space model of the vented box speaker, but also for a simple solution where the speaker is modelled as a purely ohmic resistance. Though both simulation types showed deviation, especially at above 500 Hz, the state space model of the loudspeaker was clearly more precise. Furthermore it is assumed that imprecise values from the loudspeaker datasheet, as well as an imperfect enclosure could be one of the major reasons for large deviations. Apart from this the loudspeaker showed deviations of less than 50% across large frequency areas, where the resistor model showed up to 300% deviations. Also a set of measurements with the more complex signal white noise, pink noise and IEC 268-5 were performed. Here both simulations showed to overestimate the power consumption in all three cases. However the loudspeaker model showed to perform significantly better than the resistor model. For pink noise the deviation for the loudspeaker model was found to be around 50%, whereas the resistor was found to deviate around 200% - 4 times worse. Lastly simulations with top 50 billboard music tracks were performed to demonstrate the capabilities of the model, being able to simulate power consumption when playing music signals. In short there is clearly a potential for using state space representation for modelling power consumption more precisely in sound systems. The speaker model performed significantly better than the resistor model in all measurements. The relatively large deviations at certain frequency ranges are expected to be reduced significantly by future optimization.

6 Acknowledgements

The authors would like to thank Ruben Bjerregaard from Soundboks, and Rien Oortgiesen from Merus Audio for supplying equipment and being helpful in answering any questions regarding this.

References

[1] Iversen, N. E., Oortgiesen, R., Knott, A., Andersen, M. A., and Høyerby, M., "Design of efficient sound systems for low voltage battery driven applications," in *Audio Engineering Society Convention 141*, Audio Engineering Society, 2016.

[2] Schneider, H., Jensen, L. C., Petersen, L. P., Knott, A., and Andersen, M. A., "Requirements Specification for Amplifiers and Power Supplies in Active Loudspeakers," in *Audio Engineering Society Convention 137*, Audio Engineering Society, 2014.

[3] Iversen, N. E. and Knott, A., "Small Signal Loudspeaker Impedance Emulator," *Journal of the Audio Engineering Society*, 62(10), pp. 676–682, 2014.

[4] Mijic, M., Masovic, D., Sumarac Pavlovic, D., and Petrovic, M., "Statistical properties of music signals," in *Audio Engineering Society Convention 126*, Audio Engineering Society, 2009.

[5] Iversen, N. E., Schneider, H., Knott, A., and Andersen, M. A., "Efficiency Investigation of Switch-Mode Power Audio Amplifiers Driving Low Impedance Transducers," in *Audio Engineering Society Convention 139*, Audio Engineering Society, 2015.

[6] Niels Elkjær Iversen, A. K. and Andersen, M. A. E., "Efficiency of Switch-Mode Power Audio Amplifiers - Test Signals and Measurement Techniques," 2016.

[7] Small, R. H., "Efficiency of Direct-Radiator Loudspeaker Systems," *Journal of the Audio Engineering Society*, 19(10), pp. 862–863, 1971.

[8] W. Marshall Leach, J., "Introduction to electroacoustics & audio amplifier design, Fourth Edition," 2010.

[9] Thiele, N., "Loudspeakers in vented boxes: Part 1," *Journal of the Audio Engineering Society*, 19(5), pp. 382–392, 1971.

[10] Thiele, N., "Loudspeakers in vented boxes: Part 2," *Journal of the Audio Engineering Society*, 19(6), pp. 471–483, 1971.

[11] Klippel, W., "Loudspeaker Nonlinearities–Causes, Parameters, Symptoms," in *Audio Engineering Society Convention 119*, Audio Engineering Society, 2005.

[12] Brunet, P., *Nonlinear System Modeling and Identification of Loudspeakers*, Ph.D. thesis, Citeseer, 2014.

[13] "tb-speaker," http://www.tb-speaker.com/products/w3-1876s, n/a, accessed: 15-12-2016.

[14] Chapman, P. J., "Quantifying Acoustic Measurement Tolerances and Their Importance in the Loudspeaker Supply Chain," in *Audio Engineering Society Convention 136*, Audio Engineering Society, 2014.

[15] "MA12040P Merus Amplifier," http://www.merus-audio.com/images/pdf/MA12040P.pdf, n/a, accessed: 07-01-2017.

[16] "jblpro," https://www.jblpro.com/pub/technote/spkpwfaq.pdf, n/a, accessed: 15-12-2016.

P

Class-D amplifier with modern control

Patent application submitted to Europe Patent office, June, 2017.
No. P81700213EP00.

A class-D audio amplifier

Class-D amplifiers, which are based on a switching principle, have become a common choice for audio applications. This is due to the superior efficiency these amplifiers offer compared to other traditional linear amplifiers, such as class-B amplifiers. Class-D amplifiers may reach efficiency levels close to 90%, which allow much more compact implementation than traditional linear amplifiers. In general, a class-D audio amplifier comprises a modulator, a power stage, and an output filter.

In terms of linearity, class-D amplifiers have shown great performance with total harmonic distortion as low as 0.001%. The class-D power amplifier operates by modulating an input audio signal into a high frequency discrete signal which drives an output stage. The output stage drives a load, such as a loudspeaker, via an output filter that suppresses the high frequency passes the audio signal.

The modulation of the audio signal is one of the primary sources of distortion due to the non-linearities in the modulation. Another source of distortion is the output stage. The output stage is connected directly to the supply voltage which results in disturbances in the supply voltage being reflected in the audio. To prevent these disturbances and non-linearities from introducing excessive distortion and noise to the amplified audio signal, the principals of feedback and control theory have been utilized to correct and suppress the unwanted behaviours of the class-D amplifier.

Conventional modulators use pulse width modulation (PWM) where the audio signal is modulated with a fixed high frequency carrier waveform. Typically this waveform will have a triangle or saw-tooth shape. Normally the modulation is performed by comparing the audio input with the carrier which generates a pulse train at a given frequency with varying pulse lengths. The length or on-time of the pulses are also known as the duty cycle, D, of the PWM signal.

The output stage is where the amplification takes place and it consists of semiconductor devices which are switched on and off using the PWM signal. This means that the output stage amplifies the PWM signal. The most common type semiconductor device for switch-mode power applications is the Metal Oxide Field Effect Transistor (MOSFET). The output stage is typically using a buck topology. This topology can be realized either in a half- or full-bridge configuration. The half bridge requires a dual voltage supply while the full bridge only requires a single supply. The component count in the full bridge is twice the component count in the half bridge. The full bridge configuration is commonly referred to as Bridge Tied Load (BTL).

The output filter is formed by a filter inductor, a filter capacitance, and the load impedance – which can be simplified as a purely resistive load. The output filter can in this simplified model be considered a second order low pass filter with a cut-off frequency also denoted a resonance frequency. Typically the cut-off frequency is placed one decade lower than the switching frequency. The main purpose of the filter is to remove the switching transient from the amplified audio signal. This ensures that the dissipated energy in the load is mainly coming from the audio source. Moreover it is beneficial for EMI reasons. The filter should have a flat frequency response in the audio bandwidth, i.e. 20 Hz to 20 kHz, while attenuating with 40 dB/decade above its' cut-off frequency. Moreover the filter will have a quality factor, Q, which determines how much the filter is dampened at its resonance.

Switching losses in the semiconductor devices in the output stage are among the most destructive losses as they can be of significant magnitude even at low power and thus increase the temperature of the semiconductor devices eventually destroying them if the temperature becomes too high. Conventionally, switching losses are difficult to minimize since they relate to the configuration of the semiconductor devices.

Dominating losses can be categorized as:

1) Gate losses, which are generated by charging and discharging the gate capacitances, Cgd and Cgs, of a switching device.
2) Conduction losses, which are generated when the switching device is in its' on state.
3) Switching losses, which occur while a switching device switches from an on-state to an off-state and vice versa.
4) Reverse conduction losses occur in the situation where the body diode in the switching device starts or continue conducting the instantaneous inductor current during the dead time period.
5) Filter losses, which are mainly due to the filter inductance in the output filter. These filter losses can be separated into wire losses and inductor core losses. The inductor core losses relate to the core material and the magnetic flux, B, in it.

The total losses are a sum of the above losses. Class-D amplifiers are usually designed for maximum output power, whereby the conduction losses, the switching losses, and the filter losses normally are the dominant losses. Generally, the losses occur as heat dissipation.

The majority of class-D power amplifiers have been using the principals of classical control due to its straight forward theory and the ease of implementing it in single-input, single-output systems. However, limitations in the theory often result in the control solution being only sub-optimal.

RELATED PRIOR ART

US 6,249,182 (assigned on its face to Intersil Corp.) describes a class-D amplifier with a high-Q low-pass filter which removes the resonance peak. The class-D amplifier comprises a low-pass, high-Q output filter, a pulse width modulator and a feedback compensation circuit. The pulse width modulator includes an integrator with feedback from the output of the amplifier and a comparator coupled to the output of the integrator for converting an input analogue audio signal into a digital audio signal and for

amplifying said digital audio signal. The low-pass, high-Q output filter is coupled between the output of the pulse width modulator and the load impedance for converting the amplified digital signal into an output amplified analogue audio signal. The feedback compensation circuit is coupled between the output of the low pass filter and the integrator for reducing the Q of the output filter.

The low-pass, high-Q output filter serves to keep the transfer function of the class-D amplifier independent of load impedance, but comes at unacceptable costs of creating a peak at the resonance frequency in the transfer function of the class-D amplifier. The feedback compensation circuit implements a filter that places a pole-zero combination in the transfer function of feedback loop of the class-D amplifier to compensate for the high Q output filter creating a transfer function of the class-D amplifier which has a flat frequency response at least in an audio band.

However, there remain unsolved problems in terms of enhancing performance of the class-D amplifier. The feedback compensation circuit provides only a poor reduction of audible distortion and lack of stability of the class-D amplifier may be an issue. Further, problems related to heat losses of the class-D amplifier remain unsolved.

SUMMARY

There is provided a class-D amplifier with an amplifier input and an amplifier output, comprising: an input stage with a self-oscillating pulse-width modulator configured to receive an analog input signal via the amplifier input and to output a digital signal; an output stage configured with semiconductor devices to amplify the digital signal; an output filter, configured as a low-pass, high Q filter, coupled between the output stage and the amplifier output; and a feedback circuit coupled to the output filter and to the input stage; wherein the feedback circuit is coupled at the output filter to measure a set of states comprising all of: current through the output filter inductor and output

voltage; and wherein the feedback circuit and the input stage are operatively coupled as a controller configured to control all of the states in the set of states while operatively suppressing a frequency peak at a resonance frequency of the output filter.

Thereby switching losses, conventionally resulting in heat dissipation in the semiconductor devices of the output stage, can be shifted to filter losses resulting in heat dissipation in the output filter, in the inductor thereof, rather than in the semiconductor devices. This has one or more of the advantages that heat sinks attached to the semiconductor devices may be dispensed with or reduced in size and that more output power can be delivered via the output stage. The heat dissipation shifted to the output filter is less of a problem since conventionally the inductor of an output filter is much larger than the semiconductor die of a semiconductor device and hence has a greater heat capacity which makes it able to withstand larger losses without damaging the inductor. When heat sinks are reduced in size or completely dispensed with, manufacturing costs can be lowered and the class-D amplifier can be reduced in size.

In a comparative test, semiconductor components in the output stage of a class-D amplifier configured to control all of the states above operated at temperatures in the range of 55.5 to 56.7°C compared to temperatures in the range of 93.0 to 98.9°C for a class-D amplifier

Each of the states, comprising current (IL) through the output filter inductor, output current (Ispk) and output voltage (Vspk), may be measured at the output filter by a sensing circuit and a respective signal, proportional to the current through the output filter inductor, output current and output voltage, may be supplied, via respective feedback paths, to the input stage or a circuit integrated therewith to act as a controller controlling all of the states. The controller may be implemented in this way by means of analogue circuitry i.e. as an analogue controller.

The controller may be configured based on modelling the class-D amplifier as a state-space model (cf. fig. 1) with at least the above mentioned two states, full controllability of all of the states and optionally an integration term. Controllability is ensured e.g. when the class-D amplifier is implemented in accordance with a state-space model with a controllability matrix with a full rank – representing that all states are controllable. The class-D amplifier in accordance with the state-space model may implement the integration term by means of an integrator coupled in a forward path of the input stage. The forward path couples the input signal to the output stage. The integrator corrects stationary errors and improves tracking such that the amplifier maintains proportionality between an input voltage signal and an output voltage signal across the load and prevents clipping while the input signal is in a non-clipping region. The controller may be configured as a Linear Quadratic Regulator (LQR) which can be configured by conventional methods. The Linear Quadratic Regulator may be configured using so-called penalty matrixes to emphasize performance of specific states and control signals (measured states).

A first penalty matrix may be designed to heavily penalize integration. This will move the pole of the integrator to the left in the s-plane and make it settle somewhere close to the poles of the 2^{nd} order filter, thus making the time constant of the integrator about the same as the output filters. It is thereby expected that the Linear Quadratic Regulator will further increase the damping of the output filter such that oscillations are reduced. These pole movements generate a growth in the control signal, which is limited by the supply voltage. Hence, there is a risk that the control signal is clipped – causing the class-D amplifier to act as an open-loop amplifier, which is undesired. To avoid this, a second penalty matrix is designed (by large matrix values) to emphasize the size of the control signal, thereby effectively reducing the control signal in the class-D amplifier in accordance with the state-space model. For the sake of completeness it is mentioned that the

parameters, constant gains, for the controller can be estimated by solving the well-known Riccati equation. In accordance therewith, the controller operatively suppresses the frequency peak at the resonance frequency of the high-Q output filter.

The class-D amplifier may be couple to receive an input signal from an input source, such as an audio source, via its amplifier input. At the amplifier input, the input signal is an analogue input signal. The class-D amplifier may be configured with a digital-to-analogue converter to enable reception of a digital input signal. The class-D amplifier may be coupled to a load, such as a loudspeaker, to supply an output signal, via its amplifier output, thereto.

The class-D amplifier may be implemented in discrete components on a circuit board to deliver output power in the range of a few Watts to several hundreds of Watts e.g. to thousand Watts or more. The class-D amplifier, except or including one or both of an inductor and capacitor of the output filter, may be implemented on a semiconductor die, such as on a single semiconductor die.

In some aspects the output filter is a second order filter with an inductor coupled in series with a load and a capacitor coupled in parallel with the load. In some aspects the output filter is a third order filter or a filter of a higher order, such as a fourth order filter. The inductor may have ferrite core or an air core or another type of core. The high Q of the output filter may be larger than about 2, larger than about 4 or larger than about 8. The high Q of the output filter may be in the range between 2 and 10, e.g. between 4 and 10.

In some aspects the output stage is configured as a half-bridge or as a full H-bridge. In some aspects each side of the full H-bridge comprises multiple half-bridges coupled in parallel. A semiconductor device comprises a source terminal, a drain terminal and a gate terminal. A half-bridged comprises a pair of semiconductor devices, with a first semiconductor device coupled in series with a second semiconductor device between a positive power supply

terminal and a negative power supply terminal. The first semiconductor device and the second semiconductor device are interconnected at a circuit node at their drain terminals. The output filter is coupled between the load and the circuit node at the drain terminals.

The semiconductor devices are driven by the input stage, such as by an output of the self-oscillating pulse-width modulator, via their gate terminals. The semiconductor devices in a pair of semiconductor devices are driven out-of-phase to avoid periods of short-circuiting the power supply. In some aspects a delay element, such as an inverter gate, is coupled between the output of the self-oscillating pulse-width modulator and a semiconductor device to deliberately introduce a delay between the first semiconductor device turning ‘off’ and the second semiconductor device turning ‘on’. Thereby, short-circuiting the power supply can be avoided.

In some embodiments the set of states comprises output current. The output current flows from the output of the class-D amplifier and through a load, such as a loudspeaker. When the set of states comprises the output current, the class-D amplifier has improved linearity.

In some embodiments the feedback circuit comprises: a measurement circuit outputting respective measurement signals proportional to one or more of: current through the output filter inductor, output current, and output voltage; and a gain element applying a respective gain to the respective measurement signals to output respective feedback signals to the input stage. Thereby the controller can act on signals proportional to the respective measurement signals which accurately represent the states the controller are controlling.

In some embodiments the feedback circuit has a substantially flat gain across frequencies in a frequency range between 20 Hz and 10 KHz or between 20 Hz and 20 KHz or between 20 Hz and an upper frequency; wherein the upper frequency is located approximately at the resonance frequency of the output

filter or an upper -3dB cut-off frequency of the class-D amplifier. Thereby the controller can act on signals proportional to the respective measurement signals which accurately represent the states the controller are controlling. The feedback circuit may comprise filters configured to suppress noise above or below the claimed frequency ranges.

In some embodiments the class-D amplifier is configured to perform Zero Voltage Switching (ZVS) or Reduced Voltage Switching (RVS) at least at duty-cycles in the range of 30 to 70%. This minimizes switching losses which occur in the semiconductor devices. Reduced Voltage Switching (RVS) and Zero Voltage Switching (ZVS) occur when the parasitic drain-source capacitance of the semiconductor devices in the output stage is partially (RVS) or completely (ZVS) charged/discharged by the inductor current during the dead time period. In some aspects the class-D amplifier is configured to perform Zero Voltage Switching or Reduced Voltage Switching at least at duty-cycles in the range of 15 to 85% or in the range of 10 to 90%.

In some embodiments the reactive ripple current in the output filter inductor is larger than the continuous output current at least within a range of duty-cycles from 30% to 70% duty-cycle. The duty-cycle refers to the duty-cycle of a digital signal output from the self-oscillating pulse-width modulator. In some aspects the reactive ripple current in the output filter inductor is larger than the continuous output current at least within a range of duty-cycles from 15 to 85% or 10 to 90%.

In some embodiments the class-D amplifier comprises an integrator coupled in a forward path between the amplifier input and the self-oscillating pulse-width modulator; wherein at least a first path of the feedback circuit is coupled to an input of the integrator and to a first circuit measuring the output voltage. The first circuit, measuring the output voltage, outputs a signal proportional with the output voltage to the controller implemented by one or both of the feedback circuit and the input stage. In some aspects, e.g. where

the output stage comprises a full H-bridge, the first circuit is configured as a difference amplifier sensing the voltage at each side of a two-port load, such as a loudspeaker.

In some embodiments the class-D amplifier comprises a summing circuit coupled in a forward path between the amplifier input and the self-oscillating pulse-width modulator; wherein at least a second path of the feedback circuit is coupled to an input of the summing circuit and to a second circuit measuring the current through the output filter inductor. The second circuit, measuring the current through the output filter inductor, outputs a signal proportional with the current through the output filter inductor to the controller implemented by one or both of the feedback circuit and the input stage. The second circuit may comprise a sensing resistor coupled in series with the output filter inductor and a difference amplifier sensing the voltage at each side of the sensing resistor.

In some embodiments at least a third path of the feedback circuit is coupled to an input of the summing circuit and to a second circuit sensing the output current. The third circuit, measuring the output current, outputs a signal proportional with the output current to the controller implemented by one or both of the feedback circuit and the input stage. The third circuit may comprise a sensing resistor coupled in series with the output filter inductor and a difference amplifier sensing the voltage at each side of the sensing resistor.

In some embodiments the self-oscillating pulse-width modulator is configured as an astable integrating modulator or a hysteresis offset modulator. Thereby the class-D audio amplifier achieves good audio performance with very low Total Harmonic Distortion, THD. Opposed to fixed frequency pulse width modulators, the self-oscillating pulse-width modulator operates with a modulator frequency that varies with the input signal.

In some embodiments the class-D amplifier has a step response with a peak of the output current which is limited to three times the current of a settled portion of the step response. In response to a step type input signal, the output current exhibits a conventional step response, which has some ringing towards the beginning of the step and which decays to a settled level. The peak refers to a maximum of the ringing. In some aspects the output current is limited to 2.4 times or 2.2 times the current of a settled portion of the step response.

In some embodiments the controller is implemented as an analogue controller.

There is also provided a semiconductor die comprising a class-D amplifier as set out above, excluding the output filter or an inductor thereof. Since switching losses are significantly reduced close integration of the semiconductor based output stage and input stage is possible. In some aspects the semiconductor die is integrated in a semiconductor package, such as in a plastics package. However, the output filter or an inductor thereof may require implementation as a discrete component, such as as a copper wire based coil.

In some embodiments there is provided a class-D amplifier with an amplifier input and an amplifier output, comprising: an input stage with a self-oscillating pulse-width modulator configured to receive an analog input signal via the amplifier input and to output a digital signal; an output stage configured with semiconductor devices to amplify the digital signal; an output filter, configured as a low-pass, high Q filter, coupled between the output stage and the amplifier output; and a feedback circuit coupled to the output filter and to the input stage; wherein the feedback circuit and the input stage is configured for state-space control of the class-D amplifer; wherein at least two states, e.g. three states are controlled state-space control.

Here and in the following, the terms ‘class-D amplifier’ and ‘class-D audio amplifier’ are intended to comprise any circuit and/or device suitably adapted to perform the functions described herein. In particular, the above terms comprise electronic circuits, such as electronic circuits which are integrated on fully or in part on a printed circuit board, general purpose or proprietary programmable microprocessors, Digital Signal Processors (DSP), Application Specific Integrated Circuits (ASIC), Programmable Logic Arrays (PLA), Field Programmable Gate Arrays (FPGA), special purpose electronic circuits, etc., or a combination thereof.

BRIEF DESCRIPTION OF THE FIGURES

A more detailed description follows below with reference to the drawing, in which:

fig. 1 shows a diagram for a state-space model of a class-D amplifier driving a load;

fig. 2 shows a state-space model of a class-D amplifier with state-space control;

fig. 3 shows a time-domain block-diagram of the class-D amplifier with state-space control;

fig. 4 shows a first output stage and an output filter with sensing components and sensing circuit nodes;

fig. 5 shows a second output stage and an output filter;

fig. 6 shows current sensing amplifiers;

fig. 7 shows an output voltage sensing amplifier;

fig. 8 shows an integrator with a feedback input;

fig. 9 shows a summation amplifier;

fig. 10 shows a self-oscillating pulse-width modulator;

fig. 11 illustrates ripple current over mean current as a function of duty-cycle for different filter Q; and

fig. 12 illustrates temperatures related to heat dissipation at different areas of a circuit board carrying a class-D amplifier with and without state-space control.

DETAILED DESCRIPTION

In the below the class-D amplifier is modelled as a 2^{nd} order system with a state-space controller with three states. An integrator is coupled in a forward path of the class-D amplifier inside an outer feedback loop. However, it should be noted that the integrator may be dispensed with. Also, without departing from the scope of the present invention, the class-D amplifier may be modelled as a third, fourth or higher order system. Correspondingly, the state-space controller may have a number of states equal to or greater than the order of system as it is modelled.

In general it is desired to model all the internal states of the class-D amplifier since it will provide the most accurate description of the system. However, when designing an analogue full state controller only the internal states that are directly measurable are of interest. This is because the full state controller must have a feedback path for every state which makes it crucial that the state is measureable. In embodiments wherein the class-D amplifier is configured to drive a load in the form of a speaker (i.e. a loudspeaker), the measurable states in the class-D amplifier may comprise: The speaker voltage (V_{out}), the speaker current (I_{out}) and the inductor current (I_L), where the output filter comprises an inductor coupled in series with the speaker. The measureable states are represented by a vector x(t), wherein ‘t’ denotes that x(t) is a function of time.

$$x(t) = \begin{bmatrix} I_L \\ I_{Out} \\ V_{Out} \end{bmatrix}$$

Fig. 1 shows a diagram for a state-space model of a class-D amplifier driving a load. The state-space model is an example of a model accounting for dominating poles and zeros in the transfer function for the class-D amplifier. The state-space model comprises a signal source, 101, generating an input signal, V_{in}, which is input to a gain stage 102, which is modelled as an ideal gain stage with a gain, G. The gain stage 102 supplies a signal proportional to the input signal to a 2nd order output filter which is modelled by an inductor, L_{ind}, 104 with a series resistance, R_{ind}, 103 and by a capacitor, C, 107. The load, in this example a speaker, is modelled as an inductor, L_{spk}, 106 with a series resistance, R_{spk}, 105. For this model the states can be measured as indicated by I_L, V_{out}, and I_{out} as indicated in the fig. 1.

In case the output filter of the amplifier is a 2nd order low pass filter, only two states are needed to describe it, but more states may be used. Correspondingly, the number of states is larger than or equal to the order of the output filter e.g. if the order of the filter is N, then the number of states may be N+1, wherein N is an integer number.

The states are used in a general state-space model known in the art of modern control, wherein:

$$\dot{x}(t) = Ax(t) + Bu(t)$$
$$y(t) = Cx(t) + Du(t)$$

Wherein, the matrixes A and B, when the equations governing the state-space model depicted in fig. 1 are taken into account, becomes:

$$A = \begin{bmatrix} -\frac{R_{ind}}{L_{ind}} & 0 & -\frac{1}{L_{ind}} \\ 0 & -\frac{R_{spk}}{L_{spk}} & \frac{1}{L_{spk}} \\ \frac{1}{C_O} & -\frac{1}{C_O} & 0 \end{bmatrix}$$

$$B = \begin{bmatrix} \frac{G}{L_{ind}} \\ 0 \\ 0 \end{bmatrix}$$

wherein the unified gain of the modulator and the power stage of a class-D amplifier is represented by G. The equation below provides an approximate gain through the amplifier based on the voltage amplification and a desired maximum linearized modulation index, M_{lin}.

$$G = \frac{V_{out}}{V_{in}} \cdot M_{lin}$$

5 The output of the state-space model is selected to be the voltage across the speaker, V_{out}, hence the so-called output matrix, C, and feed-through matrix, D, becomes:

$$C = [0 \quad 0 \quad 1]$$
$$D = 0$$

With this, a linear state-space model of the class-D amplifier is complete.

In one example, a class-D amplifier may have:

Cut-off freq. (fc)	155	KHz
Quality factor (Q)	4.5	
Idle switch freq. (fsw)	1.9	MHz
Modulation index (Mlin)	76	%

Input voltage, pk-pk	2	V
Gain (G)	9.12	V/V

With:

$$A = \begin{bmatrix} -\frac{37m\Omega}{1\mu H} & 0 & -\frac{1}{1\mu H} \\ 0 & -\frac{37\Omega}{1mH} & \frac{1}{1nH} \\ \frac{1}{660nF} & -\frac{1}{660nF} & 0 \end{bmatrix}$$

and

$$B = \begin{bmatrix} \frac{9.12}{1\mu H} \\ 0 \\ 0 \end{bmatrix}$$

And C and D as set out above.

As mentioned herein, the class-D amplifier in accordance with the state-space model may implement the integration term by means of an integrator coupled in a forward path of the input stage. The forward path couples the input signal to the output stage. The integrator corrects stationary errors and improves tracking such that the amplifier maintains proportionality between an input voltage signal and an output voltage signal across the load and prevents clipping while the input signal is in a non-clipping region. This is especially useful when the controller is used in a real class-D amplifier since it counteracts non-linear behaviours. The controller may be configured as a Linear Quadratic Regulator (LQR) which can be configured by conventional methods. The Linear Quadratic Regulator may be configured using so-called penalty matrixes to emphasize performance of specific states and control signals (measured states).

To dimension the integration term, the state-space model needs to be modified. This is because the controller design methods used in modern control only consider the state-space model, resulting in the integration being neglected. To solve this, an integral transform is applied to the state-space model. The matrixes below show the transformation of the state-space model to accommodate the integration term.

$$A_i = \begin{bmatrix} A & 0 \\ -C & 0 \end{bmatrix}, \quad B_i = \begin{bmatrix} B \\ 0 \end{bmatrix}, \quad C_i = [C \quad 0]$$

With this representation, a Linear Quadratic Regulator design approach is applied to the system. The Linear Quadratic Regulator (LQR) is an optimization method used to find the optimal full state controller with time varying gains. However, time varying gains are often not practical nor necessary hence a simplified steady state LQR method has been developed which will be used for the system. This method optimizes the following quadratic performance index, which is given as an example of a performance index; a person skilled in the art may choose another performance index:

$$J(u) = \lim_{t\to\infty} \int_0^t x^T(t) R_1 x(t) + u(t)\, R_2 u(t) dt$$

Wherein x(t) is the states of the model, u(t) is the control signal to the system, t designates time, and superscript ‘T’ designates the transpose. R1 and R2 are penalty matrices which are used to emphasize the performance of specific states and control signals. The index J(u) in the equation above is solved numerically for non-linear systems – and is computationally heavy i.e. very time consuming. By using a linearized state-space model the computational effort is reduced and static optimization can be used to find steady state gains for the full state feedback controller. It can be shown that the limiting constant solution P to the performance index can be found by solving the well-known Algebraic Riccati Equation below.

$$0 = A^T P + PA + R_1 - PBR_2^{-1}B^T P$$

From this, the minimum value J_{min} for the performance index J can be found to be:

$$J_{min} = \frac{1}{2} x_0^T P_\infty x_0$$

And the constant gains, K_∞, for the full state controller becomes:

$$K_\infty = R_2^{-1} B^T P_\infty$$

For the class-D amplifier it is desired to compensate for any non-linearities as fast as possible and to reduce the damped oscillation on the output. To realize this, the penalty matrix R1 is designed to heavily penalize the integration state. This will move the pole of the integrator to the left in the s-plane and make it settle somewhere close to the poles of the 2nd order filter, thus making the time constant of the integrator about the same as the output filters. Since the damped oscillation limits the movement of the integrator, it is to be expected that the LQR will further increase the damping of the output filter such that the oscillation will be reduced. All these pole movements generate a growth in the control signal which is limited by the supply voltage. It is important that the control signal does not clip since this would result in the system acting as an open-loop system. To avoid this, the penalty matrix R2 is increased to emphasize the size of the control signal thereby reducing it. Examples of penalty matrixes R1 and R2 are shown below:

$$R_1 = \begin{bmatrix} 0.7 & 0 & 0 & 0 \\ 0 & 10^{-3} & 0 & 0 \\ 0 & 0 & 10^{-3} & 0 \\ 0 & 0 & 0 & 10^{11} \end{bmatrix}, \; R_2 = 30$$

By providing a small penalty to the inductor current, the in-rush current is limited thus eliminating any overshoot at the output. Using the obtained model in and the penalty matrices, the feedback gains are found using the above equations. The resulting gains comprised by the vector K_∞ are shown below. Here it is particularly noticeable that the state, describing the current

through the speaker, is of next to no interest for the controller. This is probably because the controller focusses on controlling the voltage across the speaker and since the speaker current is a result of the voltage across the speaker, the current does not matter for the control of the amplifier.

$$K_\infty = [K_{ind\_I} \quad K_{spk\_I} \quad K_{spk\_V} \quad -K_i]$$

$$K_\infty = [0.177 \quad -1.062 \cdot 10^{-5} \quad 0.056 \quad -5.774 \cdot 10^4]$$

In the above, the last gain, K_i is the negative inverse of the time constant of the integrator, thus the time constant becomes:

$$\tau_i = \frac{1}{-K_i} = 1.8982\mu s$$

With the feedback gains and the time constant found, the loop can be closed according to the closed system shown in fig. 2.

Fig. 2 shows a state-space model of a class-D amplifier with state-space control. Please note that in fig. 2 gain elements A, B and C are multidimensional gain elements with a dimensionality in accordance with the dimensionality of state-space matrixes A, B and C in the expressions above (wherein A, B and C may be scalars). Regarding K, K in fig. 2 corresponds to K in the expressions above excluding the last element i.e. for fig. 2:

$$K = [K_{ind\_I} \quad K_{spk\_I} \quad K_{spk\_V}]$$

Thus, for example, gain element 211 has three paths with a respective gain (scalar).

In fig. 2 it is shown that the integration term is included as an integration element 203. The integration element 203 is located in a forward path of the class-D amplifier in series with a gain element 204, with gain Ki, following a summation element 202 which receives an input signal, IN, and subtracts therefrom a feedback signal provided via a gain element 212, with gain 1/G, to provide the resulting difference to the integrator term 203. The gain

element 212 receives its input signal from an output designated ‘OUT’ of the model. An outer feedback loop is thereby provided, implementing the integration term.

Further down the forward path, a summation element 205 receives a signal from the gain element 204 and subtracts therefrom a feedback signal received from a gain element 211, with gain $K = K_{\infty}$, to provide the resulting difference to a gain element 206 with gain B. Thereby a further feedback loop is provided.

Still further down the forward path, a summation element 207 receives a signal from the gain element 206 and subtracts therefrom a feedback signal received from a gain element 210, with gain A, to provide the resulting difference to an integrator element 208. Thereby a yet further feedback loop is provided. Output from the yet further feedback loop is provided to a gain element 209, with gain C, to the output.

It should be noted that Ki is the gain of the integrator. 1/G is the reciprocal of G, which is the gain of the class-D amplifier.

Using the state-space model, a linear full state integral controller can be designed, using the LQR method, and verified on a linear and non-linear model. Finally, the controller can be implemented on a class-D amplifier.

Total Harmonic Distortion, THD, measurements showed up to 10 time improvements compared to an amplifier without the controller. This proved that the principals of modern control achieve a very good performance even when the output filter has a resonance peak.

Fig. 3 shows a block-diagram of the class-D amplifier with state-space control. The block-diagram comprises elements, the details of which are explained in more detail with reference to the following figures.

The block-diagram comprises a signal source 301, an input stage 308, an output stage 305, an output filter 306 in the form of a high-Q low-pass filter,

and a load in the form of a speaker 307. The input stage comprises an integrator 302, a summing component 303 and a self-oscillating modulator in the form of a pulse-width modulator, PWM, 304. These elements form part of a forward path of the class-D amplifier.

The integrator 302 and the summing component 303 are coupled to receive a feedback signal, V_{spk}, measured at the output filter 306. The summing component 303 is additionally coupled to receive feedback signals, I_{spk} and I_L, at the output filter 306.

Fig. 4 shows a first output stage and an output filter with sensing components and sensing circuit nodes. In this embodiment, the output stage is configured as an H-bridge with semiconductor devices Q1 and Q2 in a left hand side of the H-bridge and semiconductor devices Q3 and Q4 in a right hand side of the H-bridge. The semiconductor devices Q1, Q2, Q3 and Q4 may be of the MOSFET type, FET type, BJT type or another type suitable to be operated as a switching device. The semiconductor devices Q1, Q2, Q3 and Q4 are controlled by respective control signals PWM1, PWM2, PWM3, and PWM4 where PWM1 and PWM4 are mutually in-phase control signals, which are in opposite phase with PWM3 and PWM2, which are mutually in-phase control signals. In this way short circuiting of the supply voltage through Q1 and Q2 and through Q3 and Q4 is avoided. The control signals have a square shape. The semiconductor devices Q1, Q2, Q3 and Q4 may have an ‘on-state’ and an ‘off-state’ selectively controlled by the control signals. In some time intervals, semiconductor devices Q3 and Q2 are in their on-state, while Q1 and Q4 are in their off-state, resulting in current flowing through a load, such as speaker 403, from a supply voltage terminal, Vs, to a ground terminal, Vgnd, via Q3 and via Q2. In other time intervals, semiconductor devices Q1 and Q4 are in their on-state, while Q2 and Q3 are in their off-state, resulting in current flowing through the load in the opposite direction, from the supply voltage terminal, Vs, to the ground terminal, Vgnd, via Q1 and via Q4. The

ratio between the duration of ‘on-period’ to the duration of ‘off-period’ defines the duty-cycle.

The load 403 is arranged in the path between the left hand side of the H-bridge and the right hand side of the H-bridge. The path comprises a series connection of a first output filter inductor, L1f; a first sensing resistor, R1s; the speaker, Spk; a second sensing resistor, R2s; and a second output filter inductor, L2f. The sensing resistors have relative small Ohmic impedance compared to the Ohmic impedance of the speaker.

The path also comprises a capacitor, Cf, coupled in parallel with the speaker, Spk, and the second sensing resistor, R2s.

As shown, sensing nodes are named ILs, VOA, VOB and IOs. The sensing nodes are coupled to sensing circuits as described in more detail below.

Fig. 5 shows a second output stage and an output filter. The second output stage is configured as a half-bridge, comprising semiconductor devices Q1 and Q2 as described above. The half-bridge requires a double-sided voltage power supply with a positive voltage supply terminal, Vs, a negative voltage supply terminal, -Vs, and a ground terminal, Vgnd. In this configuration a single output filter inductor, Lf, is coupled between the speaker, Spk and the half-bridge.

Sensing resistors may be coupled in series with the output filter inductor, Lf, and in series with the speaker, Spk, to provide sensing nodes ILs, VOA and IOs. In this embodiment VOB is not needed since the speaker is connected to ground, Vgnd.

Fig. 6 shows current sensing amplifiers. The current sensing amplifier 601 is coupled to the sensing nodes IOs and VOB described above and is configured to output a measurement of the current, Ispk, through the speaker. The current sensing amplifier 602 is coupled to the sensing nodes

ILs and VOA described above and is configured to output a measurement of the current, ILf, through the inductor of the output filter.

The current sensing amplifier 601 and the current sensing amplifier 602 are configured as summing amplifiers based on operational amplifiers U1 and U2 as it is known in the art.

Current sensing amplifier 601 comprises resistors R11, R16, R10 and R5. Resistor R5 is coupled to a voltage reference, Vref. The current sensing amplifier 601 provides a voltage output, Ispk, which is proportional to the difference between voltage VOB and IOs, i.e. the voltage drop across the second sensing resistor R2s, which in turn is proportional to the current through the speaker. Thus, current sensing amplifier 601 outputs a measurement of the current through the speaker.

Current sensing amplifier 602 comprises resistors R22, R23, R21 and R17. Resistor R17 is coupled to a voltage reference, Vref. The current sensing amplifier 602 provides a voltage output, ILf, which is proportional to the difference between voltage VOB and ILs, i.e. the voltage drop across the first sensing resistor R1s, which in turn is proportional to the current through the inductor of the output filter. Thus, current sensing amplifier 602 outputs a measurement of the current through the speaker.

Fig. 7 shows an output voltage sensing amplifier. The output voltage sensing amplifier 701 comprises resistors R8, R9, R7 and R6 and is based on an operational amplifier U3. Resistor R6 is coupled to a voltage reference, Vref. The output voltage sensing amplifier 701 provides a voltage output, Vspk, which is proportional to the difference between voltage VOB and VOA, i.e. the voltage drop across the speaker, Spk. Thus, output voltage sensing amplifier 701 outputs a measurement of the voltage across the speaker.

One or more of: current sensing amplifier 601, current sensing amplifier 602 and output voltage sensing amplifier 701 are comprised by a measurement circuit. The measurement circuit measures a set of states comprising two or

more of: current (IL) through the output filter inductor, output current (Ispk) and output voltage (Vspk).

Fig. 8 shows an integrator. The integrator 801 receives an input signal, Vin, via an input terminal of the class-D amplifier. The integrator 801 also receives the feedback signal, Vspk, which may be generated as described above. The output of the integrator is a voltage signal denoted, Ierr. The integrator 801 is this arranged in a forward path of the class-D amplifier and receives a feedback signal. The integrator 801 is based on an operational amplifier U4 and comprises resistors R13 and R12 and capacitors C7 and C8.

In some embodiments the integrator 801 is an implementation of the integrator 302 shown in fig. 3. The integrator 801 subtracts Vspk from Vin and provides the result thereof as its output, Ierr. The integrator improves proportionality between an input signal to the class-D amplifier and an output from the class-D amplifier. However, in some embodiments, the integrator 801 is dispensed with.

Fig. 9 shows a summation amplifier. The summation amplifier 901 is based on an operational amplifier U5 and receives feedback signals, Vspk, Ispk, ILf and forward signal, Ierr, which are summed via resistors R20, R19, R18, R14 and feedback resistor R15 to output a sum signal, Verr. The summation amplifier 901 may also be denoted a state control feedback summation amplifier which sums state control signals Vspk, Ispk and ILf.

The summation amplifier 901 is comprised by the state controller. The summation amplifier 901 has a substantially flat gain across frequencies in a frequency range between 20 Hz and 10 KHz or between 20 Hz and 20 KHz or between 20 Hz and an upper frequency; wherein the upper frequency is located approximately at the resonance frequency of the output filter or an upper -3dB cut-off frequency of the class-D amplifier. In some embodiments the summation amplifier 901 is an implementation of the summing circuit 303 shown in fig. 3.

Fig. 10 shows a self-oscillating pulse-width modulator. The self-oscillating pulse-width modulator 1001 outputs the signals PWM1 and PWM2 which are pulse width modulated signals mutually in opposite phase. From these two signals PWM3 and PWM4 may be generated as it is known in the art. The self-oscillating pulse-width modulator 1001 is based on an operational amplifier U6 and comprises resistors R1, R2, R4 and R5 and capacitor C.

The signal Verr, which is an analogue signal, is received from the summation amplifier 901 and in response to the amplitude of the signal, Verr, pulse width modulated signals PWM1 and PWM2 are output. PWM2 may be generated from PWM1. In some embodiments positively going flanks of PWM2 are slightly delayed, e.g. by one or more semiconductor elements, relative to negatively going flanks of PWM1 to ensure that short circuiting through Q1 and Q2 and through Q3 and Q4 is avoided.

Fig. 11 illustrates ripple current over mean current as a function of duty-cycle. To facilitate Zero Voltage Switching (ZVS) or Reduced Voltage Switching (RVS) for a given duty cycle span the reactive ripple current in the output filter inductor must be dimensioned so that the ripple current is larger than continuous output current for all duty cycles within that span, that is $\Delta i > I_{out}$.

It is illustrated how the ZVS/RVS region increases with higher quality factors of the output filter and a self-oscillating modulation scheme as it shows the ratio between the ripple-current and the continuous output-current vs. duty cycle for various quality factors, Q-factors, of the output filter for both conventional fixed frequency- and self-oscillating-modulators.

Fig. 12 illustrates temperatures related to heat dissipation at different areas of a circuit board carrying a class-D amplifier. The circuit board 1201 carries among other components of the class-D amplifier four semiconductor devices configured in an H-bridge in the output stage; the four semiconductor devices are arranged within a semiconductor region 1202. The four semiconductor devices are arranged e.g. as shown in the circuit shown in fig. 4. The circuit

board 1201 also carries two inductor coils arranged within an inductor coil region 1203. The two inductor coils are arranged e.g. as shown in the circuit shown in fig. 4.

Temperature measurements were conducted in connection with a class-D amplifier arranged on a circuit board as described above in a first situation without state-space control as described above and in a second situation with state-space control as described above. Six temperatures at points 1 through 6 were measured in the first situation and six temperatures were measured in the second situation:

Measurement point	With or without state-space control, $Q \sim 0.7$ [°C]	With state-space control $Q \gg 0.7$ [°C]
1	93.0	55.5
2	97.3	56.7
3	98.9	56.0
4	98.2	55.9
5	51.6	64.2
6	51.6	64.3

Thus, temperatures at the semiconductor region are lowered whereas temperatures at the conductor region are increased.

CLAIMS

1. A class-D amplifier with an amplifier input and an amplifier output, comprising:

an input stage (308) with a self-oscillating pulse-width modulator (304) configured to receive an analog input signal via the amplifier input and to output a digital signal;

an output stage (305) configured with semiconductor devices to amplify the digital signal;

an output filter (306), configured as a low-pass, high Q filter, coupled between the output stage and the amplifier output; and

a feedback circuit (309) coupled to the output filter (306) and to the input stage (308);

CHARACTERIZED in that

the feedback circuit (309) is coupled at the output filter (306) to measure a set of states comprising all of: current (IL) through the output filter inductor, and output voltage (Vspk); and

the feedback circuit (309) and the input stage (308) are operatively coupled as a controller configured to control all of the states in the set of states while operatively suppressing a frequency peak at a resonance frequency of the output filter.

2. A class-D amplifier according to claim 1, wherein the set of states comprises output current (Ispk).

3. A class-D amplifier according to any of the above claims wherein the feedback circuit comprises:

a measurement circuit outputting respective measurement signals proportional to one or more of: current (IL) through the output filter inductor, output current (Ispk), and output voltage (Vspk); and

a gain element (211) applying a respective gain to the respective measurement signals to output respective feedback signals to the input stage (308).

4. A class-D amplifier according to any of the above claims wherein the feedback circuit has a substantially flat gain across frequencies in a frequency range between 20 Hz and 10 KHz or between 20 Hz and 20 KHz or between 20 Hz and an upper frequency; wherein the upper frequency is located approximately at the resonance frequency of the output filter or an upper -3dB cut-off frequency of the class-D amplifier.

5. A class-D amplifier according to any of the above claims, configured to perform Zero Voltage Switching (ZVS) or Reduced Voltage Switching (RVS) at least at duty-cycles in the range of 30 to 70%.

6. A class-D amplifier according to any of the above claims, wherein the reactive ripple current in the output filter inductor is larger than the continuous output current at least within a range of duty-cycles from 30% to 70% duty-cycle.

7. A class-D amplifier according to any of the above claims, comprising an integrator (302) coupled in a forward path between the amplifier input and the self-oscillating pulse-width modulator (304); wherein at least a first path of the feedback circuit is coupled to an input of the integrator (302) and to a first circuit (701) measuring the output voltage (Vspk).

8. A class-D amplifier according to any of the above claims, comprising a summing circuit (303) coupled in a forward path between the amplifier input and the self-oscillating pulse-width modulator (304); wherein at least a second path of the feedback circuit is coupled to an input of the summing circuit (303) and to a second circuit (602) measuring the current through the output filter inductor.

9. A class-D amplifier according to claim 8, wherein at least a third path of the feedback circuit is coupled to an input of the summing circuit (303) and to a second circuit (601) sensing the output current.

10. A class-D amplifier according to any of the above claims, wherein the self-oscillating pulse-width modulator is configured as an astable integrating modulator or a hysteresis offset modulator.

11. A class-D amplifier according to any of the above claims, wherein the class-D amplifier has a step response with a peak of the output current which is limited to 3 times the current of a settled portion of the step response.

12. A class-D amplifier according to any of the above claims, wherein the controller is implemented as an analogue controller.

13. A semiconductor die comprising a class-D amplifier according to any of the above claims, excluding the output filter or an inductor thereof.

ABSTRACT

A class-D amplifier with an amplifier input and an amplifier output, comprising: an input stage (308) with a self-oscillating pulse-width modulator (304) configured to receive an analog input signal via the amplifier input and to output a digital signal; an output stage (305) configured with semiconductor devices to amplify the digital signal; an output filter (306), configured as a low-pass, high Q filter, coupled between the output stage and the amplifier output; and a feedback circuit (309) coupled to the output filter (306) and to the input stage (308). The feedback circuit (309) is coupled at the output filter (306) to measure a set of states comprising at least two of: current (IL) through the output filter inductor, output current (Ispk) and output voltage (Vspk); and the feedback circuit (309) and the input stage (308) are operatively coupled as a controller configured to control all of the states in the set of states while operatively suppressing a frequency peak at a resonance frequency of the output filter.

(fig. 3 should be published)

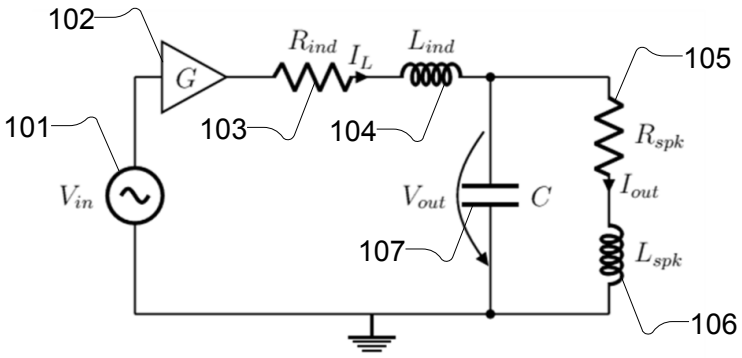

Fig. 1

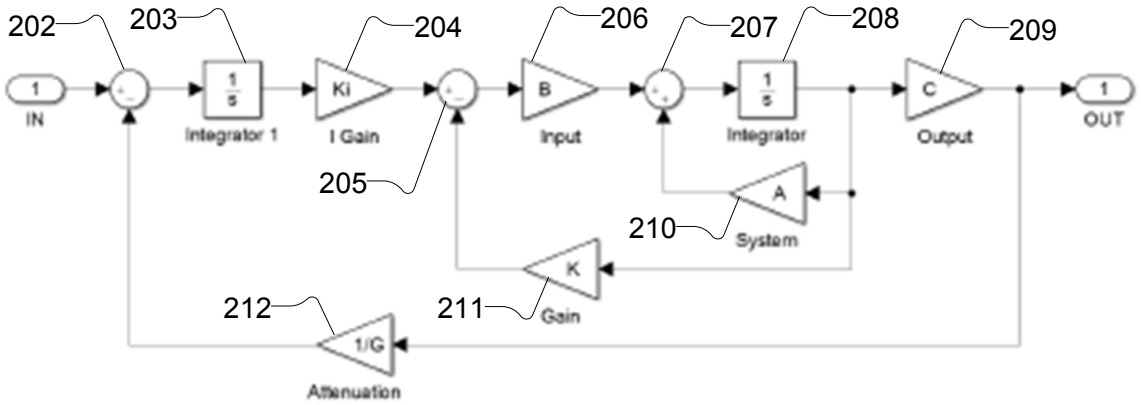

Fig. 2

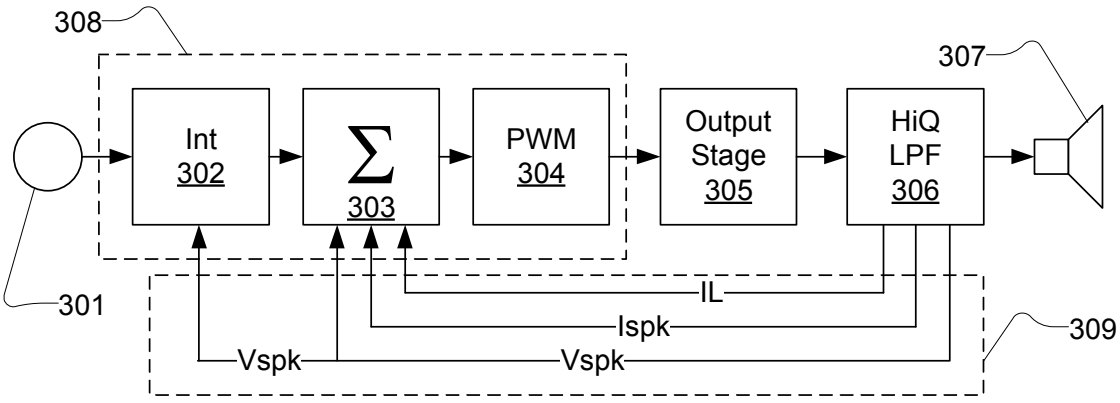

Fig. 3

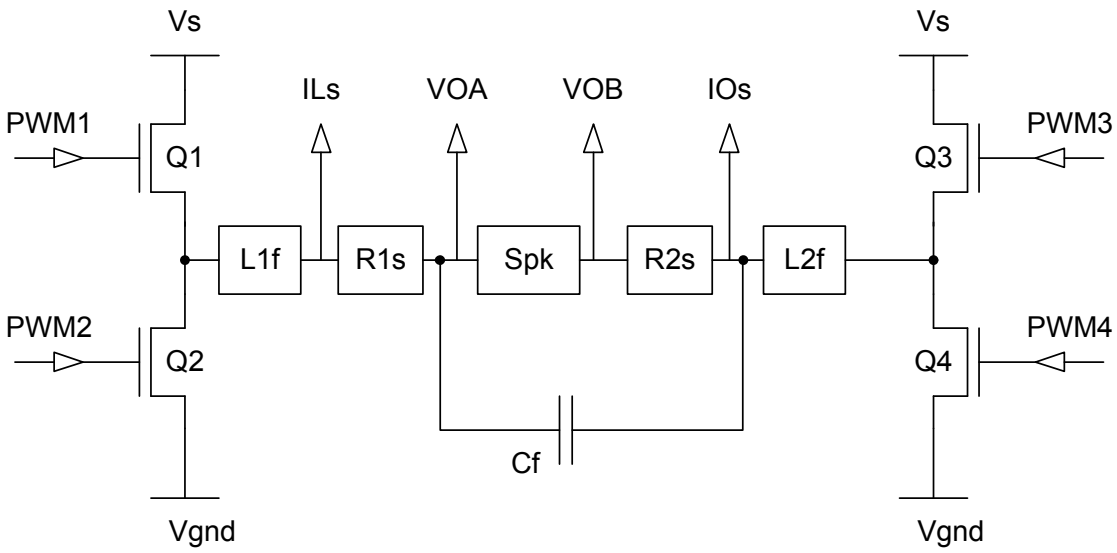
Vs
Vs
ILs
VOA
VOB
IOs
PWM1
Q1
Q3
PWM3
L1f
R1s
Spk
R2s
L2f
PWM2
Q2
Q4
PWM4
Cf
Vgnd
Vgnd

Fig. 4

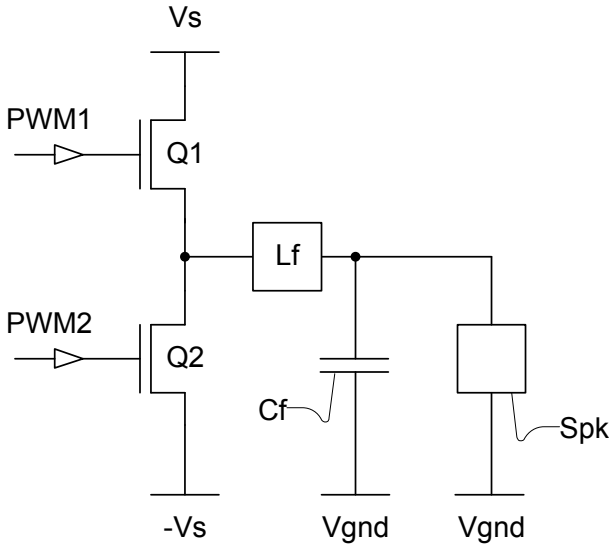
Vs
PWM1
Q1
Lf
PWM2
Q2
Cf
Spk
-Vs
Vgnd
Vgnd

Fig. 5

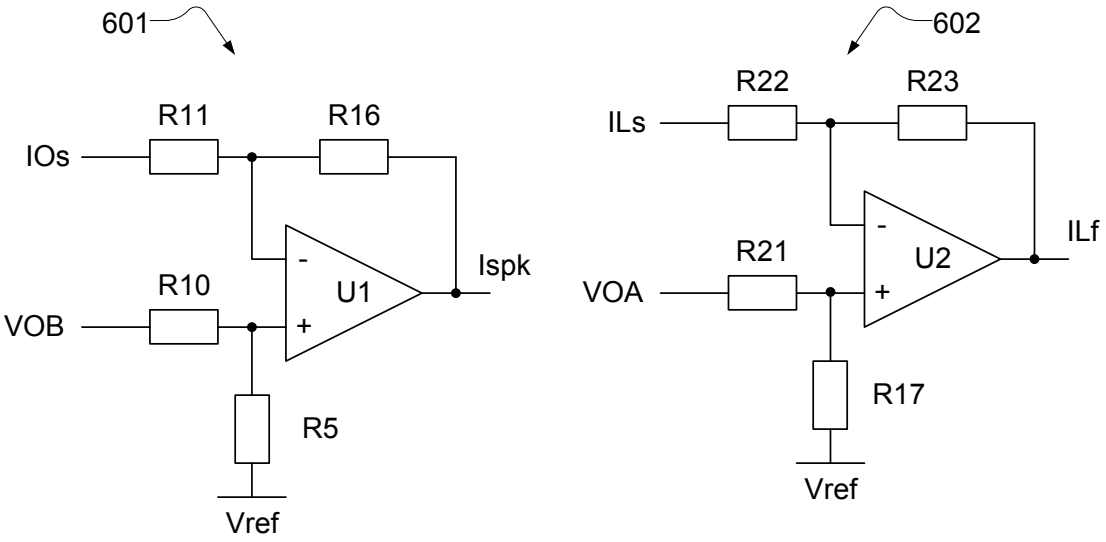
601
602
R11
R16
IOs
R10
VOB
U1
Ispk
R5
Vref
R22
R23
ILs
R21
VOA
U2
ILf
R17
Vref

Fig. 6

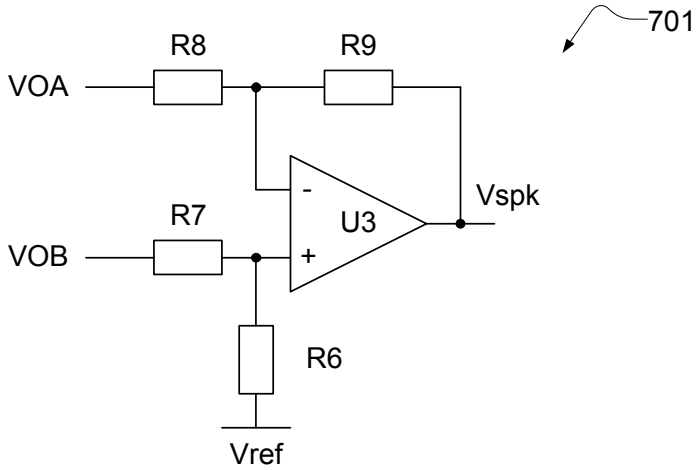
701
R8
R9
VOA
R7
VOB
U3
Vspk
R6
Vref

Fig. 7

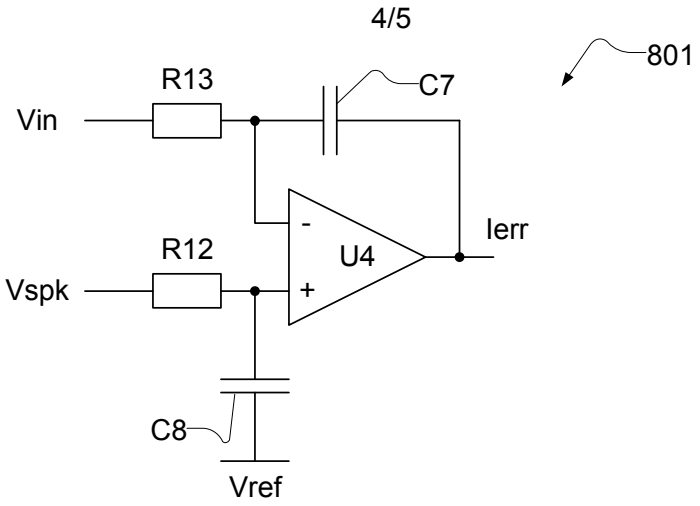

Fig. 8

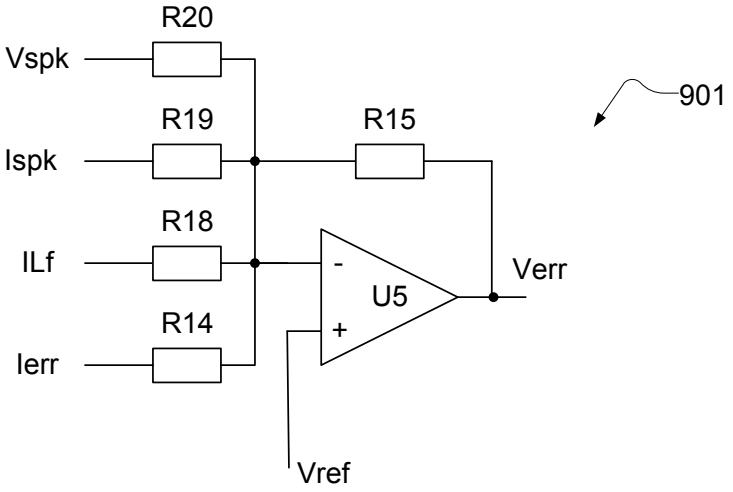

Fig. 9

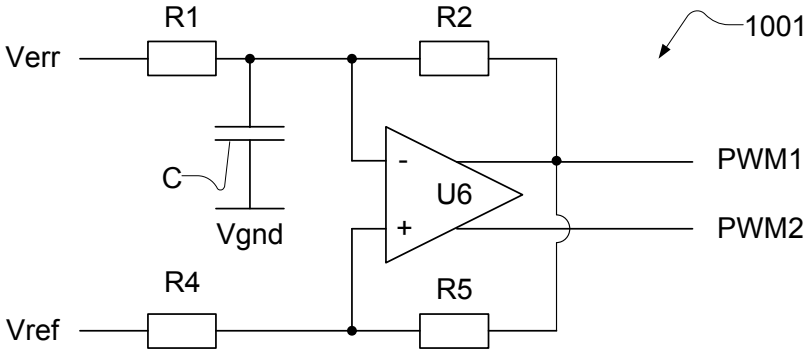

Fig. 10

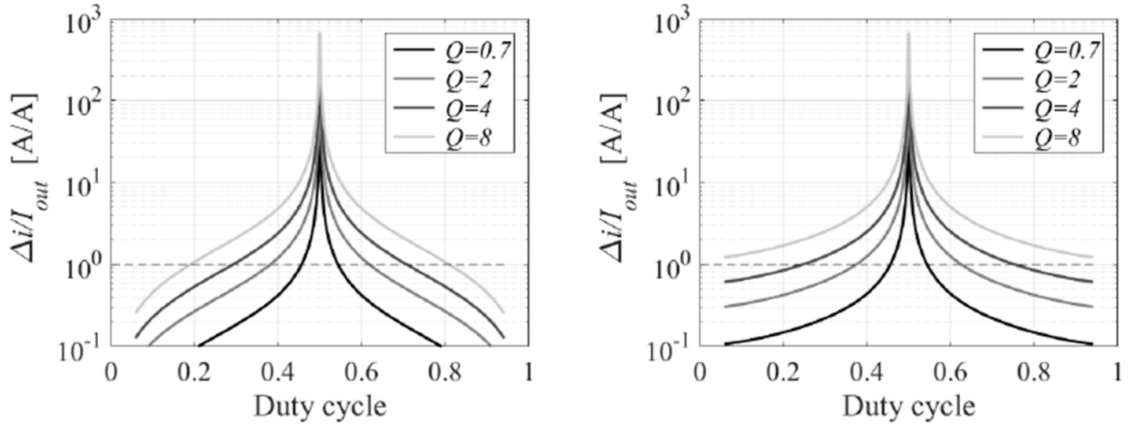

(a) Fixed frequency modulation.

(b) Self-oscillating modulation.

Fig. 11

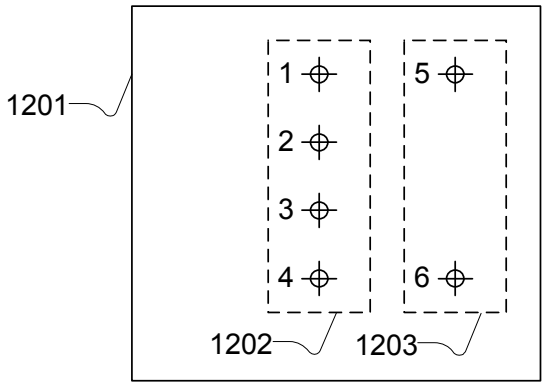

Fig. 12

DTU Electrical Engineering
Department of Electrical Engineering
(ADD GROUP OR CENTER)
Technical University of Denmark

Ørsteds Plads
Building 348
DK-2800 Kgs. Lyngby
Tel: (+45) 45 25 38 00

www.elektro.dtu.dk